INFLUENCE OF PARTICLE SIZE DISTRIBUTION ON THE PERFORMANCE OF FLUIDIZED BED REACTORS

By

Guanglin Sun

M. A. Sc. (Chemical Engineering) Zhejiang University

A THESIS SUBMITTED IN PARTIAL FULFILLMENT OF

THE REQUIREMENTS FOR THE DEGREE OF

DOCTOR OF PHILOSOPHY

in

THE FACULTY OF GRADUATE STUDIES

CHEMICAL ENGINEERING

We accept this thesis as conforming

to the required standard

THE UNIVERSITY OF BRITISH COLUMBIA

1991

In presenting this thesis in partial fulfilment of the requirements for an advanced degree at the University of British Columbia, I agree that the Library shall make it freely available for reference and study. I further agree that permission for extensive copying of this thesis for scholarly purposes may be granted by the head of my department or by his or her representatives. It is understood that copying or publication of this thesis for financial gain shall not be allowed without my written permission.

Department of Chemical Engineering

The University of British Columbia
Vancouver, Canada

Date April 8, 1991

DE-6 (2/88)

Abstract

The effect of particle size distribution (PSD) on the performance of a fluidized bed reactor was investigated using the ozone decomposition reaction, combined with the study of hydrodynamics, for fresh and spent fluid cracking catalysts, each having three particle size distributions - wide, narrow and bimodal - all with nearly the same mean diameter (60 μm), the same particle density and the same BET surface area. The superficial gas velocity was varied from 0.1 to 1.8 m/s to include the bubbling, slugging, turbulent and fast fluidization regimes. The catalytic rate constant, based on the volume of the particles, ranged from 2 to 10 s^{-1}, while the static bed height was varied from 0.15 m to 1 m. Four different multi-orifice gas distributors with different hole diameters (2.2 to 5.1 mm) and hole numbers (4 and 21) were also tested to evaluate the influence of gas distributor on the performance of fluidized bed reactors.

The particle size distribution was found to play a larger role at higher gas velocities than at lower velocities. At low gas velocities ($U_f \leq 0.2$ m/s), the reaction conversion was not greatly affected by the PSD. However, with an increase in gas velocity the PSD effect became larger. The wide size distribution gave the highest reactor efficiency, defined as the ratio of the volume of catalyst required in a plug flow reactor to that required in the fluidized bed reactor to achieve the same conversion, while the narrow blend gave the lowest. The differences are not solely a function of the "fines content".

The influence of particle size distribution on the hydrodynamics of fluidization was evaluated by measuring particle concentrations in voids, bubble sizes, and dense phase expansion. When the superficial gas velocity exceeded 0.1 m/s, the bed with the wide size distribution usually gave the highest particle concentration inside the voids, the smallest

bubble size and the greatest dense phase expansion at the same operating conditions. There is evidence that there is a greater proportion of "fines" present in the voids than in the overall particle size distribution. This has been explained in terms of the throughflow velocity inside bubbles being of the same order as the terminal velocity of typical "fines", causing these particles to spend longer periods of time inside the voids.

The effect of the PSD on the fluidization regime and its transitions was determined by measuring pressure fluctuations along the column. The earliest transition from bubbling or slugging to turbulent fluidization occurred in the bed of wide size distribution, while the latest corresponded to the narrow PSD.

For particles of wide size distribution, higher conversion was achieved for the turbulent and fast fluidization regimes than for the bubbling fluidization regime under otherwise identical conditions, while for particles of narrow size distribution, the dependence of conversion on regime was small. Hence, for reactors of wide PSD, the performance can be improved significantly by operating in the turbulent or fast fluidization regime, while for particles of narrow size distribution, the benefit of operating at high gas velocity is slight at best.

The PSD influence should be considered in modelling fluidized bed reactors. The "Two-Phase Bubbling Bed Model" has been modified to account for PSD effects. For the reactor of wide particle size distribution operated at high gas velocities, a single-phase axial dispersion model with closed inlet and open outlet boundary conditions appears to be suitable to predict the performance.

It was also found that a high pressure drop across the gas distributor was not sufficient to maintain good performance of the distributor. The reactor efficiency in the entry region was higher for a distributor with a greater number of orifices, even though it had a lower pressure drop, than for a distributor plate with fewer larger holes.

Acknowledgement

I would like to express my great appreciation to Dr. J.R. Grace for his excellent supervision and overall support.

Special thanks are also due to the ladies and gentlemen of the Department of Chemical Engineering, especially to the Workshop and the Stores, for their invaluable assistance.

This project would not have been possible without the financial assistance of the donors of the Petroleum Research Fund, administered by the American Chemical Society; a Graduate Fellowship awarded by the University of British Columbia; a Fellowship provided by Alcan; a Scholarship awarded by Pao; research funding from the Natural Sciences and Engineering Research Council of Canada. To each of these goes a very special thank-you.

The assistance of the Esso Petroleum IOCO refinery in Port Moody, B.C. in supplying the catalyst particles needed in this study is also gratefully acknowledged.

Table of Contents

List of Tables

List of Figures

Chapter 1

Introduction

Fluidized bed reactors are widely used in the process industries for solid-catalysed gas phase reactions (e.g. in catalytic cracking, acrylonitrile manufacture, phthalic anhydride production, polyethylene and polypropylene processes, etc.) and in gas-solid reactions (ore roasting, combustion, gasification, catalyst regeneration, calcination reactions, etc.). Advantages of fluid bed reactors include favourable heat transfer, temperature uniformity, capability of continuous addition and removal of particles, and ability to scale up to very large reactor sizes. A thorough review of industrial processes in fluidized bed reactors was given by Yerushalmi (1982). For a general introduction to fluidized beds and their hydrodynamic regimes see Geldart (1986).

The particle size distribution (PSD) is a key factor in determining the performance and operation of fluidized bed reactors. Although many workers have made reference to the importance of fines in determining the behaviour and performance of fluidized beds (e.g. Matheson et al, 1949; Zenz and Othmer, 1960; Agarwal and Davis, 1966; Abrahamsen and Geldart, 1980; Yates and Newton, 1986, etc.), and oil companies and other operators or designers of fluidized bed reactors commonly apply empirical criteria to ensure a level of fines which assists in establishing favourable yields and overall performance, the role of fines content and the effect of the PSD are poorly understood. There are at least three questions which need to be answered:

1. In what ways and to what extent do the PSD and the "fines" content affect the performance of fluidized bed reactors?

2. Why do the PSD and the "fines" content affect the performance of fluidized bed reactors?

3. Is it possible to characterize the influence of the PSD simply in terms of a "fines" content, as assumed by some authors (e.g. Abrahamsen and Geldart, 1980; Dry et al, 1983; Avidan and Edwards, 1986, etc.)?

The performance of a fluidized bed reactor mainly depends on the hydrodynamics of fluidization, transfer phenomena within the reactor and the kinetics of the reaction(s). We are primarily concerned in this thesis with catalytic applications of fluidized bed reactors. In such applications, the fluidized particles are generally small (almost always < 100 μm in average size, falling in Group A of the Geldart (1973) classification) with the result that catalyst effectiveness factors are very nearly one. The PSD primarily influences the reactor performance, therefore, via its effect on the hydrodynamics of fluidization and via its effect on the mass transfer in the reactor. In the present study, both of these interrelated aspects are investigated. The third question is resolved by separating the effect of fines and the effect of mean particle size in our experiments. The role of the PSD on the operation of fluidized bed reactors is modelled and discussed. Optimum PSD's for catalytic reactions are also considered.

1.1 PSD effect on the hydrodynamics of fluidized beds

The performance of fluidized bed reactors is strongly related to the hydrodynamics of fluidization, to those fundamental factors controlling the behaviour of the fluid-solid systems. Several years after the successful application of large scale commercial fluidized bed reactors composed of finely powdered solids in the cracking process of petroleum, the effect of "fines" on the character of fluidized beds began to interest a few investigators.

In an early study, Matheson et al (1949) measured the torque necessary to rotate a

paddle suspended in fluid beds made up of binary mixtures of synthetic cracking catalyst to explore the effect of the PSD on bed "viscosity". Relatively small amounts of fines added to a coarse cut were found to decrease the "viscosity" markedly. This trend was maintained up to fines concentrations of about 30%, after which the effect became less marked. Morse and Ballou (1951) investigated the uniformity of fluidization using capacitance signals and found that uniformity was better for non-uniform mixtures of particle sizes than for narrow cuts.

Zenz and Othmer (1960) evaluated early research work on the effects of the PSD on the pseudo viscosity of fluidized beds and concluded that the introduction of fines between the coarse grains could act as a lubricant to reduce the friction between the coarse paticles, thereby reducing the bed viscosity and helping to maintain "good fluidity". They also noted that PSD influences the efficiency and loading of fines recovery facilities, as well as the operation of pneumatic conveyers.

The effect of fines content on the hydrodynamic character of fluidized beds has also attracted some attention. Agarwal and Davis (1966) compared the minimum fluidization velocity for closely sized fractions of iron ore to that with a wide size range, and found that the greater the "fines"content, the lower the minimum fluidization velocities. In another study, de Groot (1967) investigated the effect of the amount of "fines" on bed expansion and reported that the expansion increased with addition of "fines", especially in columns of diameter larger than 0.5 m. While measuring the distribution of voidage in the particulate phase near rising bubbles by a capacitance technique, Lockett and Harrison (1967) observed that it became more difficult to define a real boundary between the bubble and particulate phases as the particle size distribution increased. That is, the difference between the two phases appeared to be less sharp for the system containing more fines.

More recently, Abrahamsen and Geldart (1980) measured hydrodynamic properties

of fluidized beds composed of powders with different mean particle size, density and proportion of fines (defined as particles smaller than 45 μm), and found that the minimum bubbling velocity, the dense phase interstitial gas velocity and the bed expansion all increased with the addition of fines. Similar results were reported by Sun et al (1983) with different gas properties and Dry et al (1983) with wider size range. In the latter case, the demarcation between "fines" and the rest of the material was taken to be 22 μm. In their correlations for minimum bubbling velocity, dense phase voidage and dense phase gas velocity, "fines" content was taken into account and played a significant role.

Avidan and Yerushalmi (1982) investigated the bed expansion of fine powders over a range of gas velocities spanning different fluidization regimes and noted that the presence of fines has far-reaching effects on the 'quality' of fluidization. They found that fresh catalyst with a higher proportion of fines showed less tendency to segregate, lower cluster terminal velocities and lower transition velocities to turbulent fluidization than older catalysts from which most of the fines had been lost. Werther (1984) measured the local visible bubble flow, including local bubble size and average bubble rise velocities in fluidized beds and discovered that increased fines (defined as particles with $d_p < 44$ μm) could increase the mass transfer rate due to decreasing equilibrium bubble size with an increase in the proportion of fines. Nacastro and Glicksman (1984) investigated pressure fluctuations within a fluidized bed and noted that variation in the particle size distribution could cause non-similarity of fluidization. The PSD was said to be an important parameter for modelling fluid dynamic behaviour.

While scaling up the methanol-to-gasoline process, Avidan (1986) found that bubble suppression was achieved in a turbulent fluidized bed with a minimum of 15% fines, where fines were defined as particles smaller than 40 μm. Kono et al (1986a) investigated the emulsion phase characteristics for fluidization of fine powder fluidized beds and reported that the minimum complete fluidization velocity and bed expansion ratios were somewhat

larger for beds containing more fines than for beds with few fines.

Since the quality of fluidization is supposed to be substantially determined by the characteristics of the emulsion phase of the bed, such as its viscosity (Grace, 1970), the fluid bed hydrodynamics can be related, to a certain extent, to the rheological characteristics of the powders. Generally speaking, the less rigid the structure of the emulsion phase, the more homogeneneous the fluidized system. The PSD effect on the powder rheology, therefore, has also been studied by researchers, not only in the area of fluidization, but also in other powder handling systems.

By measuring the tensile strength of powders around the minimum bubbling point, Kono et al (1986b) observed that both the tensile strength and the plastic deformation coefficient evaluated from the bed expansion could be decreased by adding fine powders to a narrow cut of particles. Lloyd and Webb (1987) measured the shear stress of powders with different fines content in both an aerated and non-aerated state. They noted that the rate of reduction of the shear stress with increased aeration is dependent on the fines content, and the addition of particles around 30 μm in size had a large effect. They also found the addition of fine particles could cause the powder to behave as 'liquid like' at lower shear velocities.

For spent FCC particles, investigators at UBC (Ip, 1988; Khoe et al, 1991), based on collapse tests, observed that U_{mb}/U_{mf} for particles of wide size distribution was 20% greater than for narrow PSD. They reported that for a given average surface-volume diameter, a wide size distribution gives a greater air retention capacity than a bimodal distribution which in turn gives greater retention than a narrow distribution. By measuring the pressure fluctuations in a fluidized bed, Ip also found that the magnitude of pressure fluctuations increases as the particle size spread become more narrow. However, the frequency of fluctuations is independent of the size spread.

Fines not only affect the hydrodynamics of fluidization, but also the flow character

of particles (Zenz and Othmer, 1960). Changing the particle size distribution allows the particle flow properties to be modified (Kurz and Münz, 1975; Geldart and Radtke, 1986). Reterman (1985) investigated catalyst circulation problems in fluid catalytic cracking units due to the loss of fines through a damaged cyclone and presented a parameter, F_{Prop}, which depended on the fines fraction (fines being defined as particles with $d_p <$ 45 μm), to express the flow properties and predict the onset of circulation problems.

Kwauk and his co-workers (Tung et al, 1989) carried out an extensive series of bed collapse experiments for different gas-solid systems and presented a dimensionless parameter, Θ, mainly depending on the collapsing time of fluidized beds at certain conditions, to express the hydrodynamic performance of fluidization. Based on the comparison of Θ values for different powders, they suggested that blending of particle fractions with different sizes can be used to improve the homogeneity of fluidization.

1.2 PSD effect on the performance of fluidized bed reactors

Very little work has been performed to determine the influence of the PSD on the performance of catalytic fluidized bed reactors. The performance of catalytic fluidized bed reactors depends not only on the hydrodynamics of fluidization, but also on other factors, such as diffusion resistance between gas and particles, catalyst activity, reactant conversion level and the nature of the reaction process. A number of these factors may be related to the mean particle size and to the particle size distribution.

Yates and Newton (1986) investigated the oxidative dehydrogenation of butene to butadiene in a reactor of 0.11 m in diameter at superficial gas velocities from 0.06 m/s to 0.32 m/s. The fines content (fines being defined as smaller than 45 μm) of the catalyst was 0%, 16% and 27%. The conversion of reactant was found to increase with the increase in the proportion of fines. The authors suggested that more gas flowed through

the emulsion phase of the bed, at the expense of gas flowing through the bubble phase, in fluidized beds with more fines.

Pell and Jordan (1988) studied the PSD effect in a pilot scale reactor where propylene was reacted with air and ammonia to produce acrylonitrile. The experiments were carried out at three different superficial gas velocities and at five different fines levels: 23, 27, 32, 40 and 44% by weight of particles smaller than 45 μm. The proportion of fines was varied by adding -45 μm enriched material to the existing charge. It was found that the conversion usually increased as the fines content increased. At higher gas velocities, the improvement in conversion due to addition of fines was much less than that at lower gas velocities.

The importance of the PSD on the performance of fluidized bed reactors has been recognized by industrial companies. It is common to control the PSD in fluidized beds during long periods of operation by adding fines from time to time to make up for those lost during the operation and to increase the collection efficiency of cyclones. It has been found (Sun and Chen, 1986) that the yield of a commercial fluidized bed reactor producing about 26000 tonnes of acrylonitrile per year can be increased by 2-3 per cent if the content of fines (less than 45 μm) is raised from 15% to 32% by weight.

Although high "fines" level can often give a better performance in fluidized beds, caution is necessary at such generalizations. Temperature runaway once happened in the freeboard region of a commercial fluidized bed reactor of propylene ammoxidation due to a large quantity of fine particles entrained from the bed with too high "fines" content (CGCPC Report, 1985). Moreover, if the fines become predominant, the behaviour of the powder becomes determined by interparticle forces, i.e. the powder behaves as a group C (cohesive) powder in the classification scheme of Geldart (1973).

Cooper and Clough (1985, 1986) have recently attempted to establish experimental methods to obtain on-line, real-time measurements of PSD in fluidized bed reactors.

Their apparatus includes a continuous flow particle sampling system, an optical spectrometer and a process computer system. The sampling system is closed-loop so that all sampled particles can return to the bed immediately after being analyzed.

1.3 Some basic problems with studies of PSD effect

Although the importance of fines on the performance of fluidized bed appears to have been established by the studies cited, the PSD effect on the performance of fluidized bed reactors has not previously been subjected to systematic investigation. Several basic problems connected with previous studies are considered in this work. Some of the key questions to be addressed are as follows:

1.3.1 Can the PSD effect be separated from the influence of the mean particle size?

Almost all studies cited above on the effect of particle size distribution discussed the problem in terms of the influence of "fines" content. It should be noted, however, that addition of fines affects both the mean particle size and the size distribution. The effect of "fines" content, therefore, can be divided into two aspects: the effect of average particle size and the effect of particle size distribution. It is clear that the influence of the mean particle size on fluidized bed performance is very significant, especially for group A materials, typical of fluid bed catalytic reactors. This effect has been considered in most correlations and results published on fluidization.

By measuring the bed expansion and bubble frequency, Matsen (1973) investigated the influence of mean particle size on the maximum stable bubble size in fluidized beds. Six kind of particles with different mean particle size (from 26 μm to 150 μm) were tested. Each kind of particles had different "fines" content (from 0% to 40% by weight)

where "fines" are defined as those less than 20 μm. Matsen found that the maximum stable bubble size was very sensitive to mean particle size, while the nature of the size distribution was also very critical. This suggests that the PSD effect should be separated from the influence of mean particle size if we want to explore the PSD effect without interference of other relative factors.

1.3.2 Is the "fines" content sufficient to express the particle size distribution?

No general method of expressing the PSD has been accepted by investigators of fluidized beds. Although most investigators characterized PSD by "fines" level, the definition of "fines" has differed from worker to worker. Some workers (e.g. Geldart and Abrahamsen, 1980; Yates and Newton, 1986) have defined fines as those particles which pass through a sieve of opening 45 μm. Dry et al (1983), however, defined the demarcation between the fines and the rest of the material to be 22 μm, while Avidan and Edwards (1986) distinguished on the basis of 40 μm. Evidently, different definitions of "fines" will lead to different results. Moreover, any such definition will be entirely arbitrary, and it is clear that addition of significant volumes of material 1 μm larger than the chosen limit will give nearly the same result as adding the same volume of material 1 μm smaller than the limit.

To illustrate the problem, consider the PSD of powders, as shown in Fig. 1.1, used by Matsen (1973) in a study of maximum stable bubble size for particles with different size and size distributions. If "fines " are defined as those less than 45 μm, coke 4 and coke 5 have the same "fines" level. If the "fines" are defined as those less than 20 μm or 15 μm, "fines" concentrations in coke 4 and coke 5 are then different. The experimental maximum stable bubble diameters determined by Matsen were different for these two distributions of particles (64 mm for coke 5 and 127 mm for coke 4), even though the

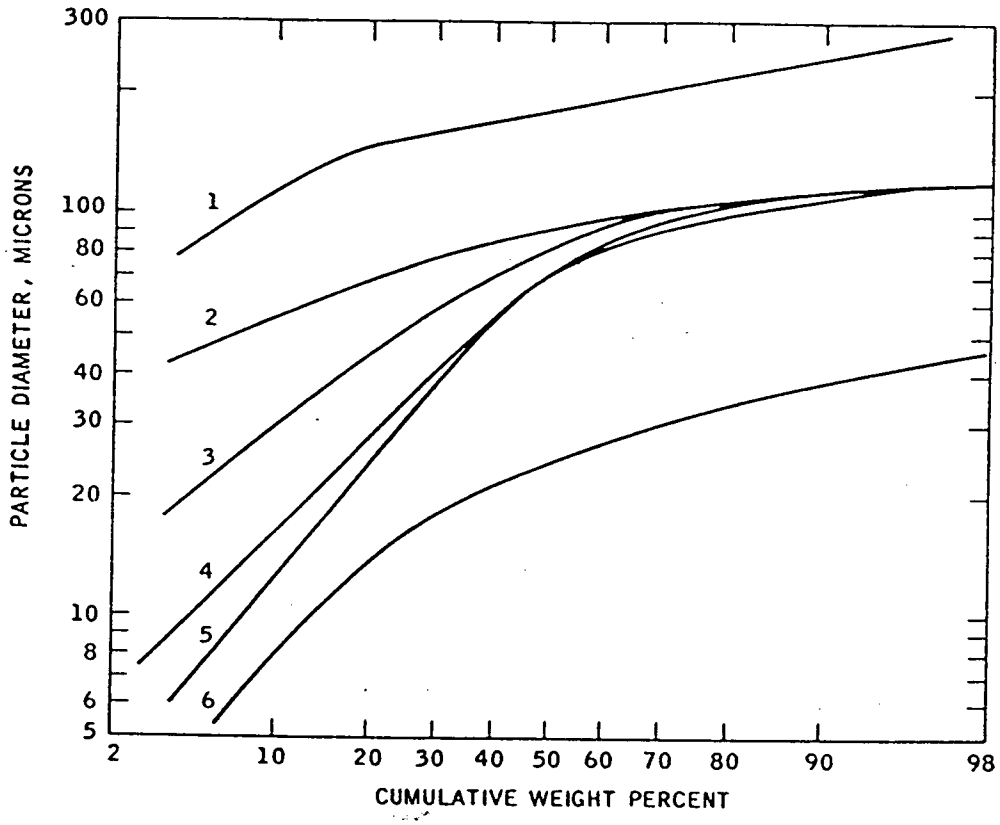

Figure 1.1: Coke particle size distributions. Identifying numbers on curves correspond to coke materials of several particle size distributions obtained by grinding. (Matsen, 1973)

mean particle diameters were almost the same for the two powders.

1.3.3 Is the influence of the PSD the same in different hydrodynamic regimes and bed regions?

Most previous experimental studies of chemical reaction in fluidized beds (e.g. Lewis et al, 1959; Hovmand and Davidson, 1968; Chavarie and Grace, 1975; Bauer and Werther, 1981; Yates and Newton, 1986) have been restricted to relatively low gas velocities, seldom exceeding 0.3 m/s. Commercial fluidized beds, however, usually operate at higher gas velocities (above 0.45 m/s) where different hydrodynamic regimes (e.g. turbulent and fast fluidization) may be encountered (Grace, 1986). It is possible that the PSD effect may differ in the various regimes, as indicated by the experimental result of Pell and Jordan (1988).

It is now well known that reactor characteristics differ widely between the region immediately above the gas distributor (grid region), the bed proper and the freeboard region. Since mass transfer resistance appears different in different regions, the extent of the PSD effect may also change from region to region.

1.4 Objectives of the present study

The objectives of this study are to analyze and explain the basic problems mentioned above. Briefly the objectives are:

1. To evaluate the PSD effect on the performance of catalytic fluidized bed reactors.
2. To examine the PSD effect in different fluidization regimes and different bed regions.
3. To investigate the PSD effect on the hydrodynamics of fluidization.
4. To explore the reasons for the influence of "fines" and of particle size distribution.

5. To express the PSD effect on the performance of fluidized bed reactors in different regimes and regions by suitable reactor models.

6. To test other factors related to the performance of catalytic fluidized bed reactors, such as the kinetic rate and the gas distributor.

Because PSD effects appear to be most significant for materials which belong in group A of the Geldart (1973) classification and fluid bed catalysts almost always fall into this category, this study will be limited to materials of this group.

Chapter 2

Experimental Particles and Apparatus

The main preparation work in this study can be divided into two parts: (a) experimental materials, including particles and gas, and (b) experimental equipment including the fluidization column, fixed bed column, instrumentation, data acquisition system and other accessories. Special attention has been paid to the catalyst powder preparation in order to achieve the objectives of this study. Two of the key points are:

1. separating the PSD effect from the influence of mean particle size, and
2. keeping the PSD within the experimental system as constant as possible during each operation period, even at high gas velocities.

2.1 Preparation of Particle Blends

Two kinds of particles, spent fluid cracking catalyst (S-FCC) and fresh fluid cracking catalyst (N-FCC), were used in the experiments. These were obtained from the Esso Ioco refinery in Port Moody, B.C. The mean diameter, defined as $1/\Sigma(x_i/d_{pi})$, was about 60 μm in each case. For each kind of particles, three batches were prepared, labelled "wide", "narrow" and "bimodal", each with the same mean diameter and nearly the same BET surface area and particle density, but different particle size distribution.

2.1.1 Particle separation and blending

The original spent and fresh cracking catalysts were separated into six different size fractions respectively using the Haultain Infrasizer in the UBC Coal and Mineral Processing

Centre. This device is based on air elutriation and is suited to split the particles into multiple fractions below 200 mesh (i.e. 75 μm) at one time (Haultain, 1937). The infrasizer consists of six steel conical chambers arranged in series. Their dimensions are given in Fig. 2.1. The separation involved two passes to minimize overlapping between adjacent fractions. The respective air flowrates for the first and the second passes were 0.0021 and 0.0022 m^3/s. The original bulk FCC particles were charged into chamber 1 of the infrasizer during the first pass. The fraction collected in cone number 3 was then passed into the sizer during the second run. Four size fractions of FCC labelled "wide", "coarse", "narrow" and "fine" were collected for our experiments. The "wide" distribution was the unseparated (i.e. original) FCC powder. The "coarse" and "fine" fractions were the powders collected in cone numbers 2 and 4, respectively, from the first pass. The "narrow" fraction was collected in cone number 3 from the second pass, i.e. all particles in this fraction ended up in cone 3 in two successive passes.

A horizontal rotating drum mixer was used to blend particles of different fractions or different activities. Bimodal batches were prepared by combining the "coarse" and "fine" fractions. The catalyst activity was adjusted by changing the weight ratio of activated to non-activated particles.

2.1.2 Catalyst activation and characterization

FCC particles were activated as the catalyst for ozone decomposition by being impregnated with ferric nitrate solution at room temperature in a stirring mixer for one hour, and then roasted in an electric oven at 450°C for one and a half hours. Both photographs and size distribution measurements before and after this activation procedure (see Figs. 2.3 and 2.4, and Appendix E) indicate that there was negligible agglomeration or change in the physical properties as a result of the impregnation and roasting. The concentration of the ferric nitrate solution used was 10% by weight. The activity of the

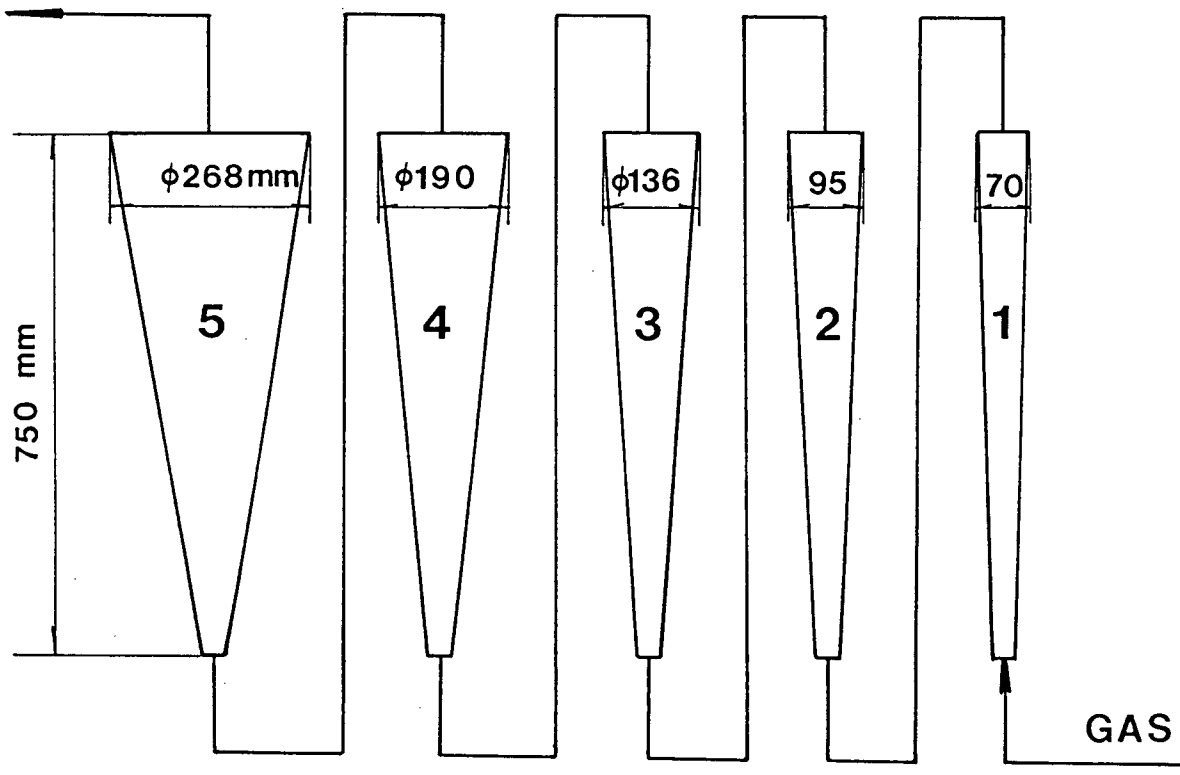

Figure 2.1: Dimensions of the infrasizer

resulting catalysts was around 15 s^{-1} at 20°C. Keeping the impregnation and roasting conditions consistent for each batch of particles was essential to ensure uniform quality of the catalysts prepared. The activities of the catalysts used in the experiments prepared by blending activated and non-activated catalysts, were measured before and after each run in a small fixed bed reactor with the same range of mean gas residence time as in the fluidized bed.

Some properties were found to differ appreciably between the fresh and spent catalysts. For example, the spent FCC particles can be used as a catalyst without activation for ozone decomposition, with a kinetic rate constant of 0.3 to 0.5 s^{-1} at room temperature, whereas the fresh FCC particles were found to be inactive for ozone decomposition. However, once activated, the activity of the fresh FCC was much more stable than that of the spent catalyst. The activity change of the activated N-FCC catalysts during a run was usually less than 3%. The experimental results on the performance of fluidized bed reactors were therefore collected mainly for the N-FCC particles.

2.1.3 Relevant properties of the particles

Relevant properties of the particles used in our experiments, including the particle density, particle diameter, particle shape and surface area, were measured.

Two kinds of density, the particle density, ρ_p, and the bulk density, ρ_b, were measured for each particle fraction and particle blend. The particle density, ρ_p, was measured with the "wet cake" method proposed by Abrahamsen and Geldart (1980). The bulk densities were determined after the bulk volume of a loose packed bed of a pre-weighted sample of particles was determined using a graduated cylinder. The resulting densities of spent and fresh FCC are shown in Table 2.1.

The particle size distributions measured by an Electrone Size Analyser, based on the same principle as that of the Coulter counter, appear in Fig. 2.2.

Table 2.1: Measured particle and bulk densities for fluid cracking catalyst

Powder	Size distribution	ρ_p (kg/m^3)	ρ_b (kg/m^3)
S-FCC	wide	1444	756
S-FCC	coarse	1384	743
S-FCC	narrow	1455	735
S-FCC	fine	1556	782
S-FCC	bimodal	1440	761
N-FCC	wide	1582	860
N-FCC	coarse	1591	895
N-FCC	narrow	1586	823
N-FCC	fine	1557	847
N-FCC	bimodal	1573	868

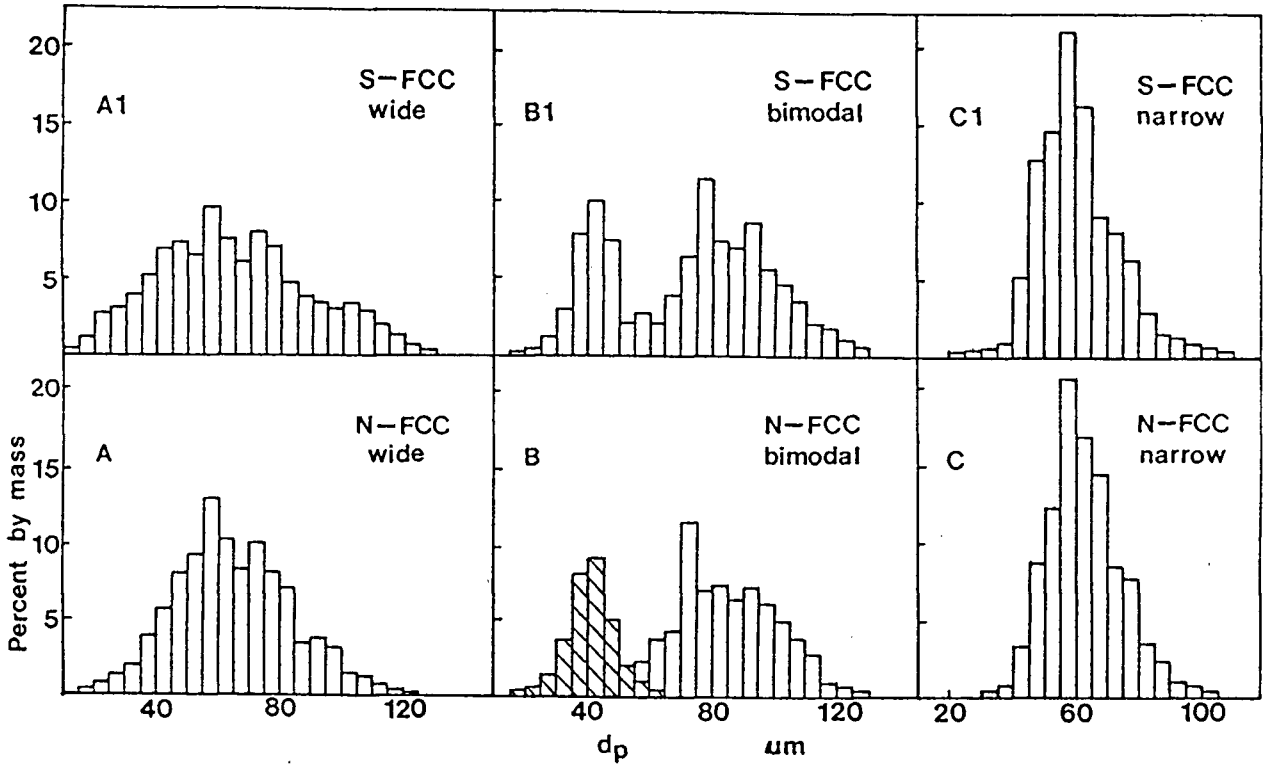

Figure 2.2: Size distributions of FCC particles

Table 2.2: Surface area of FCC particles

Powder	Size distribution	Activated?	Surface area (m^2/g)
N-FCC	wide	No	212
N-FCC	narrow	No	208
N-FCC	bimodal	No	210
N-FCC	fine	No	251
N-FCC	coarse	No	144
N-FCC	wide	Yes	172
N-FCC	narrow	Yes	164
N-FCC	bimodal	Yes	169
S-FCC	wide	No	88

The particle surface area was measured by a Micromeritics Surface Analyser based on the BET isotherm theory, with sample tubes of type P/N 230-61001-00. The results are given in Table 2.2. Some reduction in surface area resulted from the impregnation / roasting procedure, presumably due to pore blockage by the ferric oxide.

The particle surface shape was measured by the sweep electron microscope (Hitachi S-570). SEM pictures of different fractions and different blends of FCC particles are presented in Figs. 2.3 to 2.8.

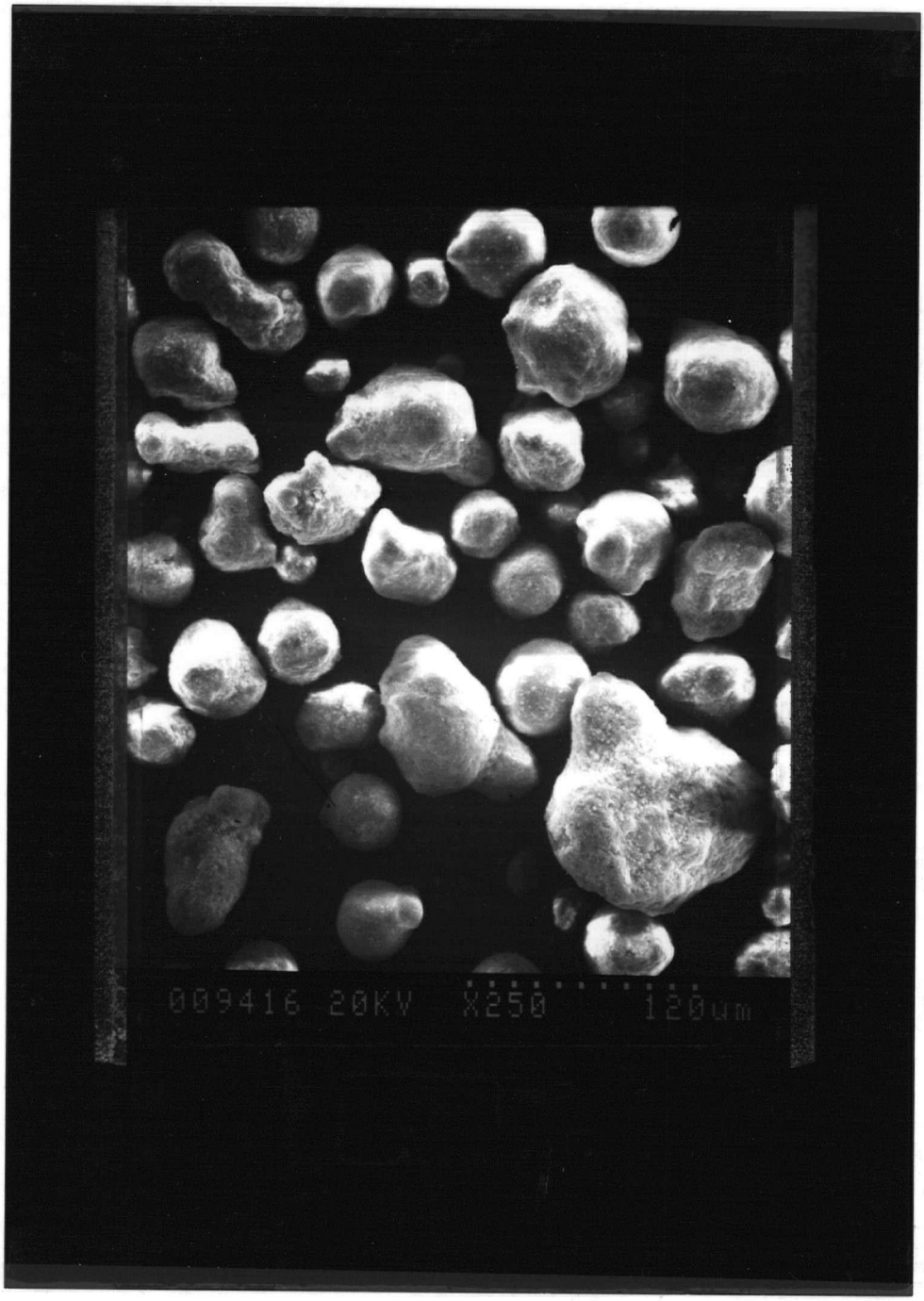

Figure 2.3: SEM photograph for N-FCC particles of wide size distribution

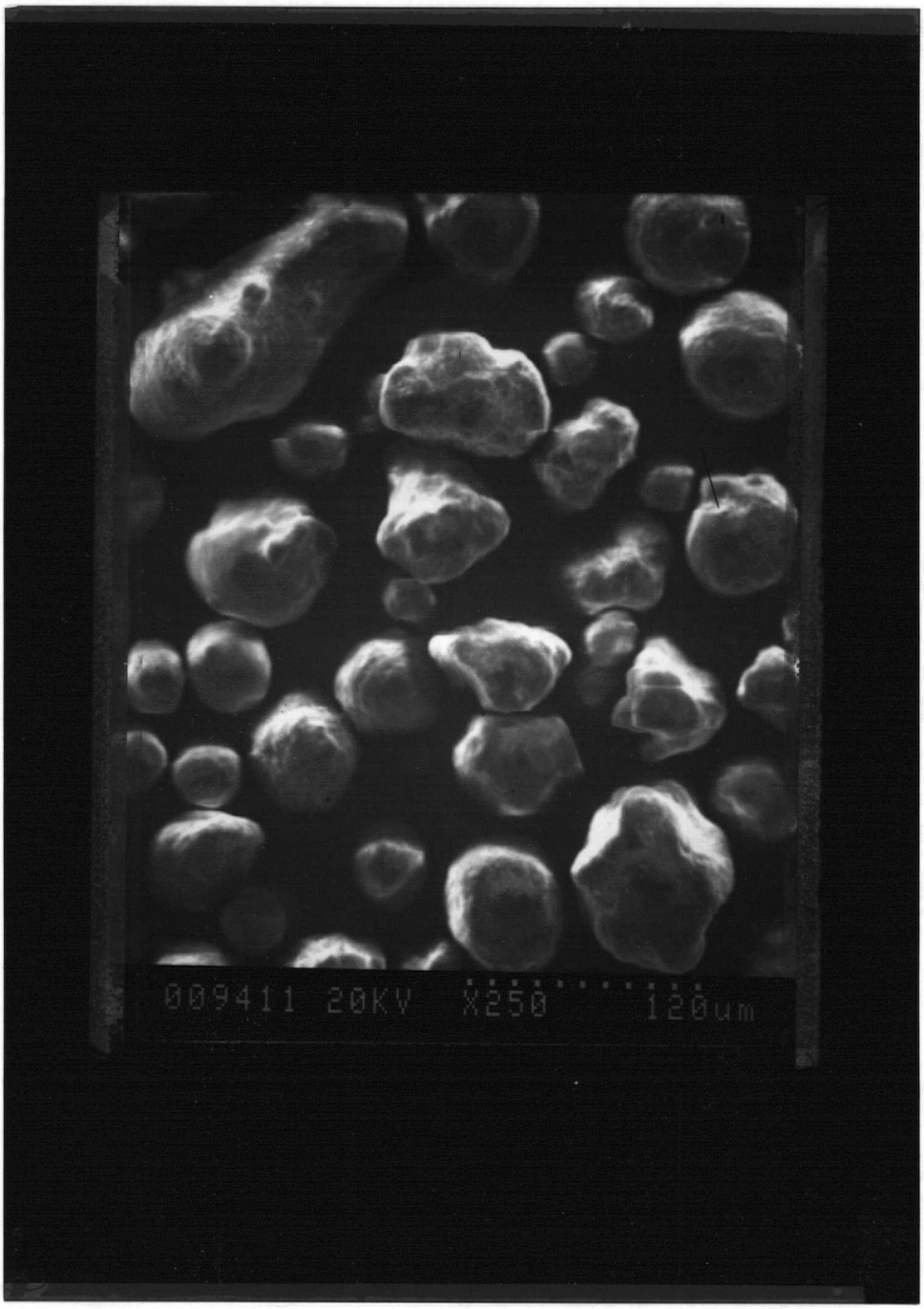

Figure 2.4: SEM photograph for N-FCC particles of wide size distribution after being activated

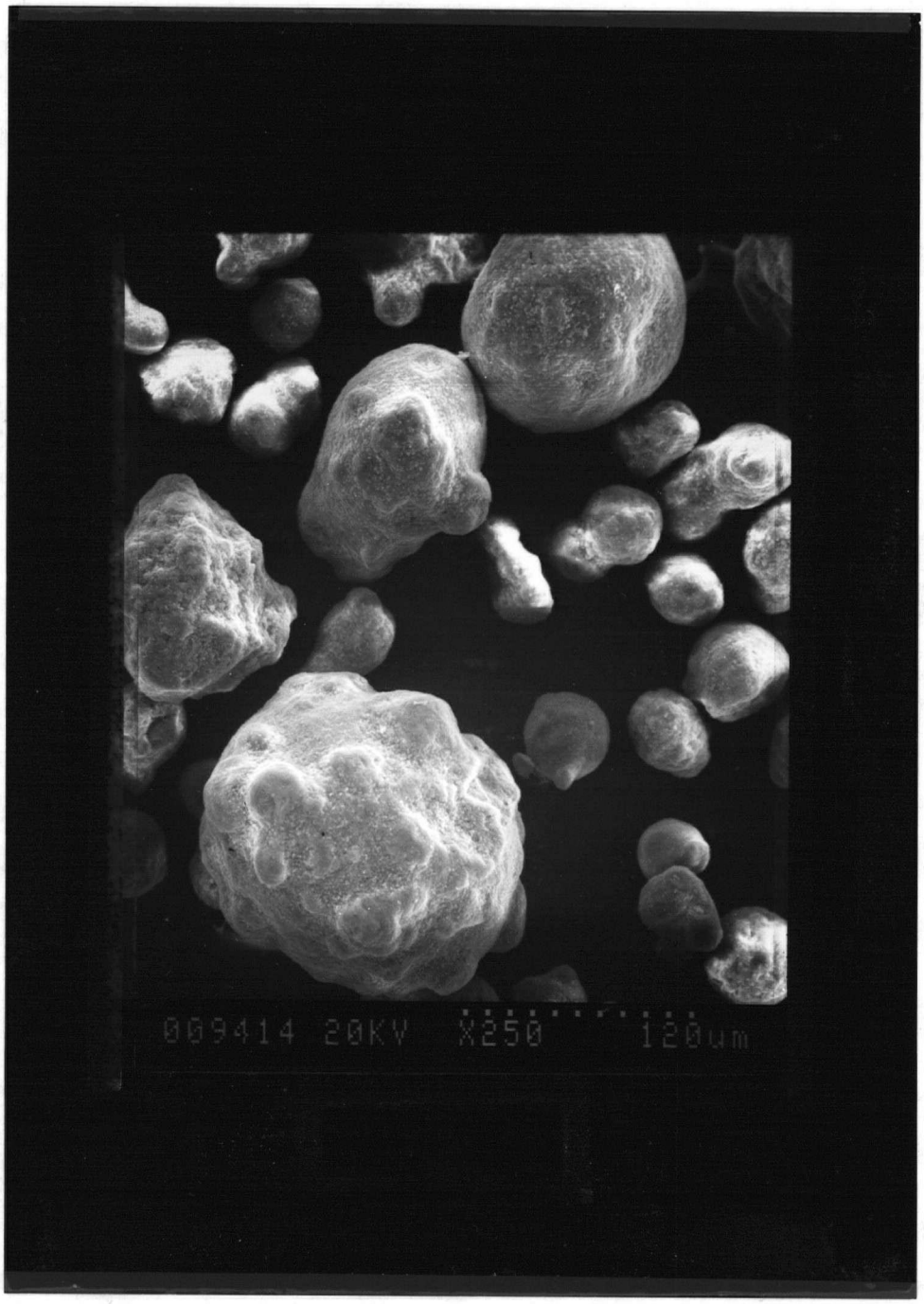

Figure 2.5: SEM photograph for N-FCC particles of bimodal size distribution

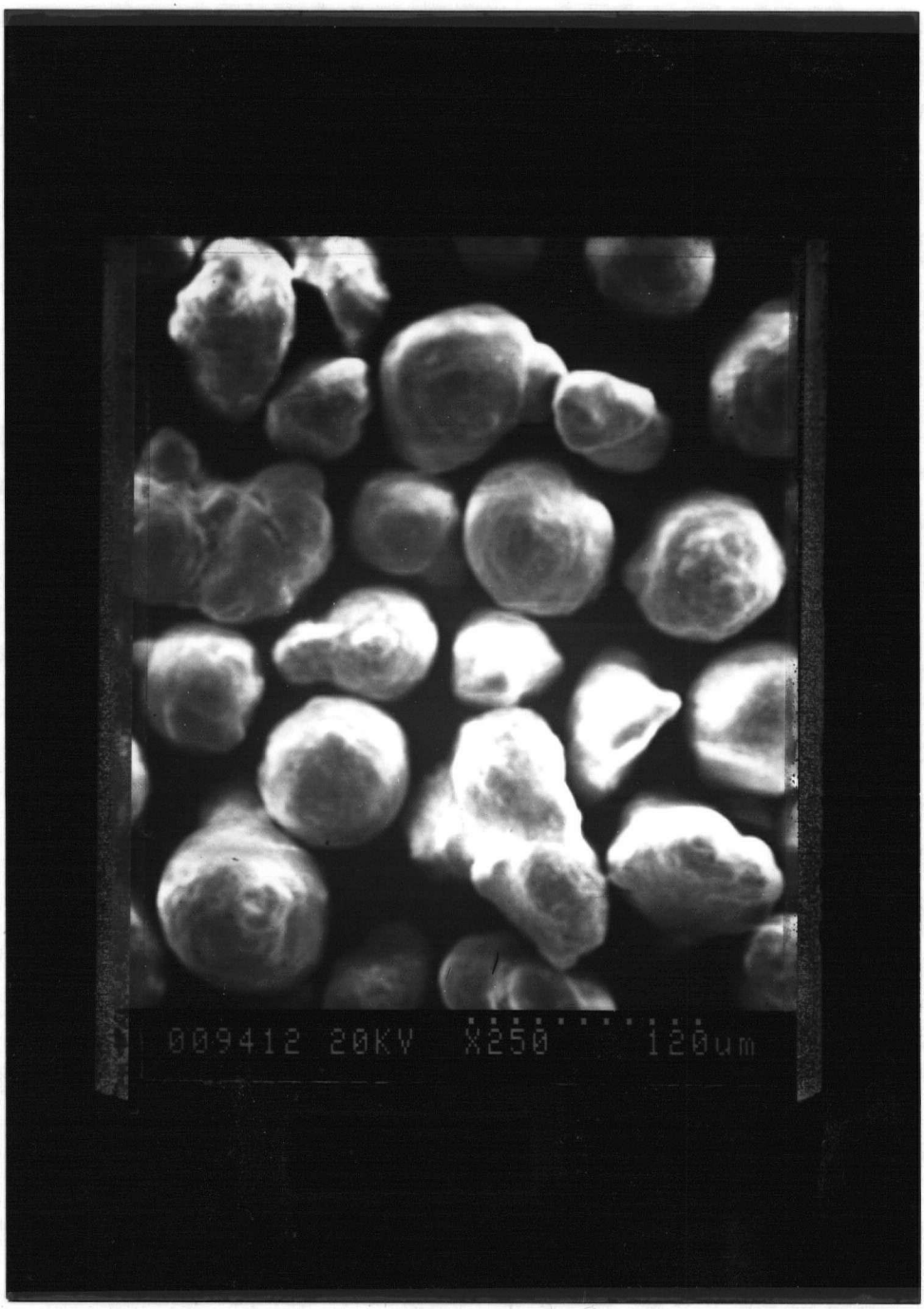

Figure 2.6: SEM photograph for N-FCC particles of narrow size distribution

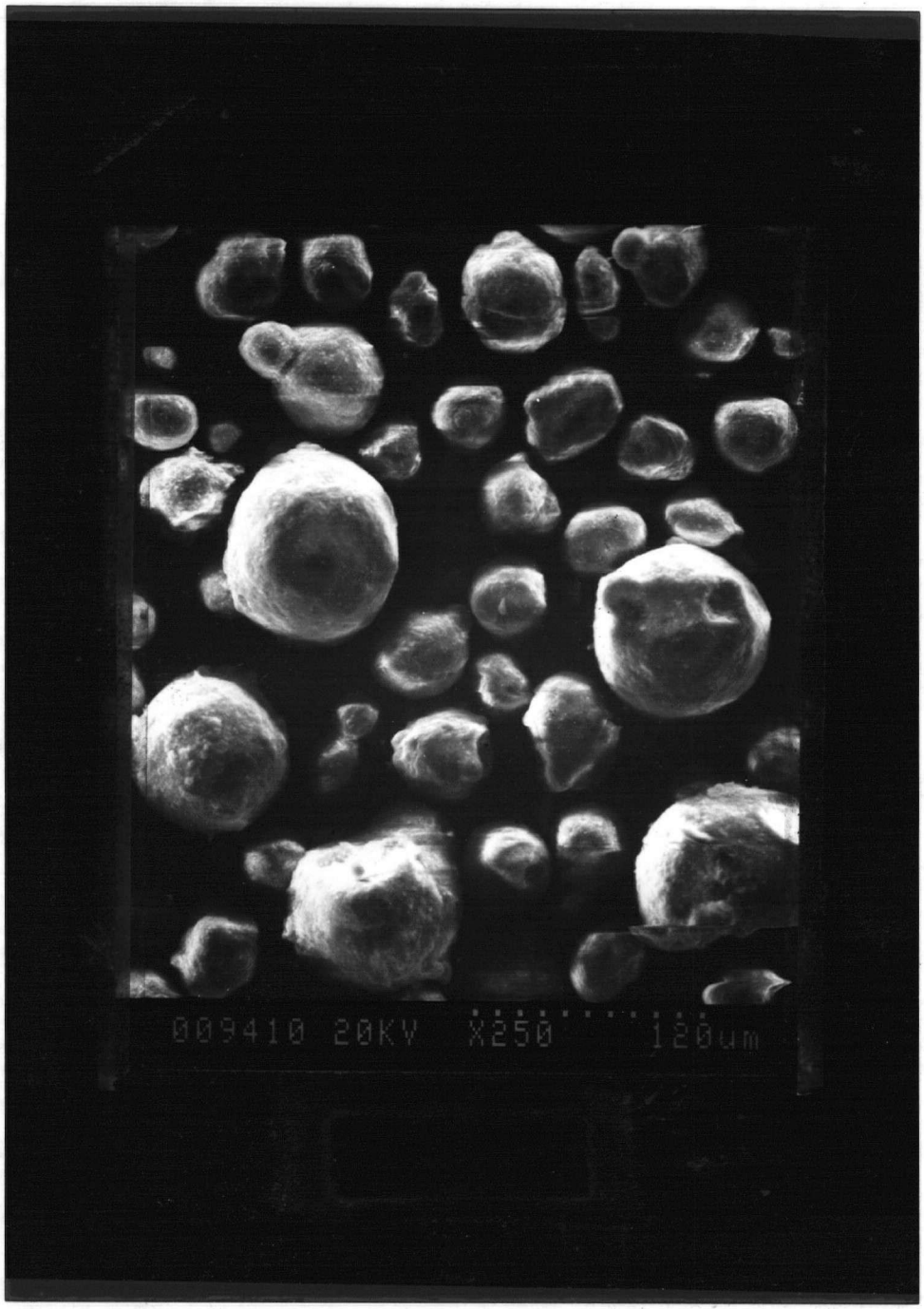

Figure 2.7: SEM photograph for S-FCC particles of bimodal size distribution

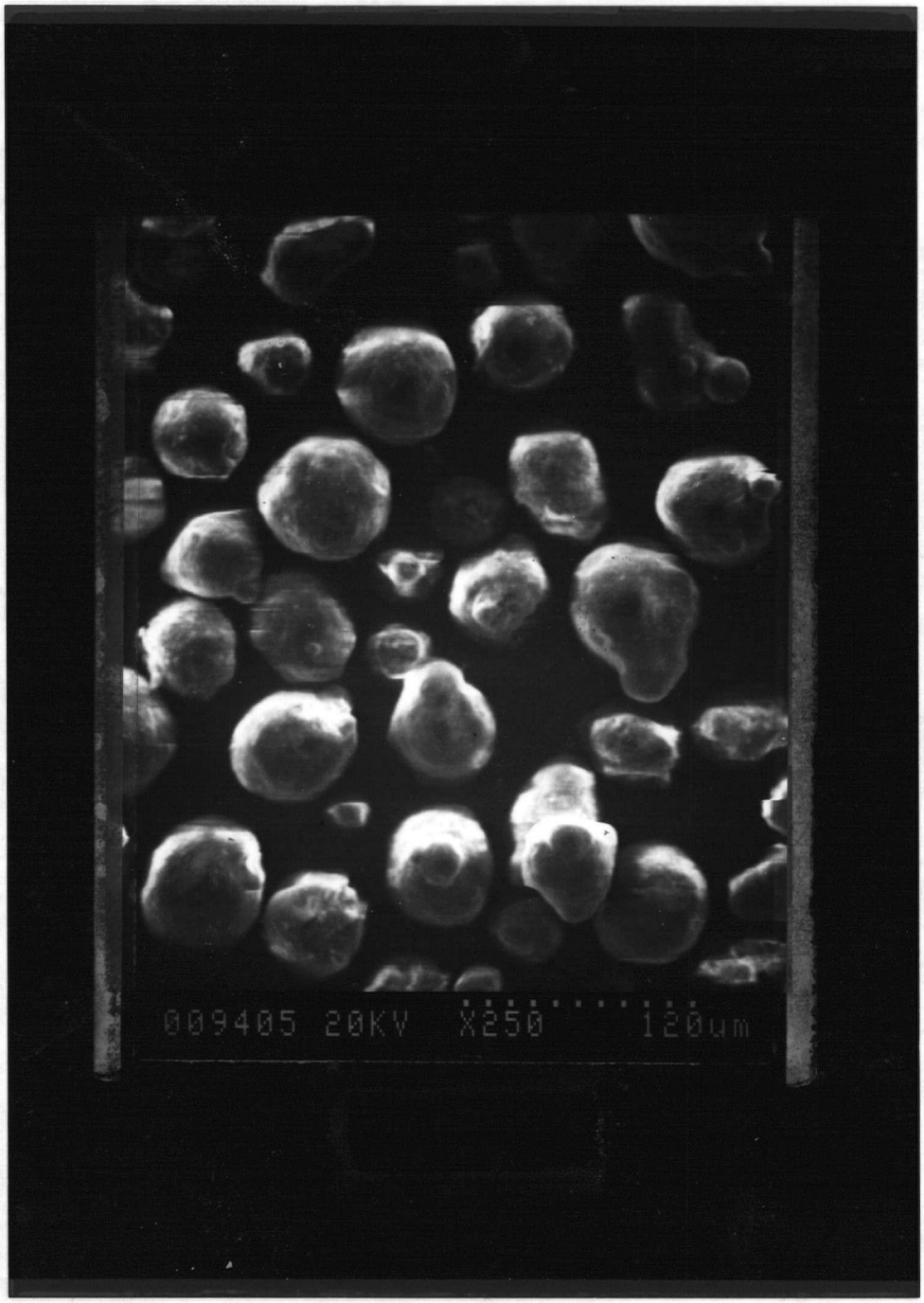

Figure 2.8: SEM photograph for S-FCC particles of narrow size distribution

2.2 Experimental Apparatus

Most experiments on the performance and hydrodynamics of fluidized bed reactors were carried out in a fluidized bed system designed and constructed for this project. Some hydrodynamic research was also carried out in a two-dimensional fluidization column which was modified for this investigation. Reliability and safety of the experimental equipment, flexibility during operation and economy of manufacture and operation were the main design considerations.

The ozone decomposition reaction,

$$O_3 \longrightarrow 1.5\ O_2 + 143\ \text{kJ/mole},$$

is a valuable laboratory reaction because it can be carried out under room temperature and pressure conditions. In addition, it is nearly first order, and ozone can be readily analysed using UV absorption. Several research workers (e.g. Frye et al, 1958; Van Swaaij and Zuiderweg, 1972; Chavarie and Grace, 1975; Bauer and Werther, 1981) have used this reaction to investigate the character of fluidized bed reactors, generally at low gas velocities and for Group B or D particles.

The apparatus is shown schematically in Fig. 2.9. It includes five major parts: (1) ozone generation and gas purification system; (2) fluidization column; (3) outlet gas treatment and particle recirculation system; (4) instruments and data acquisition system; (5) fixed bed apparatus.

2.2.1 Gas supply system

Ozone is generated by passing a stream of cylinder oxygen (breathing grade), after being further dried by calcium sulphate, through an OREC electric discharge ozone generator. The resulting O_2 - O_3 mixture, with ozone concentration 1 - 3% by volume, was then

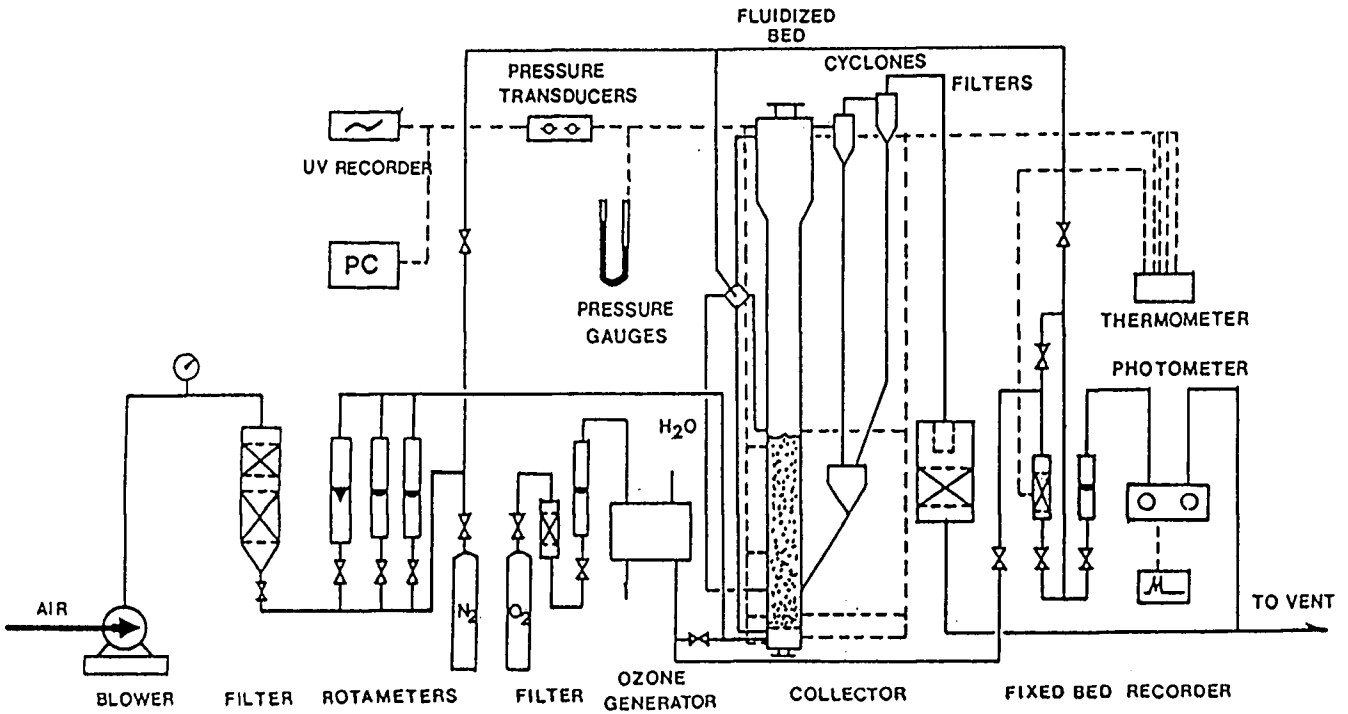

Figure 2.9: Schematic of experimental equipment

combined with the fluidizing gas before entering the bed. The fluidizing gas was blower air, purified by passing through a column containing activated carbon and silica gel.

It is found from our pretest that the rate of ozone decomposition is very sensitive to the humidity of fluidizing gas, especially at room temperature. The catalyst activity decreases very quickly if the catalysts are fluidized by unpurified air from the blower. Frye et al (1958) reported that the activity of ozone decomposition varied with the reciprocal third order of water vapor concentration.

2.2.2 Reactors

The fluidization column (Fig. 2.10) is 2.6 m tall and 0.10 m in inside diameter. There is an enlarged section above the column, 0.15 m in diameter and 0.5 m in height, to reduce carryover, with a sloping section in between having a steep enough angle that particles do not collect thereon. The fixed bed is 19 mm in diameter and 200 mm tall. The ozone concentration at different positions along the fluidized bed is sampled isokinetically by five probes. Since fines with diameters less than 20 μm can plug the filter of the sampling probe, a nitrogen backflow system is set up to purge the filter before each sampling at lower gas velocity and every 2 to 5 minutes for higher gas velocities ($U > 0.5$ m/s). The purge frequency was also dependent on the fines content of the bed material.

Since ozone is a very powerful oxidant and reacts with most substances at 25°C (Razumovskii and Zaikov, 1984), the material of the reactor vessels and connecting tubes had to be carefully chosen. The fluidized and fixed bed vessels are constructed of aluminum. The sampling and connecting tube between the manometers and the reactor are pure copper. It has been found (Horvath et al, 1985) that at room temperature and for ozone concentrations up to 7% by volume, decomposition of ozone is not catalysed by pure aluminum, lead, copper and tin, although most metals are strongly oxidized by ozone and promote its decomposition.

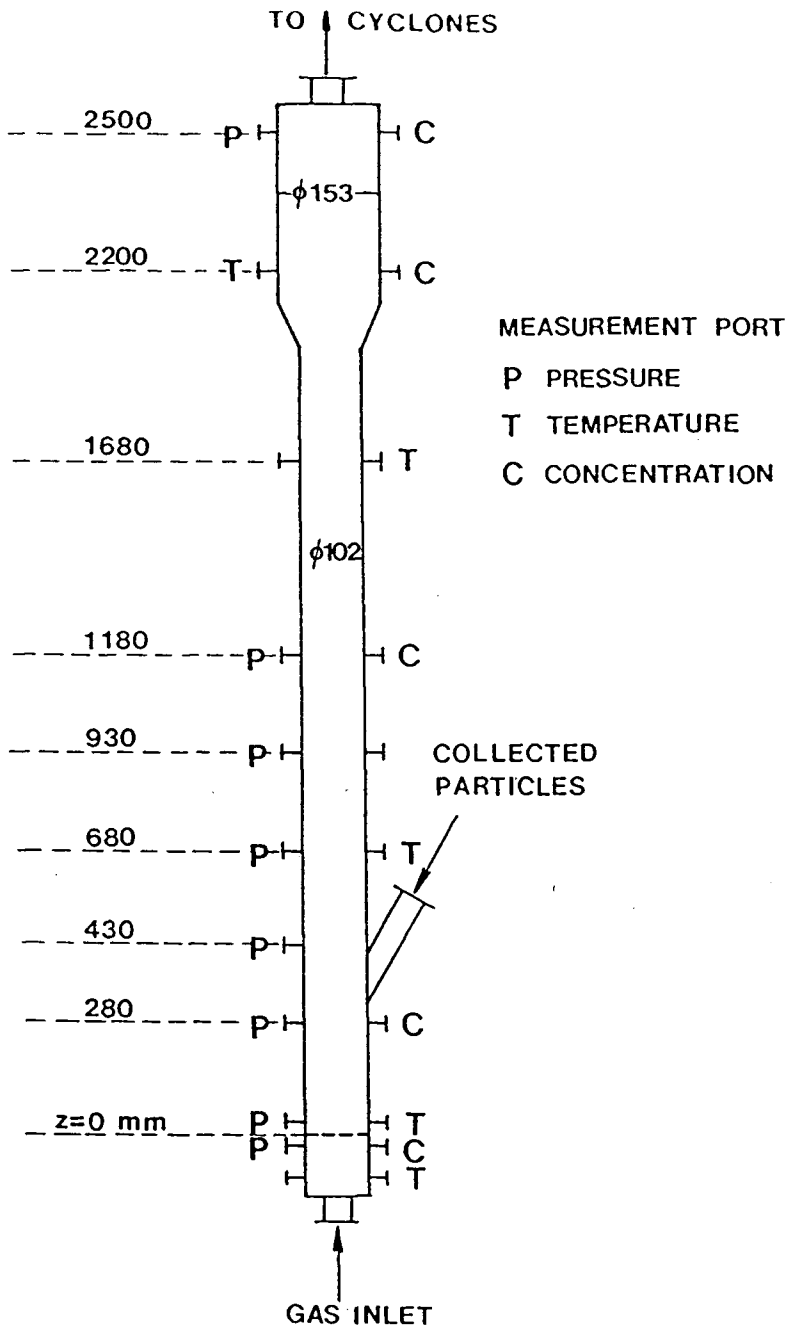

Figure 2.10: Detailed drawing of the fluidization column

2.2.3 Particle collection and return system

To keep the PSD within the experimental system as constant as possible under various operating conditions, that is, to prevent fine particles from escaping from the fluidized bed at higher gas velocities and static bed heights, a double-decked flapper system was designed (Fig. 2.11). Two factors, the space limitation and the feeding location of particles collected by the cyclones, required that this structure be used. The overall height of the experimental column was limited by the height of the ceiling. This limited the vertical length of the diplegs of the two cyclones, so that they were not long enough to provide the necessary pressure drop to prevent gas bypassing for some operating conditions. This pressure drop should be higher than the pressure drop across the cyclones, which, in turn, is related to the collection efficiency of the cyclones, especially for fine particles.

To ensure that the particles collected by the cyclones did not immediately become entrained from the reactor again, these particles were returned to the reactor in the lower dense region, not far above the distributor. This return location increased the difficulty in balancing the pressure drop of cyclones and made the flapper valve at the end of the dipleg operate inefficiently. During operation, the typical hold-up of material in the collection and return system (i.e. cyclones and standpipe) was of the order of 5 - 20 % of the inventory of solids in the system.

Gas leaving the reactor was passed through two cyclones to separate entrained particles. The cyclones were designed according to standard cyclone dimensions (Sinnott, 1983), except for modification of the inlet ducts, where two tapered joints were used to ensure high collection efficiency over a wide range of superficial gas velocity. At lower superficial gas velocities, the collection efficiency is mainly maintained by the second cyclone, whose inlet area is only half of that of the first cyclone. At $U = 0.5$ m/s, for

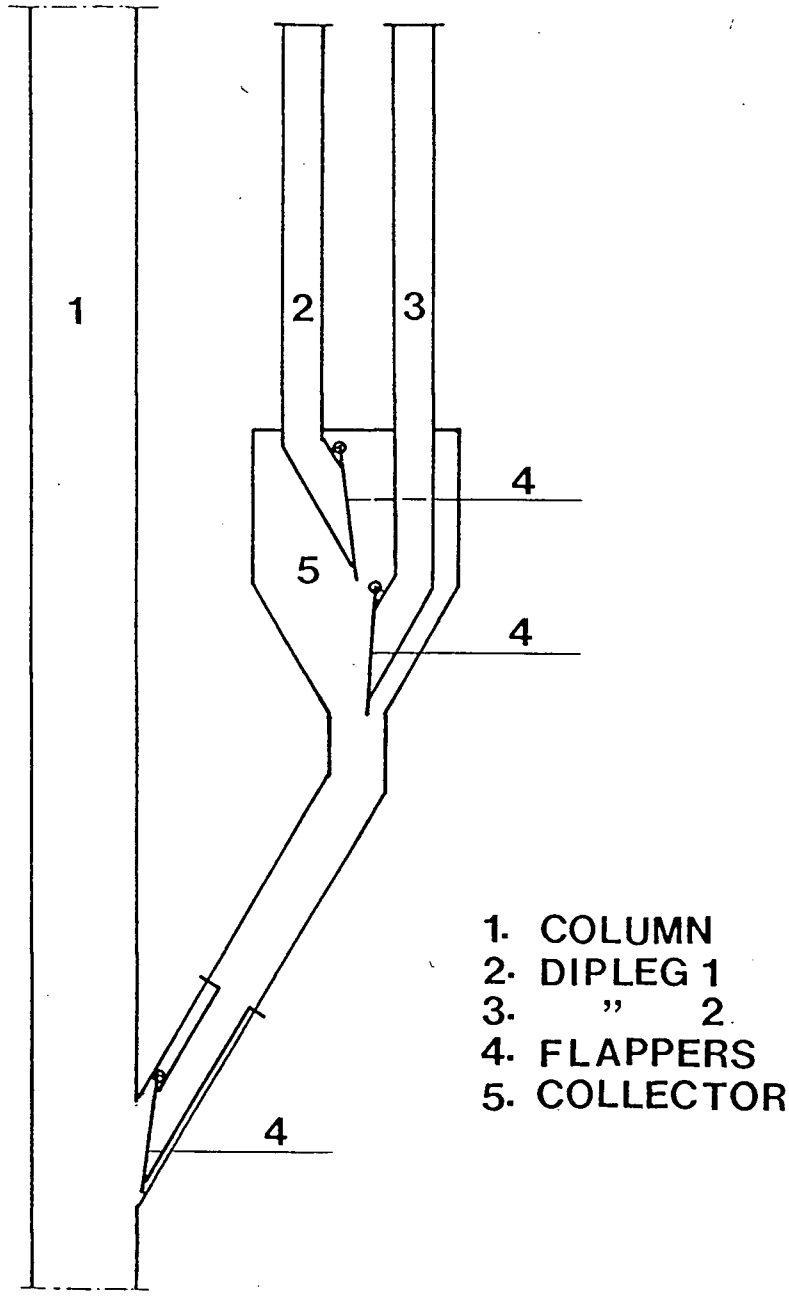

Figure 2.11: Detailed drawing of the particle collection system.

example, the inlet gas velocity of the second cyclone is 14 m/s. The collecting efficiency of this cyclone system is quite high, usually more than 99.99%, if the carryover rate is estimated from the correlations of Wen and Chen (1982).

Separated particles returned to the bed through two diplegs equipped with a double-decked flapper system (three flapper valves altogether) to prevent gas bypassing. At the outlet of the second cyclone there is a bag filter and a fixed bed of diameter 300 mm and height 600 mm filled with activated carbon to adsorb and react any remaining ozone. The maximum mass of particles collected by the bag filter during each run was less than 0.1% of the total initial mass in the bed so that the PSD and the mean diameter of particles remained nearly constant within the system, even at high gas velocities. This confirmed that the designed particle collection and return system was effective. In addition, there was negligible attrition over the duration of the experimental tests. Typical PSD results before and after operation are given in Appendix E.

2.2.4 Gas Distributors

Four sets of gas distributors with different free area ratio, orifice diameter and number of orifices, as detailed in Table 2.3, were used in the experiments to test the influence of distributor parameters. Each distributor was composed of two multiorifice plates with different free areas as shown in Fig. 2.12. The free area ratio of the two plates was between 3 to 15, with the main pressure drop produced by the upper plate. The angle α_d was maintained less than 60% of the angle of repose to prevent leakage of particles into the windbox.

Table 2.3: Distributors tested in the experiments

type*	hole diameter, mm	hole number	free area, %	pitch distance, mm
T1	2.2	21	1.0	20
T2	3.8	21	3.0	20
T3	5.0	21	5.0	20
T4	5.0	4	1.0	45
B1 - B3	8.8	21	15.5	20
B4	19.5	4	15.2	45

* Ti is the top plate and Bi is the bottom plate of distributor-i.

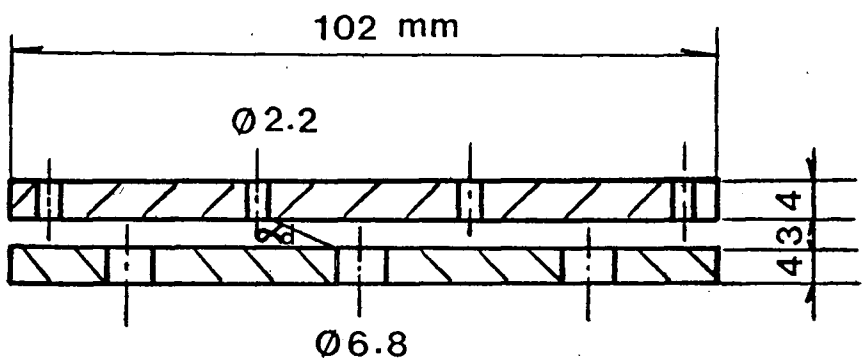

Figure 2.12: Detailed drawing of gas distributor

2.2.5 Instrumentation

The main instruments used in our experiments include a UV photometer to analyze ozone concentrations, pressure transducers to measure pressure fluctuations, a laser photometer to indicate the particle concentration inside voids and other void characteristics, a computer data-logging system and other instruments to measure gas flow rate and temperature.

Continuous analysis of ozone concentration along the column was carried out by means of UV adsorption measurements, using a Dupont Model 400 Photometric Analyser at a wavelength of 254 nm. The UV beam passed through a quartz cell with a 100 mm path length and a diameter of 20 mm flushed by the gas being analysed. Calibration of the analyser was carried out by the KI absorption method suggested by the OREC operation manual (see also Razumoskii and Zaikov, 1984) over a wide range of ozone concentration (40 to 1400 ppm).

Four differential pressure transducers (PX162 - 01D) were used to measure pressure fluctuations along the column. Each transducer had two input channels and produced an output voltage proportional to the pressure difference, with a range of 0 to 7 kPa. The lines which connected the taps and the transducers were checked experimentally to ensure that no significant damping was introduced.

Differential pressure signals at different bed heights and different operating conditions were logged to an IBM - XT minicomputer via an A/D convertor (Tecmar board) and recorded simultaneously in analogue format on a UV chart recorder.

The particle concentration inside voids, the void size and void frequency in fluidized beds were detected by means of light absorption in a "two-dimensional" plexiglass column. Detail description is provided in Chapter 5.

Chapter 3

Reactor Performance at Low Gas Velocities

Product yield is the most important indicator of the performance of commercial catalytic fluidized bed reactors. For a simple reaction, such as ozone decomposition, the yield is simply determined by the conversion. In our study, the effect of the PSD on the performance of fluidized bed reactors is therefore mainly evaluated by the measurement of ozone concentration for different PSD's under different operating conditions.

As discussed in Chapter 6, the fluidization regime and the regime transition from the bubbling or slugging regime to the turbulent fluidization regime are dependent on the PSD and on other operating parameters such as the static bed height (Fig. 6.4). The term "lower gas velocities" used here refers to the range of gas velocities at which all the fluidized beds discussed operated in the bubbling or slugging fluidization regime, regardless of the PSD and static bed height. In this study, low gas velocity signifies $U <$ 0.6 m/s. In this chapter, we mainly evaluate the PSD effect at low gas velocities, that is, in the bubbling and/or slugging fluidization regimes.

3.1 Rate Constant Determination

The rate constant of ozone decomposition for each batch of catalysts was determined in a fixed bed reactor (19 mm in diameter). If this integral microreactor is assumed to be operated isothermally with transport gradients minimized and plug-flow attained, the rate constant of ozone decomposition which can be taken as a first order reaction (Frye

Table 3.1: Determination of the rate constant for 10 g samples of N-FCC catalysts of wide size distribution

C_{Ain}, ppm	C_{Aout}, ppm	Contacting time, s (V_{cat}/v_g)	k_r, s^{-1}
330	185	0.26	2.23
509	292	0.26	2.14
686	374	0.26	2.33

et al, 1958), is readily obtained from the equation:

$$k_r = \frac{v_g \rho_p}{W} \ln \frac{C_{Ain}}{C_{Aout}} \tag{3.1}$$

where W is mass of catalyst, v_g the volumetric gas flow rate, ρ_p the bulk density, and C_{Ain}/C_{Aout} the ratio of inlet to outlet ozone concentration.

Justification for the assumptions underlying equation 3.1 are as follows:

a. Reaction order

The reaction order of ozone decomposition is dependent on the decomposing mechanism (Horvath et al, 1985). To determine the reaction order in our experiments, both inlet gas flow rate and inlet ozone concentration were changed to test the linearity of the rate constant calculated from Eqn. 3.1. As shown in Table 3.1, the rate constant for different concentrations in our experimental range is nearly constant, implying that the decomposition can be taken as a first order reaction.

b. Axial dispersion effects

The effect of axial dispersion can be minimized in packed-bed reactors by increasing the ratio of reactor length, H, to equivalent particle diameter, d_p. The deviation from plug flow is less than 5% (Mears, 1971a) if

$$\frac{H}{d_p} > \frac{20n}{Pe_p} \ln \frac{C_{Ain}}{C_{Aout}} \tag{3.2}$$

where n is the reaction order, i.e. $n = 1$ in our experiments. Pe_p is the axial Peclet number, $Pe_p = d_p U/D_e$, while D_e is an effective axial dispersion coefficient, which can be determined as a function of Reynolds number and Schmidt number (Levenspiel, 1972).

Considering a wide range of C_{Ain}/C_{Aout} and gas velocity in our experiments, we should have $H/d_p > 140$ (see Appendix 1) to satisfy the Mears criterion, eqn. 3.2. In our kinetic measurements, H/d_p was more than 600. Hence, the effect of axial dispersion is negligible.

c. Interphase and interparticle gradients

Interphase transport gradients include the concentration and the temperature gradients around the particle. Since the size of catalysts used in our experiments is small, criteria for minimizing the heat and mass transport gradients in the fixed bed (Rase, 1977) were readily achieved. This was confirmed by varying the flow rate for four measurements in which V_p/v_g was maintained constant. The interphase gradients were negligible since the resulting conversions at different flow rate were almost the same, as shown in Table 3.2.

Mears (1971b) suggests that, for a first order reaction, the intraparticle transport concentration gradient is negligible if

$$\frac{k_r d_p^2}{D} < 3 \tag{3.3}$$

This criterion is satisfied for most particles in catalytic fluidized bed reactors. For our

Table 3.2: Experimental test on the interphase transport gradient for N-FCC particles of wide size distribution

v_g, ml/min.	W_{cat}, g	V_{cat}/v_g, s	k_r, s^{-1}
1000	6.7	0.26	2.1
1500	10	0.26	2.2
2000	13.4	0.26	2.1
2800	18.7	0.26	2.3

experimental system, $k_r d_p^2/D < 0.1$, i.e. the criterion is easily satisfied.

d. Isothermicity

Isothermicity in integral reactors is favoured by having a low-activity catalyst. For catalysts used in this study, the activity was varied over a wide range, including some relatively high values (around 10 s^{-1}). Diluting of the catalysts utilized in the fixed bed with inert solids, however, was not necessary to achieve isothermal operation in our work due to the low ozone concentration of the inlet gas (< 0.1% by volume). The isothermicity of our fixed bed was confirmed experimentally by changing the position of a thermocouple in the bed.

3.2 Stability of Catalyst Activity

It is important to keep both the PSD and the catalyst activity as stable as possible during each run to ensure accuracy of the experimental results. Previous results (Frye et al, 1958; van Swaaij and Zuiderweg, 1972) have indicated that the rate of ozone decomposition can be influenced strongly by the composition of the incoming gas, due to adsorption of gaseous species at ambient temperatures. Frye et al noted that the ozone decomposition was reciprocal third order with respect to water vapor concentration over the experimental range investigated. The influence of water vapor and other impurities can be reduced by increasing the operating temperature (van Swaaij and Zuiderweg, 1972) and by purifying the fluidization gas. The latter method was used in our experiments.

In this study, the fluidization gas was purified by passing through a fixed bed of diameter 300 mm filled with activated carbon and silica gel, each with 250 mm height, to improve the catalytic activity stability. The activated carbon was mainly used to remove impurities such as oil droplets, while the silica gel was to remove water vapor.

Considerable work was done to keep the catalyst activity constant during each experimental run. It was found that catalyst-decay was very significant for catalysts prepared from S-FCC particles. For example, the activity could decrease from 3.5 s^{-1} to 2.1 s^{-1} after only 60 min, that is the deactivation rate was 40% per hour. The deactivation rate for the N-FCC particles, however, was less than 3% per hour.

3.3 Definition of Efficiency for Fluidized Bed Reactors

For a first order irreversible simple reaction, the volume of catalyst, $V_{c,p}$, required to achieve a certain conversion in a fixed bed reactor with plug flow and negligible interphase and intraparticle transport resistance can be obtained from eqn. 3.1, as

$$V_{c,p} = \frac{v_g}{k_r} \ln \frac{C_{Ain}}{C_{Aout}} \tag{3.4}$$

When the bed is fluidized at the same superficial gas velocity as in the fixed bed, the mixing and contacting deviate from those of the plug flow reactor. As a consequence, the actual volume of catalyst, $V_{c,f}$, required to achieve the same conversion with the same flow rate and catalyst activity is larger than $V_{c,p}$. The ratio of $V_{c,f}$ to $V_{c,p}$ is dependent on the performance of fluidized bed reactors. It is convenient to compare the performance of different batches of catalysts with different PSD in terms of a "contact efficiency", E, defined as

$$E = V_{c,p}/V_{c,f} \tag{3.5}$$

E can be regard as the utility efficiency of catalysts in fluidized bed reactors compared with that in the plug flow reactor. The lower the E, the poorer the reactor performance, i.e. the more the reactor deviates from that of a fixed bed with negligible axial dispersion.

3.4 Effect of PSD on Conversion and Reactor Efficiency

Experiments on the reactor efficiency were carried out over a wide range of operating conditions to test not only the effect of PSD on the reactor efficiency but also the influence of other factors. The kinetic rate constant, based on the volume of the particles, ranged from 2 to 9 s^{-1}, while the static bed height was varied from 0.15 to 1 m. The superficial gas velocity was varied from 0.1 to 1.8 m/s in order to cover a range from bubbling through the slugging and turbulent regimes just into the fast fluidization bed regime.

Attempts were made in some runs to measure ozone concentration profiles by withdrawing gas samples from three different ports along the column in order to evaluate the

PSD effect on the performance of fluidized beds in different reactor regions. For the sampling probe immersed in the dense bed, however, a plug of particles would build up on the tip of the probe very quickly just after beginning to withdraw the sampling gas. This plug may cause further reaction to occur, distorting the measurement results. For example, Figure 3.1 indicates that the apparent ozone concentration increases with height, an impossible result. A similar problem was reported by Yates and Newton (1986). For probes above the dense bed, the formation of the particle plug which appeared to be much slower than in the dense bed, depended on the vertical location of the probe, the particle size distribution and the superficial gas velocity. To reduce the interference of the particle plug on the measurement, or the frequency of gas backflow to remove the plug formed, all conversion experimental results reported here were determined with the the sampling probe at the highest level, $z = 2.5$ m, just before the outlet of the expansion section. The concentration measured after the cyclone was found to be very nearly the same as that measured at $z = 2.5$ m.

Experimental conversions for two catalyst inventories, 5.05 and 2.75 kg, corresponding to static bed heights of 750 and 420 mm, are shown in Figs. 3.2 and 3.3. The corresponding conversion for single phase plug flow (PF) reactors:

$$x = 1 - exp(-k_f^{'}) \tag{3.6}$$

and for perfect mixing (PM), i.e. CSTR reactors:

$$x = \frac{k_f^{'}}{1 + k_f^{'}} \tag{3.7}$$

are shown for reference purposes. The measured conversion never reaches the former, but may or may not exceed the latter, depending on the PSD and the operating conditions.

Each experimental point is the average of five individual readings over a period of at

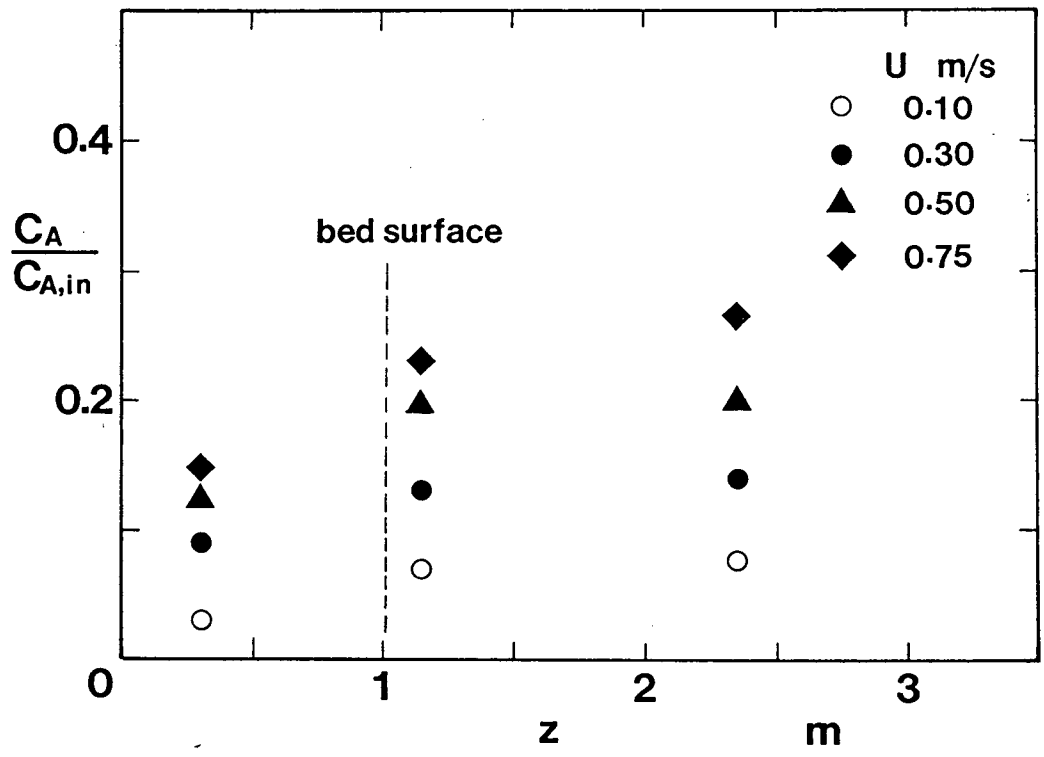

Figure 3.1: Variation of apparent reactant fraction unconverted with height above the distributor for narrow size distribution with kinetic rate = 9.1 s^{-1}; catalyst inventory: 5 kg.

least 20 min. at stable operating conditions. Statistical considerations are discussed in Appendix C. There it is shown that the gap between the error bars for each condition would be smaller than the size of the symbols on the graphs. It is clear from Figs. 3.2 and 3.3 that the PSD does affect the performance of fluidized bed reactors. Among the three blends used in our experiments the wide size distribution generally gives the highest conversion, while the narrow distribution gives the lowest. The bimodal PSD gives intermediate results, although conversions for the bimodal distribution tend to be closer to those of the wide distribution than to the narrow.

It can be seen from Figs. 3.2 and 3.3 that the effect of PSD on the performance of fluidized bed reactors is related to the gas velocities and the fluidization regimes. In the bubbling and slugging regimes, the PSD effect is enhanced by the increase of gas velocities. After transition to the turbulent fluidization, the PSD effect is reduced as the gas velocity increases. Clearly, the reason for the PSD effect may differ from regime to regime. It is better, therefore, to discuss the influence of PSD for each hydrodynamic regime, separately.

Contact efficiencies are plotted against the unconverted gas fraction in Figs. 3.4 and 3.5 for the same conditions as in Figs. 3.2 and 3.3. The wide size distribution gives the highest contact efficiency followed by bimodal distributions, with the narrow distribution again giving the poorest results except for one point in Fig. 3.4 corresponding to a very high gas velocity ($U = 1.75$ m/s) where the contact efficiency was higher for the narrow size distribution than for the bimodal distribution with the fine fraction active. The contact efficiency at low gas velocities is usually lower than for a single phase CSTR due to the two-phase nature of fluidized bed reactors.

Although the mean diameters of the wide and bimodal blends are the same and the bimodal blend contains more "fines" (about 21% by weight for N-FCC if fines are defined as particles < 45 μm compared with about 16% by weight for the wide blend), the

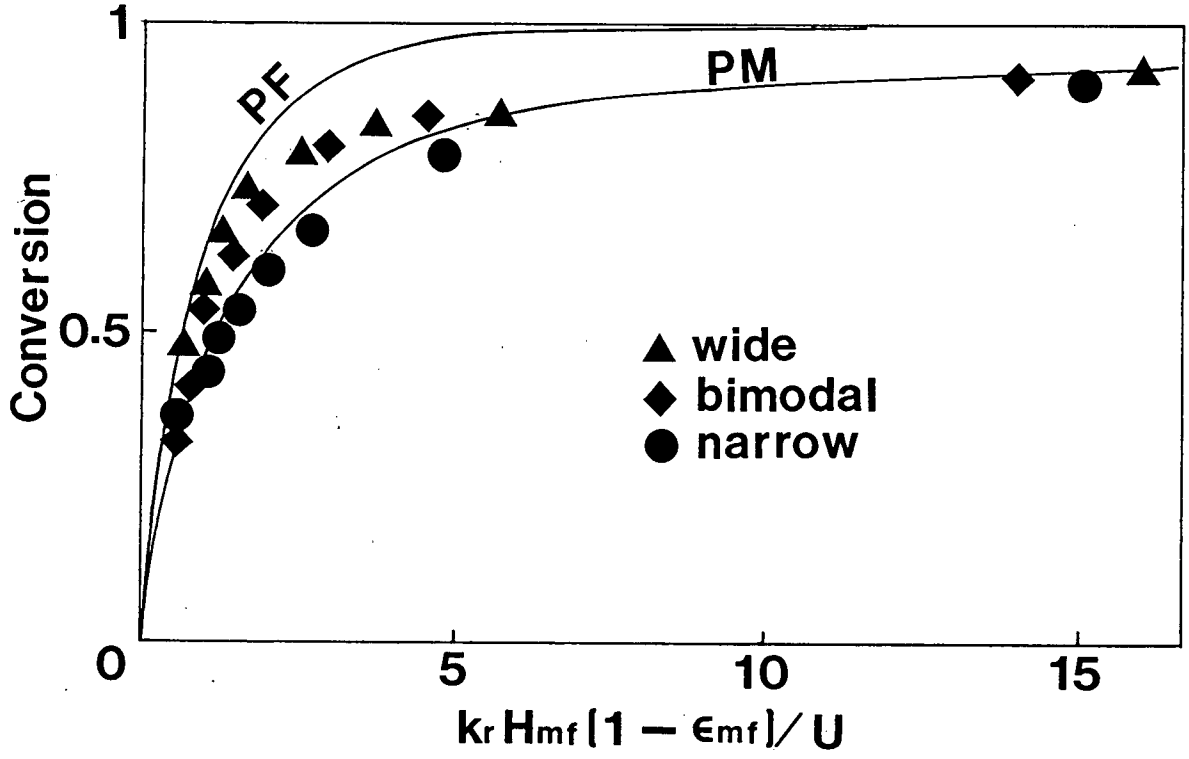

Figure 3.2: Effect of PSD on ozone conversion for N-FCC with k_r = 4.1 to 4.3 s^{-1}; catalyst inventory: 5.05 kg. PF and PM are corresponding results for single-phase plug flow and perfect mixing respectively.

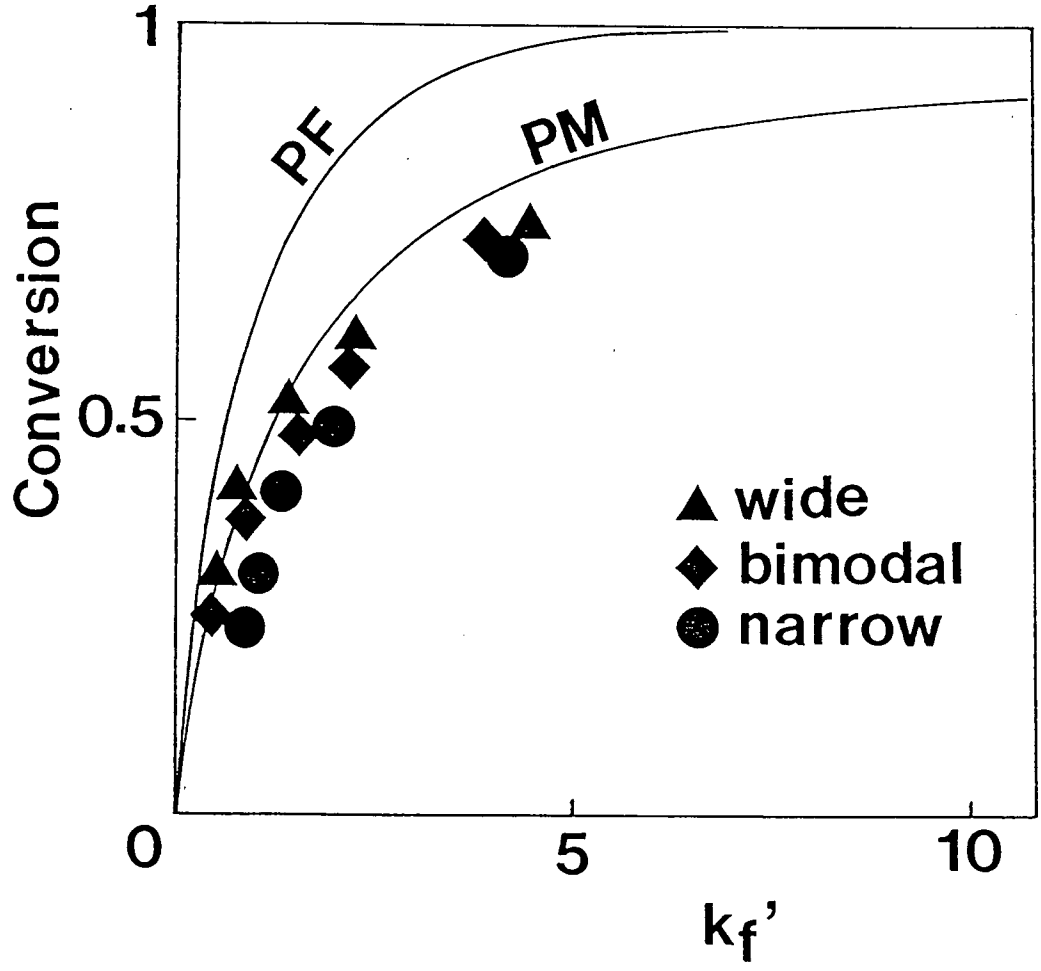

Figure 3.3: Effect of PSD on ozone conversion for N-FCC with k_r = 2.1 to 2.2 s^{-1}; catalyst inventory: 2.75 kg. PF and PM as in Fig. 3.2.

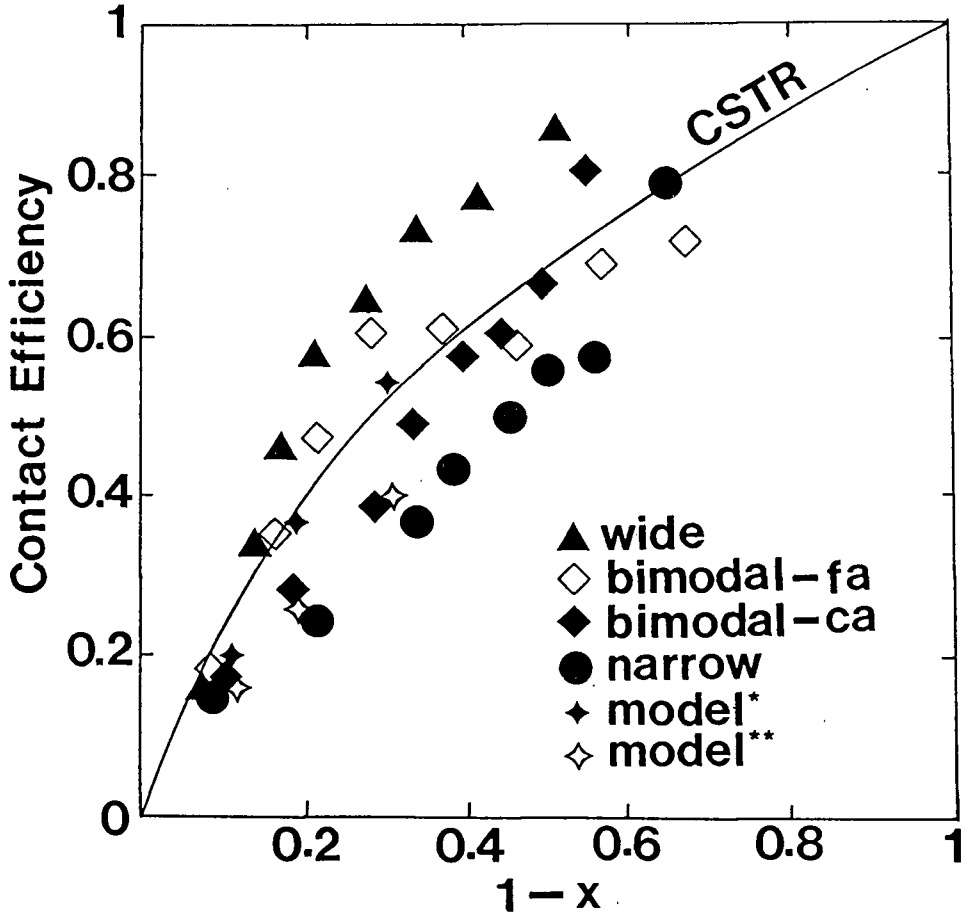

Figure 3.4: Effect of PSD on contact efficiency for N-FCC with $k_r = 4.0$ to 4.3 s^{-1}; catalyst inventory: 5.05 kg; "fa" and "ca" denote fines active and coarse active, respectively.

$\star$ with $\phi_b = 0.05\ \epsilon_b$ and $S_b = 2S$;
$\star\star$ with $\phi_b = 0.01\ \epsilon_b$ and $S_b = S$.

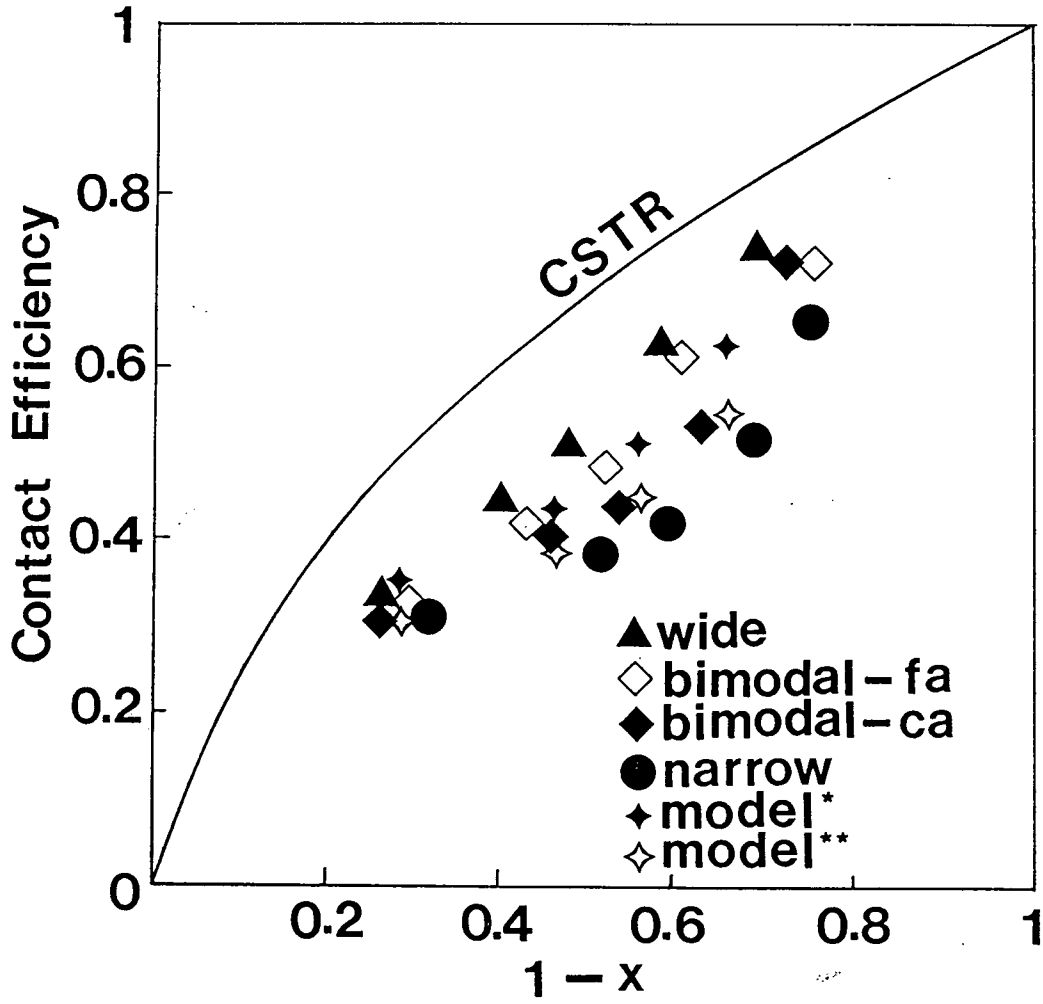

Figure 3.5: Effect of PSD on contact efficiency for N-FCC with k_r = 2.1 to 2.2 s^{-1}; catalyst inventory: 2.75 kg; "fa" and "ca" denote fines active and coarse fraction active, respectively.

$\star$ with $\phi_b = 0.05\ \epsilon_b$ and $S_b = 2S$;
$\star\star$ with $\phi_b = 0.01\ \epsilon_b$ and $S_b = S$.

performance of the wide blend is usually better. This suggests that the "fines content" is not sufficient to characterize the PSD and that the performance of fluidized particles depends not only on the quantity of "fines", but also on their nature and on the overall size distribution. It is notable that Geldart and Buczek (1989) found that fines content alone was insufficient to explain their hydrodynamic data.

3.5 Influence of Whether Fines or Coarse Particles are Active

To gain greater understanding of the importance of different size fractions and of the reasons for the influence of the PSD, the bimodal distribution was separated into two fractions, a finer fraction (mean size 40 μm) and a coarser fraction (mean size 90 μm), as shown by the shaded and unshaded portions of Fig. 2.2(b). Due to the imperfect nature of the separator, there was a small overlap between the two fractions. Three catalysts were then prepared:

(1) Both fractions (i.e. all particle sizes) activated with ferric nitrate, as described in Chapter 2;

(2) Finer fraction activated, coarser fraction inactive, designated "fa";

(3) Coarser fraction activated, finer fraction inactive, designated "ca".

In each case, the overall activity, determined in the packed bed, was nearly the same, 4.0 to 4.2 s^{-1} or 2.0 to 2.2 s^{-1}. The mixing ratio of activated particles to inactive particles was nearly the same, around 0.75. Conversions for these three catalysts appear in Fig. 3.6. It is seen that for $U < 1.1$ m/s, the catalyst with only the finer fraction activated gives higher conversion than that with only the coarser fraction active. Intermediate results were achieved with all sizes activated. Some of these results also appear in Figs. 3.4 and 3.5 in terms of contact efficiency, again showing that it is more important that the fines be active than that the coarser fraction be active. For $0.1 < U < 0.7$ m/s, i.e. within

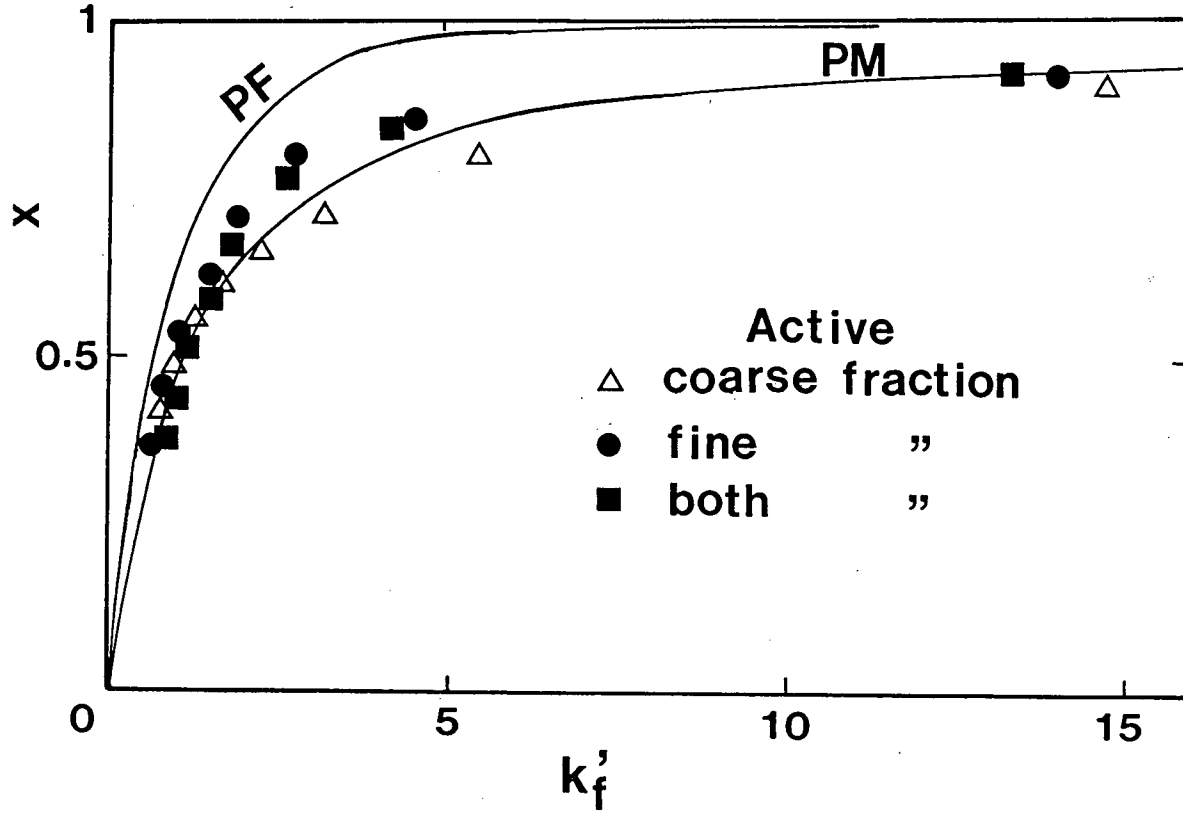

Figure 3.6: Effect of which fraction is active on conversion for bimodal catalyst; $k_r = 4.0$ to 4.2 s^{-1}; catalyst inventory: 5.05 kg.

the bubbling and slugging regimes, the influence of which fraction is active is enhanced as the overall catalyst activity and as the gas velocity are increased.

The different conversion in beds of bimodal PSD FCC with different fraction ("fines" or "coarse") active can be explained by the disproportionate fraction of "fines" reporting to the dilute (or dense) phase. The sensitivity of conversion to which fraction is active suggests that more fines are present in the dilute phase, since catalyst particles in the dilute phase can play a more important role, because they are exposed to gas of higher ozone concentration than particles in the dense phase. No other explanation can account for the results since the hydrodynamics, mixing and contacting are all independent of which fraction is activated. In the bubbling and slugging fluidization regimes, gas is usually assumed to pass through the dilute phase in plug flow (e.g. Davidson and Harrison, 1963). In fluidized beds of Group A particles, if $U \gg U_{mb}$, as in this study, most of the gas flows in the dilute phase, with exchange back and forth to the dense phase.

Based on the experimental results in this chapter and those in Chapter 5, it could be concluded that the most important effect of PSD on the performance of fluidized bed reactors operated at relatively low gas velocities is the influence on the void (bubble or slug) character, including void type (bubble or slug), void size, particle concentration in the voids and the relatively higher affinity of fine particles, compared with coarse particles, for the dilute phase. All these effects appear to be enhanced as the gas velocity increases. For example, with an increase of gas velocity, both the mean bubble size and solids concentration inside voids in a fluidized bed of wide PSD appear to increase gradually, while for beds of narrow PSD some bubbles grow large, becoming slugs, and there is much less particle hold-up within the voids.

3.6 Model Predictions of PSD Effect at Low Gas Velocities

Many models have been proposed for bubbling fluidized bed reactors. Among the subset of models which have been shown to give good predictions for the overall conversion in pilot plant and industrial-scale equipment (Grace, 1986; Johnsson et al, 1987) the two-phase bubbling bed model (Grace, 1984) is simpler than the others. For a first order irreversible reaction, the outlet concentration derived from this model can be written as:

$$\frac{C_{Aout}}{C_{Ain}} = exp\{\frac{-(k_r H/U)[X(\phi_b + \phi_d) + (k_r H/U)\phi_b\phi_d]}{X + \phi_d(k_r H/U)}\} \tag{3.8}$$

where ϕ_b is the fraction of the bed volume occupied by bubble phase solids, ϕ_d is the fraction occupied by solids assigned to the dense phase and X is a dimensionless interphase mass transfer group, given by

$$X = \frac{k_q a_b \epsilon_b H}{U} \tag{3.9}$$

The interphase mass transfer coefficient, k_q, can be calculated (Sit and Grace, 1981) from:

$$k_q = \frac{U_{mf}}{3} + (\frac{4D\epsilon_{mf}u_b}{\pi \bar{d}_{eq}})^{1/2} \tag{3.10}$$

It is straightforward to show that the contact efficiency predicted from this model is given by

$$E = \frac{1}{\phi_d}[\frac{X(\phi_d + \phi_b) + k_f'\phi_b}{X + k_f'}] \tag{3.11}$$

where k_f' is a dimensionless rate constant,

$$k_f' = \frac{k_r H_{mf}(1 - \epsilon_{mf})}{U} \tag{3.12}$$

If $X \rightarrow \infty$ and $\phi_b \rightarrow 0$, i.e. in the limit where the two phase flow fluidized bed reactor simplifies to a single phase plug flow reactor (or fixed bed reactor), $E \rightarrow 1$ as expected.

From eqn. 3.11 it is clear that changes in the contact efficiency, E, may be caused by changes in ϕ_b, ϕ_d or X with the different size distributions, or by some combination of two

or more of these factors. Clearly, the extent of the change also depends on k_f'. To express the PSD effect on the performance of bubbling fluidized bed reactors, it is necessary to account for the PSD effect on the bubble size, on the total particle concentration within the dilute phase and on the particle size distribution inside voids. We do this by extending the two-phase bubbling bed model described above.

An increase in conversion for the bimodal PSD with fines fraction active (see section 3.5 above) can be explained by postulating that a disproportionate fraction of fines reports to the dilute phase. Let S be the overall ratio of the fines fraction by volume in the bed to that of the coarser fraction, S_b be the corresponding ratio in the bubble or dilute phase and S_d the ratio in the dense phase. A mole balance on gaseous component A for the dilute or bubble phase, assuming plug flow and a first order reaction and ignoring axial variations in hydrodynamic properties is

$$U\frac{dC_{Ab}}{dz} + k_q a_b \epsilon_b (C_{Ab} - C_{Ad}) + k_{rb}\phi_b C_{Ab} = 0 \tag{3.13}$$

The corresponding mole balance for the dense phase, assuming perfect mixing in this phase, is

$$k_q a_b \epsilon_b (C_{Ad} - C_{Ab}) + k_{rd}\phi_d C_{Ad} = 0 \tag{3.14}$$

Here k_{rb} is the reaction rate constant of particles in the dilute or bubble phase, while k_{rd} is the corresponding rate constant for the dense phase. When the fines fraction is active

$$k_{rb} = k_{rp}\frac{S_b}{1+S_b} \tag{3.15}$$

and

$$k_{rd} = k_{rp}\frac{S_d}{1+S_d} \tag{3.16}$$

while

$$k_r = k_{rp}\frac{S}{1+S} \tag{3.17}$$

where k_{rp} is the kinetic rate constant of active particles. S_d can be determined from

$$S_d = \frac{H_{mf}(1-\epsilon_{mf})S(1+S_b) - H\phi_b S_b(1+S)}{H\phi_d(1+S)(1+S_b) + H\phi_b S_b(1+S) - H_{mf}(1-\epsilon_{mf})S(1+S_b)} \tag{3.18}$$

If the coarse fraction is active, then

$$k_{rb} = \frac{k_{rp}}{1+S_b} \tag{3.19}$$

and

$$k_{rd} = \frac{k_{rp}}{1+S_d} \tag{3.20}$$

while

$$k_r = \frac{k_{rp}}{1+S} \tag{3.21}$$

Equations 3.13 and 3.14 can be integrated with the boundary condition $C_{Ab} = C_{Ain}$ at $z = 0$. For a first order irreversible reaction, the outlet concentration becomes:

$$\frac{C_{Aout}}{C_{Ain}} = exp\{\frac{-(k_r H/U)[X(\phi_d \frac{k_{rd}}{k_r} + \phi_b \frac{k_{rb}}{k_r}) + \frac{k_r H}{U}\phi_b\phi_d(k_{rb}k_{rd}/k_r^2)]}{X + \phi_d(k_r H/U)\frac{k_{rd}}{k_r}}\} \tag{3.22}$$

while the contact efficiency is given by

$$E = \frac{1}{\phi_d}\{\frac{X[\phi_d \frac{k_{rd}}{k_r} + \phi_b \frac{k_{rb}}{k_r}] + k_f'\phi_b(k_{rb}k_{rd}/k_r^2)}{X + k_f'\frac{k_{rd}}{k_r}}\} \tag{3.23}$$

If $S_b = S_d = S$ or $k_{rb} = k_{rd} = k_r$, that is, if both size fractions of catalyst particles are uniformly active, Eqn. 3.23 reduces to Eqn. 3.11.

For the fine fraction active, the efficiency can be expressed as

$$E_{fa} = \frac{1}{\phi_d}\{\frac{X[\phi_d \frac{S_d(1+S)}{S(1+S_d)} + \phi_b \frac{S_b(1+S)}{S(1+S_b)}] + k_f'\phi_b \frac{S_b S_d(1+S)^2}{S^2(1+S_d)(1+S_b)}}{X + k_f'\frac{S_d(1+S)}{S(1+S_d)}}\} \tag{3.24}$$

while for the coarse fraction active,

$$E_{ca} = \frac{1}{\phi_d}\{\frac{X[\phi_d \frac{1+S}{1+S_d} + \phi_b \frac{1+S}{1+S_b}] + k_f'\phi_b \frac{(1+S)^2}{(1+S_d)(1+S_b)}}{X + k_f'\frac{1+S}{1+S_d}}\} \tag{3.25}$$

Since E_{fa} was always higher than E_{ca} in the bubbling regime for our experiments, comparing Eqn. 3.24 with Eqn. 3.25 it would appear that $S_b/S > 1$ and $S_d/S < 1$, so that $S_b > S_d$. This suggests that more fines associate with the bubble phase, consistent with the discussion in Section 3.5 and the theoretical prediction discussed in Section 5.1.3. The fact that the ratio E_{fa}/E_{ca} increases with superficial gas velocity and bed height implies that both S_b and ϕ_b may increase with gas velocity and bed height. This is also consistent with the experiments involving photometric measurements (Chapter 5), where it was found that the influence of PSD on the particle concentration in voids is strongly enhanced by an increase in gas velocity for $U > 0.2$ m/s.

In previous modelling of bubbling fluidized bed reactors (e.g. Orcutt et al, 1962; Kunii and Levenspiel, 1969; Grace, 1984; Werther, 1984), the particle concentration in bubbles was usually taken to be in the range $0 \leq \phi_b/\epsilon_b \leq 0.01$. However, even if we take $\phi_b = 0.01\ \epsilon_b$, the upper limit suggested by Kunii and Levenspiel, the predicted E_{fa}/E_{ca} from eqns. 3.24 and 3.25 is still much less than the experimental result, even if S_b approaches infinity, i.e. if all of the particles dispersed in the bubble phase were fines. This suggests that ϕ_b should be larger than $0.01\epsilon_b$ for Group A particles. As shown in Figs. 5.7 to 5.9, more than 70% of the voids contained more than 2.5% particles by volume in a two-dimensional bed, even for FCC particles of narrow size distribution. It is notable that the experiments which led Kunii and Levenspiel to suggest that $\phi_b/\epsilon_b \leq 0.01$ were conducted with coarse or Group B particles at low gas velocities (Toei et al, 1966; Kobayashi, 1966; Kunii et al, 1967). Hence $\phi_b/\epsilon_b \leq 0.01$ may be only suitable for Group B particles. For the fluidized bed reactor (Section 3.5) of bimodal particles with different fraction active, if ϕ_b were taken as $0.05\epsilon_b$, values of S_b from 2 to 5 would explain the observed results, as shown in Figs. 3.4 and 3.5. Both S_b and ϕ_b, of course, are likely to be related to the gas-solid characteristics, including the PSD, as well as superficial gas velocities and bed depth.

3.7 Influence of Overall Catalyst Activity on the PSD Effect

The influence of overall activity of catalysts on the PSD effect in fluidized bed reactors was also tested in our experiments. The catalyst rate constant was varied from 2 to 9 s^{-1} by changing the concentration of the ferric nitrate solution from 3% to 10% by weight. It can be seen from Figs. 3.7, 3.8 and 4.1 to 4.3 that the PSD effect is generally enhanced by the increase of the catalytic activity, especially at high gas velocities. It should be noted, however, that the enhancement of PSD effect on the performance of fluidized bed reactors was only significant at lower kinetic rate, that is, when k_r was increased from 2.2 s^{-1} to 4.5 s^{-1}, if the bed was operated in the bubbling or slugging fluidization regime. The influence of a further increase in k_r (from 4.5 to 9 s^{-1}) on the PSD effect seems negligible. These results suggest that mass transfer between the two phases (dilute and dense) appears to be the controlling step in determining the reaction conversion in a bubbling or slugging fluidized bed reactor if the kinetic rate is sufficiently high (e.g. $k_r \geq$ 5 s^{-1} in our experiments).

For a simple irreversible reaction, if the resistance to chemical reaction and mass transfer between two phases are of similar magnitude, the reaction conversion in a fluidized bed reactor would be dependent both on the kinetic rate constant and on the interphase mass transfer. In this range of catalyst activity, the PSD effect, via its influence on the mass transfer rate, will be enhanced by an increase in the kinetic rate, as k_r was increased from 1 s^{-1} to 5 s^{-1} in our experiments at relatively low gas velocities. When the reaction is fast enough that conversion is mainly determined by the interphase mass transfer rate, the influence of an increase in activity on the PSD effect becomes insignificant.

Based on our experimental results at low gas velocities and the prediction from the model expressed by eqns. 3.15 to 3.25, it is found that if $k_f'/X > 2$ (for $H_{mf} < 1$ m and

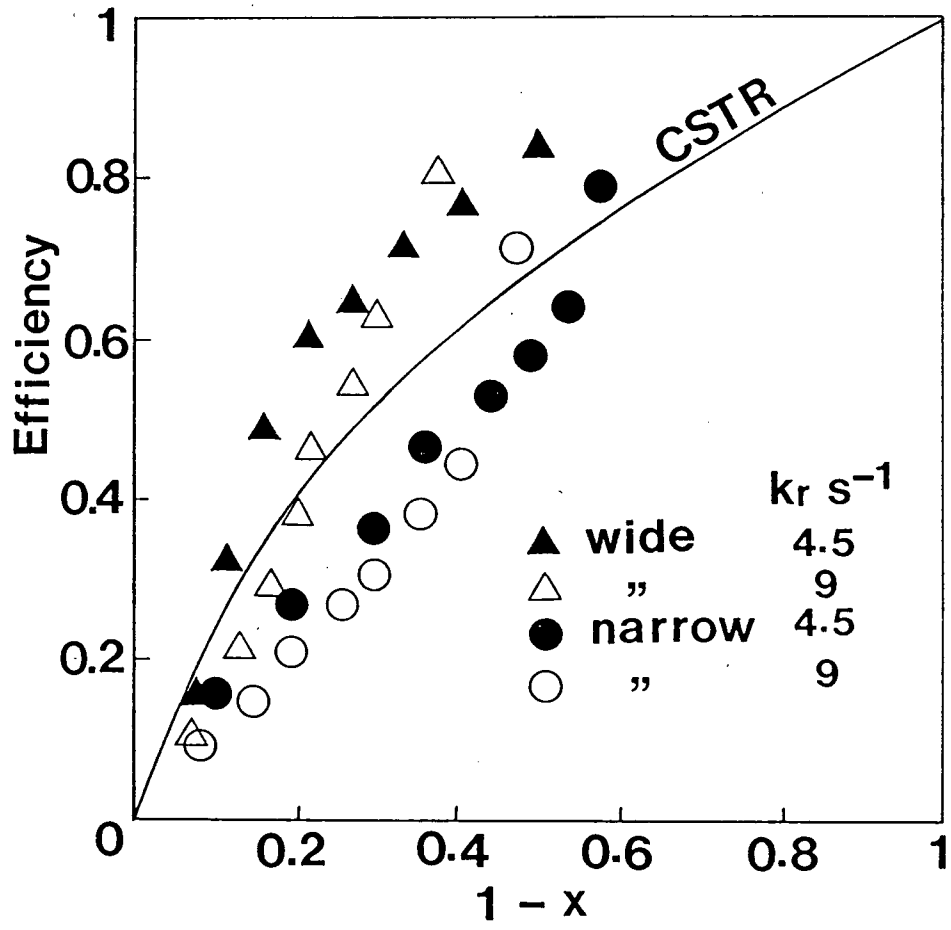

Figure 3.7: Influence of overall catalyst activity on the PSD effect; catalyst inventory: 5 kg.

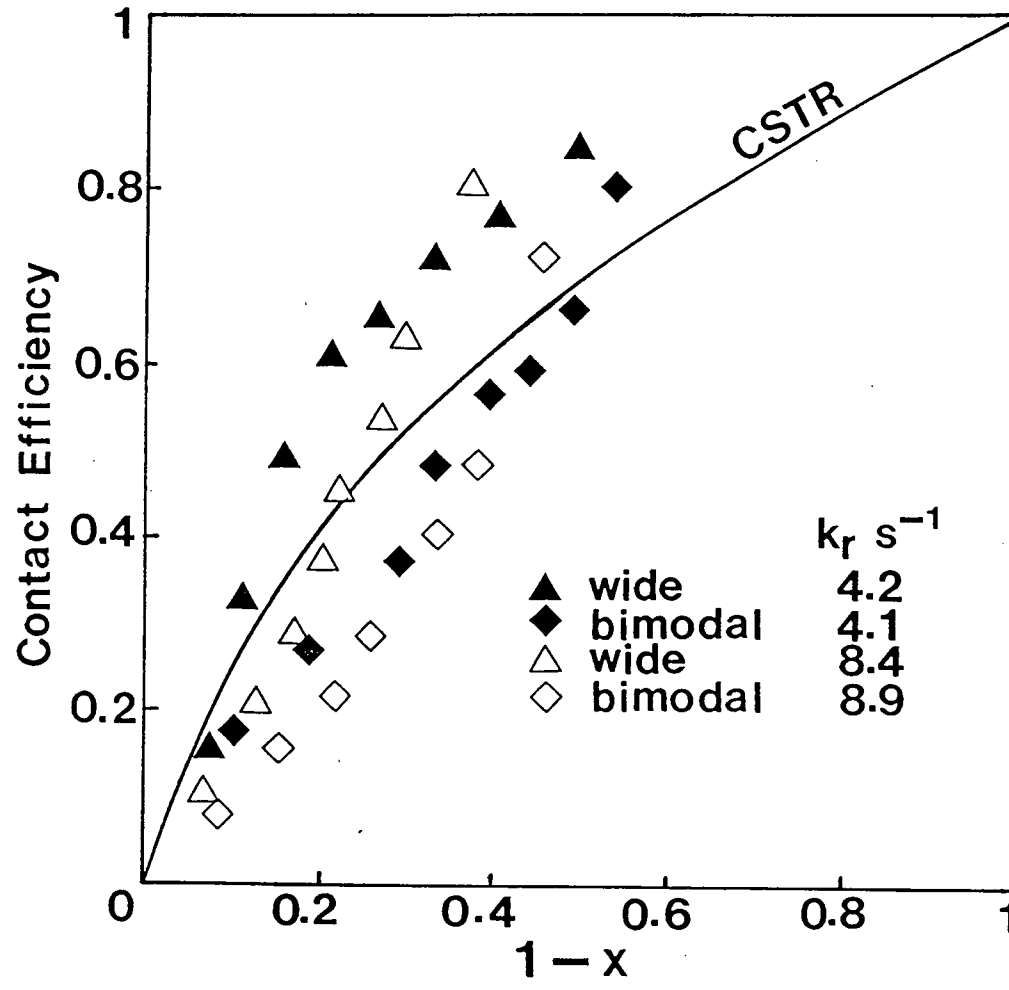

Figure 3.8: Influence of overall catalyst activity on the PSD effect; catalyst inventory: 5.05 kg.

$U < 0.8$ m/s), the PSD effect appears to be not influenced by the change of kinetic rate; if $k_f'/X < 2$, however, the PSD effect is enhanced by an increase in k_r.

Chapter 4

Reactor Performance at Higher Gas Velocities

In most previous experimental studies of chemical reaction in fluidized beds, whether for Group A or for Group B particles (e.g. Lewis et al, 1959; Massimilla and Johnstone, 1961; Hovmand and Davidson, 1968; Chavarie and Grace, 1975; Bauer and Werther, 1981; Yates and Newton, 1986), restricted ranges of gas velocity, seldom exceeding 0.3 m/s, have been investigated. Contacting efficiency tends to decrease as the gas velocity increases over this range, since bubbles or slugs grow larger with increasing gas flow. However, most successful applications of fluidized beds in the petrochemical and chemical industries, such as fluid catalytic cracking, acrylonitrile synthesis and oxychlorination of ethylene, utilize higher gas velocities, generally sufficiently high that clearly defined bubbling or slugging has given way to a more turbulent hydrodynamic region where gas-solid contacting can be improved (Yerushalmi and Avidan, 1985). Further shifts from bubbling mode to high velocity modes are expected for many processes (Horio et al, 1989).

Partially due to technical difficulties which stand in the way of research on high gas velocity fluidized beds, both fundamental research into the underling phenomena and systematic compilation of design data lag well behind commercial applications which are developing rapidly (Yerushalmi, 1986). Modelling work on high gas velocity fluidized bed reactors is even less developed, especially for reactors operated in the turbulent fluidization regime, despite their practical importance (Edwards and Avidan, 1986).

The objective of this chapter is to evaluate the effect of particle size distribution

on the performance of fluidized bed reactors operated at relatively high gas velocities ($U > 0.6$ m/s), including the transition region from bubbling (or slugging) to turbulent fluidization, the turbulent regime and a small part of the fast fluidization regime. Some modelling work on fluidized bed reactors operated at relatively high gas velocities with different PSD is also carried out.

4.1 Previous Work on Fluidization Performance at High Gas Velocities

Generally speaking, five distinct hydrodynamic regimes can be observed in gas-solid systems involving Group A particles (Yerushalmi, 1986; Yang and Chitester, 1988) beyond U_{mf}. In order of increasing gas velocities, they are:

1. bubble-free expansion between U_{mf} and U_{mb},
2. bubbling/slugging,
3. turbulent fluidization,
4. fast fluidization, and
5. dilute-phase flow.

When the gas velocity is increased, bubbling beds of fine solids undergo a transition to a turbulent regime. This transition is usually assumed to occur when the amplitude of the pressure fluctuation reaches a maximum. The corresponding superficial gas velocity, U_c, can be taken as a "pseudo" critical gas velocity to characterize the performance of fluidized beds (Yerushalmi, 1986). Below U_c, the two-phase appearance of the fluidized bed is clear, and voids grow larger with increasing gas flow at a rate depending on the gas-solid properties and equipment characteristics. Around U_c, the heterogeneous, two-phase character of the bed peaks. Above U_c, the fluidized bed gives way, usually gradually, to a condition of increasing uniformity, culminating in the "turbulent" state. Complete transition to the turbulent regime may occur at U_k, where large discrete bubbles or voids

are on the whole absent. Since U_k is much harder to measure, most people take U_c as the onset of the turbulent regime, which extends to the transport velocity U_{TR}. The approach to the transport velocity is accompanied by a sharp increase in the rate of carryover. The transport velocity may be regarded as the boundary between turbulent fluidization and fast fluidization if the solid flow rate is sufficiently high, or to a dilute phase flow regime if the solid rate is low.

Although fluidized bed reactors have advantages in many chemical processes compared with other reactors, their application is restricted by the limited mass transfer between two phases. Two approaches have been used in commercial practice to improve the fluidization performance. One is to restrict bubble growth and control gas flow by using internal baffles, or by dividing the bed into several stages. Another is to suppress the bubbling phenomena by adjusting the gas-solid properties, such as "fines" content, and increasing gas velocities (Avidan and Edwards, 1986). The latter method is more effective and interesting for most practical applications of catalytic fluidized bed reactors.

Numerous investigations have been carried out of gas-solid behaviour in fluidized beds operated at high gas velocities. Most of the studies have been concerned with the solid movement and distribution (e.g. Li and Kwauk, 1980; Hartge, 1986, Weinstein et al, 1986; Brereton, 1987; Herb et al, 1989) and the gas flow pattern - dispersion and backmixing (e.g. Cankurt and Yerushalmi, 1978; Yang et al, 1984a; Avidan and Edwards, 1986; Krambeck et al, 1987; Brereton, 1987; Weinstein et al, 1989). For catalytic fluidized bed reactors, the gas flow pattern is usually more important to the reaction results.

Cankurt and Yerushalmi (1978) conducted experiments in a 152 mm diameter column on gas backmixing in fluid cracking catalysts fluidized at gas velocities spanning the bubbling, turbulent and fast fluidization regimes, by measuring the tracer (methane) concentration upstream of the injection point. The degree of gas backmixing was high in the bubbling regime and diminished gradually over the turbulent regime. In the fast

fluidized bed, there was almost no backmixing. Yang et al (1984a) measured the tracer (helium) concentration profiles radially and axially in a fast fluidized bed of 115 mm i.d. and reported that axial mixing could be neglected in a fast fluidized bed. They also proposed an emprical correlation to express radial gas diffusion.

Gas tracer experiments were also carried out in a pilot scale reactor (100 mm i.d.) by Avidan and his colleagues (Avidan and Edwards, 1986; Krambeck et al, 1987) to study the gas residense time in bubbling and turbulent fluidization. Solids used in their experiments were typical FCC particles, while SF_6 was used as tracer. Pulse responses were measured at gas velocity from 0.2 to 1.2 m/s. They reported that at low gas velocities ($U < 0.3$ m/s), there existed a radial gradient in tracer concentration. This gradient decreased as the gas velocity was increased and appeared to be negligible at a gas velocity of 0.6 m/s. They concluded that an axial dispersion model can be used to predict conversion in a turbulent fluidized bed reactor of Group A particles with enough fines ($> 15\%$ if fines are defined as smaller than 40 μm), that the two-phase appearance of the bed is diminished and overall homogeneity is approached. They wondered (Krambeck et al, 1987) why so many models containing bubble properties were used extensively in the fluidization literature. These models are seldom claimed to be more than "learning models", while actual design models in industry are simpler. They noted that in the turbulent fluidization regime, voids are in a constant state of coalescence and break up, so that models based on discrete voids have little relation to the true physical picture, especially for most commercial applications of fine powders.

In brief, even though many investigations have been conducted on high velocity fluid beds, most results are concerned with hydrodynamics and dispersion. Information on the effect of catalyst size distribution on conversion results or contacting efficiency in a fluidized bed reactor operated at relatively high gas velocities, typical of industrial applications of catalytic fluidized bed reactors, is still not available from the literature.

4.2 Dependence of PSD Effect on the Superficial Gas Velocity

To test the dependence of the PSD effect on the superficial gas velocity, our experiments on ozone decomposition were carried out over a wide range of gas velocities, from 0.06 to 1.8 m/s, to include the bubbling, slugging, turbulent and fast fluidization regimes. It was found from our experiments that the PSD effect on the performance of fluidized bed reactors is related to the superficial gas velocity, as shown in Figs. 4.1 to 4.3. The PSD effect appears to be most significant at gas velocities between about 0.3 and 1.4 m/s. The conversion difference between the particles of wide and narrow size distribution appears to increase with gas velocity for $U < 1.2$ m/s and to decrease slightly at higher gas velocities. These results are consistent with those from hydrodynamic experiments (Chapters 5 and 6) and further suggest that different dependence of fluidized bed performance on gas velocity is associated with different particle size distributions.

As discussed in Chapter 6, at lower gas velocities, that is at $U < 0.6$ m/s in our experiments, for all three different particle size distributions tested in this study, the lower part of the fluidized bed ($z < 0.3$ m) mainly operated in the bubbling regime, while the upper part of the bed was mainly subject to the slugging regime. The characteristics of voids (i.e. bubbles and slugs), such as void size and solid concentration, however, are influenced by the PSD. The influence of the PSD appears to increase with increasing gas velocity. Although for the three blend particles of different size distribution, the void size increased with the increasing gas velocity for $U < 0.6$ m/s, the growth rate of voids was higher for the narrow PSD than for the wide PSD. At $U > 0.6$ m/s, fluidized bed reactors of wide size distribution undergo a transition from bubbling or slugging to turbulent fluidization and the turbulent fluidization regime. In these regimes, bubbles or slugs break up frequently to smaller voids of irregular shape containing a greater percentage of the total solids. For particles of narrow size distribution, however, the transition to

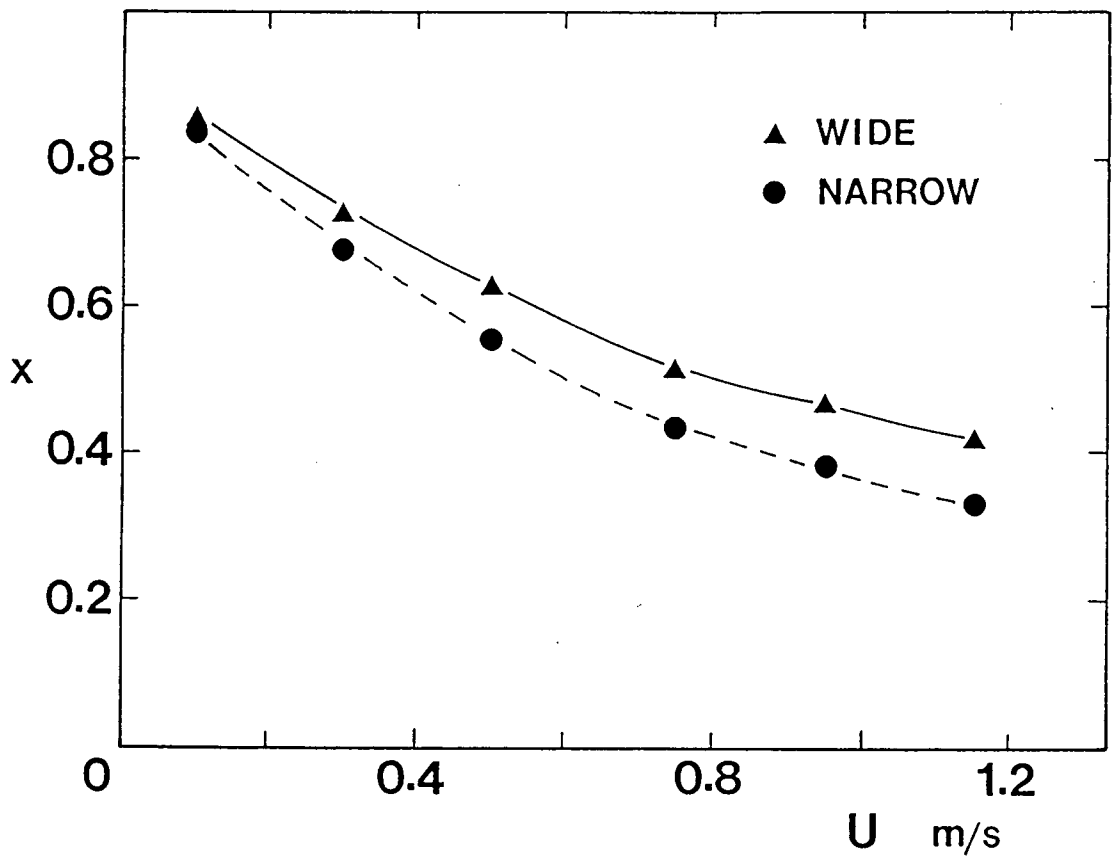

Figure 4.1: Influence of gas velocity and PSD on reactor conversion; catalyst inventory: 5 kg, $k_r \approx 2.4\ s^{-1}$.

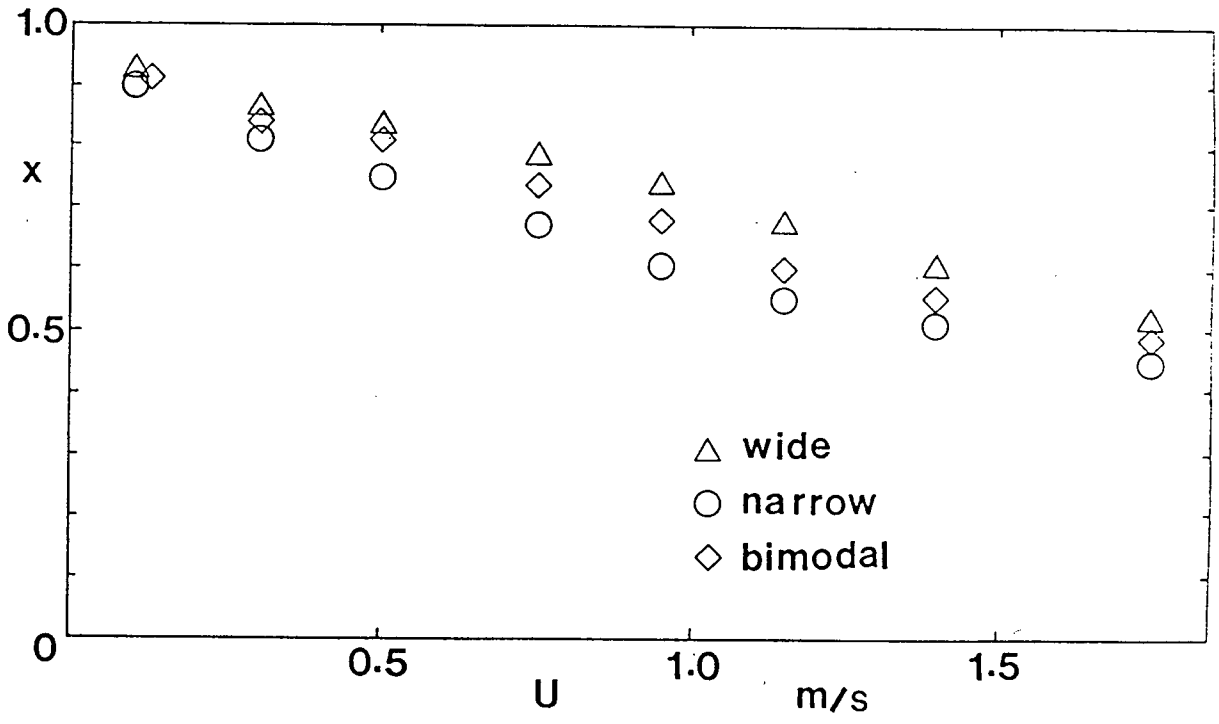

Figure 4.2: Influence of gas velocity and PSD on reactor conversion; catalyst inventory: 5 kg, $k_r \approx 4.5\ s^{-1}$.

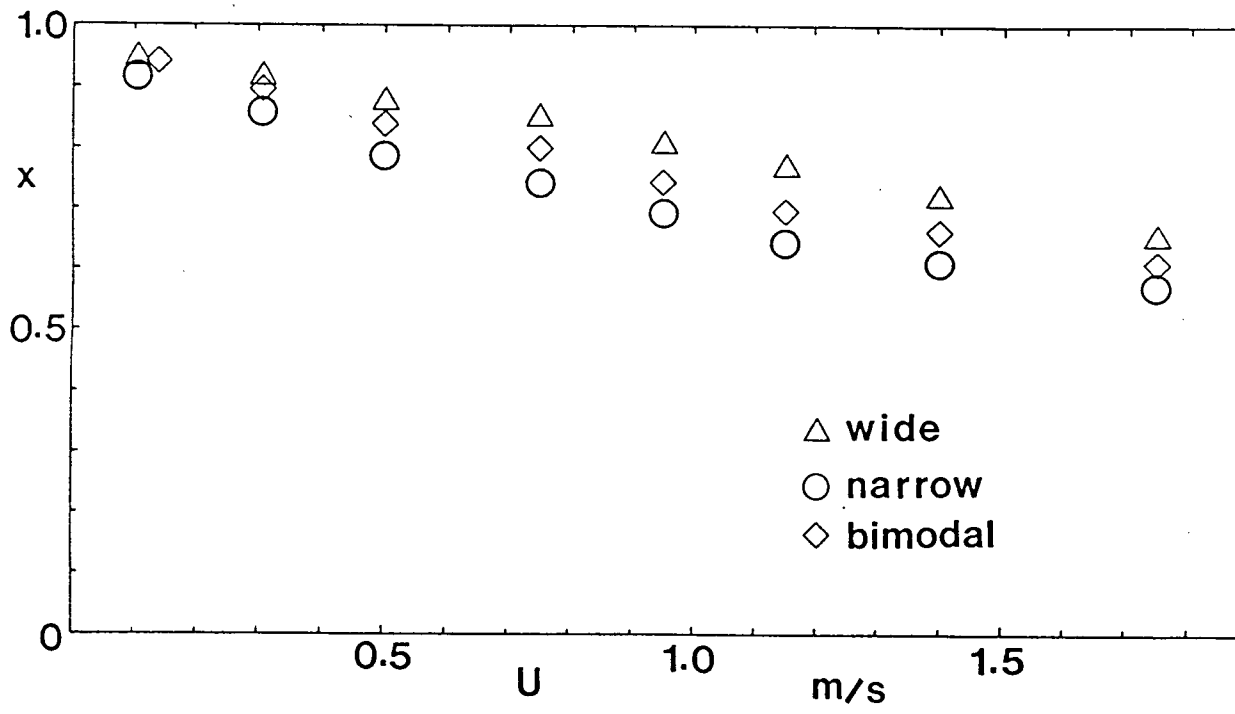

Figure 4.3: Influence of gas velocity and PSD on reactor conversion; catalyst inventory: 5 kg, $k_r \approx 9\ s^{-1}$.

turbulent fluidization not only occurred much later, but also was much less significant, that is, there were still some slugs or large bubbles of lower particle concentration at least in the upper part of the bed, even at high gas velocities (e.g. at $U = 1.2$ m/s).

The difference in particle concentration inside voids should also be noted. For particles of wide size distribution, the solids content inside bubbles appears to increase with gas velocity if $U > 0.2$ m/s (see section 5.1.3). For particles of narrow size distribution, however, the solid concentration in voids usually decreases with gas velocity, until $U > 0.6$ m/s, in contrast to the wide PSD. More reaction, therefore, is likely to occur in the voids for particles of wide size distribution than for those of narrow PSD. This difference increases with gas velocity until the two-phase character disappears in fluidized beds of both particle size distributions.

4.3 Influence of Fluidization Regime on Reactor Performance

The influence of the fluidization regime on the performance of fluidized bed reactors was investigated by changing the gas velocity and the kinetic rate constant at the same time to keep the dimensionless rate constant, k_f', constant. The gas velocity was changed from 0.1 to 1.8 m/s to include the bubbling, slugging, and turbulent regimes, and to just reach the fast fluidization regime. Further increases of the gas velocity were limited by the column height, and the requirement that the pressure drop across the dipleg be balanced against that across the bed and cyclones. The regimes tested in this study, therefore, were the bubbling, slugging, turbulent and part of fast fluidization regimes. The kinetic rate constant, k_r, was changed from 2 to 10 s^{-1}.

4.3.1 Regime influence for particles of wide size distribution

The conversion in catalytic reactors operated in different fluidization regimes is shown in Figs. 4.4 and 4.5 for particles of wide and narrow size distribution respectively. The evaluation of regime effect on reactor performance was based on the comparison of conversions achieved in fluidized beds operated in different regimes but with the same k_f'. The corresponding results for single phase plug flow and perfect mixing are also shown for reference.

It is seen from Fig. 4.4 that for particles of wide size distribution the conversion obtained in the turbulent and fast fluidization regimes appears to be 10% to 20% more than in the bubbling and slugging fluidization regimes at the same k_f'. Conversions obtained in bubbling and slugging fluidization were usually lower than in single phase perfect mixing reactors, suggesting the predominant two phase character, i.e. high mass transfer resistance between a dilute and dense phase. Conversions achieved at higher gas velocities ($U > 0.6$ m/s), or in the turbulent and the fast fluidization regimes, however, were usually higher than that in the corresponding perfectly mixed reactors, implying that the mass transfer resistance between gas and solids decreases due to the regime changes, i.e. due to break-up of the typical two-phase character. The effect of hydrodynamic regime on the contacting efficiency of fluidized bed reactors is also related to the PSD. For particles of wide size distribution, the contacting efficiency in the turbulent and fast fluidization regimes is higher than that in the bubbling and slugging regimes as shown in Fig. 4.6. Operating at higher gas velocities, therefore, can improve the performance of fluidized bed reactors of Group A particles of wide size distribution.

The effect of fluidization regime on the reactor performance should be considered in modelling fluidized bed reactors. The higher efficiency attained at higher gas velocities for particles of wide PSD, with values between those obtained for single phase perfect

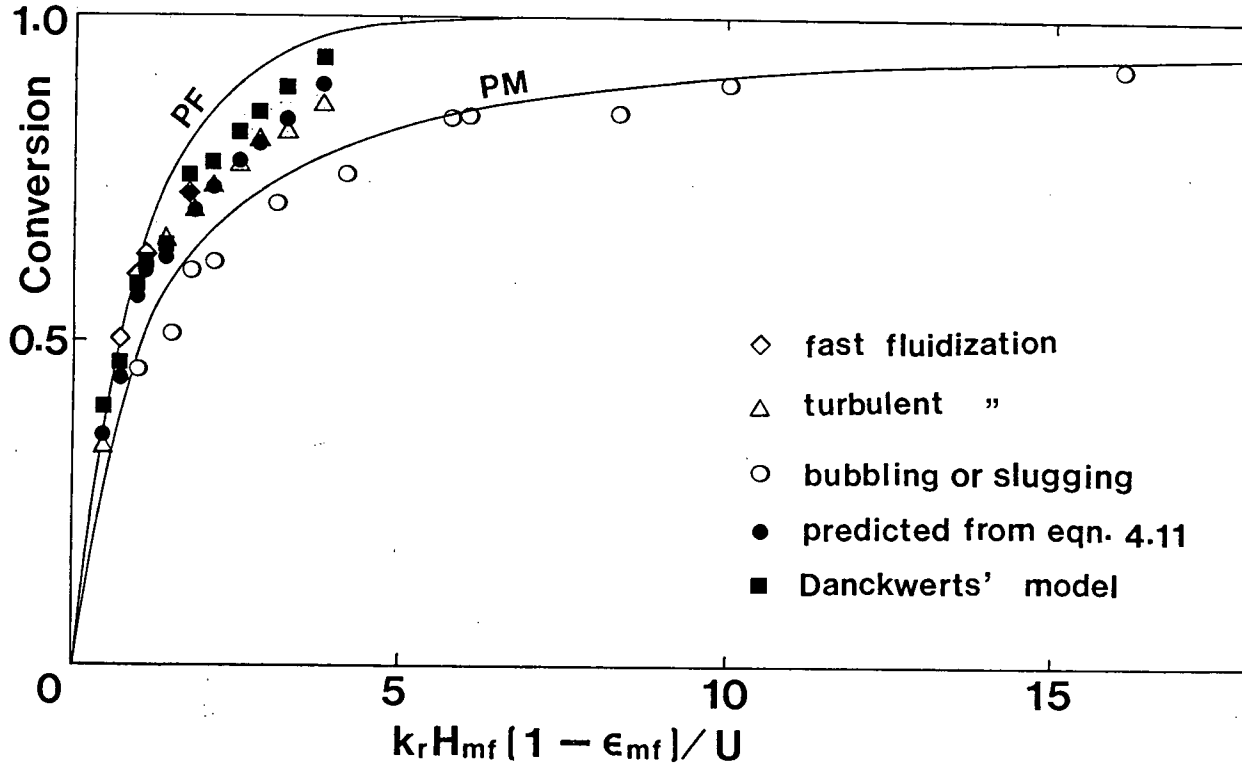

Figure 4.4: Influence of hydrodynamic regime on ozone decomposition for catalysts of wide size distribution

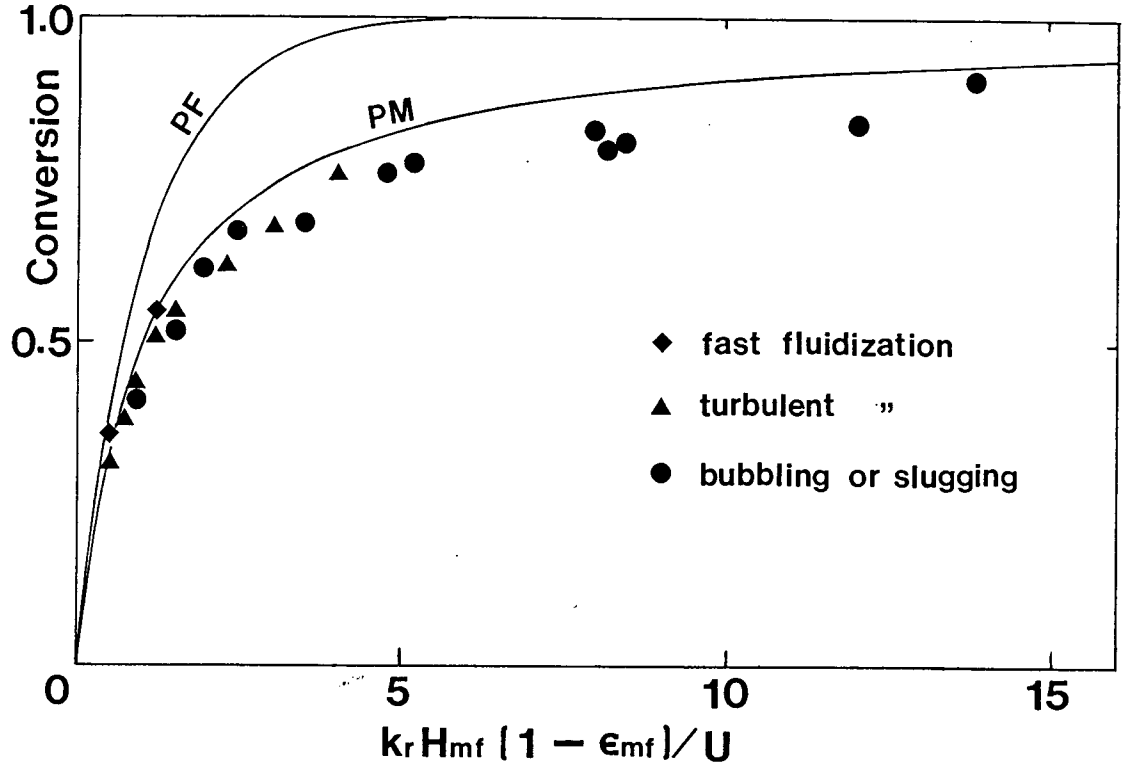

Figure 4.5: Influence of hydrodynamic regime on ozone decomposition for catalysts of narrow size distribution

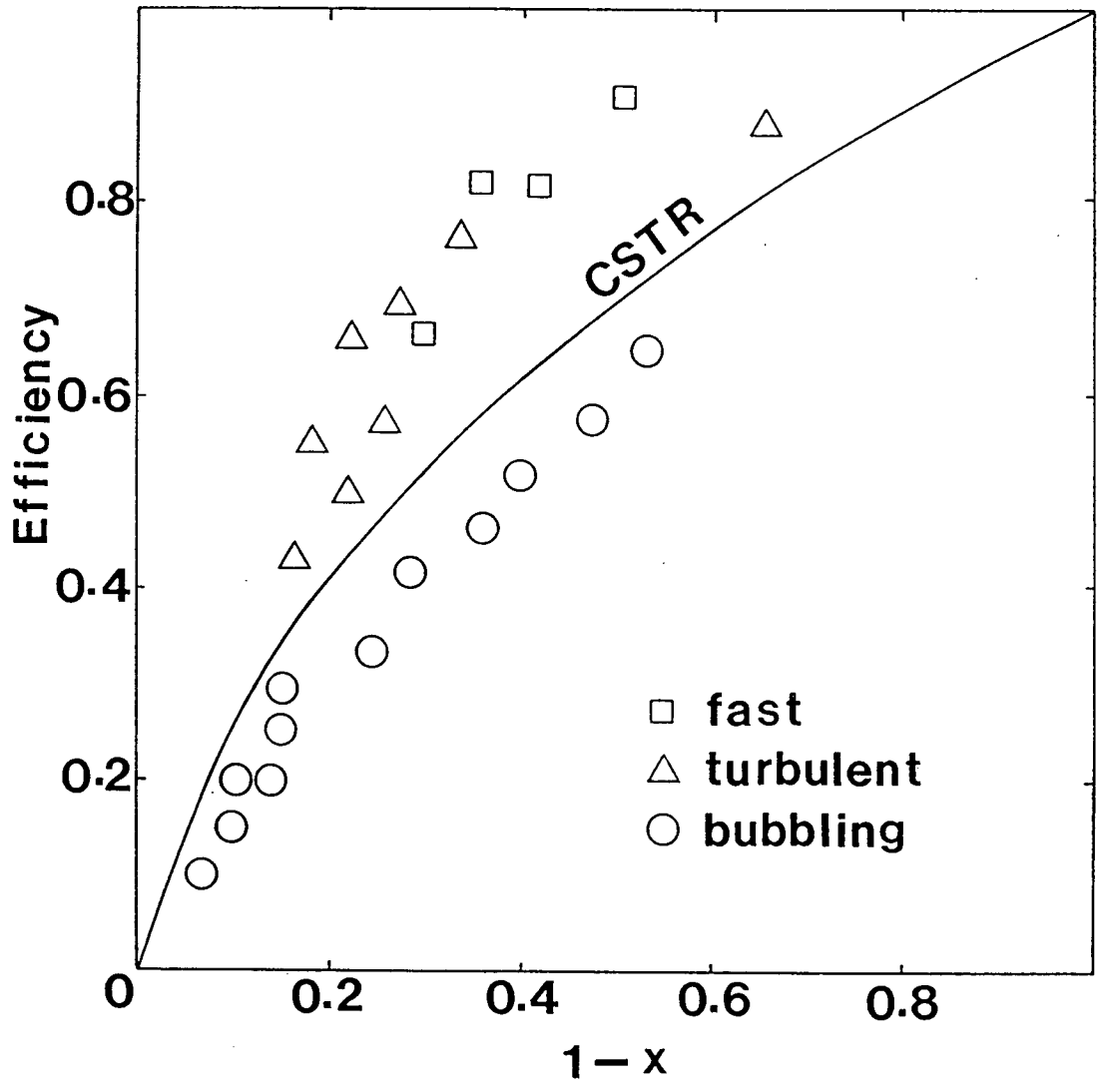

Figure 4.6: Influence of hydrodynamic regime on contacting efficiency for particles of wide size distribution

mixing and plug flow reactors, is underestimated by the two-phase bubbling bed model. Other models, such as a single phase axially dispersed model or a countercurrent flow model, may be more suitable to evaluate the performance of fluidized bed reactors which operate at high gas velocities (Avidan and Edwards, 1986; Krambeck et al, 1987).

4.3.2 Regime influence for catalysts of narrow size distribution

For particles of narrow size distribution, it can be seen from Figs. 4.5 and 4.7 that the difference among conversions obtained at the same dimensionless kinetic rate, k_f', but different hydrodynamic regime is relatively minor, in contrast to the result for the wide size distribution. These phenomena can be explained by our hydrodynamic experimental results discussed below in Chapter 6. As shown in Fig. 6.1, the dependence of F_p on the gas velocity for particles of narrow PSD differs from that of the wide size distribution catalyst. For particles of wide size distribution, U_c, corresponding to the regime transition from bubbling to turbulent fluidization, is about 0.6 m/s, while the transition is completed at around 1 m/s (or U_k). For particles of narrow size distribution, although the pressure fluctuations appear to decrease gradually with gas velocity after reaching a peak at around 0.75 m/s, the significant levelling-off, which is seen for particles of wide PSD, has not been found at the upper part of the bed in the entire range of gas velocity in this study. This suggests that even at high gas velocities, the two-phase character still appears to be significant in fluidized beds of narrow PSD. Hence, considerable voids of large size and low particle concentration exist in the bed. The proper particle size distribution, therefore, is a necessary condition to obtain optimum performance of fluidized bed reactors at high gas velocities.

The conversion achieved in fluidized bed reactors containing particles of narrow size distribution was generally less in our experiments than in a perfectly mixed single phase reactor, whether the bed operated in the bubbling, slugging or turbulent regime, except

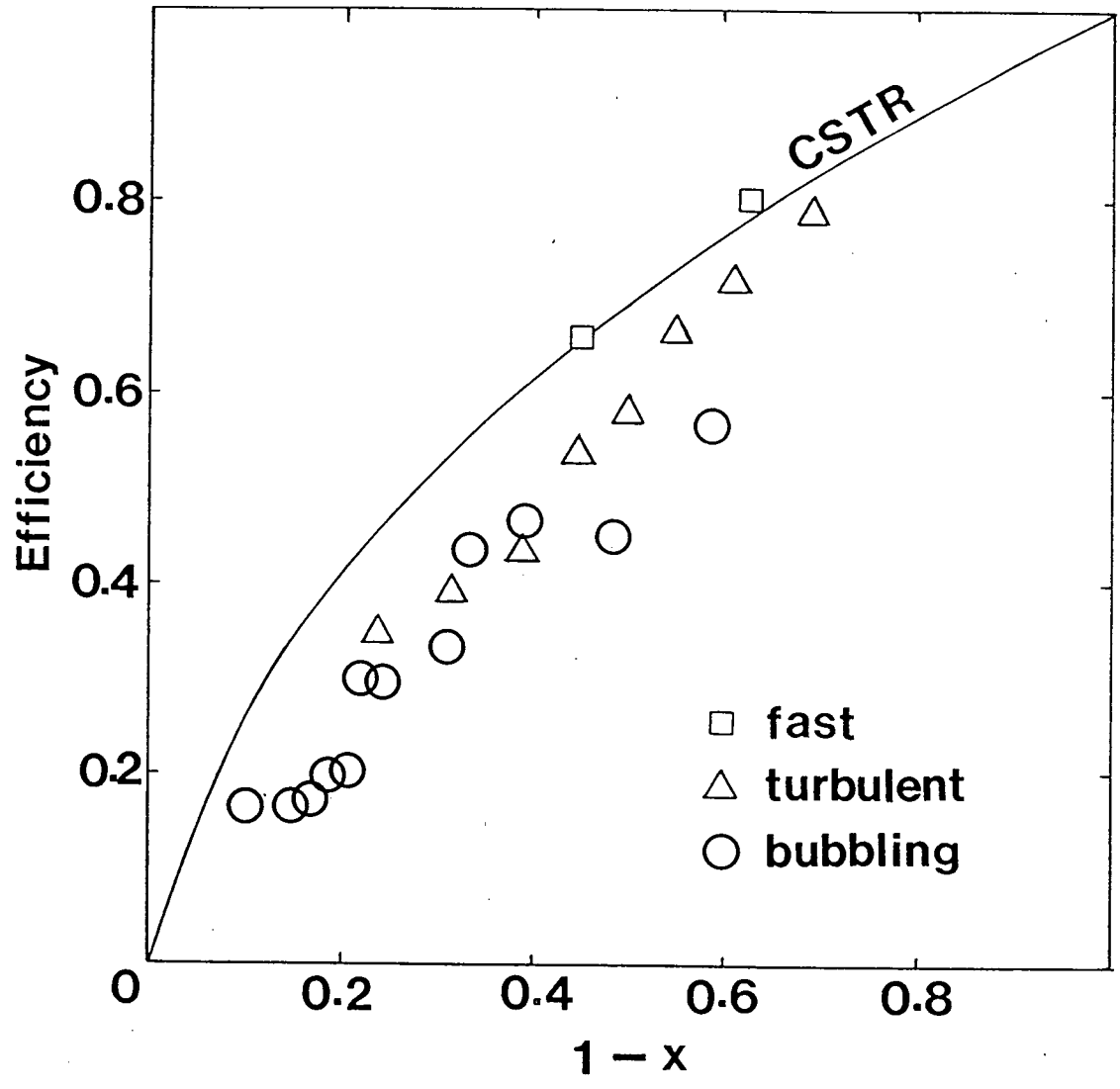

Figure 4.7: Influence of hydrodynamic regime on contacting efficiency for particles of narrow size distribution

for $U > 1.4$ m/s, as shown in Fig. 4.5. The two phase flow model, therefore, may be suitable to predict the conversion for particles of narrow size distribution at both low and high gas velocities.

4.4 Prediction of PSD Effect at High Gas Velocities

The effect of the fluidization regime and the particle size distribution on the reactor performance should be considered in modelling fluidized bed reactors. For the regime where two-phase phenomena are predominant, that is at low gas velocities for the wide PSD or over a wider range of gas velocity for the narrow PSD, the conversion achieved in a fluidized bed can be successfully predicted by the Two-Phase Bubbling Bed Model (Grace, 1984, 1986) with two modifications to express the PSD effect. First, it is neccessary to account for the effect of PSD on particle concentration in voids (as discussed in Chapter 3). Secondly, PSD has a significant influence on bubble size and/or slug length (as discussed in Chapter 5). At higher gas velocities, however, the higher efficiency attained in fluidized beds of wide PSD, with values between those obtained for single phase perfect mixing and plug flow reactors, as shown in Fig. 4.4, will usually be underestimated by the two-phase bubbling model.

The suppression of gas bubbles in fluidized bed reactors suggests the use of a homogeneous dispersion model. From the experience of scaling-up the MTG process, Avidan and Edwards (1986) suggested that the axial dispersion model can be used to predict conversion in a turbulent fluidized bed reactor under certain conditions. These conditions - high gas velocities, substantial fines contents and sufficient bed height, were almost achieved in our experiments for particles of wide PSD and at high gas velocities.

The axial dispersion model, a one-dimensional model, is often used to describe phenomena that cause a distribution of residence times. In the case of an unpacked tubular

reactor the dispersion is attributable to molecular diffusion and turbulent transport or eddy diffusion. In the fluidized bed, it is largely the result of local backmixing and by-passing, local acceleration, deceleration and trapping, as fluid elements are retained in a random manner for varying periods in the voids. These phenomena are conveniently described using an effective axial diffusivity, D_e, a Fickian-type term. D_e is usually determined from residence time distributions, which, in turn, are often derived from tracer tests.

A fluidized bed reactor can generally be divided into three sections along the column, as shown in Fig. 4.8. For a steady state flow reactor with axial diffusion and first order reaction, if reactions in the windbox and outlet section are negligible, the following differental equations result from mole balances on reactant A for these three sections:

$$D_{e,1}\frac{d^2C_A}{dz^2} - U\frac{dC_A}{dz} = 0, \qquad z \leq 0 \tag{4.1}$$

$$D_{e,2}\frac{d^2C_A}{dz^2} - U\frac{dC_A}{dz} - k_r(1-\bar{\epsilon}_f)C_A = 0, \qquad 0 \leq z \leq H \tag{4.2}$$

$$D_{e,3}\frac{d^2C_A}{dz^2} - U\frac{dC_A}{dz} = 0, \qquad z \geq H \tag{4.3}$$

where $D_{e,1}$, $D_{e,2}$ and $D_{e,3}$ are gas axial dispersion coefficients in the windbox, reaction section and outlet section respectively and $\bar{\epsilon}_f$ is the average voidage in the reaction section. The axial dispersion coefficient may differ between sections for reasons of gas velocity, presence of particles and the like.

In practical fluidized bed reactors, in order to keep the pressure drop across the distributor sufficiently high, the orifice gas velocity is maintained high and gas dispersion across the distributor is negligible. The concentration in the windbox can then be taken

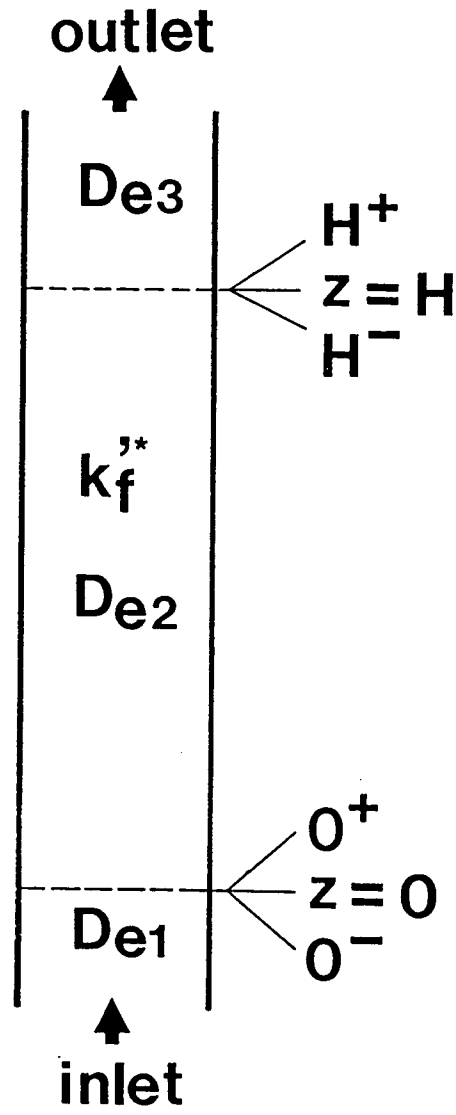

Figure 4.8: Axial dispersion model for fluidized bed reactors

as $C_{A,in}$. Equation 4.1, therefore, can be deleted. This model can then be solved with the following four boundary conditions (see Fig. 4.8):

$$(a) \qquad C_A \mid_{z=0^-} = C_A \mid_{z=0^+} = C_{A,in} \tag{4.4}$$

$$(b) \qquad (UC_A - D_{e,2}\frac{dC_A}{dz}) \mid_{z=H^-} = (UC_A - D_{e,3}\frac{dC_A}{dz}) \mid_{z=H^+} \tag{4.5}$$

$$(c) \qquad C_A \mid_{z=H^-} = C_A \mid_{z=H^+} \tag{4.6}$$

$$(d) \qquad C_A \mid_{z=+\infty} = C_{A,out} \tag{4.7}$$

Condition (b) results from the conservation of reactants at the exit of the bed, taking into account flow and diffusion. Conditions (a) and (c) arise from the intuitive argument that at steady state the concentration should be continuous between sections at the bed entrance and exit.

The general solutions for eqns. 4.2 and 4.3, containing four arbitrary constants, N_i, are:

$$\frac{C_A}{C_{A,in}} = N_1 exp\frac{U}{2D_{e,2}}(1+a)z + N_2 exp\frac{U}{2D_{e,2}}(1-a)z \quad 0 \leq z \leq H \tag{4.8}$$

and

$$\frac{C_A}{C_{A,in}} = N_3 + N_4 exp\frac{Uz}{D_{e,3}} \qquad z \geq H \tag{4.9}$$

After inserting boundary conditions, the complete solutions for equations 4.2 and 4.3 are:

$$\frac{C_A}{C_{A,in}} = \frac{exp\frac{A_1 z}{2H}[(a-1)expPe + (1-a)expA_2] - exp\frac{A_2 z}{2H}[(a+1)expPe + (1+a)expA_1]}{(1+a)exp(Pe(1+a)) + (1-a)exp(Pe(1-a)) - 2expPe} \tag{4.10}$$

$$0 \leq z \leq H$$

$$\frac{C_{A,out}}{C_{A,in}} = \frac{2aexpPe}{(1+a)exp(Pe(1+a)/2) - (1-a)exp(Pe(1-a)/2)}, \qquad z \geq H \tag{4.11}$$

where

$$Pe = \frac{HU}{D_{e,2}} \tag{4.12}$$

$$a = \sqrt{1 + \frac{4k_f'^{*}}{Pe}} \tag{4.13}$$

$$k_f'^{*} = \frac{k_r H(1-\bar{\epsilon}_f)}{U} \tag{4.14}$$

$$A_1 = (1+a)Pe \tag{4.15}$$

$$A_2 = (1-a)Pe \tag{4.16}$$

This model was tested against our experimental results. The axial dispersion coefficients used were from the tracer experiments of Guo (1987). Guo applied hydrogen as tracer gas to measure the residence time distribution and gas axial dispersion coefficient in a fluidized bed (D_T = 0.07 m) of FCC particles. The tracer flowed through a solenoid valve into the windbox of the column as an impulse input, and the sampling probe was installed in the expansion section. The measurements were carried out at superficial gas velocities from 0.1 to 1.2 m/s with H_{mf} from 0.15 to 0.9 m. These conditions are similar

to those of our systems. Using the data reported by Guo for $H_{mf} = 0.6$ m, the Peclet numbers calculated for our experimental systems were from 6 to 13, similar to values measured by Avidan and colleagues (Avidan and Edwards, 1986; Krambeck et al, 1987). As shown in Fig. 4.4, the conversions achieved in the turbulent fluidization regime for particles of wide size distribution are in good agreement with the prediction results from this simple model, with an average deviation of only 5.1%.

Conversions predicted from the axial dispersion model with boundary conditions of open inlet and closed outlet, as used by many previous investigators (e.g. Danckwerts, 1953; Avidan and Edwards, 1986), are also shown in Fig. 4.4. In this case, the average deviation between the experimental and the predicted results was larger, 8.4%.

Chapter 5

Effect of Particle Size Distribution on Two-Phase Behaviour

The performance of fluidized bed reactors is strongly related to the hydrodynamics of fluidization. In this study, the influence of particle size distribution on the hydrodynamics of fluidization was investigated in two different fluidized bed columns. In this chapter, the influence of PSD on the void phenomena - particle concentration in voids, void size and void frequency, mainly determined in the two dimensional column - is examined. The effect of PSD on pressure fluctuations, regime transitions and bed expansion, in the 102 mm diameter cylindrical column in which the ozone decomposition reaction was studied (see Chapters 3 and 4), is considered in Chapter 6. The distribution of different particle size fractions between the dense and dilute phases is discussed in Chapter 3.

The performance of bubbling and slugging fluidized beds is dominated by the dilute phase behaviour, i.e. by the characteristics of gas voids. At low gas velocities, that is, in the regime of bubbling fluidization, gas voids are conveniently termed "bubbles", while at higher gas velocity, "bubbles" become "slugs" or appear in a more irregular or transitory manner in the turbulent fluidization regime (Rowe and MacGillivray, 1980).

Considerable work has been done on the behaviour of bubbles, and a number of correlations have been proposed to predict mean bubble size. Most of them, however, are restricted to coarse particles, i.e. group B or D powders according to the Geldart (1973) classification (Horio and Nonaka, 1987). The dependency of dilute phase character on the PSD is poorly understood, with direct measurements almost totally missing from the literature.

5.1 Particle Concentration in Voids

An assumption made by some investigators in modelling fluidized bed reactors is that the bubble or dilute phase is completely free of particles (e.g. May, 1959; Van Deemter, 1961; Orcutt et al, 1962; Werther, 1980). Although this assumption appears suitable for systems of coarse particles and for slow reactions, solids dispersed in the bubbles need to be considered for a fast reaction system, even when the volumetric particle concentration is small (Grace, 1982). Previous experimental work carried out with coarse particles (Toei et al, 1966; Kobayashi, 1966; Kunii et al, 1967), has demonstrated that particles are present in bubbles. In most catalytic fluidized bed reactors, such as in catalytic cracking of petroleum, ammoxidation of propylene and chloroxidation of ethylene, not only is the reaction fast, but also the catalyst is composed of fine (Group A) particles. The particles inside the void phase, therefore, may play an important role in determining the gas-solid contacting efficiency and reactor performance.

Hiraki et al (1965) investigated the amount of particles dispersed in bubbles in a two-dimensional freely bubbling fluidized bed by means of photograpy. Microspherical catalysts (ρ_p = 1.54 g/cm^3, $\bar{d}_p$ = 150 μm) were tested at a gas velocity just above U_{mf}. Particles dispersed in a bubble were illuminated using the Tyndall phenomenon and recorded on film. The volume fraction of particles dispersed in a rising bubble was calculated by counting the number of particles on the photograph, multiplying by the average volume of each particle and dividing by the bubble volume. The volume fraction occupied by particles was found to be 0.4 to 0.6%.

Toei et al (1966) measured the particle concentration in bubbles by tomography in a two dimensional bed (cross-section 24 × 250 mm). Particles used were glass beads (150 μm < d_p < 180 μm and 710 μm < d_p < 1000 μm) and sand (125 μm < d_p < 180 μm). The gas velocity was varied from 0.06 to 0.2 m/s. The measured volumetric concentration

of particles in bubbles ranged from 0.18% to 1.2%.

Kobayashi et al (1966) determined the particle concentrations in bubbles by using a detection probe consisting of a small electric bulb and a phototransistor. The particles tested were commercial silica gel particles with size range 180 to 250 μm. The gas velocity ranged from 0.05 to 0.22 m/s. The average particle concentration in bubbles was determined to be 0.8 to 4% by volume, while the ratio of particles contained in bubbles to the total solids in the fluidized bed was 0.4 to 1.2%, increasing with increasing gas velocity.

All the above experiments were carried out with coarse or Group B particles at low gas velocities. These results, however, have often been assumed to apply to fluidized bed of Group A particles, often containing large quantities of fines, and operated at high gas velocities.

In this study, the particle concentration in voids in fluidized bed of Group A particles was estimated using a laser photometric technique, and the effect of the PSD on the particle concentration was evaluated for a wide range of gas velocities.

5.1.1 Theory underlying the measurements

Photometric techniques, depending upon light absorbance, are applicable in many industrial process units since the experimental procedure is simple and non-interfering. The extinction of a collimated beam passing through suspended particles can be used to determine the line-of-sight average particle concentration or spray concentration. Fenton and Stukel (1976) constructed a miniaturized optical probe system utilizing the attenuation of a collimated light beam passing through a particulate suspension to measure the particle concentration. Brown et al (1988) measured the size distribution and relative concentration of solid particles in liquids by small-angle laser light diffraction. By combining the Beer-Lambert Law with a theorem of Cauchy, the absolute concentration of particles

could also be evaluated. Schmidt et al (1989) developed a laser photometric probe to measure the local concentration in liquid dispersions. The technique consisted of a laser light sourse, a fiber-optic probe and an electronic device with a photodetector. Their measurements for different concentrations of oil-blue droplets in toluene demonstrated that the Lambert-Beer law holds over the range investigated.

Scattering and absorption characteristics of many particles in fluidized bed can be obtained from the single particle characteristics based on a size parameter α ($\alpha = \pi d_{pi}/\lambda$) and the particle volume fraction (Tien, 1985). The measurement system can be considered to be in the independent scattering regime if $\alpha > 20$ (Hodkinson, 1966), and the particle volume fraction < 0.15 (Tien, 1988).

For the independent scattering regime it can be assumed that each particle in the assembly scatters and absorbs radiation unaffected by other particles. Thus the extinction and scattering by the system is expressed by simple algebraic addition of the energy extinquished and scattered by each primary particle. The cross-section for the system of N particles is the sum of the cross-section of each particle, and the individual particles are assumed to scatter and absorb radiation independently of the others.

With the helium-neon laser ($\lambda = 0.632$ μm) and particles used in this study ($d_{pi} >$ 15 μm), α is always greater than 60. For the dilute phase investigated, therefore, the condition for independent scattering is easily met.

For a measurement system in the independent scattering regime, the ratio of the light intensity measured before and after the particles are placed in the laser beam is related to the total projected cross-sectional area of the particles, expressed by the Lambert-Beer Law, that is

$$\ln \frac{I}{I_0} = -\sum_{i=1}^{m} N_i A_i Q_i L \tag{5.1}$$

where I and I_0 are the light intensities with and without the particles respectively, N_i

is the number of particles of size interval i per unit volume, A_i is the cross-sectional area of the same particles, Q_i is the extinction efficiency of these particles and L is the optical path length. Q_i is related to the diameter of the particles, to the absorptivity and emmissivity of the particles, to the refractive index of the medium, and to the wavelength of the radiation.

For a spherical particle,

$$\frac{V_p}{A_p} = \frac{2d_p}{3} \tag{5.2}$$

so that

$$N_i A_i = \frac{3V_i}{2d_{pi}} \tag{5.3}$$

where V_i is the volume of particles in size range i, per unit volume.

Combining eqns. (5.1) and (5.3), we obtain

$$\ln \frac{I}{I_0} = -L \sum_{i=1}^{m} \frac{3V_i}{2d_{pi}} Q_i \tag{5.4}$$

Since $V_i = V_{p,t}\ x_i$, and $V_{p,t} = 1 - \epsilon$, where $V_{p,t}$ is the total volume of all particles in the beam per unit volume,

$$\ln \frac{I}{I_0} = -(1-\epsilon) L \sum_{i=1}^{m} \frac{3x_i}{2d_{pi}} Q_i \tag{5.5}$$

If $\alpha > 50$, the effect of particle diameter on the extinction efficiency is negligible (Brown et al, 1988), so that Q_i can be taken as Q. The particle concentration in the voids, expressed as $1 - \epsilon$, therefore, can be estimated from

$$1 - \epsilon = \frac{2\bar{d}_{p,v} \ln(I_0/I)}{3LQ} \tag{5.6}$$

where $\bar{d}_{p,v} = 1/\sum(x_i/d_{pi})_v$, is the mean particle diameter of the particles in voids.

The theory developed thus far implies that the particle concentration in voids increases logarithmically with the ratio of I_0 to I. For a measured value of (I_0/I), the particle concentration is directly proportional to the mean diameter of particles inside the void.

5.1.2 Laser photometer and its calibration

The experiment was carried out in the two dimensional column (12 × 560 mm in cross-section and 2.1 m in height). There is a tapered expansion section (Fig. 5.1) at the top of the column to reduce carryover. Above this section, there is a filter bag to collect fines escaping from the column.

The measurement equipment consisted of a laser light source, a Metrologic photometer and a UV chart recorder, as shown in Fig. 5.2. The laser was a 5 mW He-Ne tube (Spectra Physics Stablite) emitting light at a wavelength 632 nm. Power was supplied by a Model 255 Exciter. The Metrologic Photometer (Model 45-230), designed for laser measurement, includes a photo-detector and a circuit amplifier. The measurement range of the photometer was from 0.003 mW to 10 mW, adjusted by a range selector. The output of the photometer (0 - 1 vDC) was recorded continuously on the UV chart recorder.

Both N-FCC and S-FCC particles, each with three different PSD but with the same $\overline{d}_p$ for each type, were tested in the two-dimensional fluidized bed at gas velocities from 0.06 to 0.8 m/s. The static bed height was 0.9 m, and the measurement location was 0.85 m above the distributor along the center line of the front face of the column. Compressed air was used as the fluidizing gas.

Most of the experiments were carried out in darkness at night to reduce the influence of extraneous light on the measurements. Pretesting showed that interference could be prevented if both walls of the bed, except for apertures for the beam, were covered by black plastic film (900 × 500 mm). No signal was detected by the photometer if the laser

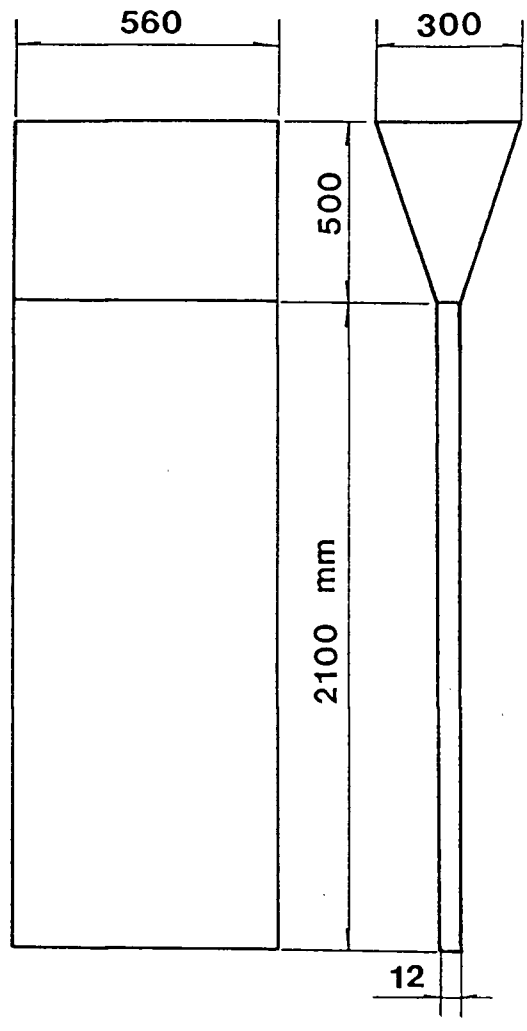

Figure 5.1: Dimensions of the two-dimensional fluidization column

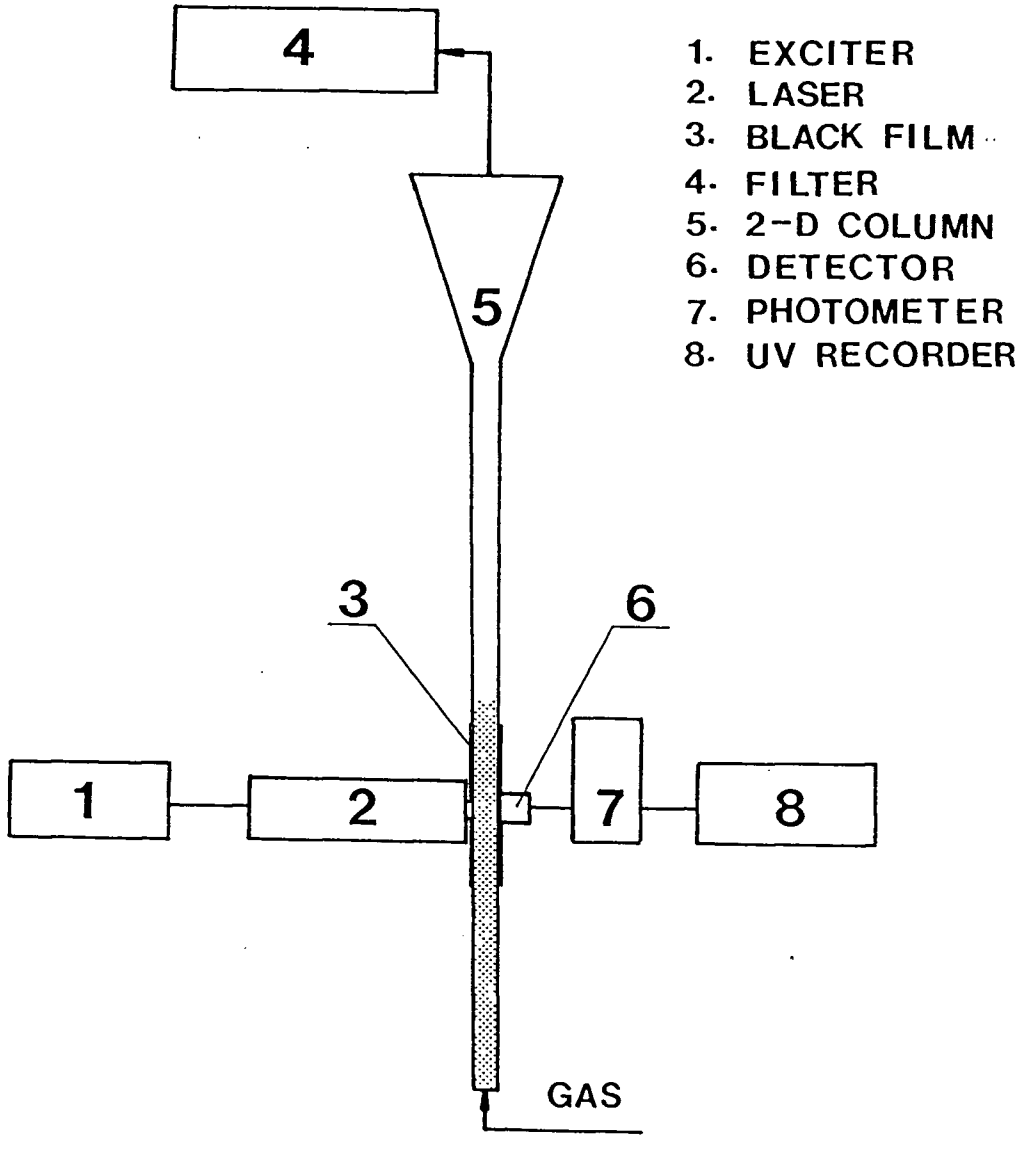

Figure 5.2: Measurement apparatus used to determine particle concentration in voids

was shut off, even in the most sensitive range (0.003 mW).

The operation procedure was as follows. The alignment of the laser tube and the detector was checked carefully before each measurement. After the laser was turned on for a half hour, particles were added to the column and fluidized by air at a predetermined gas velocity for 15 minutes. After the fluidized gas was shut off, so that the laser beam was blocked by a fixed bed, the photometer output voltage was nulled. Then approximately 1000 ml of particles were withdrawn from the bottom, so that the static bed height fell below the height of the laser beam. The photometer voltage output was thus recorded as I_0 (at zero concentration). This procedure was repeated about 3 times to make sure that I_0 was nearly constant. After I_0 was determined, the withdrawn particles and any collected by the filter were added to the column to give a static bed height of around 0.9 m. The particle concentration at different gas velocities was then measured, and the voltage output was recorded on the UV recorder continuously.

To determine the absolute particle concentration, the laser photometer was calibrated in a small two-dimensional rectangular chamber (12 $\times$ 150 $\times$ 250 mm principal dimensions) for each kind of particles measured. To ensure that the particles were dispersed uniformly, water was used as the suspending medium.. The experimental results presented by Fenton et al (1976) and Brown et al (1988) establish that the change in the extinction coefficient due to using air instead by water as the medium is insignificant. Glass beads, with mean particle size 11 μm and 22 μm respectively, were used by them, and almost the same extinction coefficient was obtained, even though Fenton et al used air as the suspending medium, while Brown et al used water.

The range of particle concentration calibrated was from 0.5 to 8% by weight (around 0.4 to 6% by volume). A weighed quality of particles was suspended in 400 g water, and maintained in suspension by vigorous hand stirring. For each sample measured, both I_0, recorded after all particles had settled, and I, recorded while particles were uniformly

dispersed, were read 5 times to obtain an average value. The calibration results, expressed by five lines, are shown in Fig. 5.3. The linearity between 1 - ϵ and $\ln(I_0/I)$ is satisfactory. Comparing lines 1 and 3, it is seen that the extinction coefficient depends on the colour of the particles. For S-FCC particles with dark-grey colour, Q was about 2, while for the N-FCC particles (white colour), Q was around 1. The calibration results seem consistent with the theory expressed by Eqn. 5.6. The difference between lines 2, 3 and 5 is caused by the change of mean particle size. For particles with the same mean size but different size distribution, the dependency of (1 - ϵ) on the ratio of light intensity, I_0/I, (lines 3 and 4) is almost the same, as predicted by Eqn. 5.6.

5.1.3 Particle and fines concentration in voids

To keep the PSD inside the bed as contant as possible during each measurement in the presence of particle carryover, the maximum gas velocity used in the two-dimensional column was 0.8 m/s. For particles tested in this study, the maximum measurable solid concentration by this photometric technique was around 2% by volume for S-FCC and 5.2% for N-FCC, as shown in Fig. 5.3, since the maximum I_0/I which can be determined accurately is around 10^4 (with reading error less than 5%). The measurement range for N-FCC particles was wider than for S-FCC particles. Most experimental results discussed here, therefore, are for the N-FCC particles. The results for the S-FCC particles are given in Appendix B.

Results for N-FCC particles are shown in Figs. 5.4 to 5.6. The intensity measured by the photometer when voids allow light to pass, is seen to be affected by both the particle size distribution and the superficial gas velocity. At low gas velocity ($U < 0.2$ m/s), the PSD influence was small. At higher gas velocities, however, the influence of PSD became significant.

The effect of PSD on the solids hold-up in voids in fluidized beds is shown in Figs. 5.7

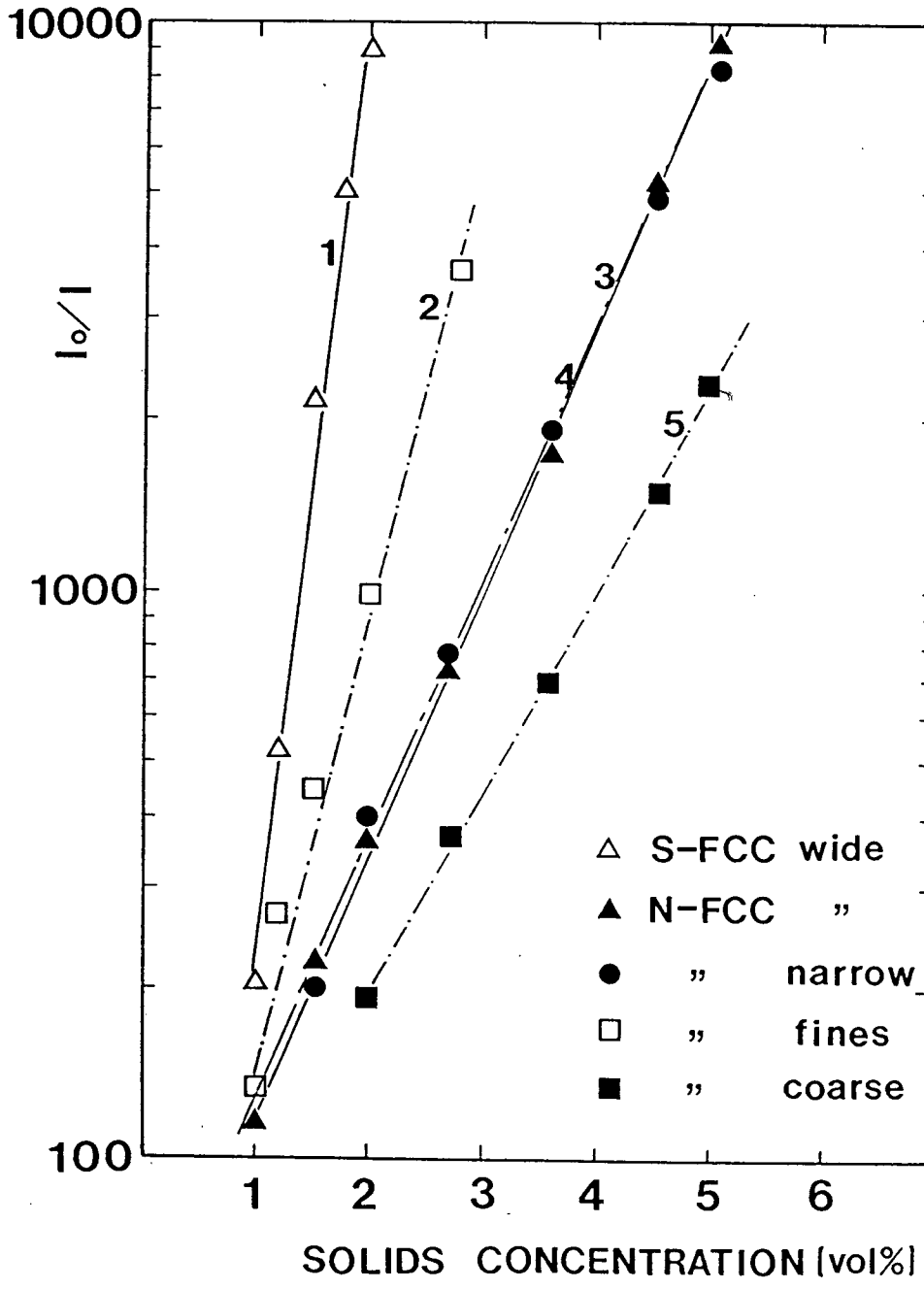

Figure 5.3: Particle concentration calibration curve

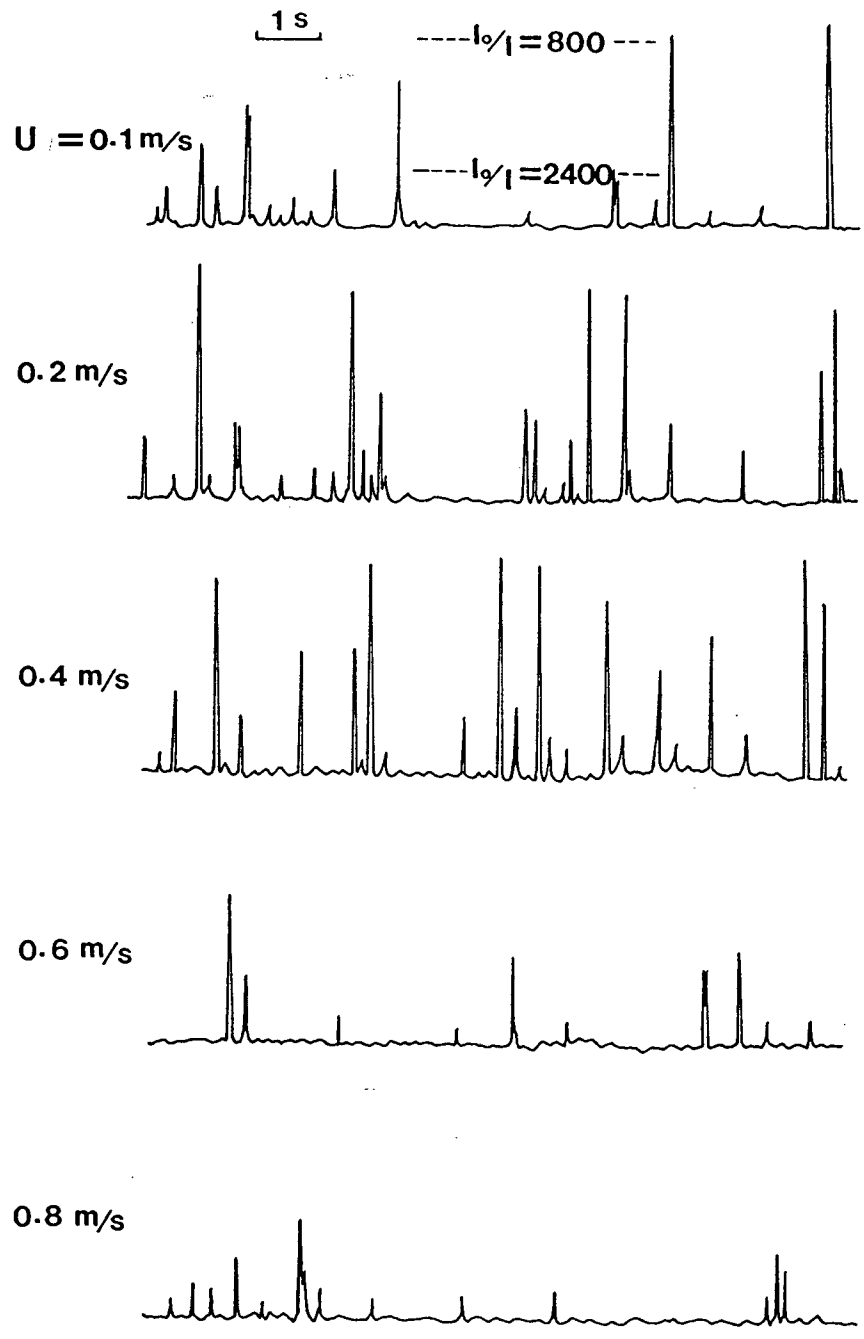

Figure 5.4: Photometric measurement for N-FCC particles with wide PSD

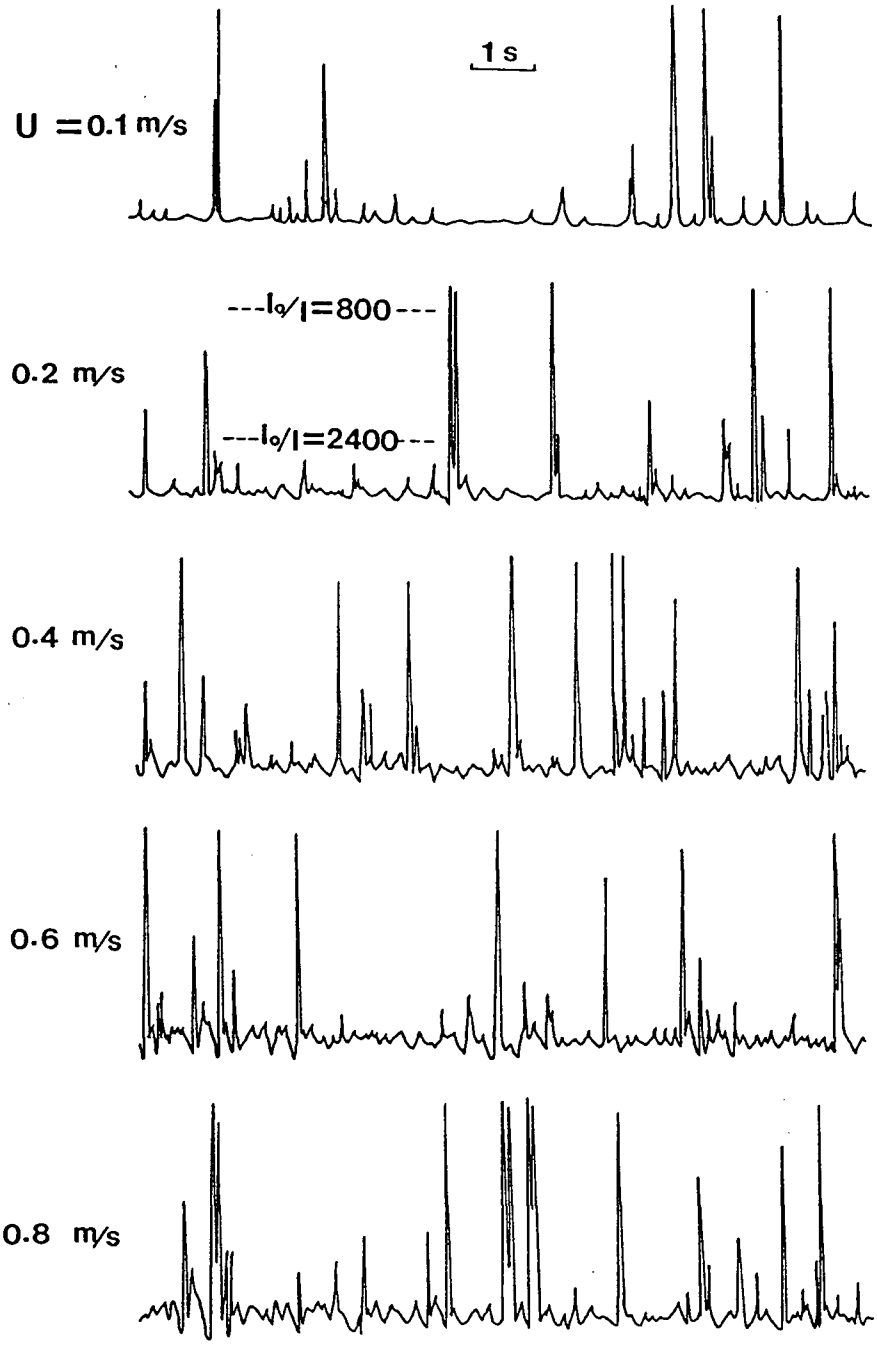

Figure 5.5: Photometric measurement for N-FCC particles with narrow PSD

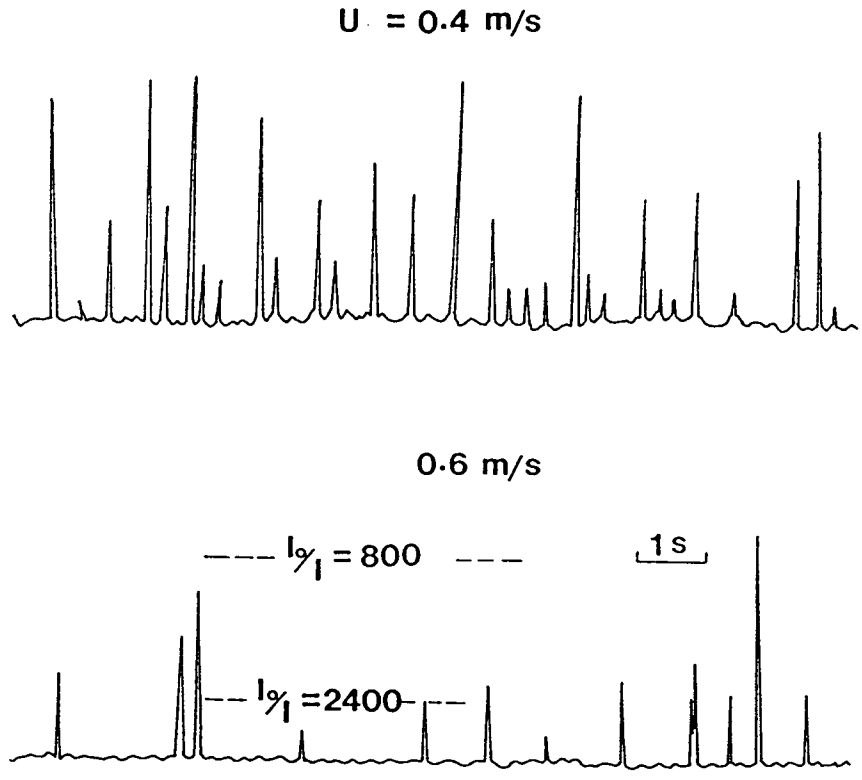

Figure 5.6: Photometric measurement for N-FCC particles with bimodal PSD

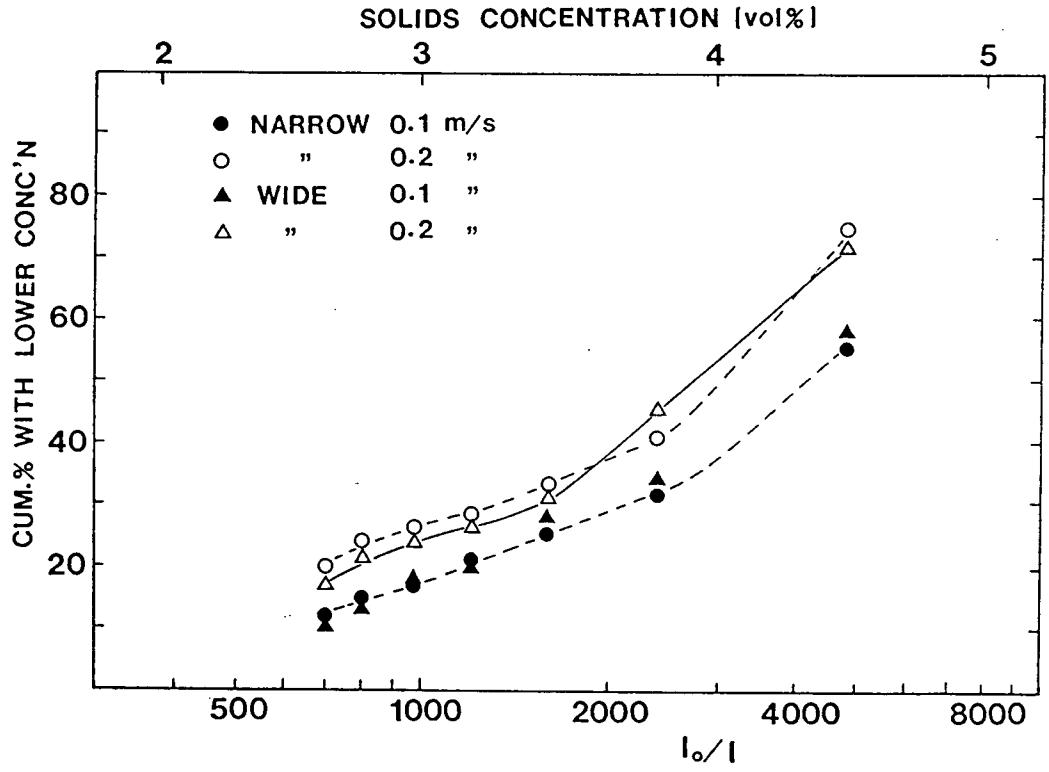

Figure 5.7: Influence of PSD on solids hold-up in voids at lower gas velocities

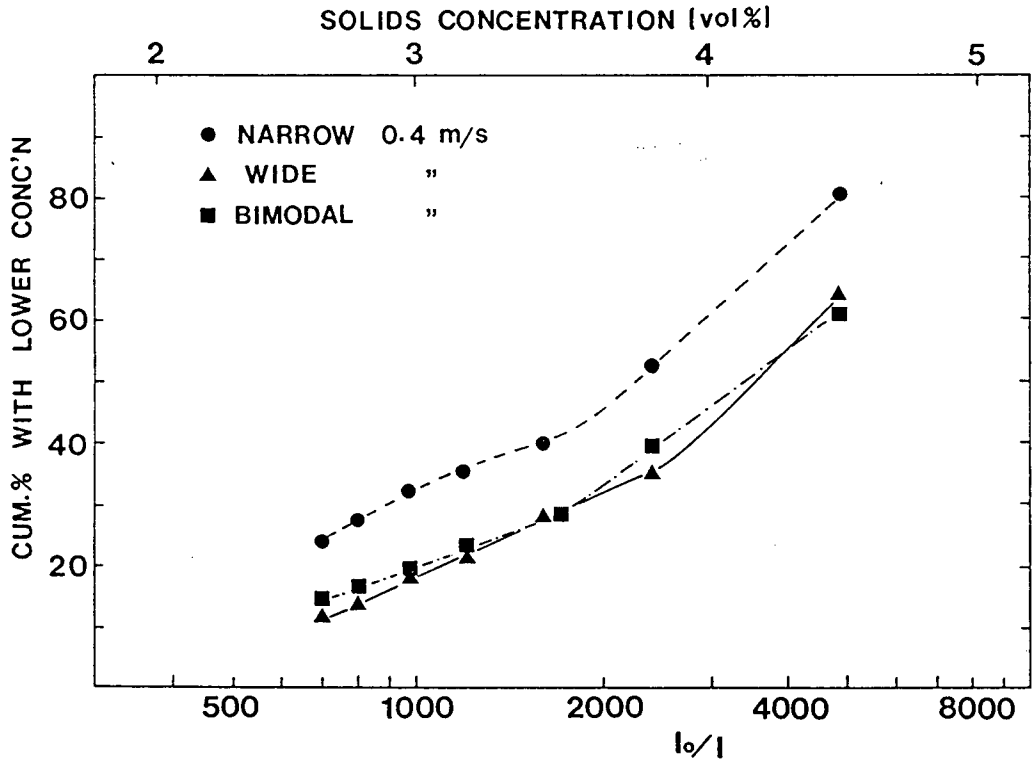

Figure 5.8: Influence of PSD on solids hold-up in voids at a gas velocity of 0.4 m/s

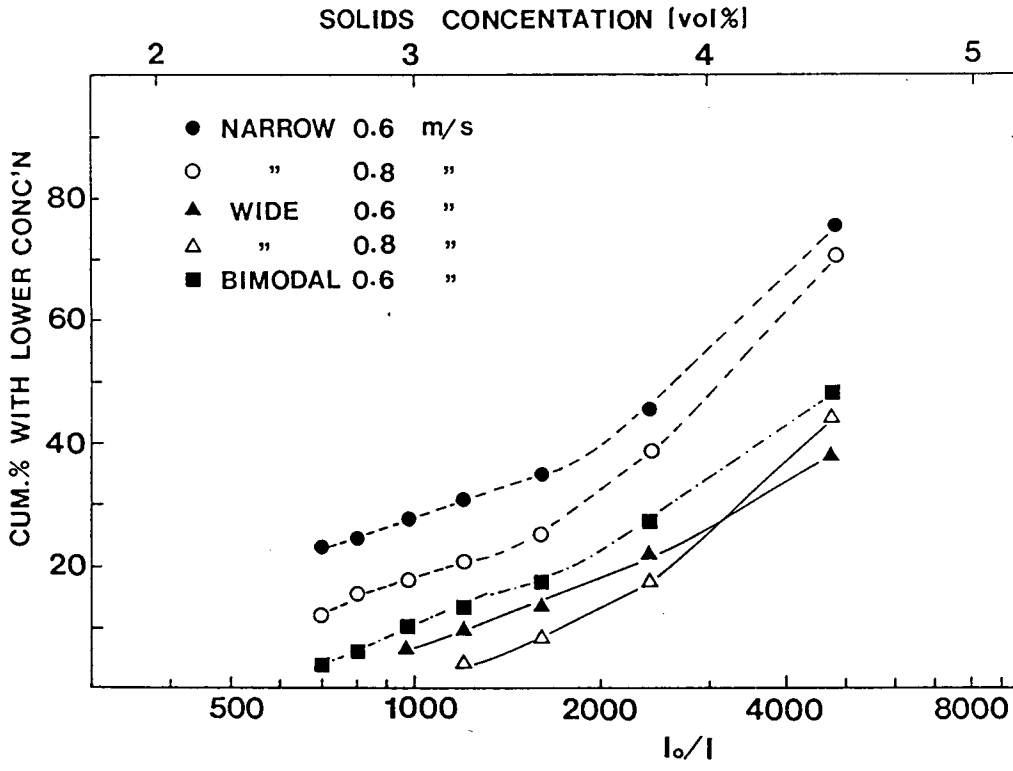

Figure 5.9: Influence of PSD on solids hold-up in voids at higher gas velocities

to 5.9 where the abscissa gives both I_o/I, and the solids concentration, while the ordinate is the ratio of the cumulative number of voids with solids concentration lower than the corresponding $(I_0/I)_k$ to the total number of voids (with solids concentration lower than 5%) for a measurement interval of 60 s. It should be noted that the solids concentration given on the top axis of Figs. 5.7 - 5.9 is for the overall PSD's. This scale should be accurate for the narrow size distribution, but there will be a small error for the wide and bimodal distributions where we have shown that there is a greater concentration of fines in the voids than in the overall bed.

For gas velocities less than 0.2 m/s, the dependency of cumulative number percent, on the particle and fines concentration in bubbles was similar for the wide and narrow particle size distributions. Even at a gas velocity of 0.2 m/s, the ratio of the cumulative number of voids with solids concentration less than 3.3% by volume to the total number of voids for the narrow size distribution is higher than for the wide PSD. With an increase of gas velocity, however, there was a significant difference between the two PSD's. This difference increased with increasing gas velocity for $U < 0.7$ m/s in our experiments. The number of voids with lower particle and fines concentrations was much greater for the narrow particle size distribution than that for the wide PSD. For the wide particle size distribution, $\sum N_i/N_T$ only increased with gas velocity if $U \leq 0.2$ m/s, and decreased dramatically with U if $U > 0.2$ m/s, except for $(I_o/I)_k = 5000$, i.e. solids concentration less than 4.5% by volume. For the narrow particle size distribution, however, this change only occurred for $U > 0.6$ m/s. For $U > 0.2$ m/s, $\sum^{(I_o/I)_i<1000} N_i/N_T$ decreased very significantly with gas velocity for the wide PSD, which means the concentration of particles or "fines" in the voids increased due to enhancement of relative movement between the two phases in fluidized bed of particles having a wide size distribution. For the bed with a narrow PSD the change of $\sum^{(I_o/I)_i<1000} N_i/N_T$ with gas velocity appears to be less significant in this range.

Comparing the measurement results for particles of bimodal size distribution with those for the wide size distribution, as shown in Figs. 5.8 and 5.9, we found that the difference of solids concentration in voids is insignificant, although at higher gas velocities solids concentration in voids for a bimodal PSD appears to be lower than for a wide PSD.

The effect of the PSD on the frequency of voids in fluidized bed is dependent on the superficial gas velocity, as shown in Fig. 5.10. For $U \leq 0.4$ m/s, the PSD effect on the frequency of voids seems insignificant, consistent with the experimental results of Ip (1988). For higher gas velocities, however, the frequency of the detectable voids in the bed of wide PSD was much smaller than that of the narrow size distribution, suggesting a progressive change towards a structure of greater homogeneity in the bed of wide PSD.

When an isolated bubble rises through a fluidized bed there is an upwards flow (often called a throughflow) from bottom to top of the void relative to the bubble, because the void offers a path of low resistance to gas seeking to rise from the bottom of the bed to the bed surface under the overall pressure gradient. The average magnitude of the relative (or throughflow) velocity can be taken as 3 U_{mf} for three-dimensional beds (Davidson and Harrison , 1963). This value only applies to isolated spherical bubbles (Clift et al, 1972) and for Group B powders, since the dense phase is assumed to correspond to the bed under minimum fluidization (rather than minimum bubbling) conditions. Considering the difference between Group A and Group B powders, we assume a typical throughflow velocity of 3 Φ U_{mf} in a freely fluidized system, where $\Phi = U_{mb}/U_{mf}$ is unity for Group B powders and > 1 for Group A. The coefficient 3 allows for some bubble interaction.

Consider a typical void rising in a fluidized bed. Imagine that into this void a small group of particles having a size distribution identical with the overall bed size distribution is introduced (either from above or below) at a particular time. If these particles are separated widely enough that hindered settling effects are of second order importance, the magnitude of the velocity of a particle relative to the void will tend towards a value

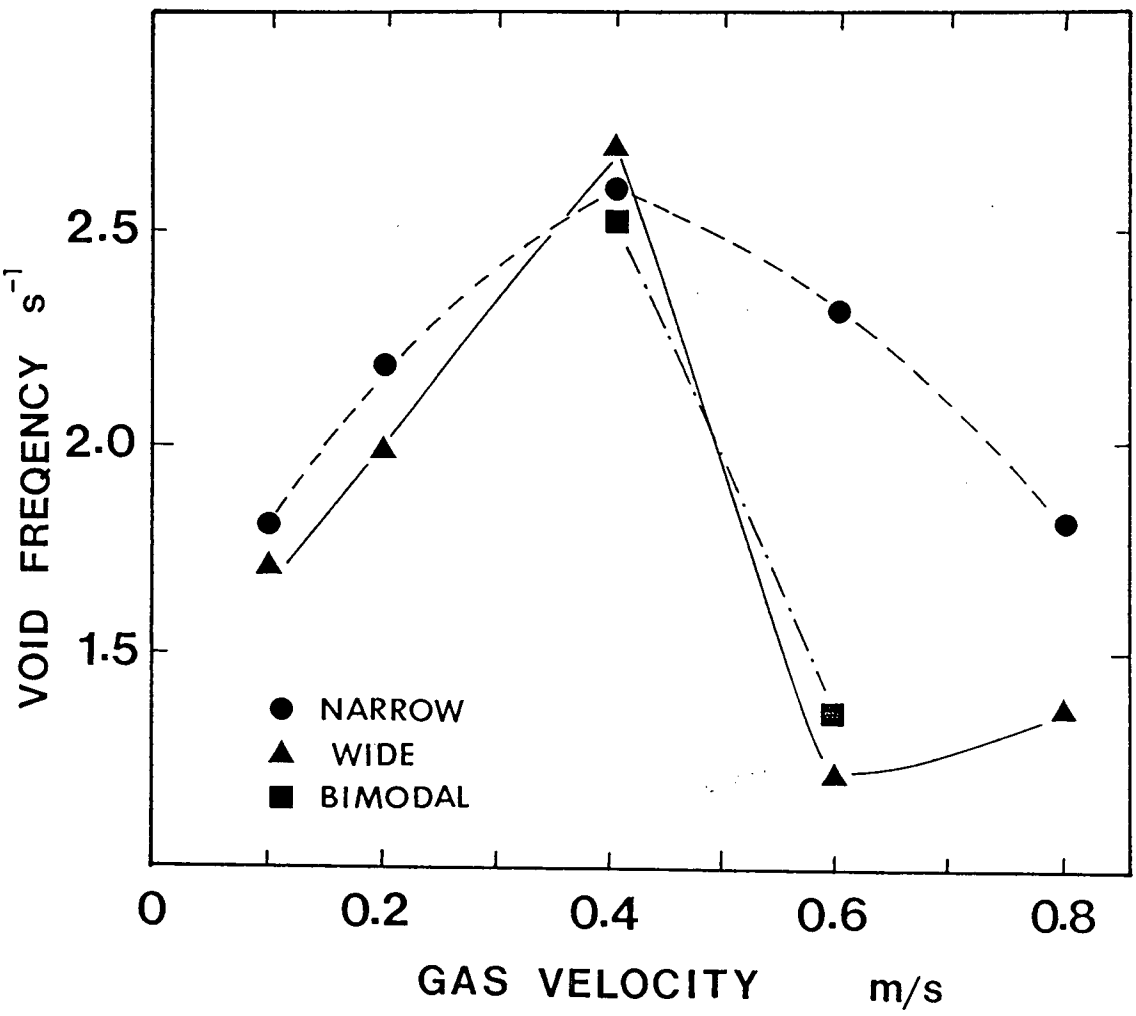

Figure 5.10: Influence of PSD on the frequency of detectable voids (i.e. with the solids concentration less than 5% by volume) at different gas velocities and at $z = 0.85$ m

of order

$$(U_{rel})_i = \mid 3\Phi U_{mf} - U_{Ti} \mid \tag{5.7}$$

where U_{Ti} is the terminal settling velocity of a particle in the i^{th} discrete size interval. For the Group A powders which are characteristic of fluid bed catalytic processes, the minimum fluidization velocity is given (Grace, 1982) by

$$U_{mf} = 7.5 \times 10^{-4} g \Delta\rho \bar{d}_p^2 / \mu \tag{5.8}$$

For fines in these Group A particles, furthermore, the terminal settling velocities are given by Stokes law, i.e.

$$U_{Ti} = g \Delta\rho d_{pi}^2 / (18\mu) \tag{5.9}$$

Substitution of Eqns. 5.8 and 5.9 into Eqn. 5.7 leads to

$$(U_{rel})_i = \frac{g\Delta\rho}{18\mu} \mid (0.0405\Phi\bar{d}_p^2 - d_{pi}^2) \mid \tag{5.10}$$

The volumetric concentration of each particle size fraction inside the voids will be proportional to the time spent by particles of that size inside the bubbles, and this, to a first approximation, will be proportional to $(U_{rel})_i^{-1}$. Assuming that the overall mass of particles in the voids is much less than that of the total mass of particles in the system, the mass fraction of particles of size i in the void phase can then be estimated from

$$(f_i)_v = \frac{f_{i,o}/(U_{rel})_i}{\sum f_{i,o}/(U_{rel})_i} \tag{5.11}$$

It is clear from the above analysis that particles with d_{pi} considerably smaller than $\bar{d}_p$, and especially particles of order $\Phi^{0.5}\bar{d}_p/5$ in diameter, where the term within the absolute value signs in Eqn. 5.10 approaches 0, will spend much longer in the bubble phase and therefore will have considerably enhanced concentration within the bubbles. Note that particles finer than this will tend to be carried upwards through the bubbles, as in the

experiments reported by Garcia et al (1973), while larger particles will fall downwards if dislodged from the roof.

It should be noted, therefore, from Eqn. 5.6, that the dependency of particle concentration, 1 - ϵ, on the ratio of light intensity, I_0/I, is affected by the mean particle size in the voids. The light intensity after passing through the suspension, I, may therefore be affected by PSD in two ways. One is via the change of particle concentration, that is, more particles are contained in voids in fluidized beds of wide PSD than for a narrow PSD. Secondly, the mean particle size in voids may differ from that of bed material since more fines are contained in voids in fluidized beds of wide size distribution, as predicted from Eqn. 5.11. Hence $\overline{d}_{p,v}$ is smaller than $\overline{d}_p$. For FCC particles of wide PSD, $\Phi = 3$, as determined by Ip (1988). The corresponding size distributions of the particles inside the voids in a bed composed of such a size distribution, calculated from Eqns. 5.10 and 5.11, are shown in Fig. 5.11, compared with the size distribution of the overall bed material, and $\overline{d}_{p,v} \approx 0.65\ \overline{d}_p$. For a fluidized bed of narrow size distribution, however, the mean particle size in voids is bound to be nearly the same as that of the overall bed material. The decrease of I therefore may also be caused by $\overline{d}_{p,v}$ being less than $\overline{d}_p$. It is found from our experiments on the PSD effect on the conversion of ozone decomposition achieved in fluidized bed reactors (Chapter 3), that both of these factors appear to be important.

It would be best therefore to be able to distinguish the two factors, i.e. to determine both (1 - ϵ) and $\overline{d}_{p,v}$. Unfortunately, it is difficult to solve this problem, i.e. to measure the particle concentration and the size distribution simultaneously. In some related work reported recently (Brown et al, 1988; Hayashi, 1988), a photometric technique, including a complex semiannular silicone photodetector array light diffraction system, could only be used to determine the volumetric concentration and size distribution of particles suspended in liquids.

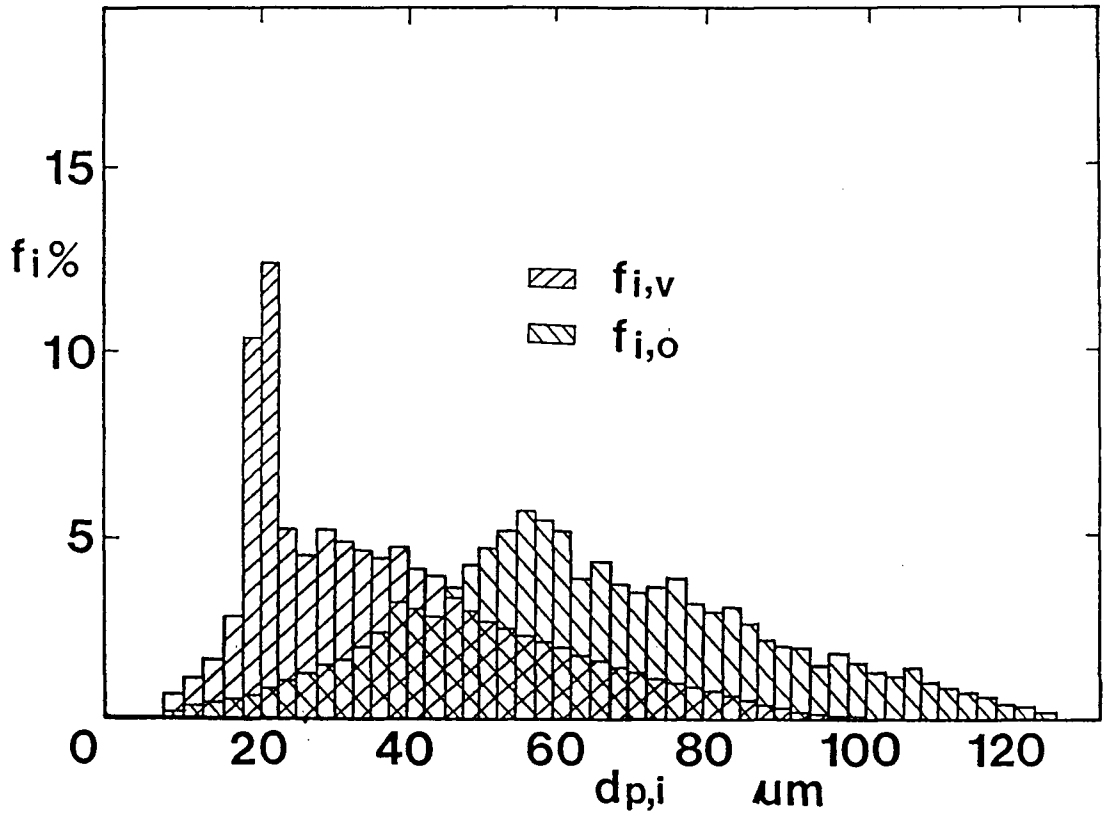

Figure 5.11: Particle size distribution for an industrial fluid cracking catalyst, $f_{i,o}$, and corresponding calculated size distribution inside voids, $f_{i,v}$.

In another study, a gamma-radiation absorption densitometer was used to try to measure the concentration and mean size of particles in voids simultaneously. For radiation attenuation (Weimer et al, 1985)

$$1 - \epsilon = \frac{\ln(I_0/I)}{\mu L} \tag{5.12}$$

where μ is the attenuation coefficient. It is clear from Eqn. 5.12 that the measured I is not influenced by $\overline{d}_{p,v}$. An attempt was made in the present work to use a gamma-ray densitometer, purchased for work in the UBC circulating fluidized bed combustion pilot plant, to determine the volumetric concentration of particles dispersed in voids in the two-dimensional column. This attempt, however, failed due to the fact that the difference between the absorbance in the empty column and with particles present was too small to be measured, since the gauge was designed to be used in a system having a much higher total absorbance.

Even if the particle concentration and particle size effects could not be separated, the following conclusions can be drawn from the experimental photometric measurements:

1. The particle concentration in most bubbles or voids in a fluidized bed of Group A particles was higher than what has been determined previously for Group B particles, i.e. 1 - ϵ was higher than the value of 1% reported for Group B particles (Kunii and Levenspiel, 1969). More than 70% of the voids contained more than 2.5% particles by volume, even for FCC particles of narrow size distribution.

2. The value of I_0/I depends on the PSD. The PSD affects both the overall particle concentration in voids and/or the relative fines content in the dilute phase. The experimental results are also consistent with the finding from Chapter 3 that more particles and a greater proportion of fines are carried by gas in voids in beds of wide PSD than in beds of narrow PSD.

3. The results of these measurements also provided information on other related parameters, such as void frequency. As shown in Fig. 5.10, for $U > 0.5$ m/s, the frequency of the detectable voids in the bed of wide PSD was much smaller than for the narrow size distribution.

5.2 Effect on the Bubble or Void Size

Bubble or void size is one of the most important indices in the design of bubbling fluidized bed reactors, since it is related to various important bed properties such as bed expansion, gas interchange between phases, particle circulation rate, heat transfer, and elutriation of fine particles from the bed surface. Numerous measurements of bubble size have been made, and many correlations have been presented (e.g. Kato and Wen, 1969; Mori and Wen, 1975; Rowe, 1976; Darton et al, 1977; Werther, 1978). These correlations have mainly been based on experimental results in fluidized beds of coarse (Group B or D) particles. In fluidized beds of fine (Group A) powders, recent work (Werther, 1984; Kai and Furusaki, 1985; Kai et al, 1987; Horio and Nonaka, 1987) has shown that the bubbles grow in size until a steady bubble size, or so-called maximum stable bubble size, is reached as a result of an equilibrium between bubble coalescence and splitting. The latter can be explained on the basis of bubble stability in fluidized beds (Grace, 1970; Clift and Grace, 1972; Clift et al, 1974). Although some modifications of the published bubble size correlations have been made to account for the bubble size in fluidized beds of Group A particles (Werther, 1984; Horio and Nonaka, 1987), less information has been reported on the effect of PSD on the void size in fluidized beds.

The effect of the particle size distribution on the bubble size, or void size at higher gas velocities, was investigated in this study by means of two methods: visual measurement and indirect evaluation from the determination of pressure fluctuations in a fluidized bed.

The former is discussed here, while the latter is described in Chapter 6.

The PSD effect on the void size was visually investigated in the two-dimensional fluidized bed. The static bed height was 0.9 m, and the superficial gas velocity ranged from 0.05 to 0.6 m/s. For each kind of particles and at each gas velocity, bubble or void phenomena were recorded by a video recorder (SONY SL-2000 with SONY HVC-2800 camera) at 30 frames/s for a period of 10 minutes. The phenomena were also recorded by a CANON T-70 still camera with 1/250 sec. shutter speed and F1.8 aperture. For each operating condition, 8 photographs were taken. The film used was Kodacolor Gold 400. The experimental schematic is shown in Fig. 5.12.

The average bubble size measured at a height 0.85 m above the distributor and the maximum bubble size in the bed are shown in Table 5.1. The effect of PSD on the bed expansion is also given in Table 5.1. Some photographs portraying bubble phenomena in beds of particles with different PSD under various conditions appear in Figs. 5.13 to 5.18.

Figs. 5.13 to 5.18 indicate that there is a significant effect of PSD on the size of bubbles in the fluidized bed, except at low gas velocity ($U < 0.2$ m/s) for the gas-solid system used in our experiments. The void size was usually smallest for the wide size distribution, while the difference between the beds with bimodal and wide PSD was small. Voids achieved the largest size in the bed with a narrow PSD, probably due to their high bed "viscosity" (Grace, 1970) or poor "fluidity".

Experimental bubble sizes measured by Werther (1984) using capacitance probes in a three-dimensional fluidized bed of wide size distribution FCC particles in a column of 0.45 m diameter at gas velocities < 0.2 m/s were lower than values obtained in the two-dimensional bed in the present study. The void sizes observed in our experiments, however, are similar to the results of Rowe and MacGillivray (1980) in a fluidization column of 140 mm diameter obtained using X-ray cinephotography. It is likely that

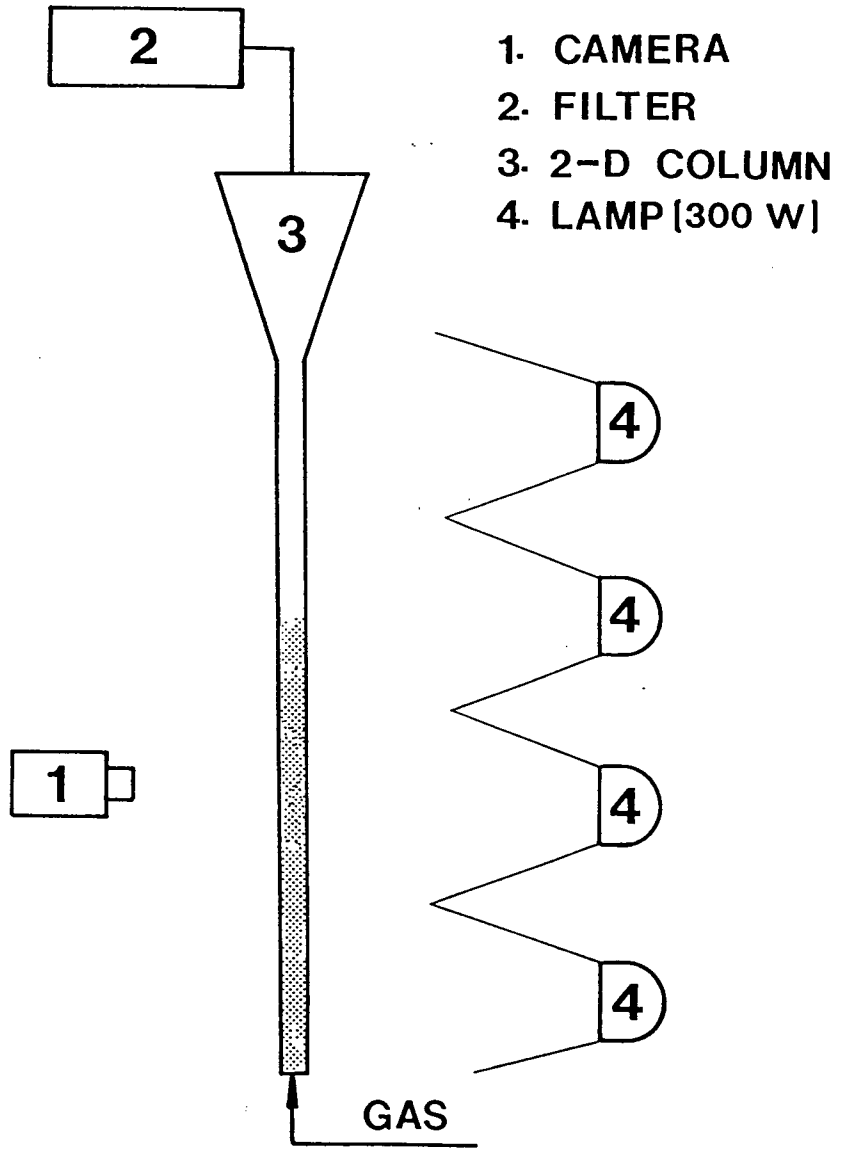

Figure 5.12: Schematic of experimental apparatus for observing bubble phenomena

Table 5.1: Void size and bed expansion in two dimensional fluidized bed

Particle	Size distribution	Gas velocity, m/s	H_f/H_{mf}	$D_{b,a}, mm^{\star}$	$D_{b,max}, mm^{\star\star}$
N-FCC	wide	0.05	1.23	27	31
N-FCC	wide	0.2	1.37	51	81
N-FCC	wide	0.4	1.55	58	83
N-FCC	wide	0.6	1.80	55	70
N-FCC	narrow	0.05	1.12	31	40
N-FCC	narrow	0.2	1.26	67	95
N-FCC	narrow	0.4	1.41	70	101
N-FCC	narrow	0.6	1.65	72	107
S-FCC	wide	0.2	1.33	44	74
S-FCC	narrow	0.2	1.26	63	93
S-FCC	bimodal	0.2	1.30	48	82
S-FCC	wide	0.6	1.73	52	76
S-FCC	narrow	0.6	1.63	71	105

$\star$ $D_{b,a}$ is the average equivalent bubble or void size at z = 0.85 m.
$\star\star$ $D_{b,max}$ is the maximum size observed over the 10 minutes period at z = 0.85 m.

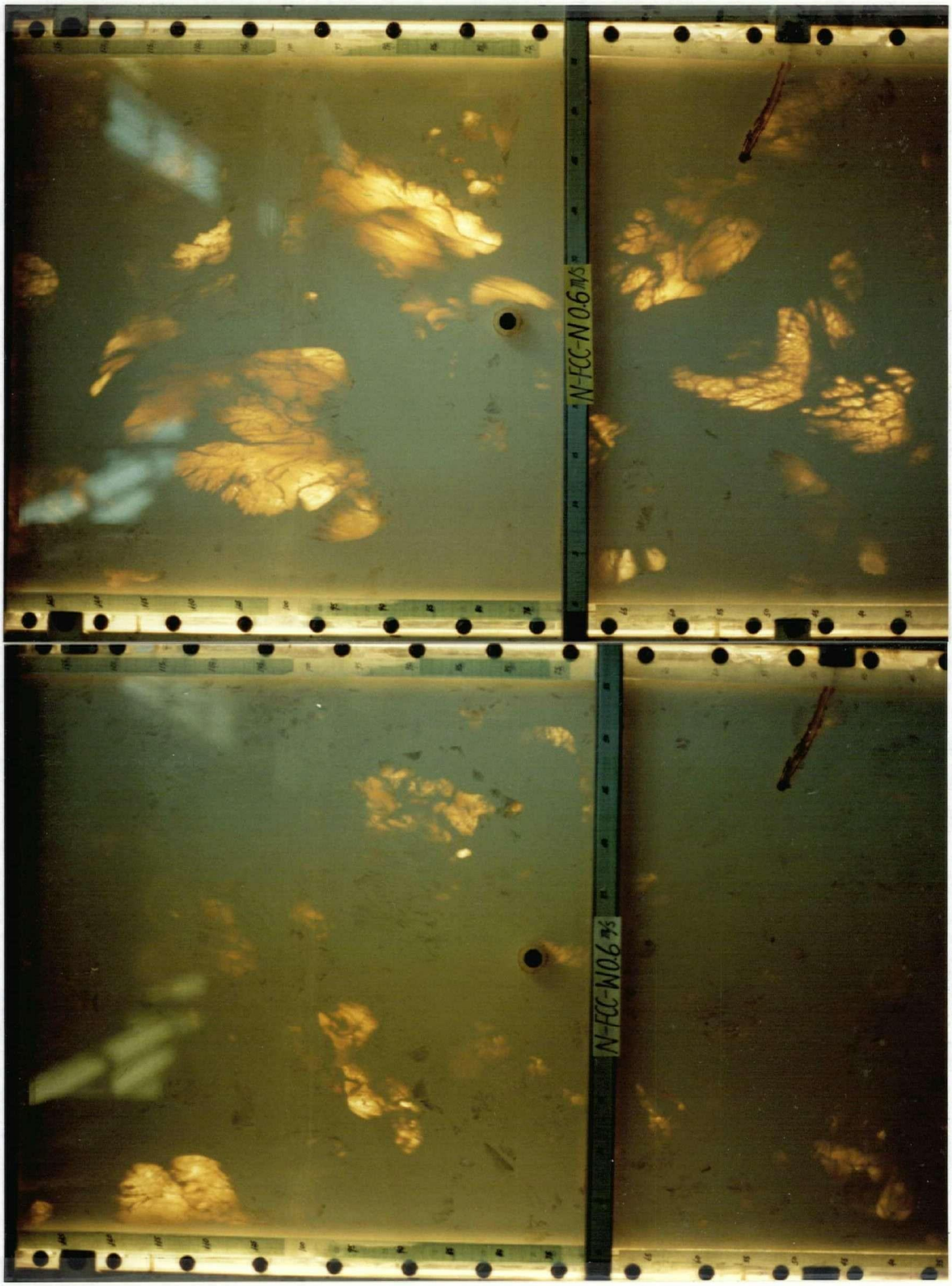

Figure 5.13: PSD effect on the properties of bubbles in fluidized beds of N-FCC particles at $U = 0.6$ m/s. Left and right photographs correspond to wide and narrow size distributions respectively.

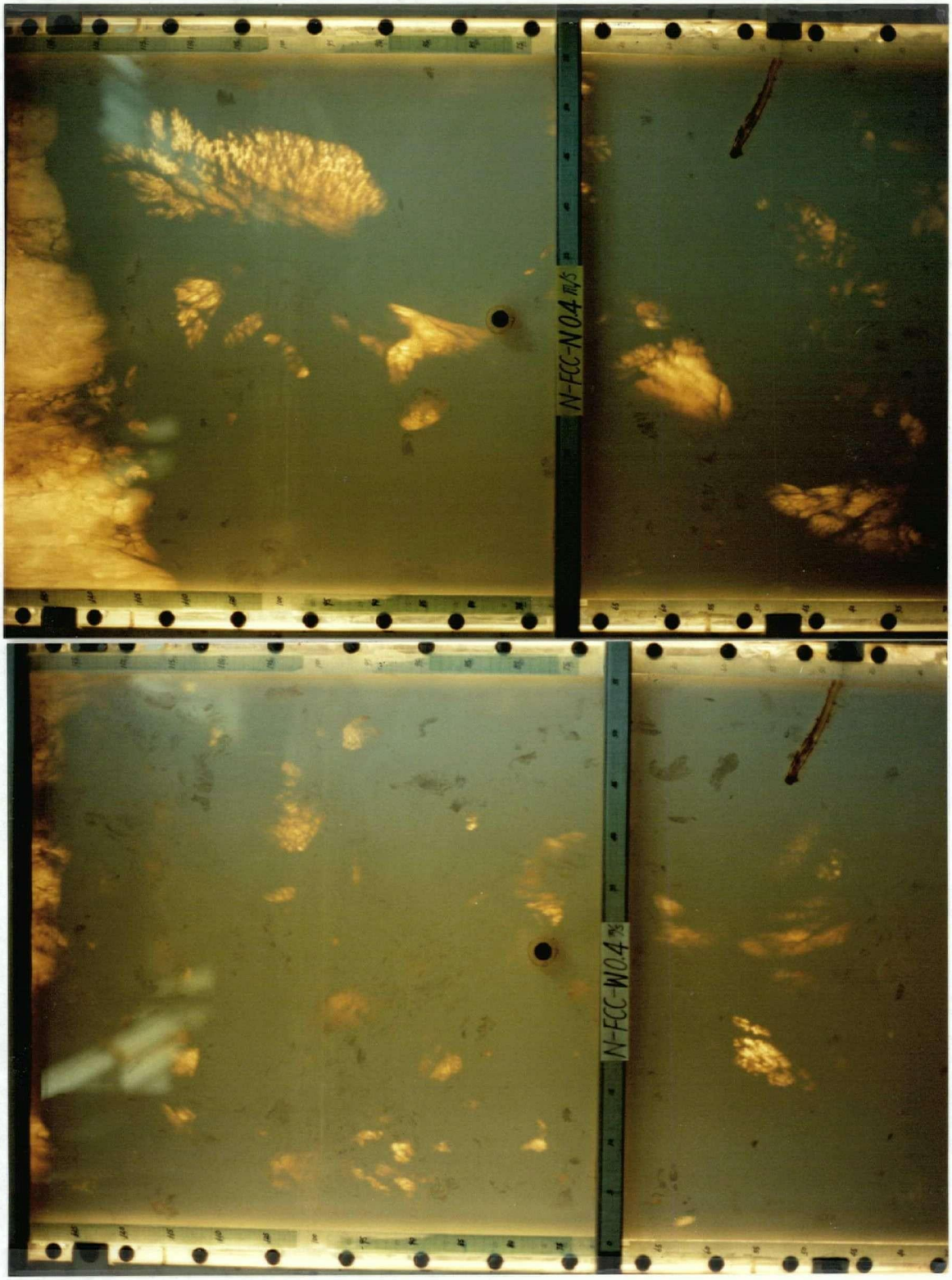

Figure 5.14: PSD effect on the properties of bubbles in fluidized beds of N-FCC particles at $U = 0.4$ m/s. Left and right photographs correspond to wide and narrow size distributions respectively.

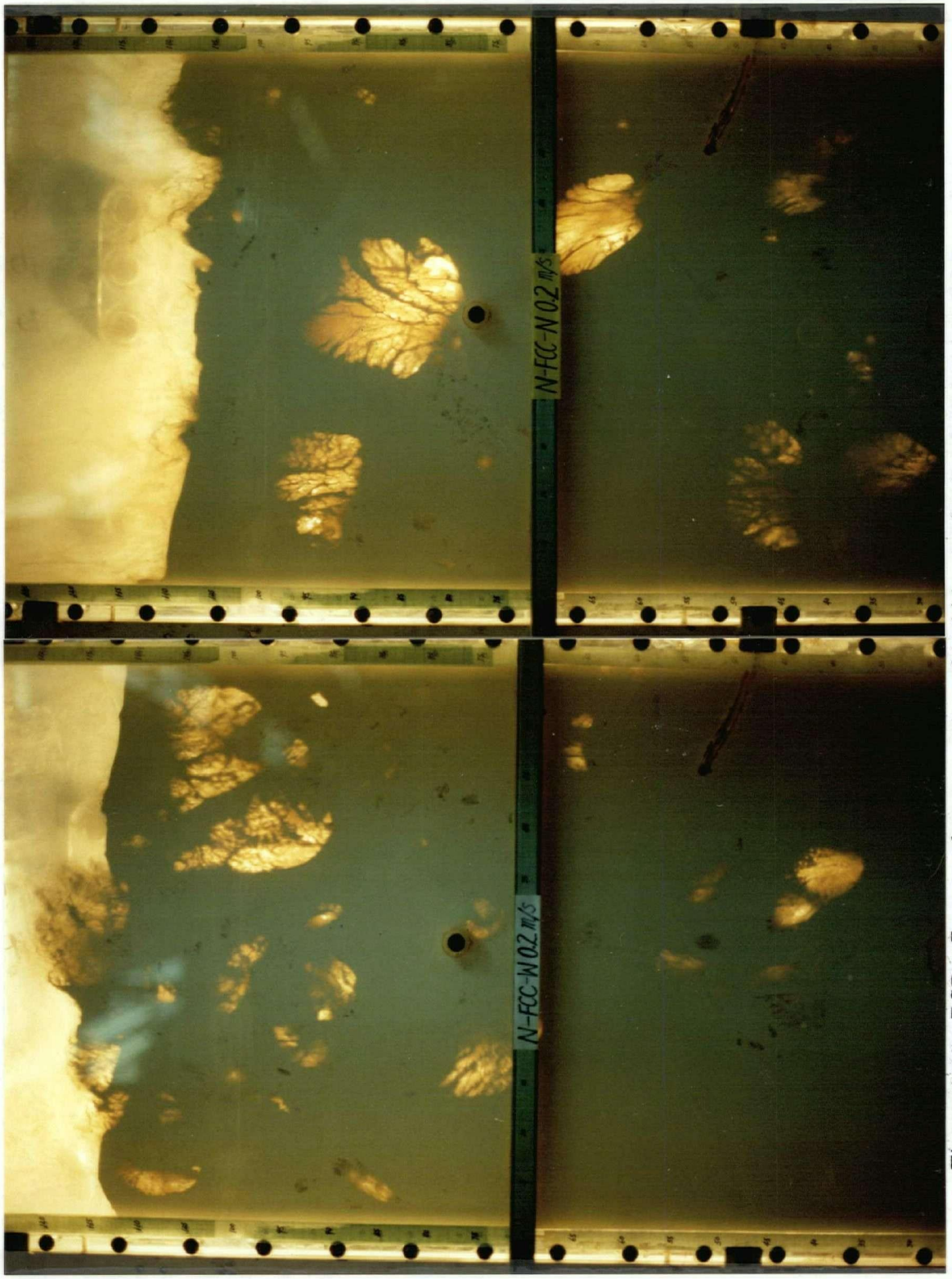

Figure 5.15: PSD effect on the properties of bubbles in fluidized beds of N-FCC particles at $U = 0.2$ m/s. Left and right photographs correspond to wide and narrow size distributions respectively.

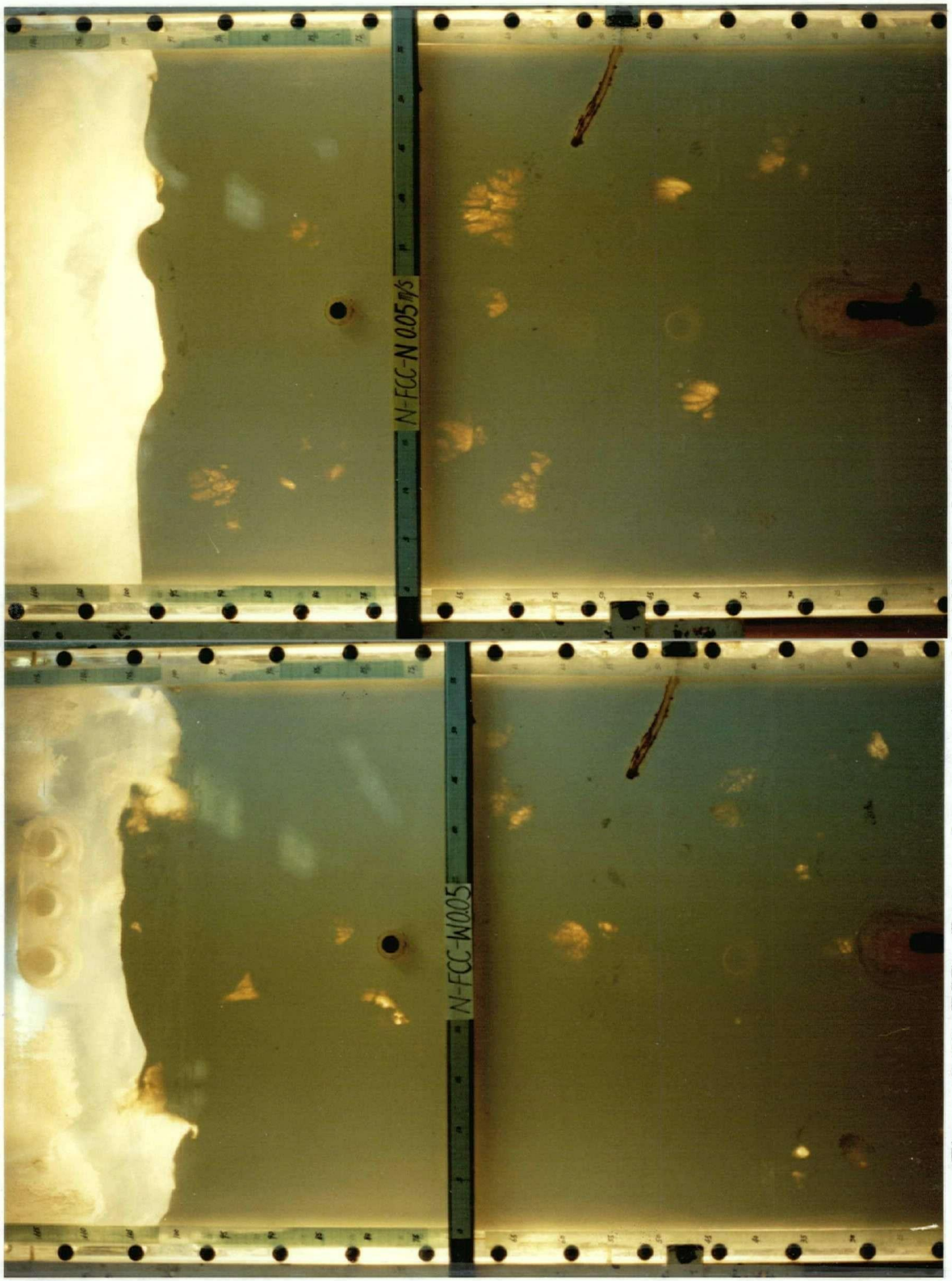

Figure 5.16: PSD effect on the properties of bubbles in fluidized beds of N-FCC particles at $U = 0.05$ m/s. Left and right photographs correspond to wide and narrow size distributions respectively.

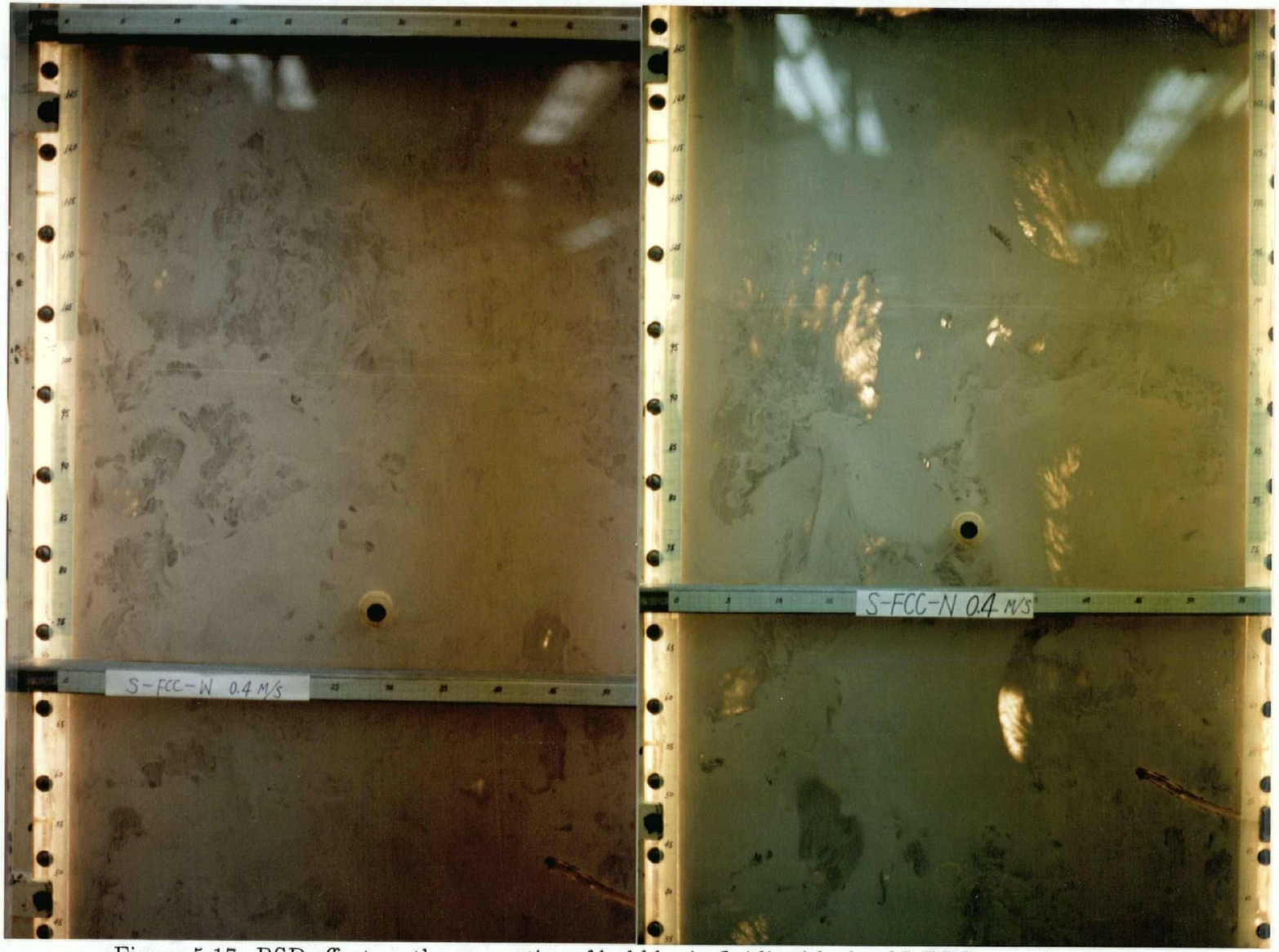

Figure 5.17: PSD effect on the properties of bubbles in fluidized beds of S-FCC particles at $U = 0.4$ m/s. Left and right photographs correspond to wide and narrow size distributions respectively.

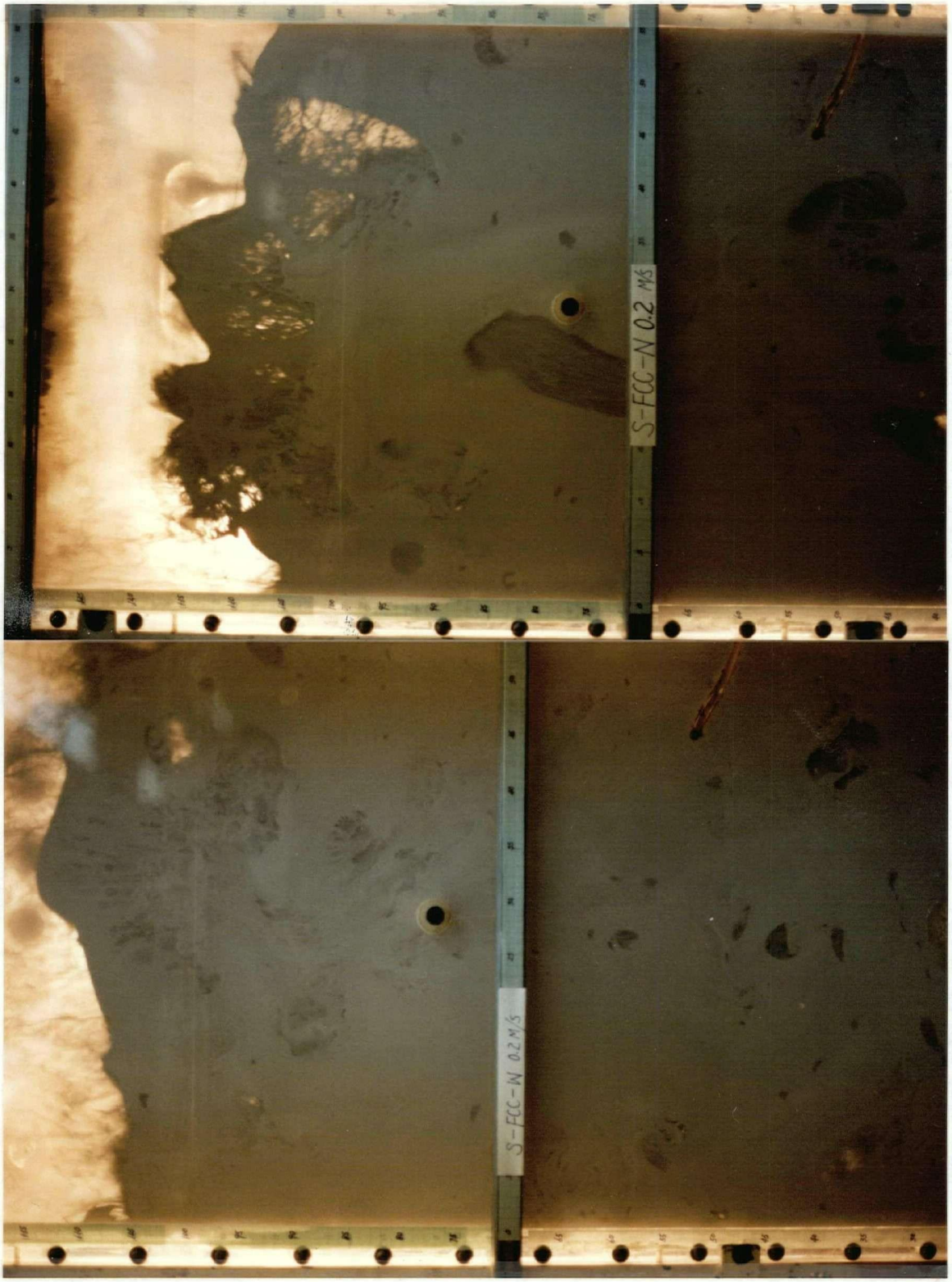

Figure 5.18: PSD effect on the properties of bubbles in fluidized beds of S-FCC particles at $U = 0.2$ m/s. Left and right photographs correspond to wide and narrow size distributions respectively.

the wall effect in the two dimensional bed or interference of the capacitance probe are responsible for differences. However, in our study, we are less interested in the absolute value of bubble size in the fluidized bed than in the relative change caused by the PSD influence.

The following qualitative and quantitative conclusions can be drawn from the photographs:

1. The bubble size is dependent on the PSD, especially as the gas velocity increases, as shown in Table 5.1.

2. As the gas velocity is increased, bubble shape becomes irregular, and the boundary between the dense phase and the dilute phase is less distinct. For FCC particles of wide and bimodal PSD, these features are especially noticeable at gas velocities beyond about 0.5 - 0.6 m/s.

3. More particles are seen inside voids of fluidized beds of Group A particles than has previously been observed in beds of Group B particles (see Section 5.1).

4. The bed expansion is also affected by the PSD, and is lowest for bed of narrow PSD. The equation

$$\frac{H}{H_{mf}} = 1 + \frac{U - U_{mf}}{0.711(gD_b)^{1/2}}, \tag{5.13}$$

based on the two-phase theory (Davidson and Harrison, 1963), is only suitable to express the bed expansion for particles with narrow PSD at lower gas velocities, as shown in Fig. 5.19. For FCC particles of wide and bimodal PSD, and at higher gas velocity, the traditional two-phase theory must be modified, for example, by the n-type two-phase theory, as suggested by Grace and Harrison (1969), to avoid overestimation of the visible bubble flow (Grace and Clift, 1974) and underestimation of the dense phase voidage (Abrahamsen and Geldart, 1980; Sun et al, 1983).

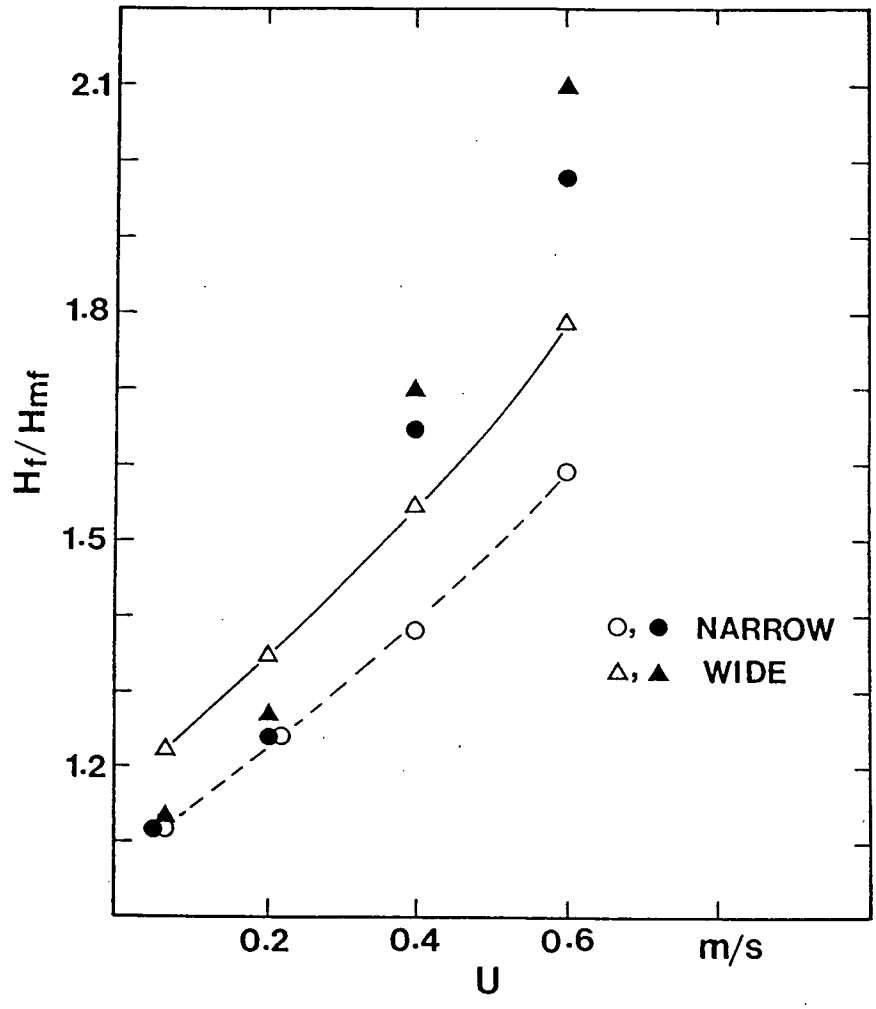

Figure 5.19: PSD effect on the bed expansion for N-FCC particles. Open symbols are experimental values; filled in symbols are the corresponding predictions from eqn. 5.13 with experimental values of $D_{b,a}$.

Chapter 6

Pressure Fluctuations and Regime Transitions

Pressure fluctuations have been used as an index of the "quality" of fluidization. The fluctuations are closely related to the gas-solid movement and depend in a complex manner on the gas and particle properties, bed geometry, and operating conditions. In this study, the character of pressure fluctuations and fluidization regime transitions, especially the transition from bubbling and/or slugging to turbulent fluidization, determined from the fluctuation measurement, were evaluated to compare the hydrodynamic performance of fluidized beds containing particles of different size distribution, but equal mean diameter and nearly the same density.

6.1 Brief review of previous work

Pressure fluctuations have been used to define the quality of fluidization by many investigators and plant operators (e.g. Shuster and Kisliak, 1952; Winter, 1968; Schnitzlein and Weinstein, 1988), with small amplitude and rapid fluctuations considered to be associated with good quality fluidization. Based on the analysis of the probabilistic and statistical characteristics of pressure fluctuations along a fluidized bed, it is also possible to estimate the size and the rising velocity of bubbles and slugs where these occur (Lirag and Littman, 1971; Fan et al, 1981; Fan et al, 1983). The average bubble size appears to be directly related to the standard deviation of the amplitude of pressure fluctuations (Sadasivan et al, 1980; Kai and Furusaki, 1985; Geldart and Rhodes, 1986).

Pressure fluctuations have also been used to monitor operating conditions and to

distinguish between hydrodynamic regimes in fluidized beds, and to explore the characteristics of these regimes (e.g. Yerushalmi and Cankurt, 1979; Li and Kwauk, 1980; Satija and Fan, 1985; Jin et al, 1986; Brereton, 1987; Lee and Kim, 1988; Sun and Chen, 1989). Generally speaking, the transition from bubbling (or slugging) to turbulent fluidization is gradual with increasing superficial gas velocity.

The character of fluidized beds operated at high gas velocities and the dependency of fluidization regime on the superficial gas velocity have been the subject of a number of investigations. In early work, Lanneau (1960) investigated bubbling phenomena in a fluidized bed (D_T = 0.075 m) of alumina catalysts ($\overline{d}_p$ = 75 μm) over a wide range of gas velocity (0.03 to 1.5 m/s) with the use of capacitance probes. He reported that the performance of fluidized beds appeared different in three gas velocity ranges:

1. low gas velocities (0.03 m/s $< U <$ 0.3 m/s), where two-phase character of the fluid bed was prominent, and discrete bubbles containing few solids were present.

2. intermediate gas velocity (0.3 m/s $< U <$ 0.9 m/s), where the bubbles began to break up as the velocity was increased, and smaller voids containing a greater percentage of the total solids were observed.

3. higher gas velocities (0.9 m/s $< U <$ 1.5 m/s), where the condition of almost uniform or "particulate" fluidization was approached, coinciding with rapid entrainment of solids from the column.

Kehoe and Davidson (1971) detected bubbles (or slugs) with increasing gas velocity in 50 and 100 mm diameter fluidized beds of fluid cracking catalyst. They described the breakdown of slugs to a so-called "turbulent" fluidization regime at gas velocities between 0.45 and 0.5 m/s. Massimilla (1973) evaluated the bubble size and size distribution inside a fluidized bed with catalysts of mean size and size distribution close to typical industrial FCC catalysts using a capacitance probe at superficial gas velocities up to 0.65 m/s. At gas velocities above 0.4 m/s, flow conditions were found to degenerate into the

turbulent regime, where the probe detected a sequence of extended low density signals, intermittently followed by bursts of short perturbances. He also provided a laboratory demonstration of the favourable solid-gas contacting efficiency of the turbulent fluidized bed reactors for propylene conversion to acrylonitrile in a pilot reactor. Conversion for the turbulent bed was higher than would have expected from a two-phase bubbling model.

Yerushalmi et al (1978) characterized the transition from the bubbling (or slugging) regime to the turbulent regime by two gas velocities, U_c, the velocity at which the pressure fluctuations reach a maximum, and U_k, the velocity at which the decay of the pressure fluctuations begins to level off. Some investigators (Yerushalmi and Cankurt, 1979; Horio et al, 1989) view U_c as the end of the bubbling or slugging regime and U_k as the onset of the turbulent regime; others (e.g. Yang, 1984; Jin et al, 1986; Lee and Kim, 1988; Judd and Goosen, 1989) have treated U_c as the gas velocity corresponding to the onset of turbulent fluidization. Still others (Satija and Fan, 1985; Brereton, 1987) found that it is difficult to define U_k directly from the amplitude of pressure fluctuations, at least for some particles.

In the bubbling and slugging regimes, pressure fluctuations are mainly associated with the formation, motion and splitting of bubbles or slugs as they rise along the bed (Fan et al, 1981), and the amplitude of the pressure fluctuations depends on the size of bubbles and/or slugs (Sadasivan et al, 1980; Kai and Furusaki, 1985; Geldart and Rhodes, 1986). U_c can therefore be regarded as the gas velocity at which bubbles reach their maximum size, dependent on the character of the gas-solid system and the geometry and size of the fluidization column (Sun and Chen, 1989). Previous work has indicated that U_c increases with particle size and density (Yerushalmi and Cankurt, 1979; Grace, 1982; Jin et al, 1986) and decreases with column size (Sun and Chen, 1989; Judd and Goosen, 1989).

Lee and Kim (1988) calculated various statistical properties such as mean amplitude, standard deviation, skewness and flatness of pressure fluctuations to determine U_c. They

found that U_c values obtained from these various methods were very similar.

The dependence of fluidization regime on the gas velocity is influenced by such factors as column diameter. Experimental results (Kehoe and Davidson, 1971; Thiel and Potter, 1977; Sun and Chen, 1989) indicate that for a given gas-solid system the transition from the bubbling (or slugging) regime to the turbulent regime in columns of smaller diameter appears later than in columns of larger diameter.

It is clear that the transition velocity from bubbling to turbulent fluidization increases with particle size and density. Little information, however, is available on the effect particle size distribution. Kehoe and Davidson (1971) added finer particles (15 μm $< d_p <$ 43 μm) to coarser fractions (40 μm $< d_p <$ 90 μm) and found that the transition velocity decreased from 0.5 m/s to 0.32 m/s. When "fines" are added to "coarse" particles, however, both the particle size distribution and the mean size are changed. Results on the effect of size distribution for solids having comparable mean size are lacking (Yerushalmi, 1986).

6.2 Experimental Equipment and Procedure

Pressure taps were installed vertically along the 102 mm diameter column with a spacing between adjacent taps of about 0.25 m, as shown in Fig. 2.10. The inside end of each tap was covered with a screen to prevent particles from entering. The two ports were always covered by dense phase, to avoid apparent regime transitions noted by Geldart and Rhodes (1986). Each tap was connected to a differential pressure transducer, which had two input channels and produced an output voidage proportional to the pressure difference between the two input channels. Differential pressure signals at different bed heights and different operating conditions were logged to an IBM-XT computer via an A/D converter. Each signal was logged for 40 s at a rate of 100 points per second and

recorded simultaneously in analogue format on a UV chart recorder.

Static bed heights of 0.15, 0.40, 0.70, 1.0 m were used in the experiments. A wide range of superficial gas velocities (from 0.04 to 1.75 m/s) was tested so that the bubbling, slugging, turbulent and fast fluidization regimes would all be included.

6.3 Influence of PSD on Pressure Fluctuations

The differential pressure fluctuations allow the two phase character of the fluidized bed to be investigated. A dimensionless standard deviation of the pressure drop or the pressure fluctuation intensity, defined as

$$F_p = \frac{\sqrt{\sum_{i=1}^{N}(\Delta P_i - \overline{\Delta P})^2/N}}{\overline{\Delta P}} \tag{6.1}$$

is used to express the amplitude of the pressure drop fluctuation, where N is the total number of data points, while $\Delta\overline{P}$ is the mean pressure drop across the measured section and ΔP_i is the instantaneous pressure drop across the same section.

Since bubbles (or slugs) are the major cause of the pressure fluctuation in aggregative fluidized beds (Fan et al, 1981), while the average bubble size appears to be directly related to the amplitude of pressure fluctuations (Kai and Furusaki, 1985; Geldart and Rhodes, 1986), analysis of the pressure fluctuations is useful in understanding the influence of the particle size distribution.

The average bubble size tends to increase with distance above the distributor due to coalescense and interaction between the bubble phase and the emulsion phase. The local bubble size in bubbling fluidization is commonly (e.g. Kato and Wen, 1969; Darton et al, 1977; Werther, 1978) expressed by an equation of the form:

$$d_b = d_{bo} + A(U - U_{mf})^B z^C \tag{6.2}$$

where d_{bo} is the initial bubble diameter at the distributor and A, B and C are constants which may depend on mean particle size (Kato and Wen, 1969). Given the dependence of pressure fluctuations on bubble behaviour, it is reasonable to seek an expression for the amplitude of pressure fluctuations of analogous form, i.e.

$$F_p = F_{po} + a(U - U_{mf})^b z^c \tag{6.3}$$

where F_{po} is the pressure fluctuation intensity at z = 0 and a, b and c are constants.

Figures 6.1 and 6.2 show the variation of F_p with superficial gas velocity for N-FCC powders with different size distributions. It is clear that the amplitude of differential pressure fluctuations is influenced by the PSD. Among the three size distributions used in our experiments, the narrow blend gives the highest F_p at given operating conditions, except at very low gas velocities ($U < 0.2$ m/s), where the values of F_p are very similar for the different PSD's.

It can also be observed from Figs. 6.1 and 6.2 that F_p first increases with the gas velocity, then reaches a peak, and finally decreases gradually. This behaviour is similar to results reported by other workers (e.g. Yerushalmi, 1986) and to our findings in a two-dimensional bed column described in Section 5.2. It was also found that F_p is dependent on the location of the measuring interval, even when all the pressure ports are immersed in the dense bed. For $H_{mf} < 0.7$ m, F_p appears to increase with the vertical position coordinate z. However, when the static bed height was increased to 1 m, F_p did not always increase with z. For the wide blend, F_p increased with z in the lower part, but decreased with z in the upper part of the bed. For narrow blend particles, the behaviour was more complex: for U < 0.7 m/s, F_p was found to increase with z, while F_p for the higher measurement interval reached a maximum, then increased with z over the lower part of the bed, while decreasing over the upper section. This suggests that if the bed is deep enough, there may be two different regions, depending on the PSD, among other

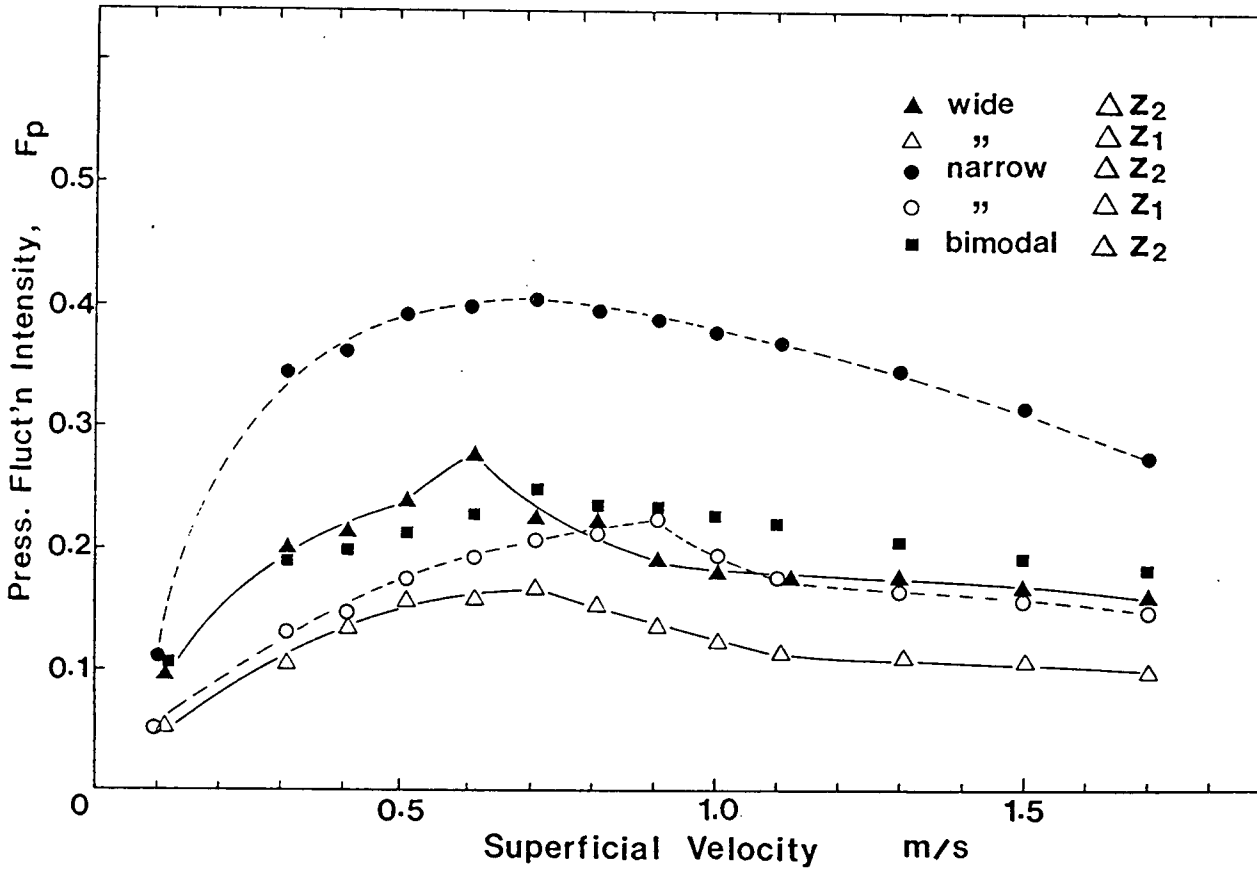

Figure 6.1: Effect of PSD on pressure fluctuations with $H_{mf} = 0.7$ m over intervals Δz_1 (30 to 280 mm), Δz_2 (430 to 680 mm) and Δz_3 (680 to 930 mm).

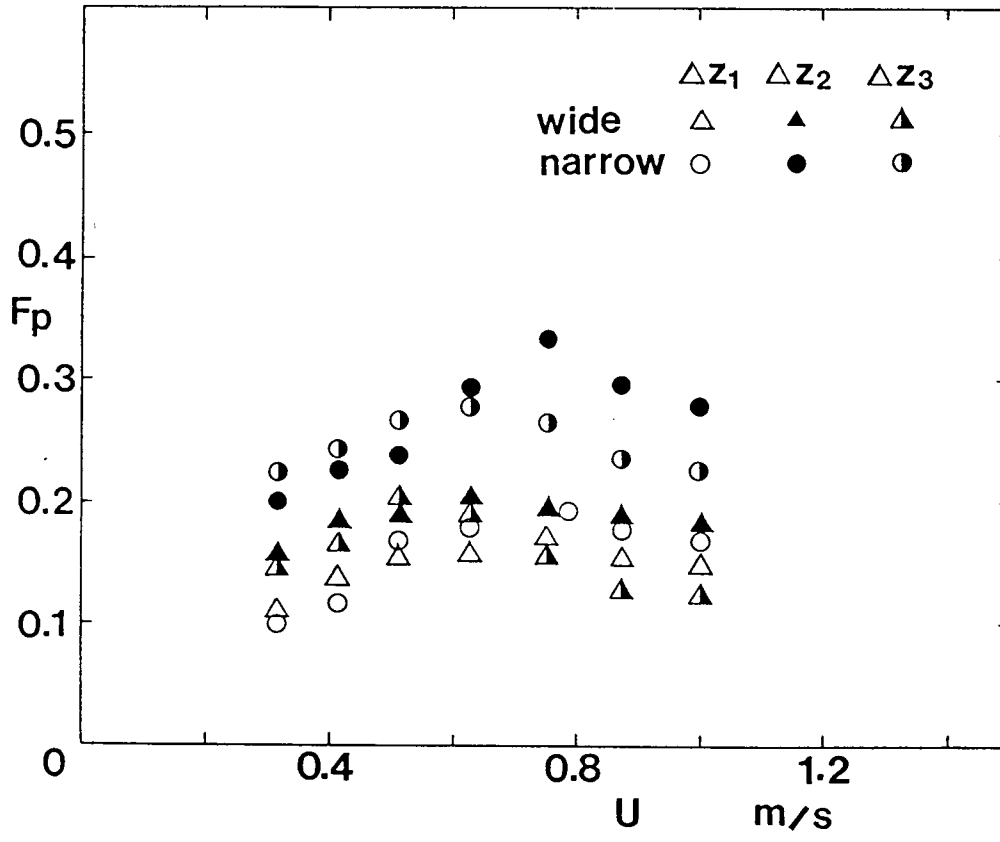

Figure 6.2: Effect of PSD on pressure fluctuations with $H_{mf} = 1$ m over intervals Δz_1, Δz_2 and Δz_3 (as in Fig. 6.1).

parameters. For particles of wide PSD in the lower region, bubble size increases with z. Bubble coalescence and growth are predominant in this region, and the coefficient c in eqs. 6.2 and 6.3 is positive. However, in the upper part of the bed, bubble splitting becomes significant and bubble size (and hence pressure fluctuations) approach limiting values.

It can be seen that the difference between the narrow and wide size distributions increased with both gas velocity and vertical position, while $F_{p,N}$ was always greater than $F_{p,W}$. Therefore, we can obtain from equation 6.3,

$$F_{p,N} - F_{p,W} = a_N(U - U_{mf})^{b_N} z^{c_N} - a_W(U - U_{mf})^{b_W} z^{c_W} > 0 \tag{6.4}$$

where the subscript N denotes the narrow blend and W the wide blend. That is,

$$\frac{a_N}{a_W}(U - U_{mf})^{b_N - b_W} z^{c_N - c_W} > 1 \tag{6.5}$$

The assumption that the effect of PSD on $F_{p,o}$ is negligible has been used to obtain the above relationships. When the bed was operated in the bubbling regime where eqn. 6.2 is suitable, it can be found from Figs. 6.1 and 6.2 that both b_N and c_N are larger than b_W and c_W. According to eqn. 6.5, a_N, should therefore also be larger than a_W, since in the range discussed here, both (U - U_{mf}) and z are smaller than 1. That is, all three constants in eqns. 6.2 and 6.3 are related to the PSD. At the same operating conditions and height, the bubble size is dependent not only on the mean particle size, as some investigators have stated, but also on the size distribution. The PSD effect, however, has not been taken into account in any of the published correlations for bubble size.

The difference in F_p between the bimodal and wide blends seems small. At low gas velocities (before reaching the maximum value of F_p), F_p is similar for these two blends over the lower portion of the bed, while for the upper part F_p was a little higher for the wide blend than for the bimodal blend. After F_p reached its peak, however, F_p was

always greater for the bimodal blend than for the wide blend, in both the upper and lower portions of the bed.

Based on the results that the average bubble size appears to be directly related to the standard deviation of the amplitude of pressure fluctuations (Sadasivan et al, 1980; Kai and Furusaki, 1985), we can assume that the bubbles (or slugs) reach their maximum sizes at the gas velocity, U_c, where F_p reaches a maximum. The maximum bubble size and superficial gas velocity at which this is achieved can be taken as two parameters to characterize the hydrodynamic performance of fluidized systems, since at given operating conditions, gas-solid contacting can be improved by reducing the bubble (or slug) size (Grace and Clift, 1974).

Comparison of F_p for different PSD's reveals that $F_{p,max}$ of the narrow blend is much higher than for the other size distributions, especially in the upper portion of the bed, while $F_{p,max}$ for the wide blend is similar to that of the bimodal distribution. This suggests that the maximum stable bubble size in the fluidized bed with a narrow PSD is larger than for a wide or bimodal PSD, as discussed in Section 5.2. This may well be caused by the lower aeration capacity of the narrow blend (Ip, 1988) and the higher bed "viscosity" for the narrow PSD .

6.4 Influence of PSD on Regime Transitions

The PSD effect on U_{mb}, the transition velocity from the particulate to bubbling fluidization, has been reported by Abrahamsen and Geldart (1980), Sun et al (1983) and Ip (1988). For the same spent FCC particles as tested in our experiments, Ip (1988) observed that U_{mb}/U_{mf} for particles of wide size distribution was 20% more than for a narrow PSD.

The gas velocity, U_c, at which F_p reaches a maximum, can be taken as the end of the

Table 6.1: Transition velocity U_c for N-FCC particles of different size distributions over intervals Δz_1 (30 to 280 mm), Δz_2 (430 to 680 mm), Δz_3 (680 to 930 mm) and Δz_4 (930 to 1180 mm).

PSD	U_c, m/s (H_{mf} = 0.7 m)			U_c, m/s (H_{mf} = 1 m)			
	Δz_1	Δz_2	Δz_3	Δz_1	Δz_2	Δz_3	Δz_4
wide	0.72	0.62	0.50	0.71	0.62	0.50	0.38
narrow	0.90	0.75	0.65	0.78	0.75	0.63	0.50
bimodal	0.75	0.65	0.55	0.75	0.64	0.53	0.45

bubbling or slugging regime and the onset of the transition to the turbulent fluidization regime (Yerushalmi, 1986). The physical meaning of U_c is that around this velocity bubbles approach a maximum size which depends on the bed "viscosity" and the aeration capacity of the particles. At velocities below U_c, bubble coalescence appears to be predominant, while above U_c, splitting becomes frequent. The value of U_c is therefore related to bubble growth and coalesence. Low U_c implies that bubbles split more readily, resulting in an improvement in gas-solid contacting. The transition velocity, U_c, determined from the pressure fluctuation curves (as shown in Figs. 6.1 and 6.2) for different particle size distributions, with different H_{mf} and at different intervals is listed in Table 6.1.

The influence of the PSD on U_c is shown in Fig. 6.3. It is clear that the PSD does

affect the transition from bubbling to turbulent fluidization. The highest U_c is attained for the narrow blend particles, while the lowest U_c occurs for the wide distribution.

From Fig. 6.3 it can also be observed that U_c decreased with increasing z, whereas F_p increased with z. Transition to the turbulent regime appears to occur sooner for deeper beds. This suggests that the growth of bubbles in fluidized bed may trigger the regime transition from bubbling to turbulent fluidization. It also implies that there does exist an "effective" maximum stable size (Harrison et al, 1961), at least for some Group A particle systems, even if this size is actually a statistical mean value.

The influence of the static bed height on pressure fluctuations has also been examined. The measurement of pressure drop between two ports which are always immersed in the dense bed avoids the effect discussed by Geldart and Rhodes (1986), whereby a change in bed level leads to an apparent transition to turbulent fluidization. It is found that the effect of static bed height on F_p (Figs. 6.1 and 6.2) and U_c (Figs. 6.4 and 6.5) is negligible, except for $H_{mf} = 0.35$ m. In this range of static bed height, U_c decreases, while F_p increases with H_{mf}, implying that the bubble size has not developed fully. For shallow beds, therefore, bubbles (or slugs) approach their "maximum size" at higher gas velocities than for deeper beds, consistent with results reported by Canada et al (1976) who found that there was no apparent effect of static bed height over a range of 250 to 700 mm. The velocity, U_c, at which the local pressure fluctuation peaks, however, appears to decrease with height. These conclusions can be explained by the nature of turbulent fluidization: with an increase of gas velocity, bubbles reached their maximum bubble size break up more readily.

The effect of bed effective viscosity can be taken as a convenient starting point to discuss the effect of particle characteristics on bubble behaviour in fluidized beds since the fluidization performance may be substantially influenced by bed viscosity (Grace, 1970; Clift, 1986). The maximum stable size a bubble can attain before splitting usually

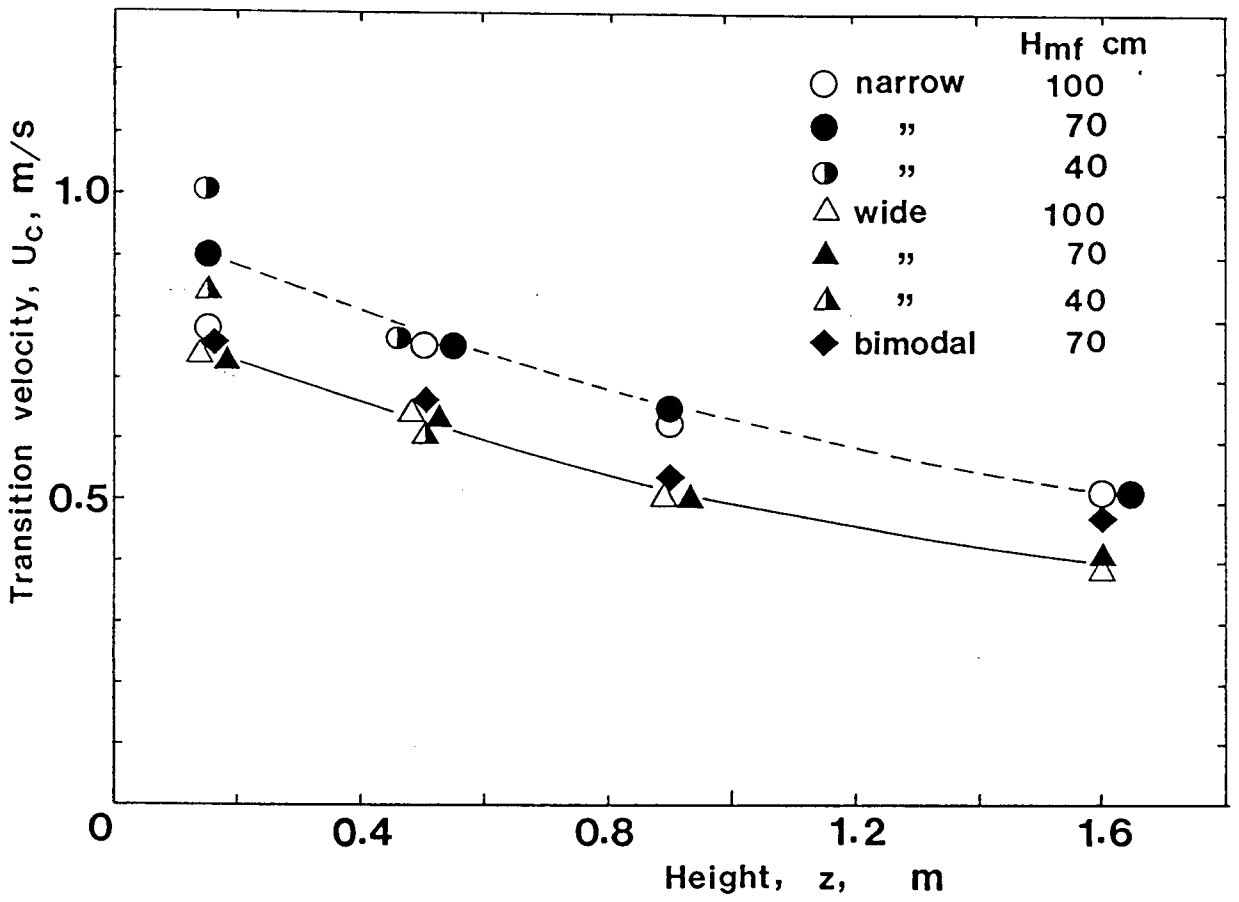

Figure 6.3: Effect of PSD on U_c for fluidized beds of N-FCC particles with different H_{mf} and at different bed heights.

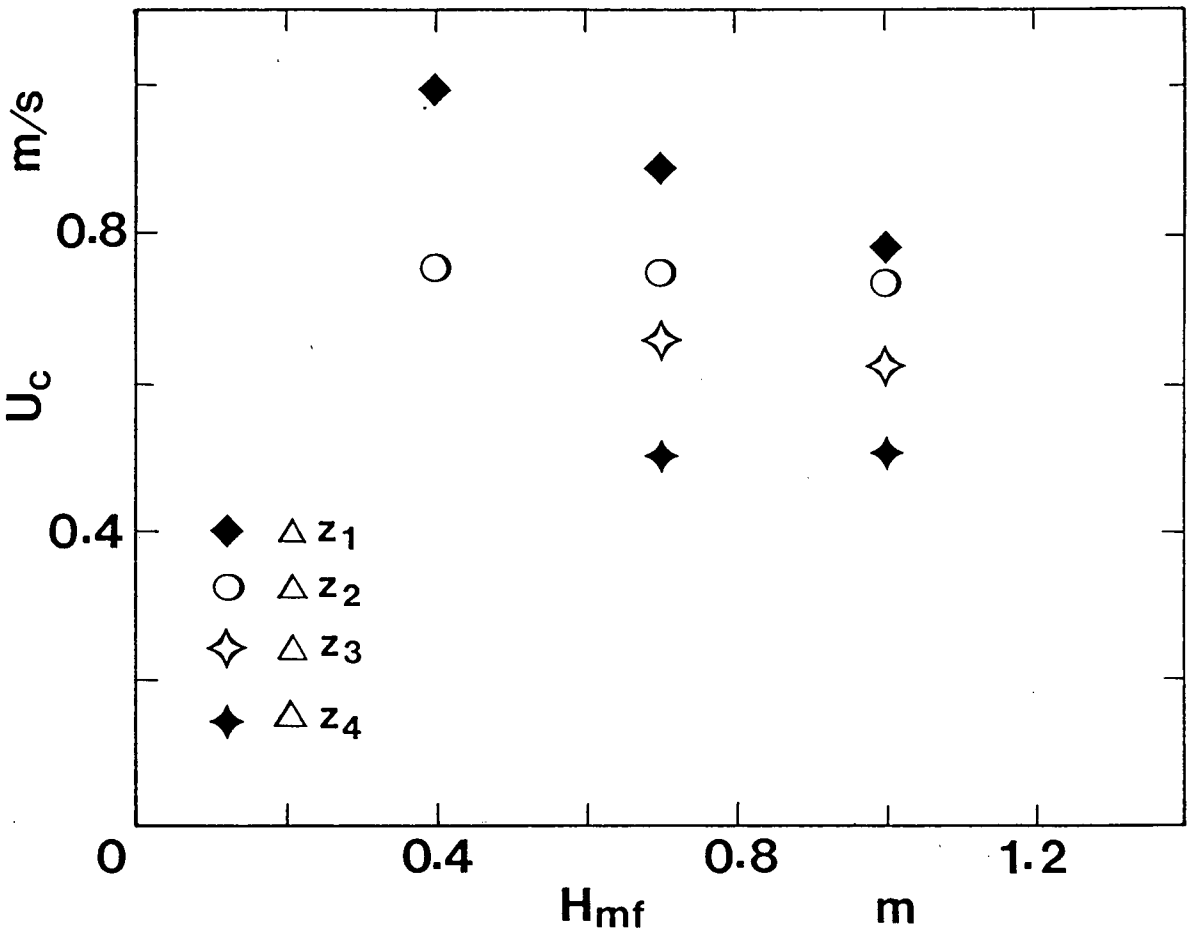

Figure 6.4: Influence of H_{mf} on U_c for N-FCC particles with narrow PSD, over intervals Δz_1 (30 to 280 mm), Δz_2 (430 to 680 mm), Δz_3 (680 to 930 mm) and Δz_4 (930 to 1180 mm).

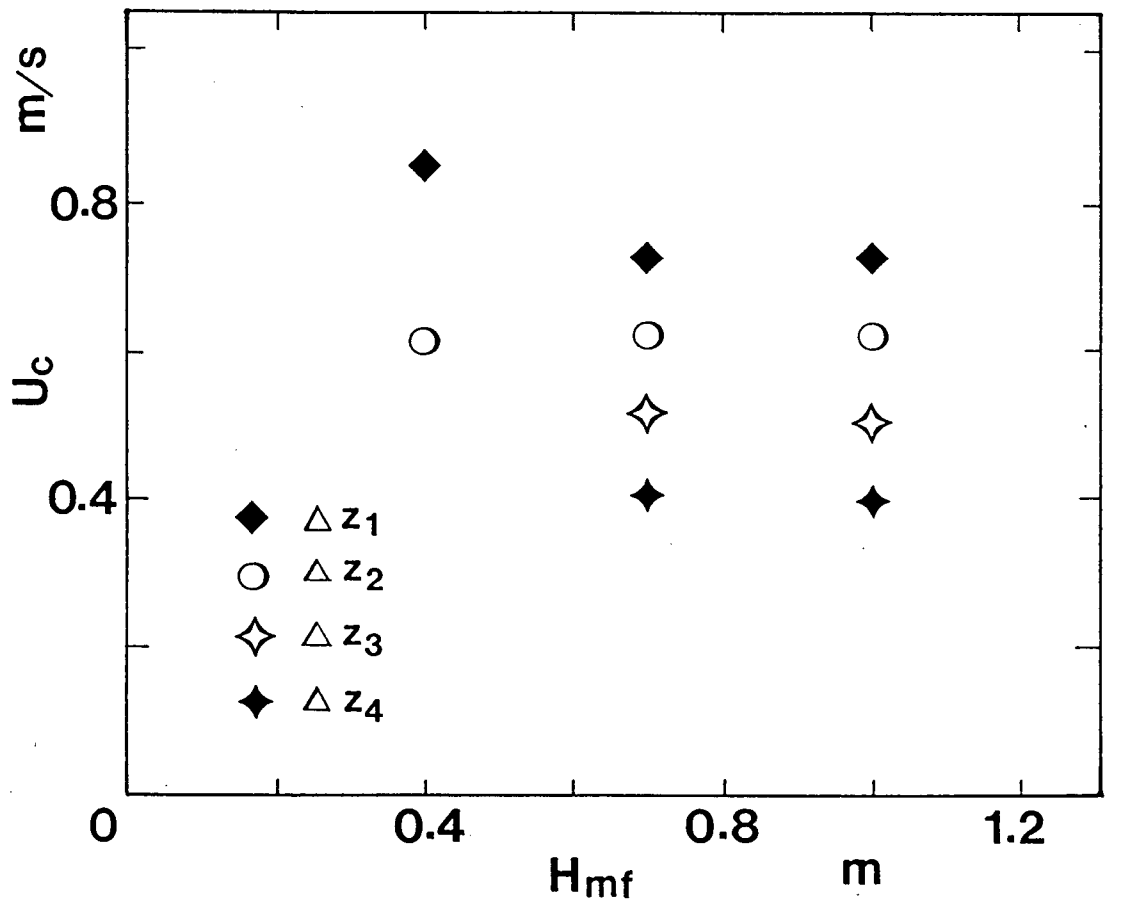

Figure 6.5: Influence of H_{mf} on U_c for N-FCC particles with wide PSD, over intervals Δz_i (as in Fig. 6.4).

increases with the effective dense phase "kinematic viscosity" (Clift et al, 1974). The lower the "viscosity", the smaller the maximum bubble size and the earlier the transition from bubbling to turbulent fluidization. In a fluidized bed of Group A particles, the effective viscosity increases with particle diameter and decreases with fines content (Kono et al, 1986a). For the gas-solid system tested in our study, Khoe et al (1991) based on the results of collapse tests, reported that for a given average surface-volume diameter, a wide size distribution gives a better air retention capacity than a narrow or a bimodal distribution, while the effective viscosity of a fluidized bed was inversely proportional to the air retention capacity of particles.

6.5 Axial Voidage Distribution

Bed expansion is one of the most important and often reported properties of fluidized beds. Better "fluidization quality" is often associated with higher dense phase voidages and smaller voids, both of which result in higher bed expansion. For given operating conditions, higher dense phase voidages probably correspond to higher average interstitial gas flow relative to particles in the dense phase and lower gas flow rates within the bubble phase (Grace and Clift, 1974). Rowe et al (1978) measured the dense phase voidage of a bubbling fluidized bed at low gas velocities ($U < 0.15$ m/s) using an X-ray technique coupled with a densitometer. They found that there were large changes in dense phase voidage with both gas velocity and fines (< 45 μm) content of the powder.

Combined with the measurement of pressure drop fluctuations along the column, the PSD effect on the axial bed voidage distribution in the fluidized bed was also investigated. The actual voidage, ϵ_f can be expressed (Weinstein and Li, 1989) as

$$\epsilon_f = 1 + \frac{dP}{dz}\left(\frac{1}{\rho_p g}\right) + \frac{dU_s}{dz}\left(\frac{G_s}{\rho_p g}\right) \tag{6.6}$$

based on momentum conservation of gas and solids in the bed. If the acceleration and/or

the flow rate of the particles is not high enough, as in the bubbling, slugging and turbulent fluidization regimes, the average local voidage between two vertical ports along the bed can be approximated by

$$\bar{\epsilon}_{f,i} = 1 - \frac{\overline{\Delta P}_i}{\Delta z_i}\left(\frac{1}{\rho_p g}\right) \tag{6.7}$$

where $\overline{\Delta P}_i$ is the mean pressure drop between ports at heights z_i and z_{i+1}.

The PSD effect on $\bar{\epsilon}_{f,i}$ and its axial distribution is shown in Figs. 6.6 and 6.7. For gas velocities less than 0.4 m/s, the narrow blend gave the highest voidage in the lower part of the bed, partially because its value of ϵ_{mf} is higher than for the other size distributions. If the gas velocity > 0.4 m/s, the overall voidage for the narrow blend is usually the lowest at all heights. The voidage increment, $\epsilon_{f,i}$ - ϵ_{mf}, due to bed expansion, always appears lowest for the narrow blend, as shown in Fig. 6.8. These results are in good agreement with the observations of the influence of PSD on the average amplitude of pressure fluctuations and bed expansion in the two dimensional bed (Table 5.1). This verifies that the highest amplitude and the lowest voidage increment, corresponding to the largest bubbles, occur for particles of narrow particle size distribution.

The axial distribution of overall voidage is also influenced by the PSD. It can be seen from Fig. 6.7 that for the wide blend powder, the local voidage always increased with height. For the narrow blend, on the other hand, this was only found for $U > U_c$. Below U_c, the change of the overall voidage along the column was small above a certain height (around 0.35 m above the distributor), where the overall voidage was always lowest.

The effect of PSD on the bed expansion can be explained by the deviation of fluidization behaviour from the two-phase theory for Group A particles of wide size distribution. Consider a section of fluidized bed, across which the visible bubble flow rate is Q_b and the average bubble velocity is u_b. The bed expansion caused by the visible bubble flow

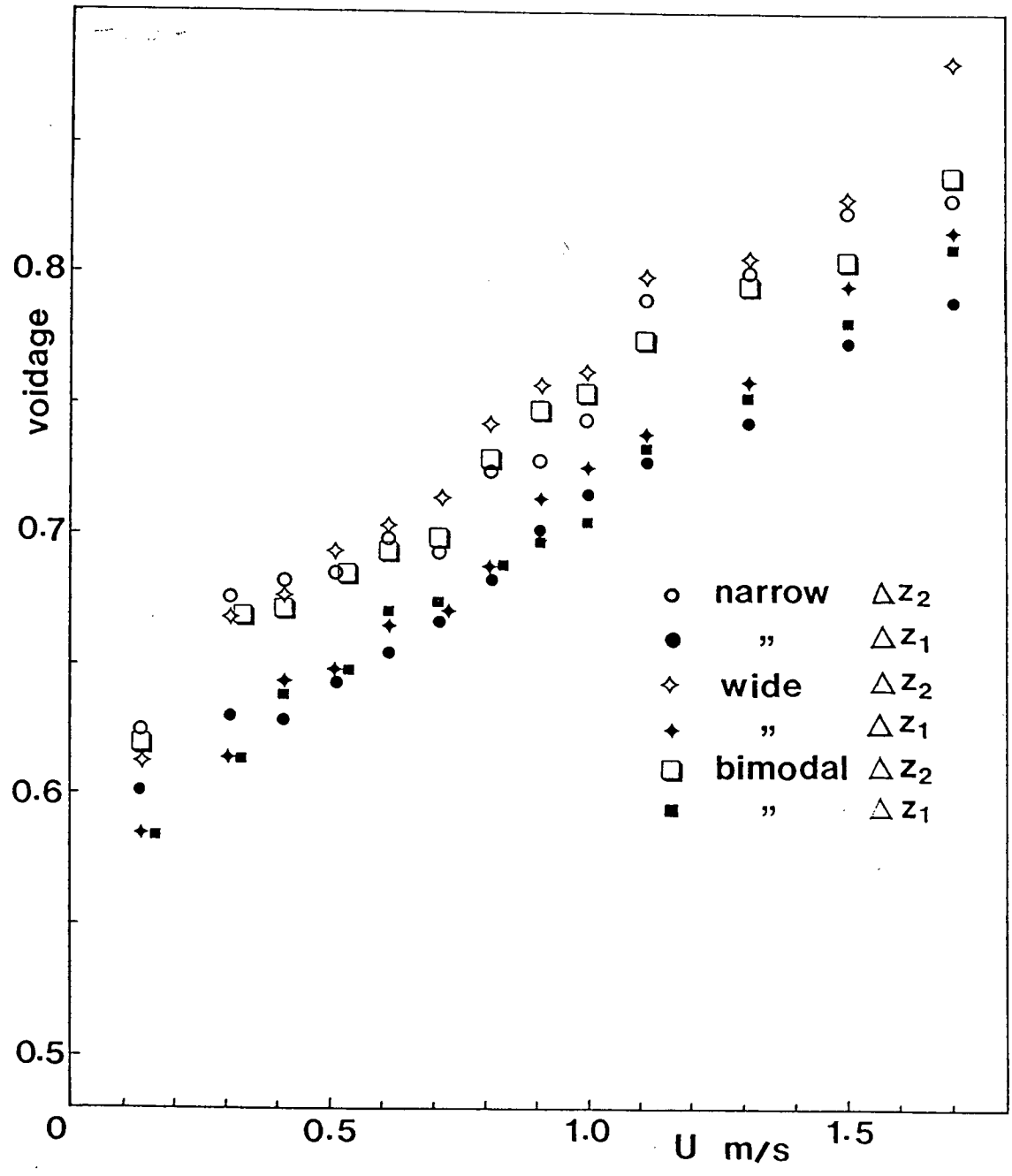

Figure 6.6: Effect of PSD on the overall voidage in fluidized bed; $H_{mf} = 0.7$ m. Intervals Δz_1 and Δz_2 are as in Fig. 6.4.

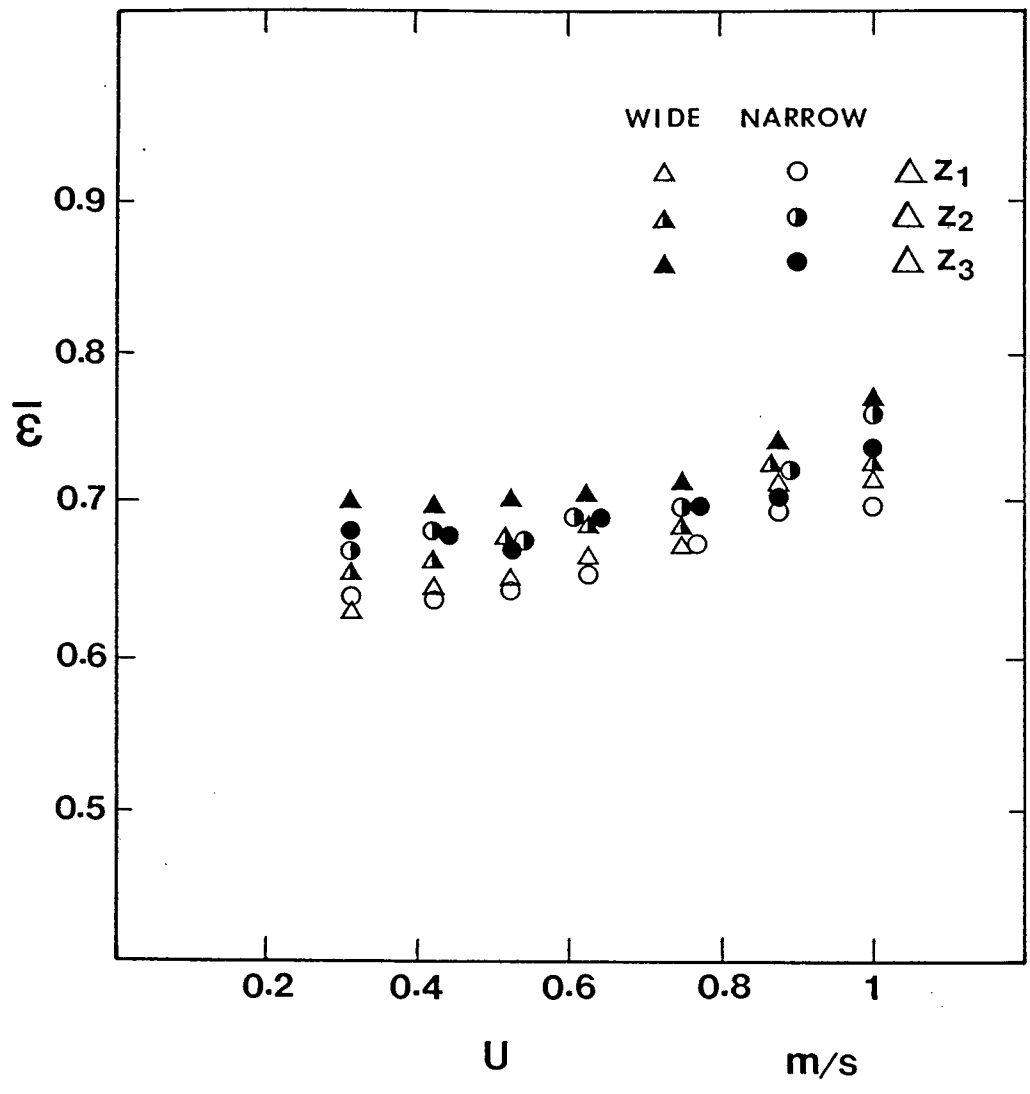

Figure 6.7: Effect of PSD on the overall voidage in fluidized bed; $H_{mf} = 1$ m. Intervals Δz_1, Δz_2 and Δz_3 are as in Fig. 6.4.

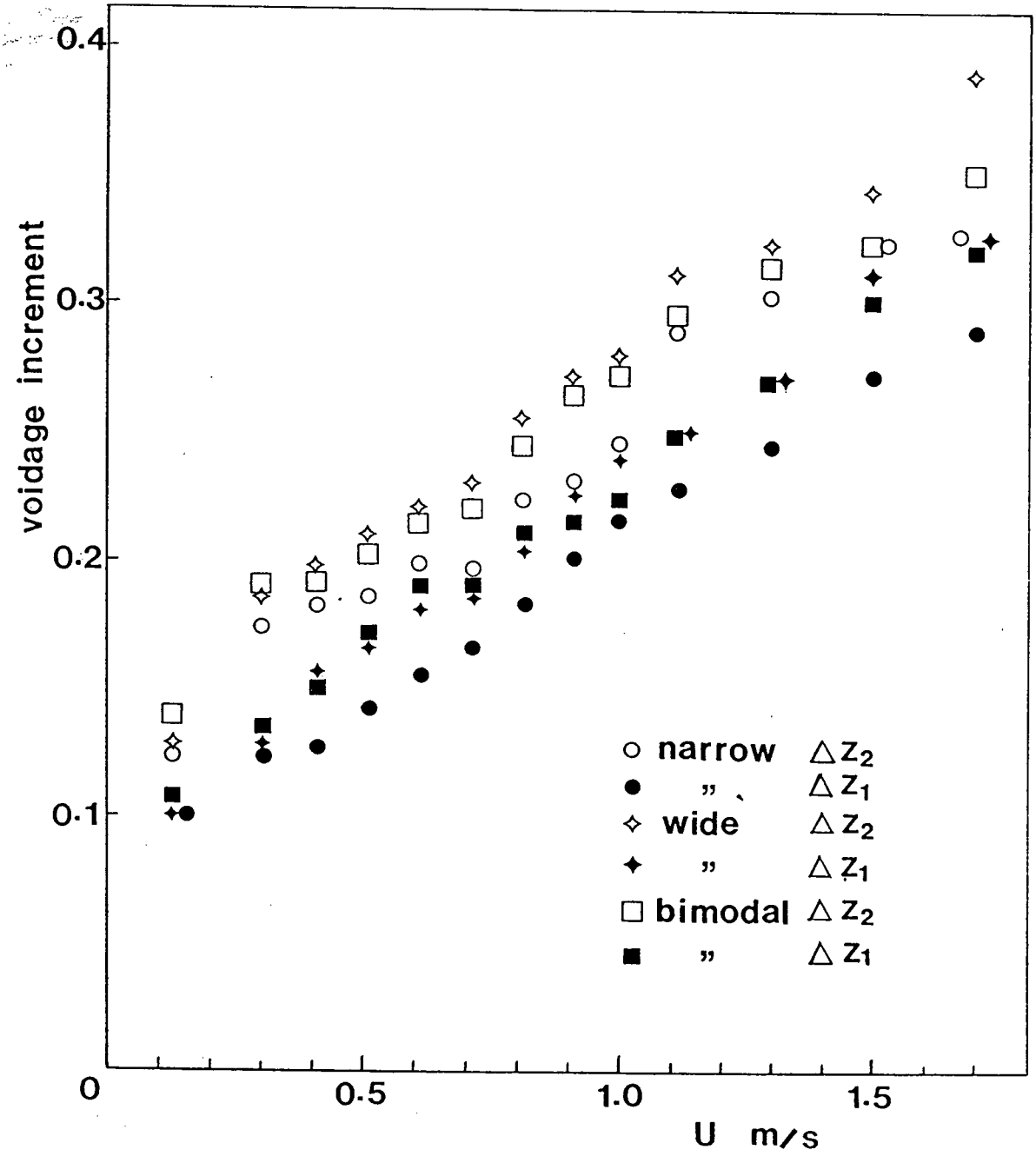

Figure 6.8: PSD effect on the voidage increment in fluidized bed; $H_{mf} = 0.7$ m. Intervals Δz_1 and Δz_2 are as in Fig. 6.4.

can then be expressed as

$$\Delta H_b = H - H_d = \int_0^H \frac{Q_b}{Au_b} dz, \tag{6.8}$$

while the expansion caused by expansion of the dense phase is given by

$$\Delta H_d = H_d - H_{mf} = \int_0^H (\epsilon_d - \epsilon_{mf}) dz \tag{6.9}$$

The total expansion of the bed

$$\Delta H = \Delta H_b + \Delta H_d = H - H_{mf}, \tag{6.10}$$

that is,

$$\Delta H = \int_0^H (\frac{Q_b}{Au_b} + \epsilon_d - \epsilon_{mf}) dz \tag{6.11}$$

It is found from Figs. 6.6 to 6.8 that for particles of wide size distribution,

$$\frac{d\bar{\epsilon}_f}{dz} > 0, \tag{6.12}$$

that is,

$$\frac{d\Delta H}{dz} > 0. \tag{6.13}$$

Therefore,

$$\frac{\partial \epsilon_d}{\partial z} > \frac{\partial u_b}{\partial z}(\frac{Q_b}{Au_b^2}) - \frac{\partial Q_b}{\partial z}(\frac{1}{Au_b}) \tag{6.14}$$

If the two-phase theory holds, $\partial \epsilon_d / \partial z = 0$ and $\partial Q_b / \partial z = 0$, so that $\partial u_b / \partial z < 0$, which means that bubble size decreases with height. Obviously, this cannot express our experimental results for particles of wide PSD, as shown in Figs. 5.13 to 5.15 and Figs. 6.1 and 6.2. Equation 6.14 therefore suggests that for Group A particles with wide size distribution, Q_b, u_b and ϵ_d vary along the bed height, and the increment of ϵ_d may be higher than that of u_b and/or the decrement of Q_b along the column.

For the narrow PSD particles with $U < U_c$ and z $\geq$ 0.35 m, it is found from Fig. 6.7, that $d\bar{\epsilon}_f/dz \approx 0$, or $d\Delta H/dz \approx 0$. If the assumption of the two-phase theory holds,

then the sign in equation 6.4 becomes an equals sign and $\partial u_b/\partial z \approx 0$, which means that the bed mainly operated in the slugging regime. This is consistent with the pressure fluctuation measurements along the bed with particles of narrow PSD (Figs. 6.1 and 6.2).

Chapter 7

Reactor Performance in the Distributor Region

The distributor region plays an important role in determining the contacting efficiency of fluidized bed reactors (Grace and de Lasa, 1978). Multiorifice distributors are commonly used in large gas fluidized beds, and their effective design has been the object of a number of studies. In this study, the PSD effect on the reactor performance in the distributor region was investigated by comparing the contacting efficiency for different distributor geometries and operating conditions. Four different multiorifice distributors with different hole numbers and hole diameters were tested for particulate materials having three different PSD's to evaluate the influence of gas distributor on the fluidized bed reactors and its interdependence with the PSD effect.

7.1 Brief Review of Previous Work

Early work on gas distributors mainly concerned the effect of distributor type and pressure drop on the "uniformity" of fluidization (e.g. Morse and Ballou, 1951; Walker, 1970; Whitehead, 1971). Compared with the types of distributors often used in the commercial fluidized bed reactors, porous plate distributors used in some small-scale laboratory tests appeared to give more "uniform" fluidization, that is smaller bubble diameters and higher bed expansion, while the influence of distributor type could persist for depths of up to 1.5 m (Walker, 1970). The reaction conversion was also found to be significantly better with a porous plate than with a sieve plate distributor (e.g. Hovmand and Davidson, 1968; Bauer and Werther, 1981). Despite these favourable characteristics, the

porous plate has rarely, if ever, been used in commercial fluidized bed reactors due to cost, difficulty in manufacture, structural considerations, pore blocking and less flexibility in operation compared with other types of distributor, such as the perforated plate or multitube distributor.

The minimum pressure drop across the grid to ensure that the distributor introduces the fluidizing gas evenly through each hole, thereby keeping the solid particles above it in constant motion and preventing the formation of defluidized zones within the bed, is generally considered in relation to that of the pressure drop across the fluidized bed itself. The required ratio of ΔP_D to ΔP_B depends on not only the fluidization performance of particles but also the ratio of H to D_T (Clift, 1986).

From experience in the development of the Nu-Iron fluidized bed reduction process, Agarwal et al (1962) suggested that for deep fluidized beds of high density material, the pressure drop across the distributor plate should be at least 10% of the pressure drop across the bed and in no case should be less than 0.5 *psi* (3.5 kPa). For relatively shallow beds of low density material, they recommended a minimum pressure drop across the distributor of 2 to 3 kPa.

Based on measurements by Hiby (1964) and Whitehead and Dent (1967), Zuiderweg (1967) proposed that for a perforated plate or nozzle distributor the pressure drop should be related to both the minimum fluidization velocity, U_{mf}, and the minimum velocity at which all nozzles operate, U_m. For U_m/U_{mf} from 1 to 2, they advocated $\Delta P_D = 0.15\ \Delta P_B$, while for $U_m/U_{mf} \gg 1$, $\Delta P_D \doteq 0.015\ \Delta P_B$.

The height of the entrance region for a multiorifice distributor was investigated by Fakhimi et al (1983) by measuring the differential pressure between the gas spout and adjacent dead zone. The principal factors influencing the height were found to be U_{mf}, mean particle size, orifice spacing and gas flow rate. They also presented an expression for the minimum $\Delta P_D/\Delta P_B$ to ensure even gas distribution.

Ho et al (1984) studied the characteristics of the distributor pressure drop in a fluidized bed corresponding to perforated distributor plates with regular and irregular (i.e. with different hole size and/or non-uniform hole location) design. They reported that abnormal conditions, e.g. hole blocking and channeling, can be detected from the analysis of the distributor and bed pressure drop data. Criteria for uniform gas distribution across the distributor holes strongly depended on the minimum fluidization velocity of the fluidizing particles, with U_m/U_{mf} higher for particles of lower U_{mf}.

Wen et al (1978) examined the formation of dead zones using two and three-dimensional fluidized beds. The dead zone height was found to be affected by the gas velocity, distributor type, orifice pitch, orifice diameter and particle size. The behaviour of the two-dimensional bed could not be readily extrapolated quantitatively to three-dimensional cases. Wen et al (1980) detected the presence and disappearance of dead zones in a cylindrial bed of diameter 262 mm using self-heating thermistor probes. Empirical correlations were proposed to calculate the critical orifice gas velocity required to eliminate the dead zone as a function of pitch, orifice diameter, particle size and particle density for a perforated plate distributor. Decreasing the pitch and increasing the orifice diameter was found to help to eliminate dead zones. Rathbone and Davidson (1986) also found that the dead zone could be avoided by suitable orifice spacing.

Patrose and Caram (1984) studied the influence of particle density (plastic and glass beads of diameter 600 to 1000 μm) and inlet gas velocity on the velocity of solids and dead zone formation by using an optical fiber probe in a two-dimensional column. They reported formation of a steady spout for the variety of bed conditions studied. The size of the dead zone decreased with increasing inlet gas velocity. The inlet grid jet was not a hollow gas cavity, but a region of active solids motion.

Briens et al (1978, 1980) investigated factors that influence grid leakage, such as gas velocity, static bed height, baffles, grid thickness and hole shape. They found that

grid leakage is caused by pressure fluctuations at the top of the grid holes, which may result from bubble formation at the grid orifices and sloshing of the bed. Inserting wavebreakers (such as baffles and tubes) and selecting the proper grid thickness could reduce grid leakage significantly.

Oki et al (1980) investigated discharge of gas into a three-dimensional fluidized bed from a multiple-orifice gas distributor using an optical-fiber array probe to test the effects of distributor orifice configurations and gas flow. They reported that orifice spacing is an important factor among the variables which affect the mode of gas discharge from the distributor.

Hsiung and Grace (1978) evaluated the effects of orifice diameter, gas velocity through the orifice, particle size and plenum chamber volume on mean frequency of bubble formation by using a sensitive pressure transducer. For each of the orifices studied, the frequency of pressure fluctuations increased with increasing gas flow rate and then levelled off at a value of 19 to 25 Hz. The gas flow for onset of multiple bubble formation decreased with decreasing orifice diameter and appeared to be independent of particle size for the range investigated (glass ballotini with size ranges of 88 to 125 μm, 149 to 250 μm, and 250 to 420 μm). The frequency spectrum also became more complex as the particle size was reduced.

Some studies have been carried out to investigate how the distributor influence reactor performance. Bauer and Werther (1981) tested the influence of distributor type (porous, perforated and nozzle plate) and free area ratio. They reported that the conversion obtained with the porous plate distributor was much better than for the perforated plates. By comparing conversion data from two perforated plates of different free area (8% and 4%), they also found that smaller holes yielded a better dispersion of the fluidizing gas and hence better conversion.

Yang et al (1984) measured the reaction conversion (butene-1 to butadiene) in the

distributor region for three different distributors, each with same proportion of free area, but with different hole numbers and diameters. They observed that a zone existed near the distributor in which the efficiency of chemical conversion is high compared with the region near the bed surface. A progressive increase in conversion was found as the initial bubble size decreased.

It has been discovered that bubbling-bed models do not properly represent reaction near the gas distributor (Chavarie and Grace, 1975) or in the freeboard (region above dense bed) (Furusaki et al, 1976). To consider the reaction and transfer process in the vicinity of the grid, Behie and Kehoe (1973) proposed a two-phase model which extended a well-known model by Orcutt et al (1962). A plug flow jet region devoid of particles was assumed to act in series with the bubble phase. Mass transfer coefficients between the jets and surrounding dense phase were based on measurements in a 0.61 m diameter bed of 60 μm cracking catalyst. Grace and de Lasa (1978) extended this model to two simple alternate models and allowed for solids dispersed in the jet phase.

Sit and Grace (1986) investigated interphase mass transfer during bubble formation in the entry region of fluidized bed by measuring tracer concentration at different radial positions and vertical levels. Interphase transfer was found to occur by two mechanisms (convection and diffusion), when bubbles formed directly at an orifice at the base of a fluidized bed of non-adsorbing particles.

Heat transfer in the grid zone between bed and tubes has also been studied (Virr and Williams, 1985; Ho et al, 1987). Heat transfer coefficients appear to be higher than in the bubbling zone of a gas-solid fluidized bed. Ho et al (1987) observed that in the bubbling zone the heat transfer coefficient increased and then decreased with the air flow, while in the grid zone region, the heat transfer coefficient increased with the air flow over the entire range of flow rates. They also determined that the heat transfer coefficient increased with decreasing open area ratio and hole pitch distance.

Most previous work on gas distributors used in industrial fluidized bed reactors has been concerned with three major issues:

1. Macroscopic criteria: What is the minimum pressure drop across the distributor and the minimum orifice gas velocity to maintain uniform gas distribution?

2. Microscopic understanding: What is the gas-solid motion and mass transfer rate at or near the grid?

3. Influence on reactor behaviour: How can the distributor be best designed to optimize the reactor performance?

Although considerable work has been carried out on issues 1 and 2, there is no clear answer to the question of how these two issues affect each other and influence the performance of a fluidized bed reactor, particularly at high gas velocities, since in previous work on grid region, U was usually less than 0.25 m/s. In this study, all three questions above are considered, at the same time as the ozone decomposition reaction is used to see the interacting influence of the PSD.

7.2 Experimental Method

In most of our reactor experiments (Chapters 3 and 4), No. 2 gas distributor (see Table 2.3) was used, in order to ensure that the pressure drop across the distributor at high gas velocities could be provided by the blower available in our building. Four multi-orifice plates with three different proportions of free area, three hole diameters and two pitch spacings were used to test the influence of the pressure drop across the distributor and the geometric nature of the grid. Their design specifications appear in Table 2.3.

Investigation of the effect of the distributor on reaction in the grid region could be impeded by particle leakage through orifices of the distributor, since significant change in catalyst inventory could occur, especially for low bed heights. A screen with very small

holes, less than the minimum size of particles tested, is often used to prevent leakage. For Group B particles with narrow size distribution, the pressure drop across the screen may be negligible. However, for Group A particles containing fines, the pressure drop across the dense screen may be higher than that across the distributor plate at high gas velocities.

In this study, particle leakage was prevented by using distributors consisting of two multi-orifice plates with very different free areas. The ratio between them was from 4 to 15, while the angle α_D (Fig. 2.12) was kept less than 60% of the angle of particle repose. Since distributor pressure drop is approximately proportional to the square of gas velocity through the orifice, the pressure drop across the lower plate is less than 10% of the total pressure drop across the distributor. The amount of particle leakage during each run was less than 0.3% of the total initial mass in the bed.

Experiments were conducted in the aluminum fluidized bed reactor at two gas velocities, 0.2 m/s and 0.6 m/s, and with two catalyst charges, 1.2 kg and 3 kg, for each of four distributors and two particle size distributions - wide and narrow. The gas velocity through the orifices was from 4 m/s to 60 m/s, while the static bed height was 0.15 m and 0.4 m. The kinetic rate constant was around 8 s^{-1}. The mixed feed gas samples withdrawn below the distributor were analysed to ensure ozone concentrations in air around 600 ppm. Outlet gas samples were withdrawn through the port at the top of the reactor (see Fig. 2.10). The distributor performance was determined by the reaction conversion or the contacting efficiency.

To evaluate the influence of gas distributor on the hydrodynamic phenomena in the grid zone, three differential pressure transducers were used to measure the pressure drop across the distributor, across a region of the bed just above the distributor and across the upper section, as shown in Fig. 7.1.

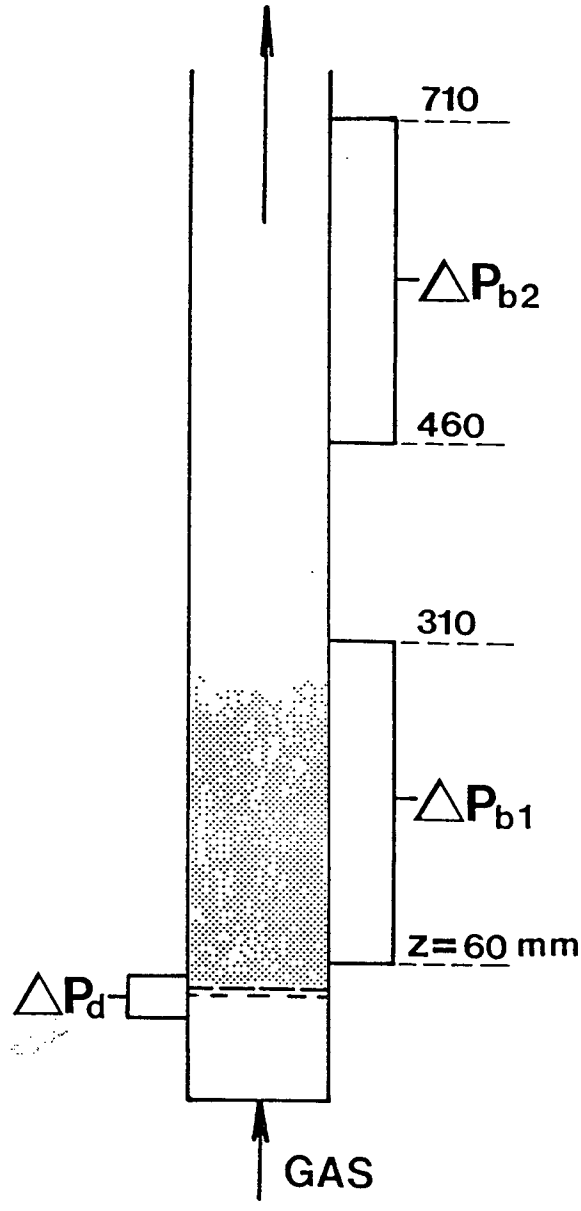

Figure 7.1: Schematic showing regions where pressure drops and their fluctuations were determined

7.3 Influence of Distributor Geometry on Reaction Conversion

Results from the conversion measurement of ozone decomposition for different gas distributors, gas velocities and catalyst inventories are shown in Figs. 7.2 to 7.5. It can be seen from Figs. 7.2 and 7.3 that for a given gas velocity, higher conversions are achieved in beds fitted with distributors with both higher orifice gas velocities and smaller pitch.

It should be noted, however, that the influence of pitch is more significant than that of free area. Although the pressure drop across distributor-4 could be much higher than that of distributor-3 or distributor-2, while the hole diameter is the same for distributors 3 and 4, the conversion was higher than for distributor-4. For columns fitted with distributor-3, the actual pressure drop across the distributor at $U = 0.2$ m/s was less than the $\Delta P_{D,min}$ required by Agarwal et al (1962). For beds fitted with distributor-4, however, the pressure drop across the distributor in our experiments was always higher than that required by Agarwal et al. This suggested that high pressure drop across the gas distributor in fluidized bed is not enough to maintain good performance of the distributor. Other factors, such as the pitch or the number of holes, should also be considered.

Based on the measurements near the grid using a self-heating miniature glass bead thermistor, Wen et al (1980) proposed the following empirical correlation to calculate the minimum orifice gas velocity needed to eliminate the dead zone completely for a perforated plate distributor of a three dimensional fluidized bed:

$$U_{jc} = U_{jmf} + 0.0803[\frac{(p - d_{or})^{0.16} d_P^{0.44}}{d_{or}^2}] \tag{7.1}$$

where U_{jc} is the minimum gas velocity through the orifice to eliminate the dead zone, p the orifice pitch, d_{or} the orifice diameter, and U_{jmf} the orifice gas velocity corresponding to minimum fluidization.

If the above correlation is applicable to our experimental system, the dead zone

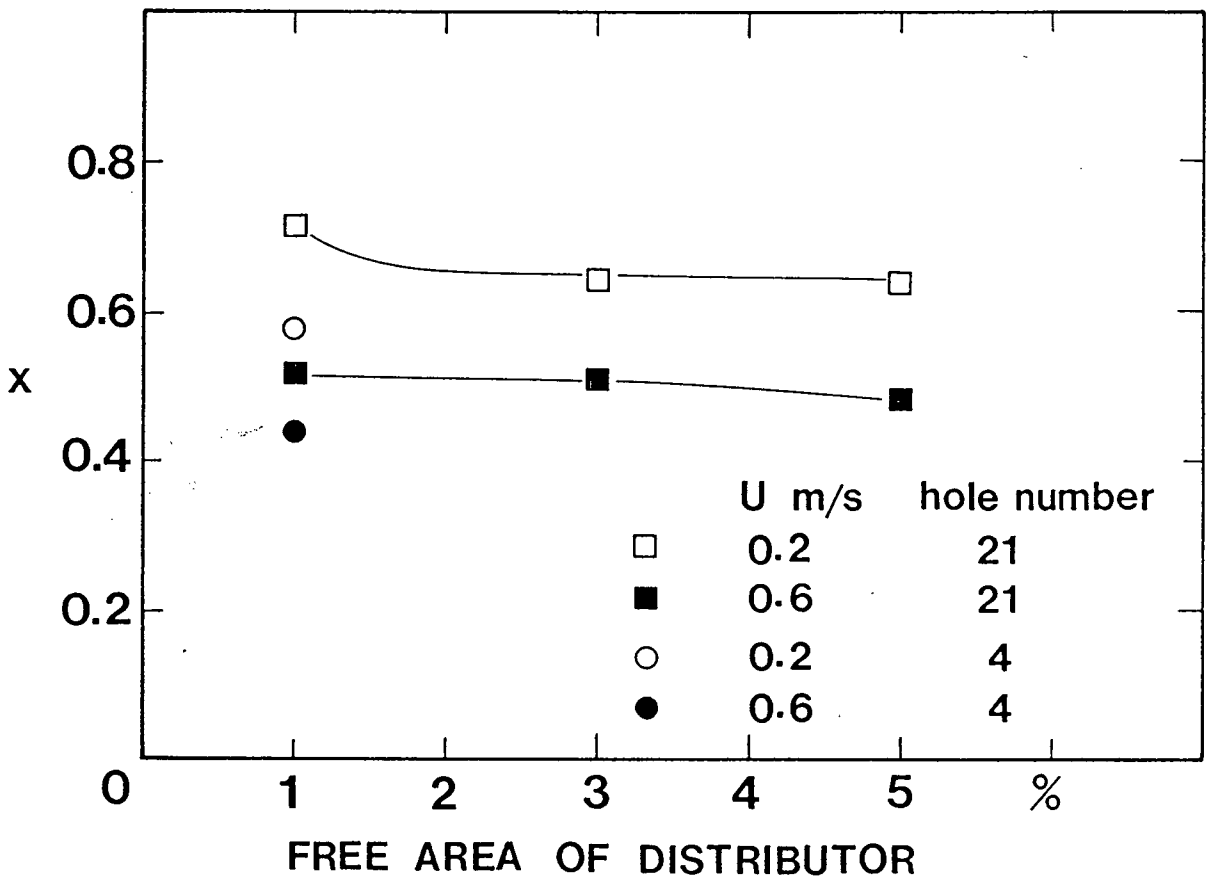

Figure 7.2: Influence of distributor free area and pitch on conversion: N-FCC particles of wide PSD, $H_{mf} = 0.15$ m.

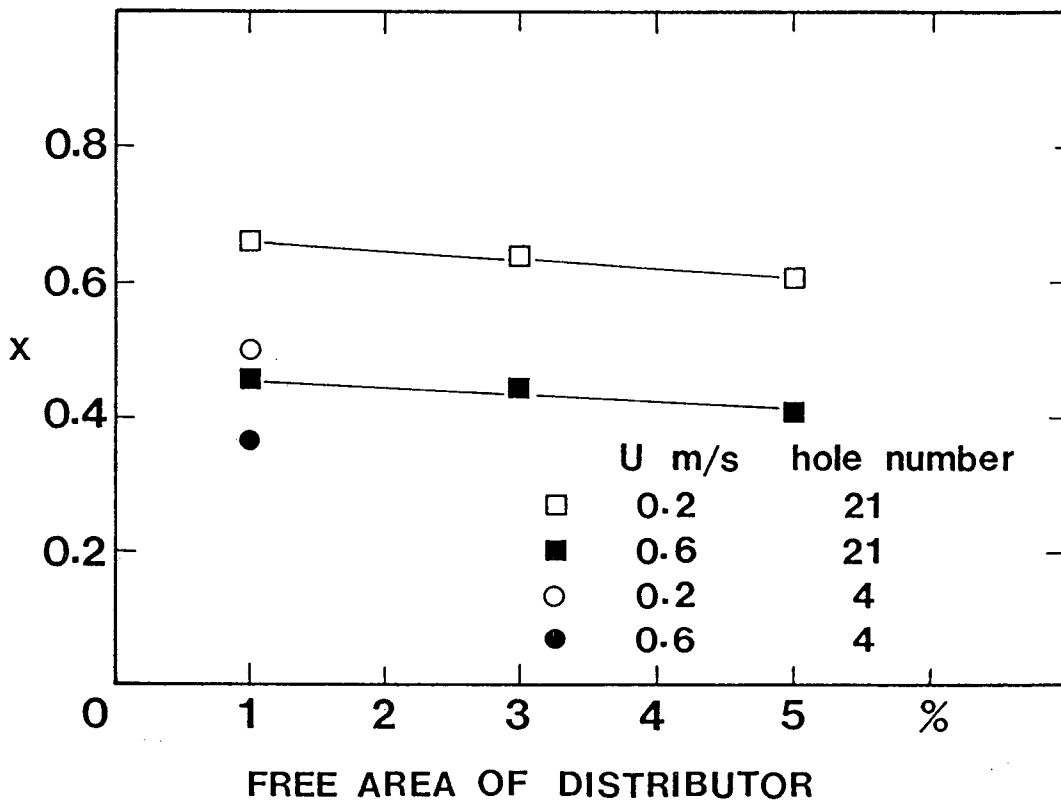

Figure 7.3: Influence of distributor free area and pitch on conversion: N-FCC particles of narrow PSD, $H_{mf} = 0.15$ m.

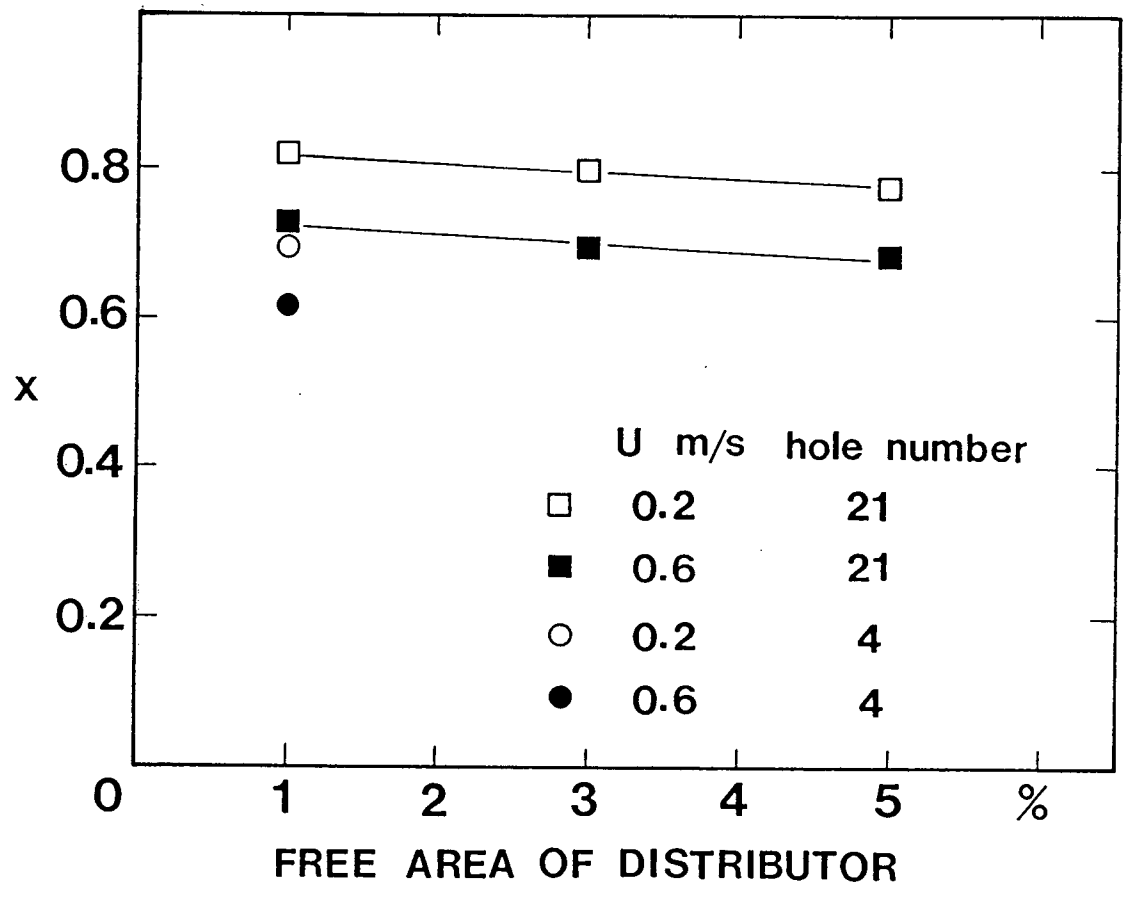

Figure 7.4: Influence of distributor free area and pitch on conversion: N-FCC particles of wide PSD, $H_{mf} = 0.4$ m.

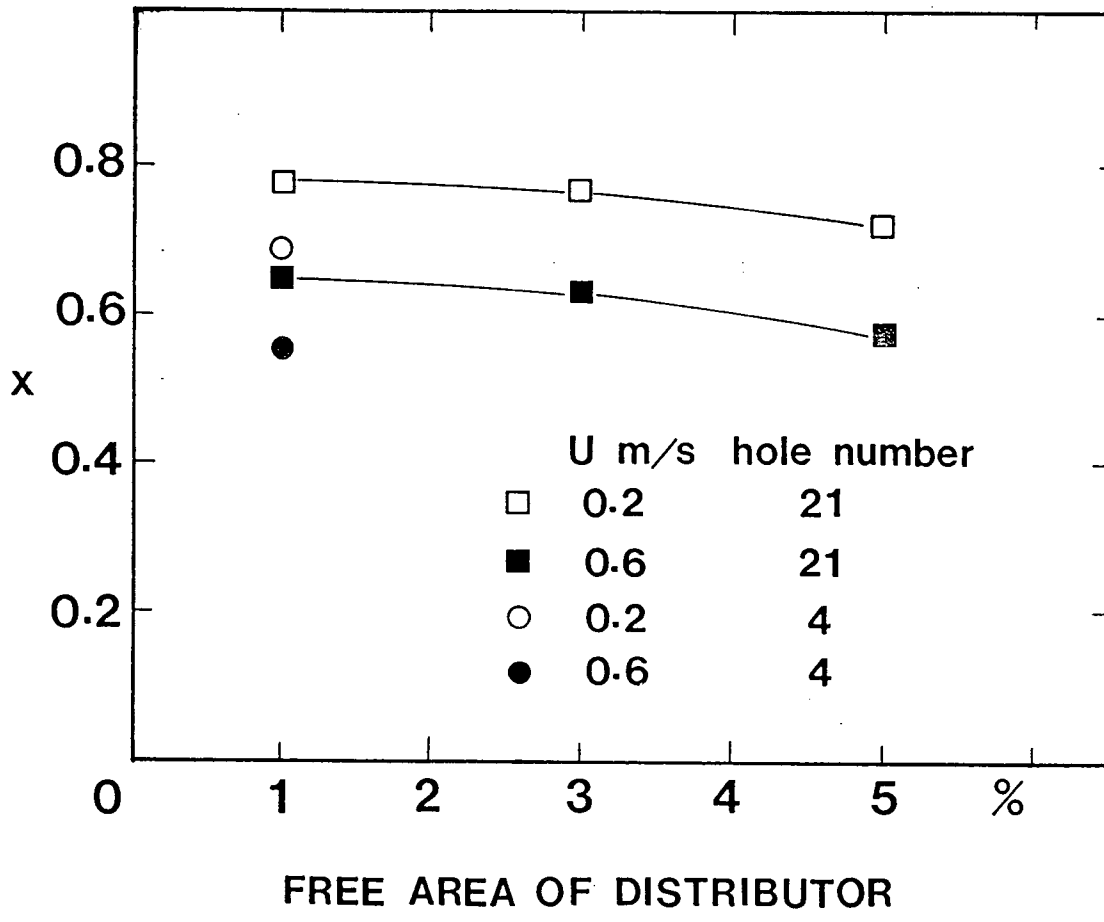

Figure 7.5: Influence of distributor free area and pitch on conversion: N-FCC particles of narrow PSD, $H_{mf} = 0.4$ m.

above the distributor-4 should be almost eliminated since $U/\alpha_{d4} \geq U_{jc}$ for all running conditions, where α_{d4} is the free area fraction of distributor-4. For distributor-3, however, $U/\alpha_{d3} < U_{jc}$, which means that a significant dead zone should occur above the plate according to eqn. 7.1. These conclusions are not consistent with our experimental results, as shown in Figs. 7.2 to 7.5. This suggests that single criteria based on hydrodynamic experiments are insufficient to determine the distributor performance in fluidized bed reactors.

The deviation of our experimental conversion results from what one would expect from Eqn. 7.1 and the criteria of Agarwal et al (1962) and Zuiderweg (1967) may be due to several reasons. One is that most previous work was carried out with Group B particles with a filter or packed material (e.g. glass wool was used by Wen et al (1978, 1980)) below the distributor plate to prevent weeping or dumping of particles. For example, the influence of pitch distance may be underestimated by Eqn. 7.1 due to the pre-distribution effect by the glass wool below the plate, and the first term on the right hand of Eqn. 7.1 can become insignificant for Group A particles due to the small magnitude of U_{mf}. It is also possible that the gas-solid movement in the grid zone was influenced by measuring probes in this region used by some investigators (e.g Wen et al, 1980; Oki et al, 1980).

Our experimental ozone conversion results reveal that the total influence of multi-orifice distributors in fluidized beds on reactor performance may consist of several aspects. Possible issues include:

1. Uniformity of gas distribution; This may be related to the pressure drop across the distributor (Agarwal et al, 1962; Zuiderweg, 1967; Fakhimi, 1983);

2. Dead zone above the distributor plate: This is related to the pitch, hole diameter and orifice gas velocity (Wen et al, 1978, 1980; Oki, 1980);

3. Initial bubble size: This is dependent on the volumetric gas flow rate per orifice (Davidson and Harrison, 1963; Yang et al, 1984).

Comparing the conversions for the column fitted with distributor-1 to that with distributors 2 and 3 (all with the same centre-to-centre pitch but different hole diameter and free area), one finds that reaction conversion in the grid zone decreases with decreasing grid pressure drop and increasing free area. The influence of the fractional free area seems small in our experiments, as shown in Figs. 7.2 to 7.5. Based on comparison of the conversions for the column fitted with distributor-4 and distributor-1 (same free area, but different hole diameter and pitch) and comparison between results for distributors 4 and 3 (same hole diameter but different pitch and free area), we see that the effect of pitch is more significant than that of pressure drop or free area.

At low gas velocity, e.g. 0.2 m/s in our experiment, the mass of particles entrained in the freeboard region is negligible compared with the total mass of particles. If the voidage in a fluidized bed is assumed to be uniform and equal to $\bar{\epsilon}_f$, except in the dead zone, the following equation can be written, based on a mass balance of particles in the grid region and other regions of the fluidized bed, as shown in Fig. 7.8:

$$\frac{W_{cat}}{\rho_p A} = (1-\bar{\epsilon}_f)H_{12} + (1-\bar{\epsilon}_f)H_{01}(1-\gamma_D) + (1-\epsilon_{mf})H_{01}\gamma_D \tag{7.2}$$

where γ_D is the ratio of dead zone volume in the grid region to the total bed volume between levels 0 and 1, H_{01} and H_{12} are bed heights between levels 0 and 1, and 1 and 2, respectively, as shown in Fig. 7.8. H_{01} is higher than H_s, the height of the dead zone, which was reported to be usually less than 60 mm (Wen et al, 1978).

From eqn. 7.2, since $H = H_{01} + H_{12}$, we can write

$$\frac{W_{cat}}{A\rho_p} = (\bar{\epsilon}_f - \epsilon_{mf})H_{01}\gamma_D + (1-\bar{\epsilon}_f)H \tag{7.3}$$

Therefore,

$$\gamma_D = \frac{1}{H_{01}(\bar{\epsilon}_f - \epsilon_{mf})}\left[\frac{W_{cat}}{A\rho_p} - (1-\bar{\epsilon}_f)H\right] \tag{7.4}$$

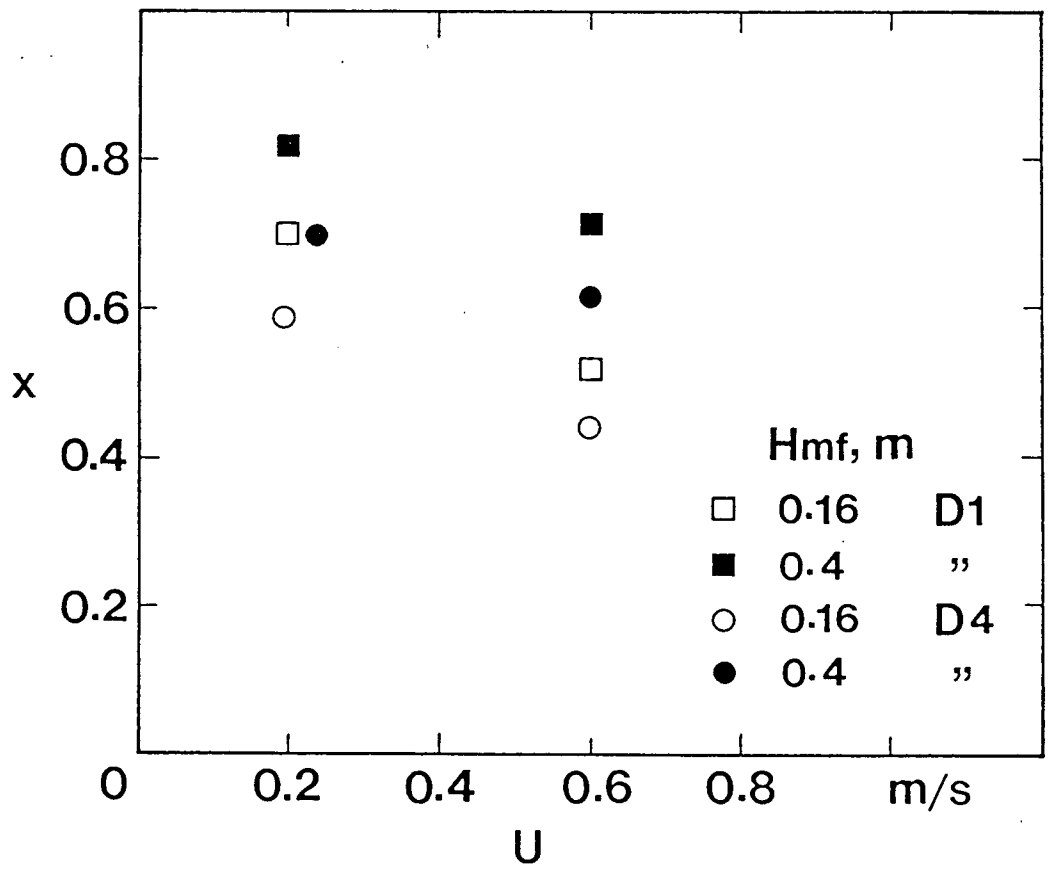

Figure 7.6: Distributor effect on reaction conversion at different bed heights: N-FCC particles of wide PSD; Di denotes distributor-i, (see Table 2.3).

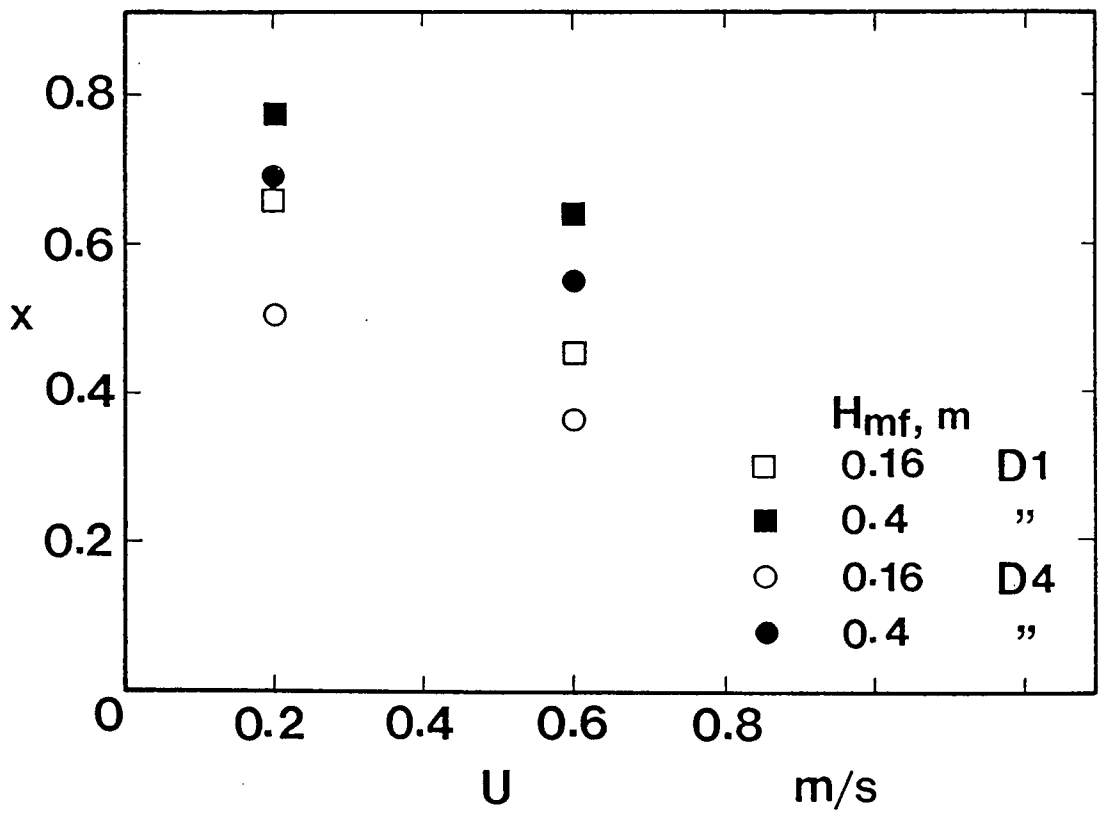

Figure 7.7: Distributor effect on reaction conversion at different bed heights: N-FCC particles of narrow PSD; Di denotes distributor-i, (see Table 2.3).

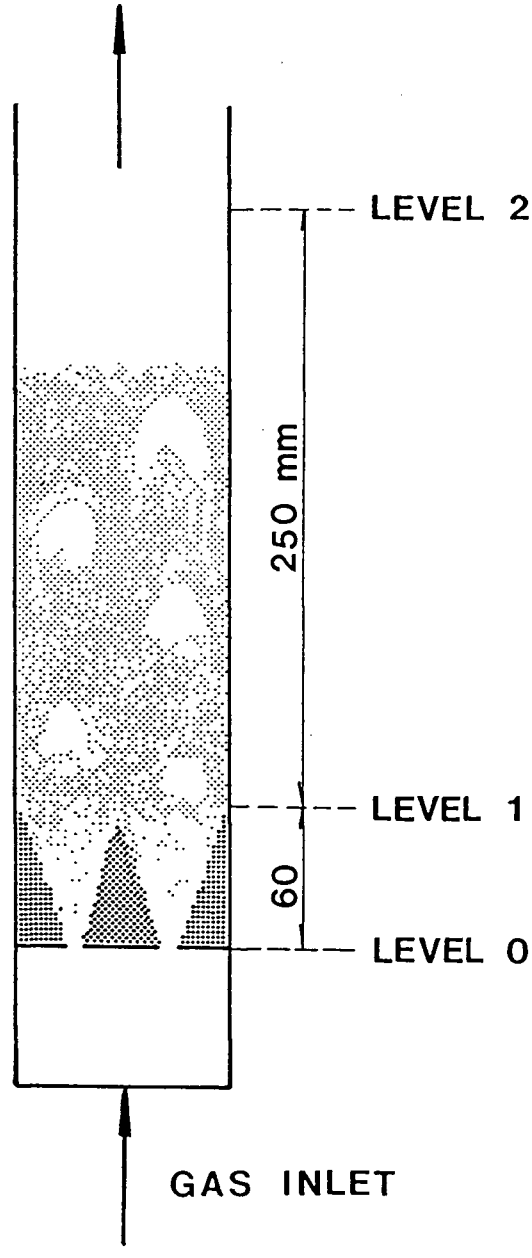

Figure 7.8: Location of taps between which differential pressures were measured.

For a given mass of particles, the lower the H, the more the γ_D, i.e. the greater the proportion of dead zone in the grid region.

Combining eqns. 7.4 and 6.7, we obtain

$$\gamma_D = \frac{1}{H_{01}(\bar{\epsilon}_f - \epsilon_{mf})}[\frac{W_{cat}}{\rho_p A} - (1 - \bar{\epsilon}_f)H_{01} - \frac{\overline{\Delta}P_{12}}{\rho_p g}] \tag{7.5}$$

For columns fitted with different distributors but operated at the same conditions, the above equation can be written as

$$\gamma_{D,i} = \frac{1}{H_{01}(\bar{\epsilon}_{f,i} - \epsilon_{mf})}[\frac{W_{cat}}{\rho_p A} - (1 - \bar{\epsilon}_f)H_{01} - \frac{\overline{\Delta}(P_{12})_i}{\rho_p g}] \tag{7.6}$$

Therefore, the difference of dead zone volume in beds fitted with distributors 4 and 1 can be evaluated from

$$V_{D,4} - V_{D,1} = AH_{01}(\gamma_{D,4} - \gamma_{D,1}) = \frac{A}{(\bar{\epsilon}_f - \epsilon_{mf})\rho_p g}[(\overline{\Delta}P_{12})_{D,1} - (\overline{\Delta}P_{12})_{D,4}] \tag{7.7}$$

From our pressure drop measurements along the column it is inferred that there were some dead or poorly fluidized zones above some distributors, such as distributor-4, used in our experiments. The volume of dead zone, $\gamma_D AH_{01}$, is dependent on some parameters of the distributor, as shown in Figs. 7.9 and 7.10. Both pitch and hole diameter (or free area) influence the volume of the dead zone. The effect of pitch appears, however, to be more significant than that of hole diameter. Based on the above model, the dead zone volume in columns fitted with distributor-4 can reach 40 - 50% of the grid zone, while for distributors 2 and 3, the dead zone volume was around 20%. This suggests that approximately 15 to 20% of the initial mass of particles may be subject to malfluidization in the dead zone on the grid for $H_{mf} = 0.15$ m and distributor-4, if distributor-1, which had the best performance in our experiments, had all particles in the grid zone being utilized fully. The reaction conversion (or contacting efficiency) achieved in vessels fitted with distributor-4 is therefore less than for distributor-1, consistent with the conversion

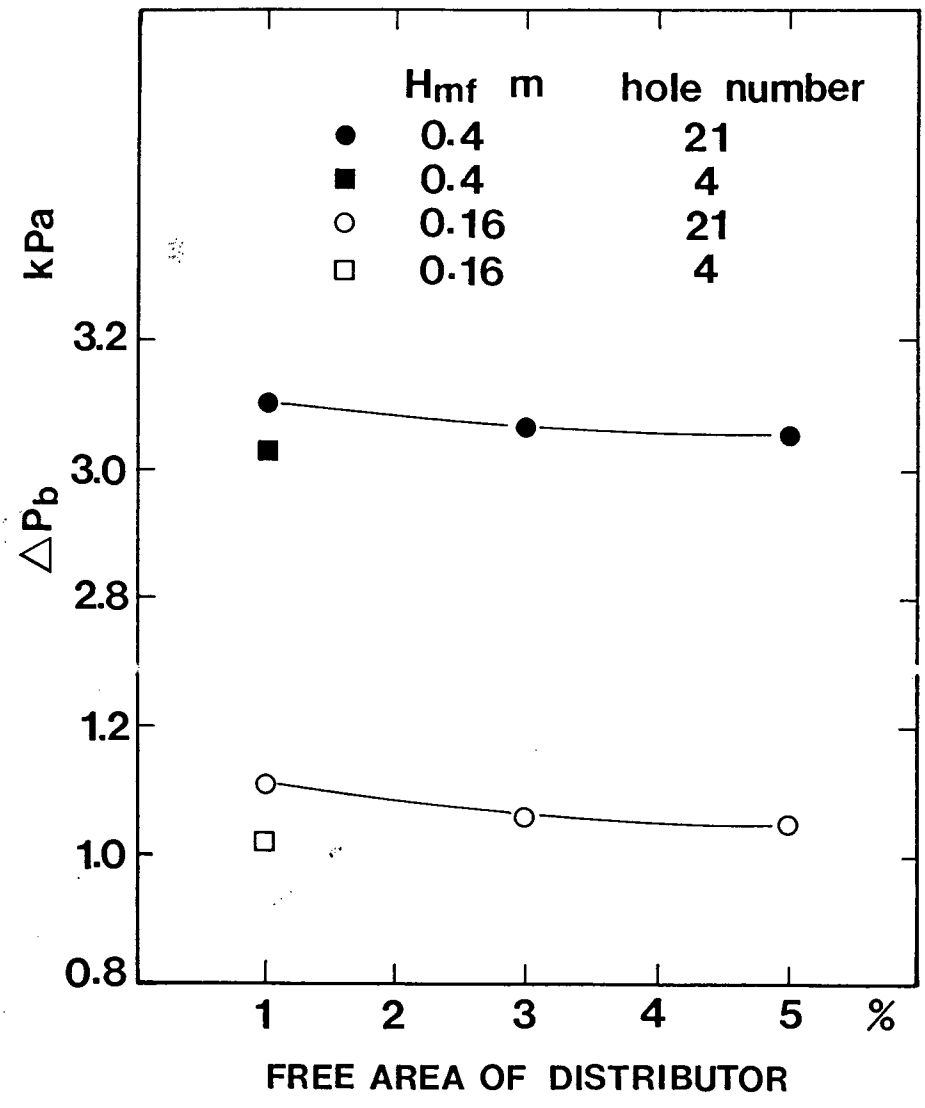

Figure 7.9: Effect of pitch on the pressure drop between ports 1 and 2: N-FCC of wide PSD, $U = 0.2$ m/s.

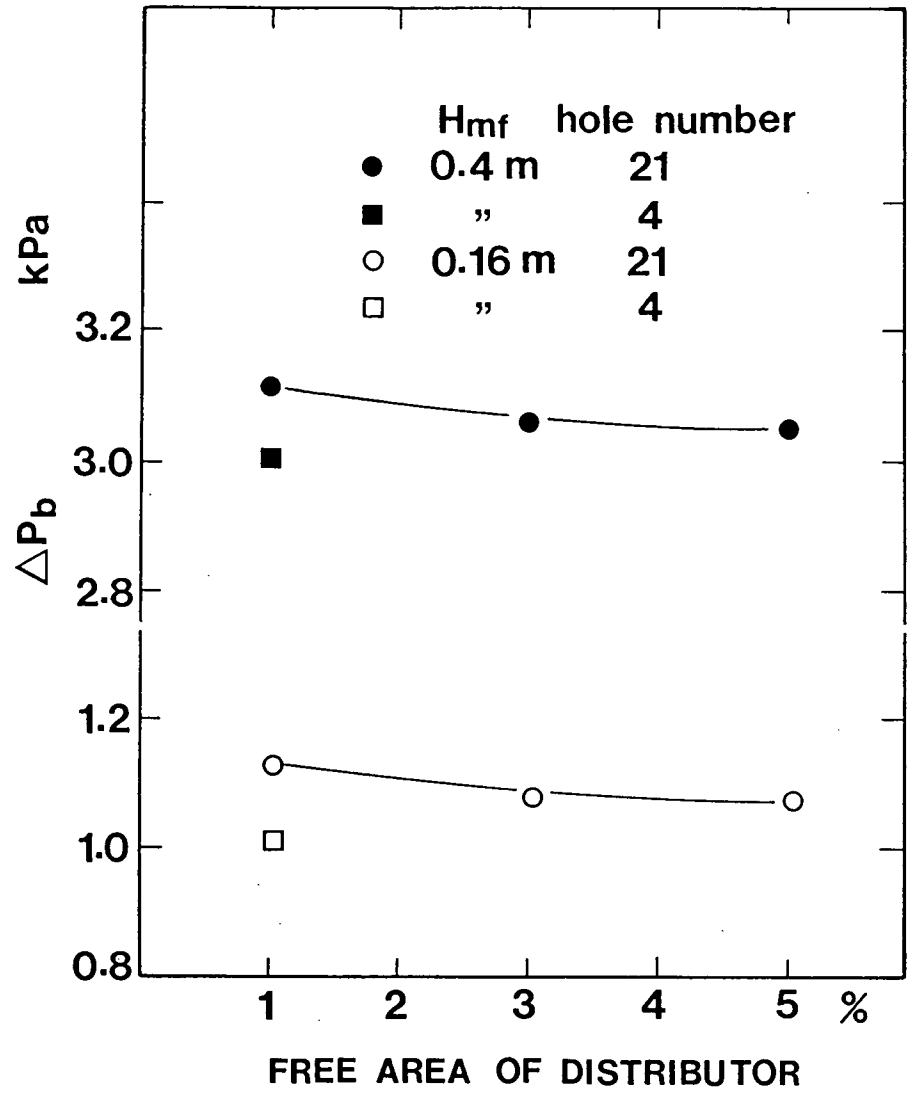

Figure 7.10: Effect of pitch on the pressure drop between ports 1 and 2: N-FCC of narrow PSD, $U = 0.2$ m/s.

results in Figs. 7.2 and 7.3. For H_{mf} = 0.15 m, therefore, the effect of a dead zone or of poorly fluidized particles may play a key role in determining the overall performance.

For H_{mf} = 0.4 m, the dead zone influence tended to be reduced, since the ratio of particles in the dead zone to the total initial mass of particles was only around 5 - 8% for distributor-4, if there was no dead zone for distributor-1. Comparison of the reaction results shown in Figs. 7.4 and 7.5, suggests that the influence of initial bubble size caused by different gas flow rate through the orifice also plays an important role, as discussed by Yang et al (1984).

By comparing the results in Fig. 7.9 with those in Fig. 7.10, we find that the particle size distribution also affected, to a certain extent, the volume of dead zone in the grid region. The dead zone volume with distributor-4 appears to be more extensive in beds of narrow PSD than in beds of wide PSD.

Comparing the conversion obtained in fluidized beds with H_{mf} = 0.15 m to that with H_{mf} = 0.4 m, it is clear that the "entrance effect" due to the grid zone is related to the PSD, as shown in Figs. 7.6 and 7.7. For particles of wide PSD, the ratio of conversion achieved in the grid zone for H_{mf} = 0.15 m to that obtained for H_{mf} = 0.4 m is higher than for the narrow PSD. This implies that the influence of the PSD on the conversion achieved in the first 150 mm of bed was greater than that on the subsequent 250 mm. Moreover, the "entrance effect" appears to be more significant for the wide PSD than for the narrow PSD.

Chapter 8

Conclusions and Recommendations for Further Work

8.1 Overall Conclusions

1. The effect of particle size distribution (PSD) on the performance of a fluidized bed reactor was investigated by combining measurements of chemical conversion (ozone decomposition reaction) with study of key aspects of the hydrodynamics for different size distributions of FCC catalyst, each having a mean particle size of about 60 μm. Fresh and spent FCC catalysts were prepared of "narrow", "bimodal" and "wide" size distributions for comparative experiments. Most of the experiments were carried out in a column of diameter 102 mm, with some of the hydrodynamic tests conducted in a two-dimensional column.

2. The influence of PSD on hydrodynamics and conversion appears to apply to a number of hydrodynamic regimes, but to be most prominent for gas velocities corresponding to the turbulent fluidization regime in the wide size distribution catalysts. In bubbling and slugging fluidized beds, the influence of the PSD became more significant with increasing superficial gas velocity.

3. Both the void size and the dense phase expansion in fluidized beds were found to be influenced by the PSD, especially for $U > 0.2$ m/s. The void size was usually smallest, while the bed expansion was highest, for the wide size distribution. Particles of narrow PSD produced the largest void size.

4. The particle concentration inside bubbles or voids in a fluidized bed of Group A

particles was higher than what has been reported in the literature for Group B particles. More than 70% of the voids contained more than 2.5% particles by volume.

5. The overall particle size distribution affects both the particle concentration in voids and the particle size distribution in the dilute phase. A greater proportion of fines was found to be present in the dilute phase than in the overall particle size distribution. The solids concentration in the voids in fluidized beds of wide PSD is higher than for the narrow PSD, especially at higher superficial gas velocities.

6. The transitions between fluidization regimes are influenced by the PSD. The earliest transition from bubbling or slugging to turbulent fluidization occurred in the wide size distribution catalyst. Both the amplitude and the frequency of pressure fluctuations are related to the PSD. A narrow size distribution gave the most vigorous fluctuations, while the wide blend corresponded to the lowest amplitude of pressure fluctuations. In the upper part of the bed, the lowest frequency of fluctuations occurred for the narrow PSD.

7. A contacting efficiency of fluidized bed catalytic reactors was defined to evaluate the influence of PSD on the reactor performance. The wide size distribution gave the highest conversion and reactor efficiency, while the narrow blend gave the lowest conversion and efficiency at the same operating conditions.

8. The commonly adopted practice of utilizing "fines content" to characterize Group A powders is not sufficient to express the effect of particle size distribution. The performance of fluidized particles depends not only on the quantity of "fines" (however defined), but also on their nature and on the overall size distribution.

9. For particles of wide size distribution, the reactor performance can be improved significantly by operating in the turbulent or fast fluidization regime. However, for particles of narrow size distribution, the benefit of operating at high gas velocities is greatly reduced.

10. The influence of the particle size distribution and the hydrodynamic regimes should be considered in modelling fluidized bed reactors. At lower gas velocities for wide PSD or over a wider range of gas velocity for narrow PSD, the conversion can be successfully predicted by the "Two-Phase Bubbling Bed Model" with modifications to express the hydrodynamic effect of PSD. For beds of wide PSD and operated at higher gas velocities, a single phase Axial Dispersion Model gave good predictions of the observed results, with closed and open boundary conditions at the inlet and top of the bed, respectively, and with the effective axial dispersion coefficient derived from measurements of Guo (1987).

11. A larger pressure drop across the gas distributors is not enough to assure good performance of the distributor. The reactor efficiency in the distributor region was found to be higher for a distributor with more holes, than for one with fewer holes even though the latter had a higher pressure drop.

8.2 Recommendations for Further Work

1. All the tests done in the current project were for Group A catalysts. It is recommended that the kind of experiments here be extended to Group B catalysts.

2. In the apparatus used in the current work, it was not possible to exceed a superficial gas velocity of about 1.8 m/s for FCC type particles. It would be useful to extend the work to higher gas velocities. This could be accomplished by modifying the apparatus employed in this project to provide a controllable particle circulation system, or by using a different set-up so that the influence of PSD within the fast fluidization regime can be explored.

3. It would be helpful to obtain more quantitative hydrodynamic results in a three-dimensional column, e.g. by using optical fibres or capacitance probes to determine void

sizes for different particle size distributions.

4. Another technique, such as energy attenuation of γ-rays, should be developed to investigate the PSD effect on solid concentrations in voids to avoid the interference of mean particle size.

5. The effect of PSD on the freeboard phenomena in fluidized beds should be evaluated by measuring the entrainment rate, solids hold-up and its distribution by particle size in the freeboard region for different particle size distributions and different gas velocities.

Nomenclature

A	cross-sectional area of fluidized bed	m^2
a_b	bubble surface area per unit volume of bubble	m^{-1}
A_p	surface area of a particle	m^2
C_{Ab}, C_{Ad}	concentration of reacting species in bubble, dense phase	$kmol/m^3$
C_{Ain}, C_{Aout}	inlet, outlet concentration of reacting component	$kmol/m^3$
D	gas molecular diffusivity	m^2/s
D_b	diameter of bubbles (volume - equivalent)	m
D_e	gas axial dispersion coefficient	m^2/s
$\overline{d}_p$	average particle diameter	m
d_{pi}	particle diameter representing i^{th} size interval	m
D_T	bed diameter	m
E	contact efficiency of fluidized bed reactor defined by eqn. 3.5	-
E_{ca}, E_{fa}	contact efficiency with coarser fraction, finer fraction active	-
f	fraction of particles by mass in given size interval	-
F_p	dimensionless standard deviation of pressure drop fluctuations	-
f_p	frequency of pressure fluctuations	s^{-1}
g	acceleration due to gravity	m/s^2
G_s	solid mass flux	kg/m^2s
H	mean expanded bed height	m
H_{mf}	bed height at minimum fluidization	m
I	intensity of transmitted light	W
I_o	intensity of transmitted light with no particles present	W

k	factor levels of the test	-
k_f'	dimensionless kinetic rate constant, $k_r H_{mf}(1 - \epsilon_{mf})/U$	-
k_q	interphase mass transfer coefficient	m/s
k_r	reaction rate constant based on the volume of the particles	s^{-1}
k_{rb}, k_{rd}	effective activity of the bubble, dense phase solids	s^{-1}
L	path length for light transmission	m
n_i	number of independent observations for one test	-
N_i	number of voids with $(I_o/I)_i$	-
N_T	total number of voids with solids concentration $< 5\%$ (vol.)	-
Pe	Peclet number, UH/D_e	-
Pe_p	axial Peclet number based on the particle size	-
Q	extinction coefficient	-
Q_b	visible bubble flow rate	m^3/s
S	ratio of finer fraction to coarser fraction by volume in the bed	-
S_b, S_d	ratio of finer to coarser fraction by volume in bubble, dense phase	-
U	superficial gas velocity	m/s
u_b	bubble velocity	m/s
U_c	superficial gas velocity at onset of turbulent fluidization regime	m/s
U_{jc}	minimum gas velocity through the orifice to eliminate the dead zone	m/s
U_{mb}	minimum bubbling superficial velocity	m/s
U_{mf}	minimum fluidization superficial velocity	m/s
U_{rel}	particle velocity relative to rising void	m/s
U_s	particle velocity	m/s
U_T	particle terminal settling velocity	m/s

U_{TR}	transport velocity of particles	m/s
V_{cat}	volume of catalyst particles	m^3
V_{cf}	volume of catalyst particles in fluidized bed reactor	m^3
V_{cp}	volume of catalysts to achieve same conversion in plug flow reactor	m^3
v_g	volumetric gas flow rate	m^3/s
V_p	volume of a particle	m^3
W_{cat}	mass of catalysts in fluidized bed	kg
X	dimensionless interphase mass transfer group	-
x	conversion of reacting component	-
x_i	mass fraction of particles having characteristic diameter d_{pi}	-
z	height coordinate measured from distributor	m
α	size parameter, $\pi d_p/\lambda$	-
α_D	angle defined in Figure 2.12	$degrees$
ϵ	voidage inside the voids in fluidized beds	-
ϵ_b	fraction of bed volume occupied by bubble phase	-
ϵ_d	dense phase voidage	-
ϵ_f	overall voidage in fluidized beds	-
ϵ_{mf}	bed voidage at minimum fluidization	-
ϵ_p	voidage in the fixed bed	-
μ_g	gas viscosity	Ns/m^2
λ	wave length	m
γ_D	ratio of volume of grid region dead zone to total bed volume	-
ρ_b	bulk density of particles	kg/m^3
ρ_g	gas density	kg/m^3
ρ_p	particle density	kg/m^3

Φ	ratio U_{mb}/U_{mf}	-
ϕ_b, ϕ_d	fraction of bed volume occupied by bubble, dense phase solids	-
ΔP_B, ΔP_D	pressure drop across bed and distributor, respectively	kN/m^2

Subscripts:

b	bubble phase
B	bimodal size distribution
d	dense phase
g	gas
i	ith particle size interval
mb	minimum bubbling
mf	minimum fluidization
N	narrow size distribution
o	overall
p	particles
v	void or dilute phase
W	wide size distribution

References

Abrahamsen, A.R. and Geldart, D. (1980). Behaviour of gas fluidized beds of fine powders, Powder Technol., **26**, 35-55.

Agarwal, J.C., W.L. Davis, and D.T. King, (1962). Fluidized-bed coal dryer, Chem. Eng. Progr., **58**, No. 11, 85-90.

Agarwal, J.C. and Davis, W.L. (1966). The dynamics of fluidization of iron and its ores, Chem. Eng. Progr. Symp. Ser., No. 67, **62**, 101-110.

Avidan, A. and Yerushalmi, J. (1982). Bed expansion in high velocity fluidization, Powder Technol., **32**, 223-232.

Avidan, A. and Edwards, M., (1986). Modelling and scale-up of Mobil's fluid-bed MTG process, in Fluidization, ed. K. Ostergaard and A. Sorensen, Eng. Foundation, New York, pp.457-464.

Baeyens, J. and Geldart, D. (1974). An investigation into slugging fluidized beds, Chem. Eng. Sci., **29**, 255-265.

Bauer, W. and Werther, J. (1981). Scale-up of fluid bed reactors with respect to size and gas distributor design - measurements and model calculations, Proceedings of 2nd World Congress of Chemical Engineering, Montreal, Canada. Vol. 3, pp.69-72.

Behie, L.A. and P. Kehoe, (1973). The grid region in a fluidized bed reactor, AIChE. J., **19**, 1070-1072.

Brereton, C. (1987). Fluid mechanics of high velocity fluidized beds, Ph.D. Thesis, The University of British Columbia.

Briens, C.L., M.A. Bergougnou and C.G.J. Baker, (1978). Leakage of solids (weeping, dumping) at the grid of a 0.6 m diameter gas fluidized bed, in Fluidization, ed. J.F. Davidson and K.L. Keairns, Cambridge University Press, Cambridge, pp.38-43.

Briens, C.L., M.A. Bergougnou and C.G.J. Baker, (1980). Grid leakage in gas fluidized beds: the effect of bed height, grid thickness, wave breakers, cone-shaped grid holes and pressure drop fluctuations, in Fluidization, ed. J.R. Grace and J.M. Matsen, Plenum Press, New York, pp.413-420.

Brown, D.J., E.J. Weatherby and K. Alexander, (1988). Shape, concentration and anomalous diffraction effects in sizing solids in liquids, in Optical Particle Sizing Theory and Practice, ed. G. Gouesbet and G. Grehan, Plenum Press, New York, pp.351-362.

Brown, G.W. (1990). Direct measurement of FCC fluidizability helps spot problems, Oil & Gas J., Jan. 15, 46-49.

Canada, G.S., McLaughlin, M. H. and Staub F.W. (1978). Flow regimes and void fraction distribution in gas fluidization of large particles in beds without tube banks, AIChE Symp. Ser. 176, **74**, 14-26.

Cankurt N.T. and J. Yerushalmi, (1978). Gas backmixing in high velocity fluidized beds, in Fluidization, ed. J.F. Davidson and D.L. Keairns, Cambridge University Press, Cambridge, pp.387-392.

Carberry, J.J. (1976). Chemical and Catalytic Reaction Engineering, McGraw-Hill, New York.

CGCPC Report, (1985). Innovation of an acrylonitrile fluidized bed reactor, China General Corporation of Petrochemical Industry.

Chavarie, C. and Grace, J.R. (1975). Performance analysis of a fluidized bed reactor, Ind. Eng. Chem., Fundam., **14**, 75-91.

Clift, R., (1986). Hydrodynamics of bubbling fluidized beds, in Gas Fluidization Technology, ed. D. Geldart, Wiley, New York, pp.53-95.

Clift, R. and Grace, J.R. (1972). The coalescence of bubble chains in fluidized beds, Trans. Instn. Chem. Engs. **50**, 364-371.

Clift, R., Grace, J.R., Cheung, L. and Do, T.H. (1972). Gas and solids motion around

deformed and interacting bubbles in fluidized beds, J. Fluid Mechanics, **51**, 187-205.

Clift, R., Grace, J.R. and Weber, M.E. (1974). Stability of bubbles in fluidized beds, Ind. Eng. Chem. Fund., **13**, 45-51.

Cooper, D.J. and D.E. Clough, (1985). Experimental tracking of particle-size distribution in a fluidized bed, Powder Technol., **44**, 169-177.

Cooper, D.J. and D.E. Clough, (1986). Optimal, real-time monitoring of particle size distribution in a fluidized bed, AIChE. J., **32**, 389-396.

Danckwerts, P.V. (1953). Continuous flow systems distribution of residence times, Chem. Eng. Sci., **3**, 1-13.

Darton, R.C., R.D. Lanauze, J.F. Davidson and D. Harrison, (1977). Bubble growth due to coalescence in fluidized bed, Tran. Inst. Chem. Eng. **55**, 274-280.

Davidson, J.F., and D. Harrison, (1963). Fluidised Particles, Cambridge University Press, Cambridge, England.

de Groot, J.H. (1967). Scaling-up of gas-fluidized bed reactors, Proc. Intern. Symp. on Fluidization, ed. A.A.H. Drinkenburg, Netherlands Univ. Press, Amsterdam, pp.348-361.

Dry, R.J., Judd, M.R. and Shingles, T. (1983). Two phase theory and fine powders, Powder Technol., **34**, 213-223.

Dry, R.J. and M.R. Judd, (1985). Fluidised beds of fine, dense powders: scale-up and reactor modelling, Powder Technol., **43**, 41-53.

Edwards, M. and A. Avidan, (1986). Conversion model aids scale-up of Mobil's fluid bed MTG process, Chem. Eng. Sci., **41**, 829-835.

Fakhimi, S., S. Sohrabi and D. Harrison, (1983). Entrance effects at a multi-orifice distributor in gas-fluidized beds, Can. J. Chem. Eng. **61**, 364-369.

Fan, L.T., Tho-ching Ho, S. Hiraoka and W.P. Walawender, (1981). Pressure fluctuations in a fluidized bed, AIChE J. **27**, 388-396.

Fan, L.T., Tho-ching Ho and W.P. Walawender, (1983). Measurements of the rise velocities of bubbles, slugs and pressure waves in a gas-solid fluidized bed using pressure fluctuation signals, AIChE. J., **29**, 33-39.

Fenton, D.L. and J.J. Stukel, (1976). Measurement of the local particle concentration in fully turbulent duct flow, Int. J. Multiphase Flow, **3**, 141-145.

Frye, C.G., W.C. Lake and H.C. Eckstrom, (1958). Gas-solid contacting with ozone decomposition reaction, AIChE. J., **4**, 403-408.

Furusaki, S., T. Kikuchi and T. Miyauchi, (1976). Axial distribution of reactivity inside a fluid bed reactor, AIChE. J., **22**, 354-359.

Garcia, A., J.R. Grace and R. Clift, (1973). Behaviour of gas bubbles in fluidized beds, AIChE. J., **19**, 369-370.

Geldart, D. (1973). Types of gas fluidization, Powder Technol., **7**, 285-292.

Geldart, D. (1986). Gas Fluidization Technology, John Wiley & Sons Ltd., New York.

Geldart, D. and A.R. Abrahamsen. (1980). The effect of fines on the behaviour of fluidized beds of small particles, in Fluidization, ed. J.R. Grace and J.M. Matsen, Plenum Press, New York, pp.453-460.

Geldart, D. and D.J. Pope, (1983). Interaction of fine and coarse particles in the freeboard of a fluidized bed, Powder Technol., **34** 95-97.

Geldart, D. and A.C. Wong, (1984). Fluidization of powders showing degrees of cohesiveness-I. bed expansion, Chem. Eng. Sci., **39**, 1481-1488.

Geldart, D. and A.C. Wong, (1985). Fluidization of powders showing degrees of cohesiveness, Chem. Eng. Sci., **40**, 653-661.

Geldart, D. and A.L. Radtke, (1986). The effect of particle properties on the behaviour of equilibrium cracking catalysts in standpipe flow, Powder Technol., **47**, 157-165.

Geldart, D. and M.J. Rhodes (1986). From minimum fluidization to pneumatic transport, in Circulating Fluidized Bed Technology, ed. F. Basu, Pergamon Press, pp.21-31.

Geldart, D. and B. Buczek. (1989). The effect of the size of the fines on the fluidization behaviour of equilibrium cracking catalyst, in Fluidization, ed. J.R. Grace, L.W. Shemilt and M.A. Bergougnou, Engineering Foundation, New York, pp.179-186.

George S.E. and J.R. Grace, (1978). Entrainment of particles from aggregative fluidized beds, AIChE Symp. Ser., No. 176, Vol. 74, 67-74.

Grace, J.R. (1970). The viscosity of fluidized beds, Can. J. Chem. Eng., **48**, 30-33.

Grace, J.R. (1981). Fluidized bed reactor modeling: an overview, American Chemical Society, Symp. Ser., No. 168, 3-18.

Grace, J.R. (1982). Fluidized-bed hydrodynamics, Chapter 8.1 in Handbook of Multiphase Systems, ed. G. Hetsroni, Hemisphere, Washington, pp.8-5 - 8-62.

Grace, J.R. (1984). Generalized models for isothermal fluidized bed reactors, Chapter 13 in Recent Advances in Engineering Analysis of Chemically Reacting Systems, ed. L.K. Doraiswamy, Wiley Eastern, New Delhi, pp.237-255.

Grace, J.R. (1986a). Fluid beds as chemical reactors, Chapter 11 in Gas Fluidization Technology, ed. D. Geldart, Wiley, New York, pp.287-341.

Grace, J.R. (1986b) Contacting modes and behaviour classification of gas-solid and other two-phase suspensions, Can. J. Chem. Eng., **64**, 353-361.

Grace, J.R. and R. Clift, (1974). On the two-phase theory of fluidization, Chem. Eng. Sci., **29**, 327-334.

Grace, J.R. and H.I. de Lasa, (1978). Reaction near the grid in fluidized beds, AIChE. J., **24**, 364-366.

Grace, J.R. and D. Harrison, (1969). The behaviour of freely bubbling fluidized beds, Chem. Eng. Sci., **24**, 497-508.

Guo, F. (1987). Gas flow and mixing behaviour in fine-powder fluidized bed, AIChE

J., **33**, 1895-1898.

Harrison, D., J.F. Davidson and J.W. de Kock, (1961). On the nature of aggregative and particulate fluidisation, Trans. Instn Chem. Engrs. **39**, 202-211.

Hartge, E.-U., Y. Li, and J. Werther, (1986). Flow structures in fast fluidized beds, in Fluidization, ed K. Ostergaard and A. Sorensen, Engng. Foundation, New York, pp.345-352.

Haultain, H.E. (1937). Splitting the minus-200 with the superpanner and infrasizer, The Canadian Institute of Mining and Metallurgy, pp.229-240.

Hayashi, S. (1988). Measurements of absolute concentration and size distribution of particles by laser small angle scattering, in Optical Particle Sizing Theory and Practice, ed. G. Gouesbet and G. Grehan, Plenum Press, New York, pp.549-558.

Herb, B., K. Tuzla and J.C. Chen, (1989). Distribution of solid concentrations in circulating fluidized bed, in Fluidization, ed. J.R. Grace, L.M. Shemilt and M.A. Bergougnou, Engng. Foundation, New York, pp.65-72.

Hiby, J.W., (1964). Untersuchungen *ü*ber den kritischen mindestdruckverlust des antrömbodens bei fluidalbetten, Chem. Ingr. Tech., **36**, 228-229.

Hiraki, I., Yoshida, K. and Kunii, D. (1966). Behaviour of bubbles in a two- dimensional fluidized bed, Kagaku Kogaku, Vol. 4, No. 1, 139-142.

Ho, T-C., T.K. Chen and J.R. Hopper, (1984). Pressure drop across the distributor in fluidized beds with regular and irregular distributor design, AIChE Symposium Ser., No. 241, Vol. 80, 34-40.

Ho, T.C., R.C. Wang and J.R. Hopper, (1987). Characteristics of grid zone heat transfer in a gas-solid fluidized bed, AIChE. J., **33**, 843-847.

Hodkinson, J.R. (1966). The optical measurement of aerosols, in Aerosol Science, ed. Davies, C.N., Academic Press, New York, pp.931-932.

Hogg, R.V. and Ledolter, J. (1987). Engineering Statistics, Macmillan Publishing

Company, New York.

Horio, M., M. Nishimuro, and H. Ishii, (1989). On the nature of "turbulent fluidized beds", Proceedings of the 3rd SCEJ Symp. on Circulating Fluidized Beds, Tokyo, Japan, 54-61.

Horio, M. and A. Nonaka, (1987). A generalized bubble diameter correlation for gas-solid fluidized beds, AIChE. J., **33** 1865-1872.

Horvath, M., L. Bilitzky and J. Huttner, (1985). Ozone, Elsevier Science Publishing Co., New York.

Hovmand, S. and J.F. Davidson, (1968). Chemical conversion in a slugging fluidized bed, Trans. Instn. Chem. Engrs., **46**, 190-203.

Hovmand, S., Freedman, W. and Davidson, J.F. (1971). Chemical reaction in a pilot-scale fluidized bed, Trans. Instn. Chem. Engrs, **49**, 149-162.

Hsiung, T.P. and J.R. Grace, (1978). Formation of bubbles at an orifice in fluidized beds, in Fluidization, ed. J.F. Davidson and D.L. Keairns, Cambridge University Press, Cambridge, England, pp.19-24.

Ip, T. (1988). Influence of particle size distribution on fluidized bed hydrodynamics, M.A.Sc. Thesis, The University of British Columbia.

Jin, Y., Yu, Z., Wang, Z. and Cai, P. (1986). A criterion for transition from bubbling to turbulent fluidization, in Fluidization, ed. K. Ostergaard and A. Sorensen, Engng. Foundition, New York, 289-296.

Johnsson, J.E., J.R. Grace and J.J. Graham, (1987). Fluidized-bed reactor model verification on a reactor of industrial scale, AIChE. J., **33**, 619-627.

Judd, M.R. and Goosen, R. (1989). Effects of particle shape on fluidization characteristics of fine particles in freely bubbling and turbulent regimes, in Fluidization, ed. J.R. Grace, L.W. Shemilt and M.A. Bergougnou, Engng. Foundation, New York, pp.41-48.

Kai, T. and Furusaki, S. (1985). Behaviour of fluidized beds of small particles at

elevated temperatures, J. Chem. Eng. Japan, **18**, 113-118.

Kai, T., Shirakawa, Y., Takahashi, T. and Furusaki, S. (1987). "Change in bubble behaviour for different fluidizing gases in a fluidized bed", Powder Technol., **51**, 267-271.

Kato, K. and C.Y. Wen, (1969). Bubble assemblage model for fluidized bed catalytic reactors, Chem. Eng. Sci., **24**, 1351-1369.

Kehoe, P.W.K. and Davidson, J.R. (1971). Continuously slugging fluidized beds, Inst. Chem. Eng. Symp. Ser., **33**, 97-116.

Kehoe, P.W.K. and J.R. Davidson, (1973). Pressure fluctuations in slugging fluidized beds, AIChE Symp. Ser., No. 128, Vol. 69, 34-40.

Khoe, G.K., Ip, T. and Grace, J.R. (1991). Rheological and fluidization behaviour of powders of different particle size distribution, Powder Technol., in press.

Kobayashi, H., Arai, F. and Chiba, T. (1966). Behaviour of bubbles in a gas-solid fluidized bed, Kagaku Kogaku, Vol. 4, No. 1, 147-150.

Kono, H.O., Chiba, S., Ells, T. and Suzuki, M. (1986a). Characterization of emulsion phase in fine particle fluidized beds, Powder Technol., **48**, 51-58.

Kono, H.O., S. Chiba, T. Ells, P. Daniell and M. Suzuki, (1986b). The effect of emulsion phase characteristics on Fluidization - selection of powder properties, in Fluidization, ed. K. Ostergaard and A. Sorensen, Engng. Foundation, New York, pp.143-150.

Krambeck, F.J., A.A. Avidan, C.K. Lee and M.N. Lo, (1987). Predicting fluid-bed reactor efficiency using absorbing gas tracers, AIChE. J., **33**, 1727-1734.

Kunii, D. and O. Levenspiel, (1969). Fluidization Engineering, John Wiley & Sons, New York.

Kurz, H.P. and Münz, G. (1975). The influence of particle size distribution on the flow properties of limestone powders, Powder Technol., **11**, 37-40.

Lanneau, K.P. (1960). Gas-solids contacting in fluidized beds, Trans. Instn. Chem. Engrs, **38**, 125-143.

Lee, G.S. and Kim, S.D. (1988). Pressure fluctuations in turbulent fluidized beds, J. Chem. Eng. Japan, **21**, 515-521.

Levenspiel, O. (1972). Chemical Reaction Engineering, 2nd ed. Wiley, New York.

Lewis, M.K., Gilliland, E.R. and Glass, M. (1959). Solid-catalyzed reaction in a fluidized bed, AIChE. J., **5**, 419-426.

Li, Y. and M. Kwauk, (1980). The dynamics of fast fluidization, in Fluidization, ed. J.R. Grace and J.M. Matsen, Plenum Press, New York, pp.537-544.

Lirag, R.C., and H. Littman, (1971). Statistical study of the pressure fluctuations in a fluidized bed, AIChE Symp. Ser. No. 116, Vol. 67, pp.11-22.

Lloyd, P.J. and P.J. Webb, (1987). The flooding of a powder - the importance of particle size distribution, Powder Technol., **51**, 125-133.

Lockett, J. and Harrison, D. (1967). The distribution of voidage fraction near bubbles rising in gas-fluidized beds, Proc. Intern. Symp. on Fluidization, ed. A.A.H. Drinkenburg, Netherlands Univ. Press, Amsterdam, 257-270.

Massimilla, L. (1973). Behaviour of catalytic beds of fine particles at high gas velocities, AIChE Symp. Ser. Vol. 69, No. 128, 11-15.

Matsen, J.M. (1973). Evidence of maximum stable bubble size in a fluidized bed, AIChE Symp. Ser. No. 128, Vol. 69, 30-33.

Matheson, G.L., W.A. Herbst and P.H. Holt, (1949). Characteristics of fluid-solid systems, Industrial and Engineering Chemistry, **41**, 1099-1104.

May, W.G. (1959). Fluidized-bed reactor studies, Chem. Eng. Prog. **55**(12), 49-56.

Mears, D.E. (1971a). The role of axial dispersion in trickle-flow laboratory reactors, Chem. Eng. Sci., **26**, 1361-1366.

Mears, D.E. (1971b). Tests for transport limitations in experimental catalytic reactors, I&EC. Process Des. Develop., **10**, 541-547.

Monceaux, L., M. Azzi, Y. Molodtsof and J.F. Large, (1986). Particle mass flux

profiles and flow regime characterization in a pilot-scale fast fluidized bed unit, in Fluidization, ed. K. Ostergaard and A. Sorensen, Eng. Foundation, New York, pp.337-344.

Mori, S. and C.Y. Wen, (1975). Estimation of bubble diameter in gaseous fluidized beds, AIChE. J., **21**, 109-115.

Morse, R.D. and Ballou, C.O. (1951). The uniformity of fluidization - its measurement and use, Chem. Eng. Progr. **47**, 199-204.

Nicastro M.T. and L.R. Glicksman, (1984). Experimental verification of scaling relationships for fluidized bed, Chem. Eng. Sci., **39**, 1381-1391.

Oki, K., M. Ishida, and T. Shirai, (1980). The behaviour of jets and particles near the gas distributor grid in the three-dimensional fluidized bed, in Fluidization, ed. J.R. Grace and J.M. Matsen, Plenum Press, New York, pp.421-428.

Orccutt, J.C., Davidson, J.F, and Pigford, R.L. (1962). Reaction time distributions in fluidized catalytic reactors, Chem. Eng. Prog. Symp. Ser. **58**(38), 1-5.

Patrose B. and H.S. Caram, (1984). The mechanics of particle motion in a grid jet, AIChE Symp. Ser. No. 241, Vol. 80, 48-56.

Pell, M. and S.P. Jordan, (1988). Effects of fines and velocity on fluid bed reactor performance, AIChE Symp. Ser. No. 262, Vol. 84, 68-73.

Rase, H.F. (1977). Chemical Reaction Design for Process Plants, Vol. 1, John Wiley & Sons, New York.

Rathbone, R.R. and J.F. Davidson, (1986). Design of distributors for air gasification of char in fluidized bed, in Fluidization, ed. K. Ostergaard and A. Sorensen, Engng. Foundation, New York, pp.63-70.

Raterman, M.F. (1985). FCC catalyst flow-problem predictions, Oil & Gas J. Technology, Jan. 7, 87-92.

Razumovskii, S.D. and G.E. Zaikov, (1984). Ozone and its Reactions with Organic Compounds, Elsevier Science Pub., New York.

Rhodes, M.J. and D. Geldart, (1986). Transition to turbulence?, in Fluidization, ed. K. Ostergaard and A. Sorensen, Eng. Foundation, New York, pp.281-288.

Rhodes, M.J., T. Hirama, G. Cerutti and D. Geldart, (1989). Non-uniformities of solids flow in the risers of circulating fluidized beds, in Fluidization, ed. J.R. Grace, L.W. Shemilt and M.A. Bergougnou, Engng. Foundation, New York, pp.73-80.

Rietema, K. (1967). Application of mechanical stress theory to fluidization, Proc. Intern. Symp. on Fluidization, ed. A.A.H. Drinkenburg, Netherlands Univ. Press, Amsterdam, pp.154-175.

Rowe, P.N. (1976). Prediction of bubble size in a gas-fluidized bed, Chem. Eng. Sci., **31**, 285-288.

Rowe, P.N. and D.J. Everett, (1972). Fluidised bed bubbles viewed by X-rays, Trans. Instn. Chem. Engrs., **50**, 43-60.

Rowe, P.N. and H.J. MacGilivray, (1980). The structure of a 15 cm diameter gas fluidised bed at up to 1 m/s and seen by X-rays, in Fluidization, ed. J.R. Grace and J.M. Matsen, Plenum Press, New York, 545-553.

Sadasivan, N., Barreteau, D. and Laguerie, C. (1980). Studies on frequency and magnitude of fluctuations of pressure drop in gas-solid fluidized beds, Powder Technol., **26**, 67-74.

Satija, S. and L-S. Fan, (1985). Characteristics of slugging regime and transition to turbulent regime for fluidized beds of large coarse particles, AIChE. J., **31**, 1554-1562.

Schmidt, H., C. Tsouris, E. Eggert, L.L. Tavlarides, (1989). Laser photometric probe for concentration measurements in liquid dispersions, AIChE. J., **35**, 507-510.

Schnitzlein, M.G. and H. Weinstein, (1988). Flow characterization in high-velocity fluidized beds using pressure fluctuations, Chem. Eng. Sci., **43**, 2605-2614.

Shuster, W.W., and P. Kisliak, (1952). The measurement of fluidization quality, Chem. Eng. Prog., **48**, 455-460.

Sinnott, R.K. (1983). An Introduction to Chemical Engineering Design, Vol. 6 in Chemical Engineering, ed. J.M. Coulson and J.F. Richardson, Pergamon Press, Oxford, pp.354-360.

Sit, S-P., and J.R. Grace, (1981). Effect of bubble interaction on interphase mass transfer in fluidized beds, Chem. Eng. Sci., **36**, 327-335.

Sit, S-P., and J.R. Grace, (1986). Interphase mass transfer during bubble formation in fluidized beds, in Fluidization, ed. K. Ostergaard and A. Sorensen, Eng. Foundation, New York, pp.39-46.

Sun, G., Wang, Z. and Chen, G.T. (1983). The incipient bubbling velocity and voidage of gas-solid particle systems, Jl. Zhejiang University, China, 4, 97-108.

Sun, G. and Chen, G.T. (1986). Development of novel reacting flow technology in fluidization systems, A Report to China General Corporation of Petrochemical Industry.

Sun, G. and Chen, G.T. (1989). Transition to turbulent fluidization and its prediction, in Fluidization, ed. J.R. Grace, L.W. Shemilt and M.A. Bergougnou, Eng. Foundation, New York, pp.33-41.

Thiel, J. and Potter, O.E. (1977). Slugging in fluidized beds, Ind. Eng. Chem. Fundam., **16**, 242-247.

Tien, C.L. (1985). Radiation properties of particulates, in Handbook of Heat Transfer Fundamentals, 2nd ed. Hemisphere, New York, pp.14.83-14.91.

Tien, C.L. (1988). Thermal radiation in packed and fluidized beds, ASME Jl. of Heat Transfer, **110**, 1230-1242.

Toei, R., Matsuno, R., Kojima, H., Nagai, Y., Nakagawa, K. and Yu, S. (1966). Behaviour of bubbles in the gas-solid fluidized bed, Kagaku Kogaku, Vol. 4, No. 1, 142-146.

Tung, Y., Z. Yang, Y. Xia, W. Zhang, Y. Yang and M. Kwauk, (1989). Assessing fluidizing characteristics of powders, in Fluidization, ed. J.R. Grace, L.W. Shemilt and

M.A. Bergougnou, Engng. Foundation, New York, pp.169-178.

Van Deemter, J.J. (1961). Mixing and contacting in gas-solid fluidized beds, Chem. Eng. Sci., **13**, 143-154.

Van Deemter, J.J. (1967). The counter-current flow model of a gas-solids fluidized bed, Proceedings Intern. Symp. on Fluidization, ed. A.A.H. Drinkenburg, Netherlands University Press, Amsterdam, pp.334-347.

Van den Aarsen, F.G., A.A.C.M. Beenackers and W.P.M. van Swaaij, (1986). Bubble-to-dense-phase mass transfer kinetics in gas-solid fluidized beds, in Heat and Mass Transfer in Fixed and Fluidized Beds, ed. W.P.M. van Swaaij and N.H. Afgan, Hemisphere, Washington, pp.397-415.

Van Swaaij, W.P.M. and F.J. Zuiderweg, (1972). Investigation of ozone decomposition in fluidized beds on the basis of a two-phase model, in Proceedings of 5th European/ 2nd International Symposium on Chem. Reaction Engineering, Amsterdam, B 9-25 - B 9-36.

Virr, M.J. and H.W. Williams, (1985). Heat recovery by shallow fluidized beds, Chem. Eng. Prog., **81**(7), 50-56.

Walker, B.V., (1970). Gas-solid contacting in bubbling fluidized beds, Ph.D. Thesis, Cambridge University, Cambridge, England.

Warren, H.V., C. Madsen and W.H. White, (1939). Some studies with the Haultain superpanner and infrasizer, Canadian Institute of Mining and Metallurgy, pp.53-56.

Wehner, J.F. and Wilhelm, R.H. (1956). Boundary conditions of flow reactor, Chem. Eng. Sci., **6**, 89-93.

Weimer, A.W., D.C. Gyure and D.E. Clough, (1985). Application of a Gamma- radiation density gauge for determining hydrodynamic properties of fluidized beds, Powder Technol., 44, 179-194.

Weinstein, H., M. Shao, M. Schnitzlein and R.A. Graff, (1986). Radial variation in void fraction in a fast fluidized bed, in Fluidization, ed. K. Ostergaard amd A. Sorensen,

Engng. Foundation, New York, pp.329-336.

Weinstein, H. and J. Li, (1989). An evaluation of the actual density in the acceleration section of vertical risers, Powder Technol., **57**, 77-79.

Weinstein, H., J. Li, E. Bandlamudi, H.J. Feindt and R.A. Graff, (1989). Gas backmixing of fluidized beds in different regimes and regions, in Fluidization, ed. J.R. Grace, L.W. Shemilt and M.A. Bergougnou, Eng. Foundation, New York, pp.57-64.

Wen, C.Y. and Chen, L.H. (1982). Fluidized bed freeboard phenomena; entrainment and elutriation, AIChE. J., **28**, 117-128.

Wen, C.Y., R. Krishnan, R. Khosravi and S. Dutta, (1978). Dead zone heights near the grid of fluidized beds, in Fluidization, ed. J.F. Davidson and D.L. Keairns, Cambridge University Press, Cambridge, England, pp.32-37.

Wen, C.Y., R. Krishnan, and R. Kalyanaraman, (1980). Particle mixing near the grid region of fluidized beds, in Fluidization, ed. J.R. Grace and J.M. Matsen, Plenum Press, New York, pp.405-412.

Werther, J. (1978). Effect of gas distributor on the hydrodynamics of gas fluidized beds, Ger. Chem. Eng. **1**, 166-174.

Werther, J. (1980). Mathematical modelling of fluidized bed reactors, Int. Chem. Eng., **20**, 529-541.

Werther, J. (1984). Hydrodynamics and mass transfer between the bubble and emulsion phases in fluidized beds of sand and cracking catalyst, in Fluidization, ed. D. Kunii and R. Toei, Eng. Foundation, New York, pp.93-101.

Werther, J. and M. Schoessler, (1986). Modeling catalytic reactions in bubbling fluidized beds of fine particles, in Heat and Mass Transfer in Fixed and Fluidized Beds, ed. W.P.M. van Swaaij and N.H. Afgan, Hemisphere Washington, pp.355-370.

Whitehead, A.B. and D.C. Dent, (1967). Behaviour of multiple tuyere assemblies in

large fluidized beds, in Proceedings Intern. Symp. on Fluidization, ed. A.A.H. Drinkenburg, Netherlands University Press, Amsterdam, pp.802-820.

Winter, O. (1968). Density and pressure fluctuations in gas fluidized beds, AIChE. J., **14**, 426-432.

Yacono, C. and H. Angelino, (1978). The influence of gas distributor on bubble behaviour: comparison between "ball distributor" and "porous distributor", in Fluidization, ed. J.F. Davidson and D.L. Keairns, Cambridge University Press, Cambridge, England, pp.25-31.

Yang, G., Z. Huang and L. Zhao, (1984a). Radial gas dispersion in a fast fluidized bed, in Fluidization, ed. D. Kunii and R. Toei, Engng. Foundation, New York, pp.145-152.

Yang, W.C. and Chitester, D.C. (1988). Transition between bubbling and turbulent fluidization at elevated pressure, AIChE Symp. Ser. No. 262, Vol. 84, 10-21.

Yang, X., D.G. Horne, J.G. Yates and P.N. Rowe, (1984b). Distributor-zone reaction in a gas-fluidized bed, AIChE Symp. Ser. No. 241, Vol. 80, 41-47.

Yates, J.G. and Newton, D. (1986). Fine particle effects in a fluidized bed reactor, Chem. Eng. Sci., **41**, 801-806.

Yerushalmi, J. (1982). Applications of fluidized beds, Chapter 8.5 in Handbook of Multiphase Systems, ed. G. Hetsroni, Hemisphere, Washington, pp.8-152 - 8-214.

Yerushalmi, J. and A. Avidan, (1985). High velocity fluidization, in Fluidization, ed. J.F. Davidson, R. Clift and D. Harrison, Academic Press, London, pp.226-293.

Yerushalmi, J., Cankurt, N.T., Geldart, D. and Liss, B. (1978). Flow regimes in vertical gas-solid contact systems, AIChE Symp. Ser., Vol. 74, No. 176, 1-13.

Yerushalmi, J. and N.T. Cankurt, (1979). Further studies of the regimes of fluidization, Powder Technol., **24**, 187-205.

Yerushalmi, J. (1986). High velocity fluidized beds, Chapter 7 in Gas Fluidization Technology, ed. D. Geldart, Wiley, New York, pp.155-196.

Zenz, F.A. and Othmer, D.F. (1960). Fluidization and Fluid-Particle Systems, Reinhold Publishing Corp., New York.

Zuiderweg, F.J. (1967). "Session report" in Proceedings of Intern. Symp. on Fluidization, ed. A.A.H. Drinkenburg, Netherlands University Press, Amsterdam, pp.739-750.

Appendix A

Minimum integral reactor length to minimize axial diffusion effects

For fixed bed reactors, it is generally considered that backmixing effects can be negligible if the ratio of reactor bed length to equivalent particle diameter is more than 50 for gaseous reactions (Carberry, 1976). A more stringent criterion should, however, be used for laboratory fixed bed reactors, or integral reactors, because of the small particle size used, except for differential reactors where disperion dose not affect the measurement results. This criterion can be derived by combining the solution of the continuity equation including the axial diffusion term with the solution for plug flow. A minimum reactor length required to maintain the deviation from plug flow at less than 5% was obtained (Mears, 1971a), giving

$$\frac{H}{\bar{d}_p} = \frac{20n}{Pe_p} \ln \frac{C_{A,in}}{C_{A,out}} \tag{A.1}$$

where n is the reaction order, i.e. $n = 1$ in our experiments. Pe_p is the axial Peclet number, corresponding to the particle size,

$$Pe_p = \frac{\bar{d}_p U}{D_e} \tag{A.2}$$

The effective axial dispersion coefficient, D_e, can be estimated after the Reynolds number and Schmidt number have been calculated (Levenspiel, 1972). The calculation was based on the harshest conditions, that is, the lowest superficial gas velocity ($U = 0.089$ m/s) and the highest reaction conversion ($x = 0.99$) in the fixed bed during the experiments. Other typical operating conditions used were:

operating temperature $T = 20\ ^{o}C$;

operating pressure $P = 0.15$ bar;

bed voidage $\epsilon_p = 0.46$.

Hence

$$S_c = \frac{\mu_g}{\rho_g D} = \frac{1.8 \times 10^{-5}}{1.2 \times 0.204 \times 10^{-4}} = 0.735 \tag{A.3}$$

and

$$Re_p = \frac{\bar{d}_p U \rho_g}{\mu_g} = \frac{60 \times 10^{-6} \times 0.089 \times 1.2}{1.8 \times 10^{-5}} = 0.355 \tag{A.4}$$

while these correspond (Levenspiel, 1972) to:

$$\frac{D_e \epsilon_p}{U \bar{d}_p} = 0.7 \tag{A.5}$$

That is,

$$Pe_p = \frac{\bar{d}_p U}{D_e} = \frac{\epsilon_p}{0.7} = 0.657 \tag{A.6}$$

Hence, from equation A.1, we can obtain:

$$\frac{H}{\bar{d}_p} > 140 \tag{A.7}$$

In our experiments, the height of fixed bed $H > 40$ mm, so that

$$\frac{H}{\bar{d}_p} > 600 \tag{A.8}$$

the axial dispersion effects, therefore, was negligible.

Appendix B

Photometric measurement for spent FCC particles

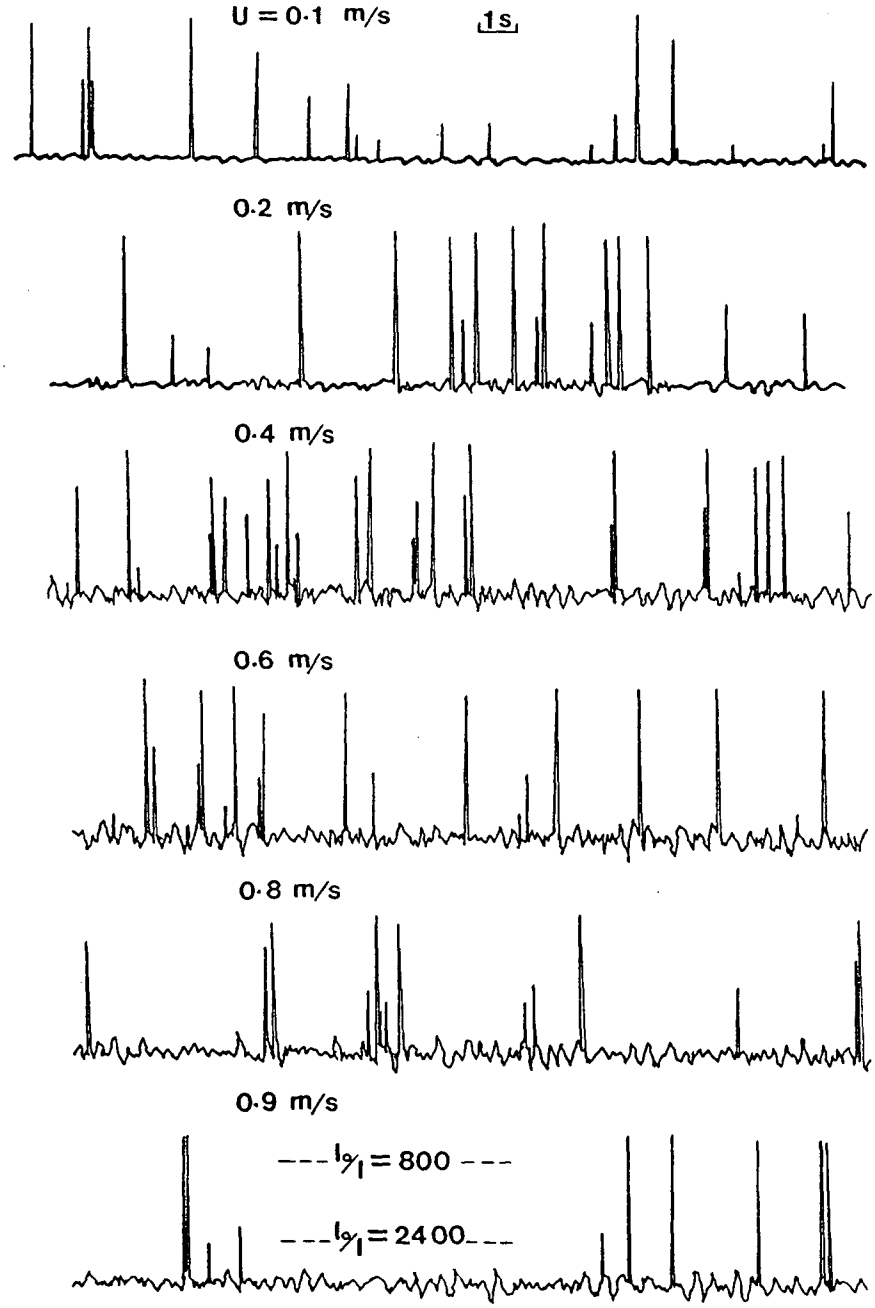

Figure B.1: Photometric measurement for S-FCC particles with narrow PSD

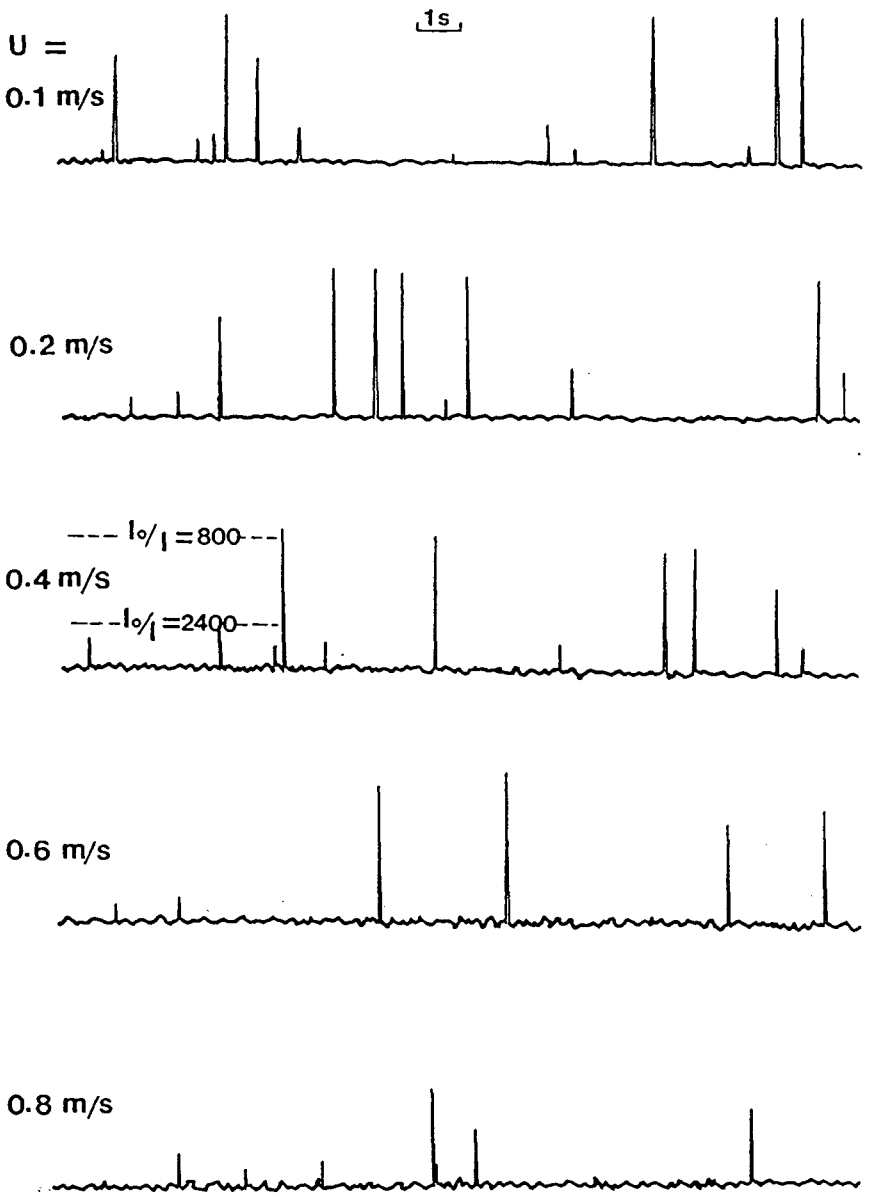

Figure B.2: Photometric measurement for S-FCC particles with wide PSD

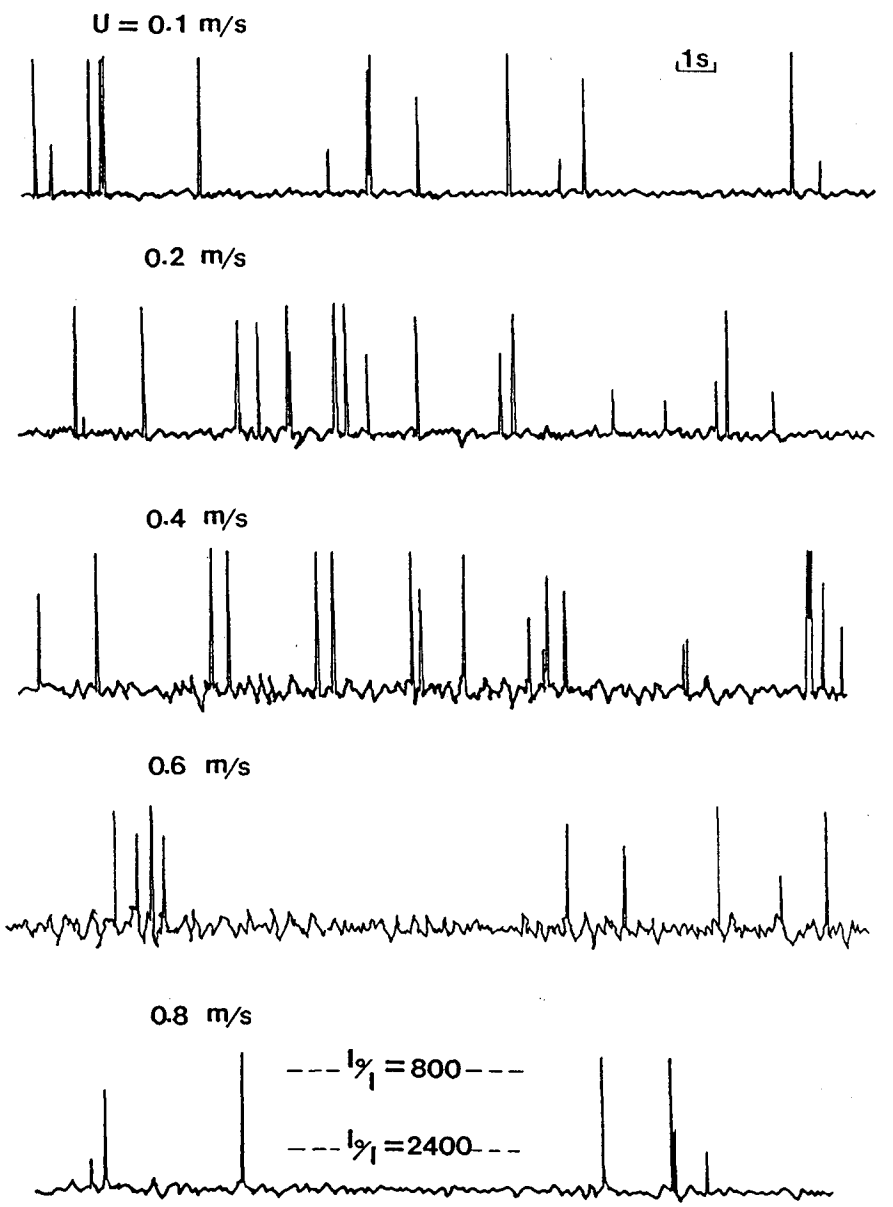

Figure B.3: Photometric measurement for S-FCC particles with bimodal PSD

Appendix C

Statistical Analysis of Experimental Results

C.1 Significance test of the influence of the PSD

The significance of the effect of the PSD on the performance of fluidized bed reactors at certain operating conditions (e.g. same U, k_r, W_{cat} and $\overline{d}_p$ etc.) has been examined using the F-test based on the assumption of randomization (Hogg and Ledolter, 1987).

Two type sources of variation may occur, the "between" and the "within", originating from the influence of the PSD and from the experimental error, respectively. The ratio of the mean squares, F, can be expressed as

$$F = \frac{MS_{PSD}}{MS_{ERROR}} = \frac{\sum_{i=1}^{k} n_i(\overline{Y}_i - \overline{Y})^2/(k-1)}{\sum_{i=1}^{k}\sum_{j=1}^{n_i}(Y_{ij} - \overline{Y}_i)^2/(N-k)} \qquad (i = 1, 2, \ldots, k;\ j = 1, 2, \ldots, n_i) \tag{C.1}$$

where

$$\overline{Y}_i = \frac{1}{n_i}\sum_{i=1}^{n_i} Y_{ij} \tag{C.2}$$

$$\overline{Y} = \frac{1}{N}\sum_{i=1}^{k}\sum_{j=1}^{n_i} Y_{ij} \tag{C.3}$$

$$N = \sum_{i=1}^{k} n_i \tag{C.4}$$

and Y_{ij} is the experimental value (e.g. reaction conversion) obtained in the jth trail for the ith PSD.

Table C.1: Reaction conversions measured in the fluidized bed reactor for particles of different size distributions; $U = 0.5$ m/s, $k_r = 9\ s^{-1}$, catalyst inventory = 5 kg.

PSD	$x_{i,j}$					$\overline{x}_i$	$\sum_{j=1}^{5}(x_{i,j} - \overline{x}_i)^2$
wide	0.875	0.882	0.870	0.893	0.886	0.881	0.000327
narrow	0.802	0.811	0.805	0.791	0.803	0.802	0.000211
bimodal	0.858	0.832	0.850	0.845	0.849	0.847	0.000363

The above mean square (or F) ratio has an F distribution with $(k-1)$ and $(N-k)$ degrees of freedom. If $F \geq F(\alpha; k-1, N-k)$, we accept the hypothesis that there is a significant influence of the PSD on the reactor performance. On the other hand, if the F-ratio is smaller than the critical value, then there is not enough evidence in the data to reject the null hypothesis, i.e. we must consider the effect of the PSD to be insignificant.

As typical example, consider a set of experimental results obtained under typical operating conditions for three different particle size distributions shown in Table C.1.

In this case, $k = 3$ and $n_i = 5$, i.e. there were three size distributions and five measured conversions for each size distribution. According to eqns. C.1 to C.4, $F = \frac{MS_{PSD}}{MS_{ERROR}} = 104.4$. It can be seen from the F distribution table, $F\ (0.01,\ 2,\ 12) = 6.93 < F$. Thus, the effect of PSD on the reactor performance at these operating conditions is significant at significance level $\alpha = 0.01$, i.e. at the 99% probability level.

If we compare the results of the bimodal PSD with those of the wide PSD, similar conclusions are obtained. The F-ratio calculated is 33.5, while $F(0.01,\ 1,\ 8) = 11.26 < F$. This means that for the operating conditions of Table C.1 the difference between reaction

conversions for the two particle size distributions were again significant at a significance level $\alpha = 0.01$. In most cases ($U > 0.2$ m/s), it is possible, as in the example given here, to shown that the differences between the results for the three particle size distributions is statistically significant.

C.2 Confidence intervals of experimental results

For a random sample $x_1, x_2, \ldots, x_n$ arises from a distribution with unknown mean μ and variance $\sigma^2 > 0$, the computed $100(1-\alpha)$ percent confidence interval can be expressed (Hogg and Ledolter, 1987) as:

$$\overline{x} \pm z(\frac{\alpha}{2})\frac{\sigma}{\sqrt{n}} \tag{C.5}$$

where $\overline{x}$ is the sample mean and the probability $(1-\alpha)$ is called the confidence coefficient. If the population mean μ is unknown, in many situations, the population standard deviation σ is also unknown. In this case, if the sample size is quite large (> 30), the sample standard deviation can be taken as σ. If the sample size is small, however, a $100(1-\alpha)$ percent confidence interval for μ can be expressed by

$$\overline{x} \pm t(\frac{\alpha}{2}; n-1)\frac{s}{\sqrt{n}}, \tag{C.6}$$

provided that the random sample arises from the normal distribution. Here t is the "student t" tabulated in most statistics texts.

The confidence intervals for our experimental results were examined against eqn. C.6. As an example, conversion data for the bimodal particle size distribution in Table C.1 were analyzed to evaluate the confidence interval.

In this case, $n = 5$, $\overline{x}_i = 0.847$, and $t(0.05/2, 4) = 2.776$, while

$$s = \sqrt{\frac{\sum(x_{i,j} - \overline{x}_i)^2}{(n-1)}} = 0.00953$$

Therefore, a 95 percent confidence interval for the mean of the reaction conversion for the bimodal PSD in Table C.1 is 0.847 ± 0.012. The interval breadth is of the same order as the height of the symbols used on the graphs. Note, however, that the different points used to determine the variance are from the same run, with the points taken at different times. In tables D.1 to D.6, results are shown for six conditions that were totally repeated for U = 0.1 and 0.11 m/s. These show that the reproducibility is nearly as good for complete repeats as for different points taken during the same experiments.

Appendix D

Raw Data from Chemical Reaction Tests

Table D.1: Raw conversion data of ozone decomposition for particles of wide size distribution

operating condition	k_r=2.15s^{-1}, W_{cat}=1.1kg		k_r=2.25s^{-1}, W_{cat}=2.75kg	
U, m/s	mean	standard deviation	mean	standard deviation
0.10	0.528	0.006	0.736	0.007
0.21	0.351	0.004	0.602	0.006
0.31	0.290	0.005	0.518	0.009
0.53	0.208	0.004	0.404	0.002
0.77			0.306	0.005
0.10	0.533	0.005	0.729	0.004

Table D.2: Raw conversion data of ozone decomposition for particles of narrow size distribution

operating condition	k_r=2.12s^{-1}, W_{cat}=1.1kg		k_r=2.17s^{-1}, W_{cat}=2.75kg	
U, m/s	mean	standard deviation	mean	standard deviation
0.10	0.455	0.005	0.686	0.006
0.21	0.300	0.002	0.466	0.008
0.31	0.225	0.003	0.392	0.005
0.53	0.153	0.004	0.298	0.004
0.77			0.237	0.002
0.10	0.450	0.006	0.682	0.005

Table D.3: Raw conversion data of ozone decomposition for particles of bimodal size distribution with coarse fraction active

operating condition	k_r=2.21s^{-1}, W_{cat}=1.1kg		k_r=2.25s^{-1}, W_{cat}=2.75kg	
U, m/s	mean	standard deviation	mean	standard deviation
0.10	0.476	0.006	0.733	0.007
0.21	0.338	0.003	0.549	0.008
0.31	0.264	0.004	0.447	0.005
0.53	0.185	0.005	0.345	0.006
0.77			0.270	0.003
0.10	0.490	0.005	0.724	0.006

Table D.4: Raw conversion data of ozone decomposition for particles of bimodal size distribution with fine fraction active

operating condition	k_r=2.16s^{-1}, W_{cat}=1.1kg		k_r=2.20s^{-1}, W_{cat}=2.75kg	
U, m/s	mean	standard devaition	mean	standard deviation
0.10	0.513	0.007	0.740	0.009
0.21	0.371	0.003	0.562	0.006
0.31	0.295	0.005	0.485	0.005
0.53	0.222	0.004	0.391	0.008
0.77			0.259	0.003
0.10	0.518	0.006	0.728	0.010

Table D.5: Raw conversion data of ozone decomposition for particles of bimodal size distribution with different fraction active; catalyst inventory: 5.05 kg

active condition	both fractions k_r=4.03s^{-1}		coarse fraction k_r=4.14s^{-1}		fine fraction k_r=4.10s^{-1}	
U, m/s	mean	deviation	mean	deviation	mean	deviation
0.11	0.911	0.009	0.897	0.006	0.906	0.011
0.31	0.844	0.007	0.814	0.007	0.848	0.005
0.51	0.767	0.006	0.714	0.004	0.783	0.005
0.71	0.689	0.008	0.663	0.006	0.712	0.006
0.91	0.585	0.007	0.600	0.003	0.628	0.008
1.10	0.512	0.005	0.547	0.010	0.539	0.002
1.35	0.445	0.003	0.495	0.002	0.460	0.004
1.70	0.406	0.004	0.431	0.004	0.398	0.003
0.11	0.902	0.008	0.908	0.006	0.914	0.008

Table D.6: Raw conversion data of ozone decomposition for particles of different size distributions; catalyst inventory: 5.05kg

PSD	wide (k_r=4.27s^{-1})		narrow (k_r=4.20s^{-1})	
U, m/s	mean	standard deviation	mean	standard deviation
0.11	0.915	0.009	0.900	0.008
0.31	0.875	0.005	0.798	0.007
0.51	0.822	0.008	0.676	0.004
0.71	0.789	0.004	0.623	0.007
0.91	0.724	0.011	0.556	0.003
1.10	0.655	0.003	0.508	0.002
1.35	0.580	0.005	0.455	0.006
1.70	0.486	0.006	0.410	0.004
0.11	0.904	0.007	0.895	0.010

Table D.7: Raw conversion data of ozone decomposition for particles of wide size distribution with different activities; catalyst inventory: 5 kg

condition	k_r=2.41s^{-1}		k_r=4.46s^{-1}		k_r=8.95s^{-1}	
U, m/s	mean	deviation	mean	deviation	mean	deviation
0.10	0.838	0.008	0.923	0.013	0.940	0.007
0.30	0.741	0.009	0.872	0.006	0.911	0.010
0.50	0.622	0.004	0.846	0.003	0.881	0.009
0.75	0.515	0.005	0.775	0.006	0.845	0.004
0.95	0.456	0.007	0.728	0.005	0.813	0.004
1.15	0.420	0.002	0.664	0.009	0.764	0.006
1.40			0.596	0.004	0.722	0.008
1.75			0.503	0.007	0.650	0.005

Table D.8: Raw conversion data of ozone decomposition for particles of narrow size distribution with different activities; catalyst inventory: 5 kg

condition	k_r=2.32s^{-1}		k_r=4.49s^{-1}		k_r=9.10s^{-1}	
U, m/s	mean	deviation	mean	deviation	mean	deviation
0.10	0.816	0.009	0.902	0.007	0.916	0.011
0.30	0.665	0.006	0.816	0.008	0.855	0.007
0.50	0.551	0.007	0.723	0.010	0.802	0.007
0.75	0.430	0.008	0.651	0.004	0.730	0.008
0.95	0.382	0.003	0.590	0.009	0.700	0.005
1.15	0.325	0.005	0.529	0.003	0.634	0.004
1.40			0.482	0.006	0.609	0.006
1.75			0.435	0.005	0.571	0.003

Table D.9: Raw conversion data of ozone decomposition for particles of bimodal size distribution with different activities; catalyst inventory: 5 kg

condition	k_r=4.62s^{-1}		k_r=9.04s^{-1}	
U, m/s	mean	standard deviation	mean	standard deviation
0.10	0.913	0.008	0.931	0.015
0.30	0.846	0.011	0.890	0.007
0.50	0.804	0.005	0.847	0.010
0.75	0.720	0.003	0.793	0.009
0.95	0.663	0.009	0.750	0.006
1.15	0.594	0.005	0.692	0.008
1.40	0.520	0.007	0.648	0.006
1.75	0.455	0.003	0.606	0.004

Table D.10: Raw conversion data of ozone decomposition in fluidized beds with different gas distributors, for particles of wide size distribution; catalyst inventory: 1.2 kg

test condition	U = 0.2 m/s		U = 0.6 m/s	
distributor No.	mean	deviation	mean	deviation
No. 1 (k_r=8.02s^{-1})	0.703	0.006	0.516	0.007
No. 2 (k_r=8.10s^{-1})	0.645	0.005	0.495	0.008
No. 3 (k_r=7.95s^{-1})	0.622	0.007	0.469	0.004
No. 4 (k_r=8.23s^{-1})	0.581	0.009	0.440	0.006

Table D.11: Raw conversion data of ozone decomposition in fluidized bed with different gas distributors, for particles of wide size distribution; catalyst inventory: 3 kg

test condition	U = 0.2 m/s		U = 0.6 m/s	
distributor No.	mean	deviation	mean	deviation
No. 1 (k_r=8.16s^{-1})	0.808	0.007	0.716	0.009
No. 2 (k_r=8.00s^{-1})	0.792	0.004	0.700	0.005
No. 3 (k_r=7.93s^{-1})	0.775	0.010	0.684	0.004
No. 4 (k_r=8.04s^{-1})	0.707	0.008	0.610	0.006

Table D.12: Raw conversion data of ozone decomposition in fluidized bed with different gas distributors for particles of narrow size distribution; catalyst inventory: 1.2 kg

test condition	U = 0.2 m/s		U = 0.6 m/s	
distributor No.	mean	deviation	mean	deviation
No. 1 (k_r=7.96s^{-1})	0.650	0.009	0.441	0.008
No. 2 (k_r=8.13s^{-1})	0.631	0.006	0.437	0.009
No. 3 (k_r=8.00s^{-1})	0.592	0.007	0.402	0.005
No. 4 (k_r=7.90s^{-1})	0.485	0.006	0.348	0.003

Table D.13: Raw conversion data of ozone decomposition in fluidized bed with different distributors for particles of narrow size distribution; catalyst inventory: 3 kg

test condition	U = 0.2 m/s		U = 0.6 m/s	
distributor No.	mean	deviation	mean	deviation
No. 1 (k_r=8.11s^{-1})	0.770	0.011	0.633	0.004
No. 2 (k_r=8.09s^{-1})	0.764	0.005	0.620	0.005
No. 3 (k_r=8.00s^{-1})	0.732	0.002	0.584	0.006
No. 4 (k_r=7.96s^{-1})	0.681	0.008	0.540	0.007

Table D.14: Axial dispersion model test for particles of wide size distribution at higher gas velocities; catalyst inventory: 5 kg.

test condition			model of this study		Danckwerts' model	
U, m/s	k_r, s^{-1}	$x_{exp.}$	$x_{cal.}$	$(x_{exp.} - x_{cal.})/x_{exp.}$	$x_{cal.}$	$(x_{exp.} - x_{cal.})/x_{exp.}$
0.75	2.41	0.515	0.516	- 0.041	0.603	- 0.171
0.95	2.41	0.456	0.483	- 0.059	0.540	- 0.184
1.15	2.41	0.420	0.410	+ 0.024	0.465	+ 0.107
0.75	4.46	0.775	0.772	+ 0.004	0.821	- 0.059
0.95	4.46	0.728	0.715	+ 0.018	0.749	- 0.029
1.15	4.46	0.664	0.619	+ 0.068	0.650	+ 0.021
1.40	4.46	0.596	0.554	+ 0.070	0.582	+ 0.023
1.75	4.46	0.503	0.417	+ 0.171	0.435	+ 0.135
0.75	8.95	0.845	0.886	- 0.049	0.937	- 0.104
0.95	8.95	0.813	0.865	- 0.064	0.896	- 0.093
1.15	8.95	0.764	0.780	- 0.021	0.824	- 0.079
1.40	8.95	0.722	0.730	- 0.011	0.758	- 0.050
1.75	8.95	0.650	0.608	+ 0.065	0.630	+ 0.031
average deviation				0.051		0.084

Appendix E

Typical measurement results of particle size and size distribution

Table E.1: Size and size distribution for N-FCC particles of wide PSD

Sample Id: 0 Date: 18.11.88 380 micron Orifice Tube, serial # 937 Volumetric: 2007.9 microliters

True Log	Dia. Ch 1	Dia. Ch 128	Current	Gain	Counts		Preset Time	Elapsed Time	Preset Peak	Preset Total
14.3 (14)	6.63	181.51	5.5	1.0	1574	0	.0	3.7	25600	8000000

Total = 147679 Mean at 59.20 Median at 59.20 Mode at 64.01

Chnl	Size	Volume	%Larger	Chnl	Size	Volume	%Larger	Chnl	Size	Volume	%Larger	Chnl	Size	Volume	%Larger
5	7.36	1	100.00	33	15.27	14	99.93	61	31.67	552	97.24	89	65.70	5987	36.81
6	7.55	1	100.00	34	15.67	17	99.92	62	32.51	619	96.87	90	67.43	4344	32.73
7	7.75	1	100.00	35	16.09	15	99.91	63	33.37	774	96.45	91	69.21	4318	29.81
8	7.96	1	100.00	36	16.51	21	99.90	64	34.25	988	95.93	92	71.04	3801	26.85
9	8.17	1	100.00	37	16.95	17	99.89	65	35.15	1044	95.26	93	72.91	4037	23.98
10	8.38	1	100.00	38	17.39	28	99.87	66	36.08	1134	94.55	94	74.84	3851	21.24
11	8.60	1	100.00	39	17.85	31	99.86	67	37.03	1291	93.78	95	76.82	2734	18.65
12	8.83	1	100.00	40	18.32	37	99.83	68	38.01	1486	92.91	96	78.84	3225	16.00
13	9.06	1	99.99	41	18.81	46	99.81	69	39.01	1835	91.91	97	80.92	2616	14.61
14	9.30	1	99.99	42	19.30	45	99.78	70	40.04	1814	90.67	98	83.06	3300	12.84
15	9.55	1	99.99	43	19.81	43	99.75	71	41.10	2069	89.44	99	85.25	2209	10.61
16	9.80	1	99.99	44	20.34	61	99.72	72	42.19	2608	88.04	100	87.50	1653	9.11
17	10.06	2	99.99	45	20.87	72	99.68	73	43.30	2879	86.27	101	89.81	1589	7.99
18	10.33	2	99.99	46	21.43	76	99.63	74	44.44	2865	84.32	102	92.19	1575	6.91
19	10.60	2	99.99	47	21.99	99	99.58	75	45.62	3323	82.38	103	94.62	1548	5.85
20	10.88	1	99.99	48	22.57	98	99.51	76	46.82	3425	80.13	104	97.12	1005	4.89
21	11.17	3	99.99	49	23.17	109	99.44	77	48.06	3825	77.81	105	99.68	815	4.12
22	11.46	4	99.99	50	23.78	150	99.37	78	49.33	4223	75.22	106	102.31	979	3.57
23	11.76	3	99.98	51	24.41	165	99.27	79	50.63	4247	72.36	107	105.01	1164	2.90
24	12.08	4	99.98	52	25.05	139	99.16	80	51.96	5079	69.49	108	107.79	687	2.42
25	12.39	5	99.98	53	25.71	207	99.06	81	53.34	5451	66.05	109	110.63	247	1.65
26	12.72	5	99.97	54	26.39	212	98.92	82	54.74	5084	62.36	110	113.55	669	1.43
27	13.06	6	99.97	55	27.09	274	98.78	83	56.19	5108	58.91	111	116.55	434	1.03
28	13.40	7	99.97	56	27.80	350	98.59	84	57.67	5699	55.45	112	119.63	156	.74
29	13.76	8	99.96	57	28.54	325	98.36	85	59.20	4767	51.60	113	122.79	338	.63
30	14.12	8	99.95	58	29.29	386	98.14	86	60.76	5371	48.23	114	126.03	183	.30
31	14.49	10	99.95	59	30.06	378	97.88	87	62.36	5099	44.59	115	129.36	198	.28
32	14.88	16	99.94	60	30.86	356	97.62	88	64.01	6400	41.14	116	132.77	214	.24

Table E.2: Size and size distribution for N-FCC particles of wide PSD after being activated

Sample Id: 2 Date: 18.11.85 380 micron Orifice Tube, serial # 937 Volumetric: 2007.9 microliters

True Log	Dia. Ch 1	Dia. Ch 128	Current	Gain	Counts		Preset Time	Elapsed Time	Preset Peak	Preset Total
14.3 (14)	6.63	181.51	5.5	1.0	686	0	.0	3.6	25600	8000000

Total = 150435 Mean at 65.70 Median at 67.43 Mode at 67.43

Chnl	Size	Volume	%Larger	Chnl	Size	Volume	%Larger	Chnl	Size	Volume	%Larger	Chnl	Size	Volume	%Larger
5	7.36	6	100.00	33	15.27	5	99.92	61	31.67	88	99.39	89	65.70	5775	54.07
6	7.55	22	100.00	34	15.67	3	99.92	62	32.51	148	99.34	90	67.43	6400	50.23
7	7.75	16	99.98	35	16.09	5	99.92	63	33.37	160	99.24	91	69.21	5620	45.98
8	7.96	8	99.97	36	16.51	7	99.91	64	34.25	249	99.13	92	71.04	5215	42.24
9	8.17	4	99.97	37	16.95	10	99.91	65	35.15	247	98.97	93	72.91	5590	38.78
10	8.38	3	99.96	38	17.39	12	99.90	66	36.08	363	98.80	94	74.84	4613	35.06
11	8.60	1	99.96	39	17.85	12	99.90	67	37.03	424	98.56	95	76.82	5332	32.00
12	8.83	2	99.96	40	18.32	11	99.89	68	38.01	605	98.28	96	78.84	4836	28.45
13	9.06	1	99.96	41	18.81	13	99.88	69	39.01	729	97.88	97	80.92	4492	25.24
14	9.30	1	99.96	42	19.30	16	99.87	70	40.04	829	97.39	98	83.06	3262	22.25
15	9.55	0	99.96	43	19.81	10	99.86	71	41.10	1221	96.84	99	85.25	2900	20.08
16	9.80	1	99.96	44	20.34	19	99.85	72	42.19	1634	96.03	100	87.50	3560	18.15
17	10.06	2	99.96	45	20.87	15	99.84	73	43.30	1941	94.94	101	89.81	3024	15.79
18	10.33	2	99.96	46	21.43	19	99.83	74	44.44	2099	93.65	102	92.19	3072	13.78
19	10.60	2	99.95	47	21.99	15	99.82	75	45.62	2102	92.26	103	94.62	2572	11.74
20	10.88	2	99.95	48	22.57	26	99.81	76	46.82	2688	90.86	104	97.12	2549	10.03
21	11.17	1	99.95	49	23.17	24	99.79	77	48.06	2850	89.07	105	99.68	2005	8.53
22	11.46	2	99.95	50	23.78	24	99.78	78	49.33	3887	87.18	106	102.31	1761	7.00
23	11.76	2	99.95	51	24.41	24	99.76	79	50.63	3119	84.59	107	105.01	2344	5.83
24	12.08	3	99.95	52	25.05	28	99.74	80	51.96	3337	82.52	108	107.79	1742	4.27
25	12.39	4	99.95	53	25.71	47	99.73	81	53.34	3973	80.30	109	110.63	1199	3.11
26	12.72	3	99.94	54	26.39	40	99.69	82	54.74	4587	77.66	110	113.55	1111	2.32
27	13.06	4	99.94	55	27.09	43	99.67	83	56.19	4533	74.61	111	116.55	1001	1.59
28	13.40	3	99.94	56	27.80	41	99.64	84	57.67	5145	71.60	112	119.63	650	.91
29	13.76	5	99.94	57	28.54	74	99.61	85	59.20	5353	68.18	113	122.79	468	.48
30	14.12	3	99.93	58	29.29	48	99.56	86	60.76	4937	64.62	114	126.03	253	.17
31	14.49	7	99.93	59	30.06	86	99.53	87	62.36	5124	61.34				
32	14.88	5	99.93	60	30.86	119	99.47	88	64.01	5806	57.73				

Table E.3: Size and size distribution for N-FCC catalysts of wide PSD after being fluidized in the reactor for 5 hours

Sample Id: 1 Date: 18.11.88 380 micron Orifice Tube, serial # 937 Volumetric: 2007.9 microliters

True Log	Dia. Ch 1	Dia. Ch 128	Current	Gain	Counts		Preset Time	Elapsed Time	Preset Peak	Preset Total
14.3 (14)	6.63	181.51	5.5	1.0	433	0	.0	3.7	25600	8000000

Total = 154901 Mean at 64.01 Median at 65.70 Mode at 67.43

Chnl	Size	Volume	%Larger	Chnl	Size	Volume	%Larger	Chnl	Size	Volume	%Larger	Chnl	Size	Volume	%Larger
5	7.36	14	100.00	33	15.27	9	99.84	61	31.67	336	98.39	89	65.70	5051	50.04
6	7.55	46	99.99	34	15.67	13	99.83	62	32.51	468	98.18	90	67.43	6400	46.73
7	7.75	35	99.96	35	16.09	9	99.82	63	33.37	486	97.86	91	69.21	5536	42.65
8	7.96	17	99.94	36	16.51	16	99.82	64	34.25	514	97.55	92	71.04	5487	39.08
9	8.17	7	99.93	37	16.95	14	99.81	65	35.15	653	97.21	93	72.91	5502	35.54
10	8.38	4	99.92	38	17.39	15	99.80	66	36.08	1046	96.79	94	74.84	5366	31.98
11	8.60	3	99.92	39	17.85	14	99.79	67	37.03	1018	96.12	95	76.82	4415	28.52
12	8.83	2	99.92	40	18.32	34	99.78	68	38.01	1208	95.46	96	78.84	3001	25.67
13	9.06	1	99.92	41	18.81	28	99.76	69	39.01	1422	94.68	97	80.92	5457	23.73
14	9.30	3	99.92	42	19.30	18	99.74	70	40.04	1072	93.76	98	83.06	3827	20.21
15	9.55	3	99.91	43	19.81	35	99.73	71	41.10	1411	93.07	99	85.25	3276	17.74
16	9.80	3	99.91	44	20.34	16	99.71	72	42.19	1609	92.16	100	87.50	2237	15.62
17	10.06	4	99.91	45	20.87	38	99.70	73	43.30	2034	91.12	101	89.81	4032	14.18
18	10.33	4	99.91	46	21.43	55	99.67	74	44.44	2028	89.81	102	92.19	3052	11.58
19	10.60	5	99.91	47	21.99	38	99.64	75	45.62	2642	88.50	103	94.62	1414	9.61
20	10.88	4	99.90	48	22.57	77	99.61	76	46.82	2485	86.79	104	97.12	2294	8.69
21	11.17	5	99.90	49	23.17	45	99.56	77	48.06	3521	85.19	105	99.68	1654	7.21
22	11.46	5	99.90	50	23.78	71	99.53	78	49.33	2973	82.92	106	102.31	2384	6.13
23	11.76	7	99.89	51	24.41	97	99.49	79	50.63	3973	81.00	107	105.01	1934	4.61
24	12.08	6	99.89	52	25.05	79	99.42	80	51.96	4530	78.43	108	107.79	1045	3.36
25	12.39	5	99.89	53	25.71	118	99.37	81	53.34	4012	75.51	109	110.63	1130	2.68
26	12.72	7	99.88	54	26.39	143	99.30	82	54.74	4338	72.92	110	113.55	0	1.75
27	13.06	7	99.88	55	27.09	149	99.20	83	56.19	4098	70.12	111	116.55	441	1.95
28	13.40	7	99.87	56	27.80	144	99.11	84	57.67	5659	67.47	112	119.63	953	1.67
29	13.76	15	99.87	57	28.54	181	99.02	85	59.20	5311	63.82	113	122.79	1030	1.05
30	14.12	13	99.86	58	29.29	168	98.90	86	60.76	5431	60.39	114	126.03	0	.59
31	14.49	8	99.85	59	30.06	272	98.79	87	62.36	5265	56.88	115	129.36	602	.39
32	14.88	10	99.85	60	30.86	344	98.61	88	64.01	5328	53.48				